

**PRECISE ORBIT DETERMINATION OF GLOBAL  
NAVIGATION SATELLITE SYSTEM OF SECOND GENERATION  
(GNSS-2)**

**-Orbit Determination of IGSO, GEO and MEO Satellites-**

M.Sc. Hua Su

Vollständiger Abdruck der an die Fakultät für Bauingenieur- und Vermessungswesen der Universität der Bundeswehr München zur Erlangung des akademischen Grades eines Doktor-Ingenieurs (Dr.-Ing.) genehmigten Dissertation.

Vorsitzender:	Univ.-Prof. Dr.-Ing.	K. Brunner
1. Berichterstatter:	Univ.-Prof. Dr.-Ing.	G. Hein
2. Berichterstatter:	Univ.-Prof. Dr.-Ing.	E. Groten (TU Darmstadt)
3. Berichterstatter:	Univ.-Prof. Dr.-Ing.	B. Eissfeller

Die Dissertation wurde am 20. Mai 2000 bei der Universität der Bundeswehr München, Werner-Heisenberg-Weg 39, D-85577 Neubiberg eingereicht.

Tag der mündlichen Prüfung: 07. August 2000



# Zusammenfassung

GNSS -2 (Global Navigation Satellite System of Second Generation) ist eine neue Generation eines satellitenbasierten Navigationssystems. Das Hauptziel des Navigationssystems ist es die vorhandenen Satellitensysteme wie GPS und GLONASS zu verbessern. Europas Beitrag zu einem neuen Navigationssatellitensystem von GNSS -2 wird Galileo genannt.

Das typische Raumsegment eines GNSS -2 Systems besteht aus inclined geosynchronous (IGSO), geostationary (GEO) und Medium Earth Orbit (MEO) Satelliten. Das Raumsegment des Galileo Systems ist jetzt nur aus MEO Satelliten zusammengesetzt. Mit diesem neuen Satellitennavigationssystem kann genaue Navigation und Ortsbestimmung mit einer Genauigkeit von mindestens 10 Metern ohne die Differentialtechnik erreicht werden. Deshalb ist eine sehr präzise Orbitbestimmung für erfolgreiche Anwendungen von GNSS -2/Galileo Systemen mit dieser Genauigkeit gefordert.

Die genauen Orbitbestimmungen von IGSO, GEO und MEO Satelliten werden mit Hilfe von dynamischen und kinematischen Methoden in dieser Dissertation diskutiert. Die Hauptaugenmerk wird jedoch auf IGSO und GEO Satelliten auf Bodenbeobachtungsstationen gerichtet.

In Kapitel 1 werden der GNSS-2/Galileo Entwicklungsplan und die Entwicklungsphase vorgestellt. In Kapitel 2 werden die Grundbeobachtungen der Satellitenbahnbestimmung diskutiert; in Kapitel 3 sind die, für verschiedene Satellitenbahnbestimmungen verwendeten, gegenwärtige Systeme beurteilt; in Kapitel 4 werden größere Quellen von Beobachtungsfehlern analysiert; in Kapitel 5 wird die Störung von IGSO, GEO und MEO modelliert und geschätzt; in Kapitel 6 werden größere Algorithmen zur Orbitbestimmung von IGSO, GEO und MEO Satelliten, wie zum Beispiel Dynamik, reduzierte Dynamik und kinematische Methoden entwickelt und diskutiert; in Kapitel 7 wird die hohe Genauigkeit der IGSO und GEO Orbitbestimmung, die Trägerphasenbeobachtung verwendet, diskutiert; in Kapitel 8 wird ein ernstes Problem der GEO Orbitbestimmung während Satellitenmanövern gezeigt und gelöst. Zuletzt werden in Kapitel 9 die Simulationsergebnisse eines möglichen Satellitenverfolgungssystems von GNSS-2/Galileo gezeigt.

## Summary

GNSS-2 (Global Navigation Satellite System of Second Generation) is a new generation of satellite-based navigation system. The primary goal is to improve the existing satellite systems such as GPS and GLONASS. Europe's contribution to a new navigation satellite system of GNSS-2 is called Galileo.

The typical space segment of a GNSS-2 system is composed of inclined geosynchronous (IGSO), geostationary (GEO) and Medium Earth Orbit (MEO) satellites. The space segment of the Galileo system is now only composed of MEO satellites. With this new satellite navigation system precise navigation and positioning with accuracy of at least 10 meters without differential techniques may be achieved. Therefore high precision orbit determination is required for successful applications of GNSS-2/Galileo systems with this accuracy level.

The precise orbit determinations of IGSO, GEO and MEO satellites are discussed using dynamic and kinematic methods in this dissertation. The effort is focused, however, on IGSO and GEO satellites on ground tracking stations.

In Chapter 1, GNSS-2/Galileo development plan and phase are presented. In Chapter 2, the basic observations of orbit determination are discussed; in Chapter 3 current systems used for various orbit determination applications are evaluated; in Chapter 4 major sources of observation errors are analyzed; in Chapter 5 perturbations on IGSO, GEO and MEO are modeled and estimated; in Chapter 6 major algorithms of orbit determination of IGSO, GEO and MEO, for examples, dynamic, reduced dynamic and kinematic methods are developed and discussed; in Chapter 7 high accuracy of IGSO and GEO orbit determination using carrier phase observation are discussed; in Chapter 8 a serious problem of GEO orbit determination during satellite maneuvers is presented and solved, and finally in Chapter 9 the simulation results of a possible satellite tracking system of GNSS-2/Galileo are presented.

# CONTENTS

<b>CHAPTER 1 INTRODUCTION .....</b>	<b>1</b>
1.1 EUROPE'S CONTRIBUTION TO A NAVIGATION SATELLITE SYSTEM .....	1
1.2 DEVELOPMENT PHASE.....	2
1.3 ORBIT DETERMINATION OF GNSS-2/GALILEO.....	2
<b>CHAPTER 2 OBSERVATIONS OF ORBIT DETERMINATION .....</b>	<b>3</b>
2.1 ONE-WAY SYSTEM .....	3
2.1.1 Range.....	3
2.1.1.1 Basic Observation .....	3
2.1.1.2 Error Budgets .....	4
2.1.2 Doppler.....	6
2.1.2.1 Basic Observation .....	6
2.1.2.2 Error Budget .....	9
2.1.3 Carrier Phases.....	10
2.1.3.1 Basic Observation .....	10
2.1.3.2 Error Budget .....	11
2.2 TWO-WAY SYSTEM.....	11
2.2.1 Range.....	12
2.2.1.1 Basic Observation .....	12
2.2.1.2 Error Budget .....	13
2.2.2 Doppler.....	14
2.2.2.1 Basic Observation Equation.....	14
2.2.2.2 Error Budget .....	16
2.3 CONCLUSION .....	16
<b>CHAPTER 3 ORBIT TRACKING SYSTEMS AND THEIR ERROR BUDGETS .....</b>	<b>17</b>
3.1 GROUND TRACKING SYSTEMS.....	17
3.1.1 Satellite Laser Ranging (SLR).....	17
3.1.1.1 Principle.....	17
3.1.1.2 Error Budget .....	18
3.1.2 S-Band .....	19
3.1.2.1 Principle.....	19
3.1.2.2 Error Budget .....	19
3.1.3 IGS Tracking Station Network .....	20
3.1.3.1 Principle.....	20
3.1.3.2 Error Budget .....	21
3.2 SPACE-BORNE TRACKING SYSTEMS .....	21
3.2.1 DORIS (Doppler Orbitography and Radio Positioning Integrated by Satellite).....	21
3.2.1.1 Principle.....	22
3.2.1.2 Error Budget .....	22
3.2.2 PRARE (Precise Range and Range rate Equipment).....	22

3.2.2.1	Principle.....	22
3.2.2.2	Error Budget.....	26
3.2.3	Inter-Satellite-Links (ISL).....	27
3.2.3.1	Principle.....	27
3.2.3.2	Error Budget.....	28
3.2.3	Navigation System (GPS/GLONASS).....	28
3.2.3.1	Principle.....	29
3.2.3.2	Error Budget.....	29
3.3	CONCLUSION.....	30
<b>CHAPTER 4 MAJOR ERROR SOURCES OF SATELLITE OBSERVATIONS.....</b>		<b>31</b>
4.1	ATMOSPHERIC ERRORS.....	31
4.1.1	Tropospheric Error.....	32
4.1.2	Ionospheric Effect.....	33
4.2	MULTIPATH EFFECT.....	35
4.2.1	Multipath Envelopes.....	36
4.2.2	Influence of Multipath Errors on Range and Phase Observations.....	38
4.3	CLOCK ERRORS.....	41
<b>CHAPTER 5 PERTURBATION MODELS OF IGSO, GEO AND MEO SATELLITE ORBITS.....</b>		<b>43</b>
5.1	THE EARTH GRAVITATIONAL PERTURBATION.....	43
5.1.1	Computation of Legendre Polynomials.....	43
5.1.2	Computation of Geopotential Perturbation.....	44
5.1.3	The Effect of Geopotential Perturbation.....	45
5.1.3.1	Influence of Geopotential on IGSO Satellites.....	46
5.1.3.2	Geopotential Influence on GEO Satellite.....	51
5.1.3.3	Geopotential Influence on MEO (GPS).....	55
5.2	THE SOLAR AND LUNAR ATTRACTIONS.....	56
5.3	THE SOLAR RADIATION PRESSURE MODEL.....	58
5.3.1	Direct Radiation Pressure.....	58
5.3.2	Effect of Eclipses.....	60
5.4	OTHER PERTURBATIONS.....	62
5.4.1	Solid Earth Tides.....	62
5.4.2	Ocean Tides.....	63
5.4.3	Ocean Tide Loading.....	64
<b>CHAPTER 6 ALGORITHMS OF ORBIT DETERMINATION FOR IGSO, GEO &amp; MEO SATELLITES.....</b>		<b>65</b>
6.1	NUMERICAL INTEGRATION.....	65
6.1.1	Runge-Kutta Integration.....	65
6.1.2	Adams-Cowell Algorithm.....	66
6.1.3	Cowell Algorithm.....	67
6.1.4	Numerical Integration of Satellite Dynamic Movement Equation.....	67
6.2	ORBIT DETERMINATION METHODS.....	68
6.2.1	Kalman Filter for Orbit Determination.....	68

6.2.2	Dynamic Orbit Determination Method.....	71
6.2.3	Kinematic Orbit Determination .....	77
6.2.4	Reduced-Dynamic Method.....	79
6.3	DATA PROCESSING.....	79
6.3.1	Batch Processing.....	80
6.3.2	Sequential Processing.....	81
6.3.3	Comparison Between Batch and Sequential Processing.....	81
<b>CHAPTER 7 ORBIT DETERMINATION USING CARRIER PHASE OBSERVATIONS.....</b>		<b>85</b>
7.1	MATHEMATICAL MODELS FOR CARRIER PHASE OBSERVATIONS .....	85
7.1.1	Carrier Phase.....	85
7.1.2	Doppler.....	85
7.1.3	Effects of Initial Ambiguities on Orbit Determination .....	86
7.1.4	Kalman Filter for Orbit Determination using Carrier Phase Observation.....	86
7.2.	PROBLEMS OF CARRIER PHASE OBSERVATION .....	88
7.2.1	Ambiguity Solution Convergence .....	88
7.2.2	Geostationary Satellite Orbit Determination using Carrier Phase Observation.....	89
7.3	AMBIGUITY RESOLUTION APPROACHES .....	90
7.3.1	LAMBDA Method .....	91
7.3.2	Three Carrier Ambiguity Resolution - TCAR .....	92
<b>CHAPTER 8 GEOSTATIONARY ORBIT DETERMINATION AND PREDICTION DURING SATELLITE MANEUVERS.....</b>		<b>95</b>
8.1	PERTURBATIONS OF GEOSTATIONARY SATELLITE.....	95
8.1.1	Nonspherical Earth Gravitation .....	96
8.1.2	Solar and Lunar Attractions.....	99
8.2	ORBIT DETERMINATION DURING SATELLITE MANEUVERS .....	104
8.2.1	Orbit Determination Without Maneuver Operation.....	105
8.2.2	Orbit Determination With Maneuver Operation.....	106
8.3	MANEUVER FORCE MODEL.....	107
8.3.1	Nominal Model.....	109
8.3.2	Approximation using Kinematic Orbit Determination .....	109
<b>CHAPTER 9 SOFTWARE AND SIMULATION RESULTS.....</b>		<b>113</b>
9.1	SOFTWARE .....	113
9.1.1	Coordinate System.....	113
9.1.2	Distribution of Tracking Stations .....	114
9.1.3	Satellite Visibility .....	115
9.2	THE SIMULATION RESULTS OF DYNAMIC ORBIT DETERMINATION USING CODE RANGE OBSERVATIONS . .....	117
9.3	SIMULATION RESULTS USING CARRIER OBSERVATIONS.....	122
9.3.1	Orbit Determination with Float Ambiguity Solution.....	123
9.3.1.1	The Accuracy of Orbit Determination without Satellite Visibility Considered.....	123
9.3.1.2	The Accuracy of Orbit Determination Considering Satellite Visibility .....	126
9.3.2	Effects of Sample Rate on the Accuracy of Orbit Determination.....	130

9.3.3	The Effect of Distribution of Tracking Stations .....	138
9.3.4	Orbit Determination With Integer Ambiguity Solution.....	140
<b>CONCLUSION .....</b>		<b>143</b>
<b>REFERENCES .....</b>		<b>145</b>
<b>ACKNOWLEDGMENTS.....</b>		<b>151</b>



## CHAPTER 1

## INTRODUCTION

### 1.1 Europe's Contribution to a Navigation Satellite System

Satellite navigation is already being used in many fields. Geodesy, geodynamics, airline pilots, fleet management, car navigation and telematics are increasingly relying on it. Information systems are also on the increase for controlling road traffic or with satellites being used to calculate positioning data. However, there is one main condition to be met before Global Navigation Satellite Systems (GNSS) can be used even more extensively, particularly in civil aviation. That is: the satellite-based navigation system should be controlled under civil institutions.

GNSS-2 (Global Navigation Satellite System of Second Generation) will be a new generation of satellite-based navigation system. The primary goal is to improve the existing satellite systems such as GPS and GLONASS, in particular for integrity, accuracy and safety. If the possibilities offered by satellite navigation were fully exploited by civil applications, the result would be better control of air, sea and road traffic, leading to considerable savings in resources and therefore costs. For that reason the European institutions are cooperating in a joint program, called Galileo, which is Europe's contribution to a new navigation satellite system of GNSS-2.

GNSS-2/Galileo will be a civil system and provide a three-dimensional performance over Europe, with accuracy better than 10 meters and provide a universal independent time of reference on a global basis..

According to the document of EU Commission Communication to the European Parliament and the Council on Galileo 2000, Galileo will offer three major categories of navigation services: a general service, a commercial service and a public service. The general service can be used for positioning, navigation and timing service compatible with the existing services but with a great degree of accuracy. This service like GPS SPS will be opened to public free of charge. The commercial services will be suitable for service providers which can give added value to their range of products. This service will be charged by Galileo operators. As a return, the Galileo operator will be able to offer certain service guarantees. The signals to access this service will be controlled on protected access keys. The public service will be offered to users who are highly dependent on precision, signal quality and signal transmission reliability. It will be offered at a very high level of integrity. This service like GPS PPS may be restricted to authorised users.

The space segment of GNSS-2/Galileo consists of a constellation of 30 medium earth satellite or MEO + GEO (Geostationary) satellites. The ground segment is composed of the satellite control centres and the centres needed to provide the services.

In the first phase of GNSS-2/Galileo, EGNOS (European Geostationary Navigation Overlay Service) will be developed. Satellites stationed in geostationary orbit at an altitude of about 36 000 km will relay on GPS and GLONASS and ensures integrity of both systems to aircraft, ship or road vehicle information that will enable the users to determine their actual positions with higher precision than possibly using GPS/GLONASS data alone. EGNOS in particular will enable to increase the number of satellites that can be seen by a given user within the geostationary broadcast area.

One requirement for EGNOS is, that the position of a geostationary satellite must be known with a high precision. For that reason several Earth stations must be deployed in order to determine the position of geostationary satellites with the required accuracy, through range measurements. All data will be forwarded to a central processing facility and used to compute navigation information similar to that provided by GPS. The results are transmitted to users with a GPS-like signal via Earth stations, one for the Inmarsat III AOR East and the other for the Inmarsat III IOR satellite. The GPS-like signal must be synchronized with the GPS clock. In a second phase, upload stations will be deployed. This will measure not only the ranges to the geostationary satellites but also the distances to all visible GPS and GLONASS satellites. With the aid of corrections transmitted by those stations and relayed through EGNOS, users will be able to determine their positions with high precision.

## 1.2 Development Phase

GNSS-2/Galileo system will be developed in the period from 2000 to 2008, building on the experience acquired from GNSS-1.

The time schedule for the different steps can be summarized as follows: (Commission Communication to the European Parliament and the Council on Galileo, 2000)

Development and Validation Phase	2001 to 2005
Deployment Phase	2006 to 2007
Start of Operation	2008

## 1.3 Orbit Determination of GNSS-2/Galileo

In the early study phase, the typical space segment of GNSS-2/Galileo system was composed of inclined geosynchronous (IGSO), geostationary (GEO) and medium earth orbit (MEO) satellites. Now the space segment of Galileo system is composed of 30 MEO satellites or MEO + GEO satellites. According to the document of EU Commission Communication to the European Parliament and the Council on Galileo 2000, the advantage of the system using such satellites is more uniform in performance both in terms of accuracy and availability and greater robustness in crippled mode. With this new satellite navigation system under control of civilian institutions, the precise navigation and positioning with accuracy of at least 10 meters without differential techniques may be achieved. Therefore high precision orbit determination is required for successful applications of GNSS-2/Galileo system with this accuracy level.

There are some new problems for orbit determination of GNSS-2 satellites. For example, due to high altitude of IGSO and GEO satellites, the geometrical distribution of tracking stations will have a greater influence on the accuracy of orbit determination than any other earth satellites, the distances between the satellites and tracking stations will change slowly as satellites move, which leads to some problems in the solution of observation equation, because there are no big differences for observations measured in several minutes. In other words, more observations in a short time will not contribute to improve the accuracy of orbit determination, and when using Doppler-based methods it also does not enhance the accuracy of orbit determination because the Doppler effect will not be significantly sensitive to slow changing of the range rate.

Until now the actual accuracy of geostationary orbit determination is in kilometers. The precise orbit determination of a GNSS-2 satellite with comparable accuracy to a GPS satellite, therefore, is a great challenge. In order to achieve highly accurate orbit determination of GNSS-2 satellites, the satellite tracking station distribution and related data processing methods should be carefully chosen to satisfy the accuracy requirement of GNSS-2 system.

The tracking systems of orbit determination can be classified as two major types: ground-based tracking systems such as S-Band and Satellite Laser Ranging (SLR) and space-borne tracking systems, for examples, DORIS and PRARE. There are two major kinds of observations for orbit determination: optical and radio microwaves. Basic optical observations are directions and angles. The microwave observation may consist of ranges, range rates (Doppler), and carrier phases.

In the dissertation, the current systems of orbit determination using ranges, range rates (Doppler) and carrier phases will be discussed and evaluated. The focus is on ground orbit determination methods. In Chapter 2, the basic observations of orbit determination are discussed; in Chapter 3 current systems used for various orbit determination applications are evaluated; in Chapter 4 major sources of observation errors are analyzed; in Chapter 5 perturbations on IGSO, GEO and MEO are modeled and estimated; in Chapter 6 major algorithms of orbit determination of IGSO, GEO and MEO, for examples, dynamic, reduced dynamic and kinematic methods are developed and discussed; in Chapter 7 high accuracy of IGSO and GEO orbit determination using carrier phase observation are discussed; in Chapter 8 a serious problem of GEO orbit determination during satellite maneuvers is presented and solved, and finally the simulation results of a possible satellite tracking system of GNSS-2 are presented in Chapter 9.

IGSO, GEO and MEO satellites are all possible candidates for a GNSS-2/Galileo system. MEO satellites are actually the same type as GPS/GLONASS satellites, therefore in the dissertation, my focus is on IGSO and GEO satellites, i.e. precise orbit determination of IGSO and GEO satellites, including special situation during GEO satellite maneuvers.

## CHAPTER 2 OBSERVATIONS OF ORBIT DETERMINATION

The basic observations of orbit determination are ranges, range rates (Doppler), carrier-phases, laser ranging, etc. According to the applications, these observations may be used for one-way or two-way systems. In this chapter, the basic observations of orbit determination, the possible error budgets, the error models related to the receivers and the advantages and disadvantages based on current satellite navigation systems, GPS/GLONASS are discussed.

### 2.1 One-Way System

In a one-way system the signal transmitted from satellite is received by the ground tracking stations or the signal transmitted from ground tracking stations is received by satellites. The received signal is then processed for orbit determination. In a typical one-way system, the measurement is done by comparing a clock time at the transmitter antenna with a clock time at the receiver antenna. The travel time of the signal is scaled into a range measurement using signal propagation velocity. All microwave observations mentioned above can be used in a one-way system.

#### 2.1.1 Range

##### 2.1.1.1 Basic Observation

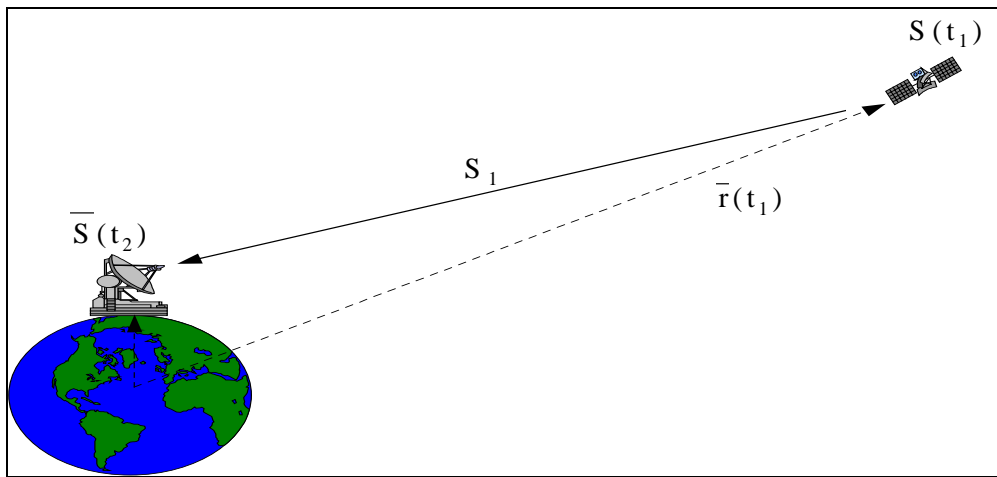


Figure 2-1 One-way Range Measurement

As shown in Figure 2-1, assuming a clock time at the receiver antenna is  $t_2$ , and a clock time at the transmitting antenna is  $t_1$ , the one-way range measurement  $S_1$  can be expressed by

$$L = S_1 = c(t_2 - t_1) + \varepsilon \quad (2-1)$$

where

- $S_1$  the geometrical distance between the satellite and ground tracking station
- $c$  speed of light in vacuum
- $\varepsilon$  measurement noises such as ionospheric and tropospheric errors, multipath effect satellite and receiver errors, and random noises
- $\bar{r}(t_1)$  satellite geocenter position vector at  $t_1$

$\bar{S}(t_2)$  the geocenter vector of ground tracking station at  $t_2$

From Figure 2-1,

$$S_1 = \|\bar{r}(t_1) - \bar{S}(t_2)\| = \{[\bar{r}(t_1) - \bar{S}(t_2)]^T [\bar{r}(t_1) - \bar{S}(t_2)]\}^{\frac{1}{2}} \quad (2-2)$$

$$\begin{aligned} S_1^2 &= [\bar{r}(t_1) - \bar{S}(t_2)]^T [\bar{r}(t_1) - \bar{S}(t_2)] = [\bar{r}^T(t_1)\bar{r}(t_1) - \bar{r}^T(t_1)\bar{S}(t_2) - \bar{S}^T(t_2)\bar{r}(t_1) + \bar{S}^T(t_2)\bar{S}(t_2)] \\ &= \bar{r}^T(t_1)\bar{r}(t_1) + \bar{S}^T(t_2)\bar{S}(t_2) - 2\bar{r}^T(t_1)\bar{S}(t_2) \end{aligned} \quad (2-3)$$

Eq.(2-1) can be written as

$$L = c(t_2 - t_1) = \|\bar{r}(t_1) - \bar{S}(t_2)\| \quad (2-4)$$

By linearizing Eq. (2-4), Eq.(2-1) becomes

$$L = L^0 + \delta L = \|\bar{r}^0(t_1) - \bar{S}^0(t_2)\| + \frac{\partial L}{\partial \bar{r}(t_1)} \delta \bar{r}(t_1) + \frac{\partial L}{\partial \bar{S}(t_2)} \delta \bar{S}(t_2) \quad (2-5)$$

where the partial derivatives are

$$\frac{\partial L}{\partial \bar{r}(t_1)} = \frac{[\bar{r}(t_1) - \bar{S}(t_2)]^T}{\|\bar{r}(t_1) - \bar{S}(t_2)\|} = \frac{[\bar{r}(t_1) - \bar{S}(t_2)]^T}{L} \quad (2-6)$$

$$\frac{\partial L}{\partial \bar{S}(t_2)} = -\frac{[\bar{r}(t_1) - \bar{S}(t_2)]^T}{\|\bar{r}(t_1) - \bar{S}(t_2)\|} = -\frac{[\bar{r}(t_1) - \bar{S}(t_2)]^T}{L} \quad (2-7)$$

$$\delta \bar{r}(t_1) = \frac{\partial \bar{r}(t_1)}{\partial \bar{r}(t_0)} \delta \bar{r}(t_0) + \frac{\partial \bar{r}(t_1)}{\partial \bar{p}(t_1)} \frac{\partial \bar{p}(t_1)}{\partial \bar{p}(t_0)} \delta \bar{p}(t_0) \quad (2-8)$$

where

$\bar{p}$  dynamical model parameters of satellite orbit

Inserting Eq.(2-6) - Eq.(2-8) into Eq.(2-5), the final linear observation equation can be written as

$$\delta L = \frac{[\bar{r}(t_1) - \bar{S}(t_2)]^T}{L^0} \left[ \frac{\partial \bar{r}(t_1)}{\partial \bar{r}(t_0)} \delta \bar{r}(t_0) + \frac{\partial \bar{r}(t_1)}{\partial \bar{p}(t_1)} \frac{\partial \bar{p}(t_1)}{\partial \bar{p}(t_0)} \delta \bar{p}(t_0) \right] - \frac{[\bar{r}(t_1) - \bar{S}(t_2)]^T}{L^0} \delta \bar{S}(t_2) \quad (2-9)$$

where

$t_0$  initial epoch

### 2.1.1.2 Error Budgets

The accuracy of range observations is dependent on the chip rate or frequency. Discussion in detail about influence on range measurements from various error sources such as tropospheric, ionospheric errors and multipath effect are given in Chapter 4. In this section the major error sources of range measurement related to the receiver are discussed and the error budget based on experiences of current satellite navigation systems is presented.

Range measurements are implemented inside the receiver in two ways: 1) tone range; 2) pseudocode ranging like GPS C/A code measurements. The major error sources related to receivers are the following two types.

#### i) Tone Range Error

The accuracy of ranging is set by the highest major carrier frequency and the signal-to-noise ratio:

$$\sigma_r = \frac{c}{2} \frac{1}{2\pi f_s} \frac{K}{\sqrt{S/N}} \quad (2-10)$$

where

$\sigma_r$  distance error

$c$  speed of light

$f_s$  major tone frequency

$S/N$  signal-to-noise ratio

$K$  receiver-related parameter

#### ii) Pseudonoise(PN)-Code Ranging Error with Delay Lock Loop (DLL)

For a Delay Lock Loop, the accuracy of range measurement can be expressed by

$$\sigma_r = D \sqrt{\frac{B_L}{2(C/N_0)}} \quad (2-11)$$

where

- $B_L$  loop bandwidth  
 $D$  chip-length of single PN-code chip  
 $C/N_0$  carrier-to-noise ratio in 1 Hz bandwidth

Using GPS as an example, the total error budget for one-way range measurement is listed in Table 2-1.

Table 2-1 Error Budget of One-Way GPS Ranging (NATO GPS Interface Document, 1988)

Segment Source	Error Source	P-Code Error 1 $\sigma$ [m]	C/A-Code Error 1 $\sigma$ [m]
Space	Clock & Nav. Sub-System Stability	3.0	3.0
	Predictability of Satellite Perturbations	1.0	1.0
	Other	0.5	0.5
Control	Ephemeris Prediction Model Implementation	4.2	4.2
	Other	0.9	0.9
User	Ionospheric Delay Compensation	2.3	5.0-10.0
	Tropospheric Delay Compensation	2.0	2.0
	RCVR Noise & Resolution	1.5	7.5
	Multipath	1.2	1.2
	Other	0.5	0.5
1 $\sigma$ System UERE [m]	Total	6.6	10.8-13.9

## 2.1.2 Doppler

### 2.1.2.1 Basic Observation

Due to relative movement between the satellite and the receiver, the received frequency is different from the frequency transmitted from the satellite. The variation is called Doppler effect. The frequency variation measured in a very short time is defined as Doppler shift measurement, also called differential Doppler measurement.

Doppler observations can be divided into two types: Doppler shift and integrated Doppler count.

(1) Doppler shift (Figure 2-2)

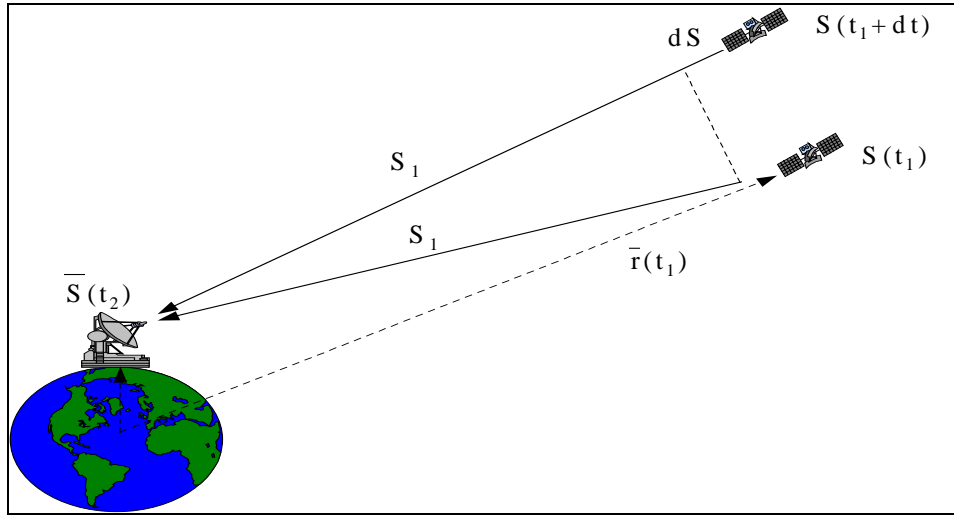


Figure 2-2 Doppler Shift Measurement

Doppler shift is usually used for measurement of the relative velocity between two objects, satellite and receiver. The relationship between received frequency and transmitted frequency due to Doppler effect is:

$$f_r = f_t \left(1 - \frac{\dot{S}_1}{c}\right) + \varepsilon \quad (2-12)$$

where

$f_t$  frequency transmitted from satellites

$f_r$  frequency received at ground tracking stations

$\dot{S}_1$  range rate between satellite and ground tracking station

$c$  speed of light in vacuum

$\varepsilon$  measurement noises i.e. ionospheric error, tropospheric error, multipath effect  
satellite clock error, receiver error and random noises

From Figure 2-2, we can obtain

$$S_1 = \|\bar{r}(t_1) - \bar{S}(t_2)\| = \{[\bar{r}(t_1) - \bar{S}(t_2)]^T [\bar{r}(t_1) - \bar{S}(t_2)]\}^{\frac{1}{2}} \quad (2-13)$$

$$\dot{S}_1 = \frac{dS_1}{dt} = \frac{[\bar{r}(t_1) - \bar{S}(t_2)]^T [\dot{\bar{r}}(t_1) - \dot{\bar{S}}(t_2)]}{S_1} \quad (2-14)$$

where

$\bar{r}(t_1)$  satellite geocentric position vector at  $t_1$

$\bar{S}(t_2)$  geocentric vector of ground tracking station at  $t_2$

Therefore, basic linear observation  $L$  can be written as follows

$$L = \Delta f = f_r - f_t = f_t \left(1 - \frac{S_1^{\&}}{c}\right) - f_t = -f_t \frac{S_1^{\&}}{c} \quad (2-15)$$

$$L = L^0 + \delta L = -f_t \frac{S_1^0}{c} + \frac{\partial L}{\partial \bar{r}(t_1)} \delta \bar{r}(t_1) + \frac{\partial L}{\partial \bar{r}^{\&}(t_1)} \delta \bar{r}^{\&}(t_1) + \frac{\partial L}{\partial \bar{S}(t_2)} \delta \bar{S}(t_2) + \frac{\partial L}{\partial \bar{S}^{\&}(t_2)} \delta \bar{S}^{\&}(t_2) \quad (2-16)$$

where

$$\frac{\partial L}{\partial \bar{r}(t_1)} = \frac{\partial(\Delta f)}{\partial \bar{r}(t_1)} = -f_t \frac{1}{c} \frac{\partial S_1^{\&}}{\partial \bar{r}(t_1)} \quad (2-17)$$

$$\frac{\partial L}{\partial \bar{r}^{\&}(t_1)} = \frac{\partial(\Delta f)}{\partial \bar{r}^{\&}(t_1)} = -f_t \frac{1}{c} \frac{\partial S_1^{\&}}{\partial \bar{r}^{\&}(t_1)} \quad (2-18)$$

$$\frac{\partial L}{\partial \bar{S}(t_2)} = \frac{\partial(\Delta f)}{\partial \bar{S}(t_2)} = -f_t \frac{1}{c} \frac{\partial S_1^{\&}}{\partial \bar{S}(t_2)} \quad (2-19)$$

$$\frac{\partial L}{\partial \bar{S}^{\&}(t_2)} = \frac{\partial(\Delta f)}{\partial \bar{S}^{\&}(t_2)} = -f_t \frac{1}{c} \frac{\partial S_1^{\&}}{\partial \bar{S}^{\&}(t_2)} \quad (2-20)$$

From Eq.(2-14),

$$\frac{\partial S_1^{\&}}{\partial \bar{r}(t_1)} = \frac{[\bar{r}^{\&}(t_1) - \bar{S}^{\&}(t_2)]^T}{S_1} - \frac{S_1^{\&}}{S_1^2} [\bar{r}(t_1) - \bar{S}(t_2)]^T \quad (2-21)$$

$$\frac{\partial S_1^{\&}}{\partial \bar{r}^{\&}(t_1)} = \frac{[\bar{r}(t_1) - \bar{S}(t_2)]^T}{S_1} \quad (2-22)$$

$$\frac{\partial S_1^{\&}}{\partial \bar{S}(t_2)} = -\frac{[\bar{r}^{\&}(t_1) - \bar{S}^{\&}(t_2)]^T}{S_1} + \frac{S_1^{\&}}{S_1^2} [\bar{r}(t_1) - \bar{S}(t_2)]^T \quad (2-23)$$

$$\frac{\partial S_1^{\&}}{\partial \bar{S}^{\&}(t_2)} = -\frac{[\bar{r}(t_1) - \bar{S}(t_2)]^T}{S_1} \quad (2-24)$$

and

$$\delta \bar{r}(t_1) = \frac{\partial \bar{r}(t_1)}{\partial \bar{r}(t_0)} \delta \bar{r}(t_0) + \frac{\partial \bar{r}(t_1)}{\partial \bar{p}(t_0)} \delta \bar{p}(t_0) \quad (2-25)$$

$$\delta \bar{r}^{\&}(t_1) = \frac{\partial \bar{r}^{\&}(t_1)}{\partial \bar{r}^{\&}(t_0)} \delta \bar{r}^{\&}(t_0) \quad (2-26)$$

where

$\bar{p}$  dynamical model parameters of satellite orbit

The final linear observation equation can be obtained by inserting Eq.(2-21) to Eq.(2-26) into Eq.(2-16).

## (2) Integrated Doppler Count

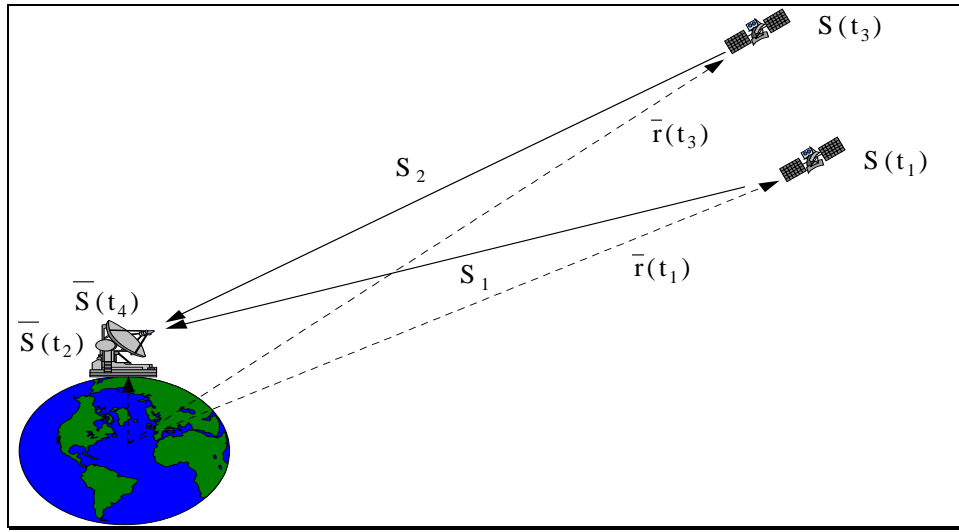


Figure 2-3 Doppler Count Measurement

The equation of integrated Doppler count measurement can be written by

$$L = (f_0 - f_t)(t_3 - t_1) + \frac{f_0}{c}(S_2 - S_1) \quad (2-27)$$

where

- $f_0$  the reference frequency of receiver
- $f_t$  the transmitting frequency of satellite signal

From Figure 2-3,

$$S_1 = \|\bar{r}(t_1) - \bar{S}(t_2)\| = \{[\bar{r}(t_1) - \bar{S}(t_2)]^T [\bar{r}(t_1) - \bar{S}(t_2)]\}^{\frac{1}{2}} \quad (2-28)$$

$$S_2 = \|\bar{r}(t_3) - \bar{S}(t_4)\| = \{[\bar{r}(t_3) - \bar{S}(t_4)]^T [\bar{r}(t_3) - \bar{S}(t_4)]\}^{\frac{1}{2}} \quad (2-29)$$

where

- $\bar{r}(t_1)$  satellite geocentric position vector at  $t_1$
- $\bar{r}(t_3)$  satellite geocentric position vector at  $t_3$
- $\bar{S}(t_2)$  the geocentric vector of ground tracking station at  $t_2$
- $\bar{S}(t_4)$  the geocentric vector of ground tracking station at  $t_4$

The basic linear observation  $L$  is expressed as

$$L = L^0 + \delta L = (f_0 - f_t)(t_3 - t_1) + \frac{f_t}{c}(S_2^0 - S_1^0) + \frac{f_t}{c} \left\{ \left[ \frac{\partial L}{\partial \bar{r}(t_3)} \delta \bar{r}(t_3) + \frac{\partial L}{\partial \bar{S}(t_4)} \delta \bar{S}(t_4) \right] - \left[ \frac{\partial L}{\partial \bar{r}(t_1)} \delta \bar{r}(t_1) + \frac{\partial L}{\partial \bar{S}(t_2)} \delta \bar{S}(t_2) \right] \right\} \quad (2-30)$$

where

$$\frac{\partial L}{\partial \bar{r}(t_3)} = \frac{f_t}{c} \frac{\partial S_2}{\partial \bar{r}(t_3)} \quad (2-31)$$

$$\frac{\partial L}{\partial \bar{S}(t_4)} = \frac{f_t}{c} \frac{\partial S_2}{\partial \bar{S}(t_4)} \quad (2-32)$$

$$\frac{\partial L}{\partial \bar{r}(t_1)} = \frac{f_t}{c} \frac{\partial S_1}{\partial \bar{r}(t_1)} \quad (2-33)$$

$$\frac{\partial L}{\partial \bar{S}(t_2)} = \frac{f_t}{c} \frac{\partial S_1}{\partial \bar{S}(t_2)} \quad (2-34)$$



$$\frac{\partial S_1}{\partial \bar{r}(t_1)} = \frac{[\bar{r}(t_1) - \bar{S}(t_2)]^T}{\|\bar{r}(t_1) - \bar{S}(t_2)\|} = \frac{[\bar{r}(t_1) - \bar{S}(t_2)]^T}{S_1} \quad (2-35)$$

$$\frac{\partial S_2}{\partial \bar{r}(t_3)} = \frac{[\bar{r}(t_3) - \bar{S}(t_4)]^T}{\|\bar{r}(t_3) - \bar{S}(t_4)\|} = \frac{[\bar{r}(t_3) - \bar{S}(t_4)]^T}{S_2} \quad (2-36)$$

$$\frac{\partial S_1}{\partial \bar{S}(t_2)} = -\frac{[\bar{r}(t_1) - \bar{S}(t_2)]^T}{\|\bar{r}(t_1) - \bar{S}(t_2)\|} = -\frac{[\bar{r}(t_1) - \bar{S}(t_2)]^T}{S_1} \quad (2-37)$$

$$\frac{\partial S_2}{\partial \bar{S}(t_4)} = -\frac{[\bar{r}(t_3) - \bar{S}(t_4)]^T}{\|\bar{r}(t_3) - \bar{S}(t_4)\|} = -\frac{[\bar{r}(t_3) - \bar{S}(t_4)]^T}{S_2} \quad (2-38)$$

$$\delta \bar{r}(t_1) = \frac{\partial \bar{r}(t_1)}{\partial \bar{r}(t_0)} \delta \bar{r}(t_0) + \frac{\partial \bar{r}(t_1)}{\partial \bar{p}(t_0)} \delta \bar{p}(t_0) \quad (2-39)$$

$$\delta \bar{r}(t_3) = \frac{\partial \bar{r}(t_3)}{\partial \bar{r}(t_0)} \delta \bar{r}(t_0) + \frac{\partial \bar{r}(t_3)}{\partial \bar{p}(t_0)} \delta \bar{p}(t_0) \quad (2-40)$$

where

$\bar{p}$  satellite dynamical model parameters

### 2.1.2.2 Error Budget

Doppler shift measurement is indirectly made by Phase-Lock-Loop (PLL). PLL measures the difference in the carrier phase between the incoming carrier and a reference carrier generated by local receiver. The standard error of phase measurement by PLL is given by

$$\sigma_\phi = \frac{\lambda}{2\pi} \sqrt{\frac{B_L}{C/N_0}} \quad (2-41)$$

where

$\lambda$  carrier wave-length

$C/N_0$  carrier-to-noise ratio in 1 Hz bandwidth

Because Doppler shift is the difference between the instantaneous phases at two continuous epochs, the standard error of Doppler measurement can be evaluated by following a simple formular

$$\sigma_D = \sqrt{2} \frac{\sigma_\phi}{T_i} \quad (2-42)$$

where

$T_i$  Doppler integration time constant

The errors of Doppler measurements are composed of ionospheric, tropospheric, multipath, satellite clock and receiver errors. Table 2-2 shows the error budget for integrated Doppler count measurement of the TRANSIT satellite system.

Table 2-2 Error Budget for One-Way Doppler Count Measurement (Seeber, 1993)

Error Source	Error (m)
Ionosphere	1-5
Troposphere	2
Multipath	*
Satellite Clock	*
Receiver Error	1-6
Total (1 $\sigma$ )	>8

\* not determined

The accuracy listed in Table 2-2 does not look good. For the precise Doppler shift measurements, please refer to Chapter 3.

### 2.1.3 Carrier Phases

#### 2.1.3.1 Basic Observation

The carrier-phase observations are biased on the integer number of cycles and oscillator frequency offsets between transmitter and receiver. During a data processing session the initial ambiguities should be included as parameters in the observation equations and solved with other parameters. The basic observation equation of carrier phase measurement is written by

$$L = \varphi_r(t) - \varphi_i(t) = \frac{2\pi}{\lambda_1} S_1 + 2\pi N_1 + \varepsilon \quad (2-43)$$

where

- $\varphi_r$  local copy of the transmitted phase produced by the receiver
- $\varphi_i$  received satellite phase at the nominal reception time  $t$
- $N_1$  initial integer ambiguity
- $\lambda_1$  wavelength of signal frequency
- $c$  speed of light in vacuum,
- $\varepsilon$  carrier-phase measurement noises

From Figure 2-1 and Eq.(2-2), the linear observation  $L$  of carrier phase can be expressed as follows

$$L = L^0 + \delta L = \frac{2\pi}{\lambda_1} S_1^0 + \left[ \frac{\partial L}{\partial \bar{r}(t_1)} \delta \bar{r}(t_1) + \frac{\partial L}{\partial \bar{S}(t_2)} \delta \bar{S}(t_2) \right] + \frac{\partial L}{\partial N_1} \delta N_1 \quad (2-44)$$

where

$$\frac{\partial L}{\partial \bar{r}(t_1)} = \frac{2\pi}{\lambda_1} \frac{\partial S_1}{\partial \bar{r}(t_1)} \quad (2-45)$$

$$\frac{\partial L}{\partial \bar{S}(t_2)} = \frac{2\pi}{\lambda_1} \frac{\partial S_1}{\partial \bar{S}(t_2)} \quad (2-46)$$

$$\frac{\partial L}{\partial N_1} = 2\pi \frac{\partial S_1}{\partial N_1} \quad (2-47)$$

and

$$\frac{\partial S_1}{\partial \bar{r}(t_1)} = \frac{[\bar{r}(t_1) - \bar{S}(t_2)]^T}{\|\bar{r}(t_1) - \bar{S}(t_2)\|} = \frac{[\bar{r}(t_1) - \bar{S}(t_2)]^T}{S_1} \quad (2-48)$$

$$\frac{\partial S_1}{\partial \bar{S}(t_2)} = -\frac{[\bar{r}(t_1) - \bar{S}(t_2)]^T}{\|\bar{r}(t_1) - \bar{S}(t_2)\|} = -\frac{[\bar{r}(t_1) - \bar{S}(t_2)]^T}{S_1} \quad (2-49)$$

$$\frac{\partial S_1}{\partial N_1} = I \quad (2-50)$$

$$\delta \bar{r}(t_1) = \frac{\partial \bar{r}(t_1)}{\partial \bar{r}(t_0)} \delta \bar{r}(t_0) + \frac{\partial \bar{r}(t_1)}{\partial \bar{p}(t_1)} \frac{\partial \bar{p}(t_1)}{\partial \bar{p}(t_0)} \delta \bar{p}(t_0) \quad (2-51)$$

$$\frac{\partial L}{\partial N_1} = I \quad (2-52)$$

Eq.(2-43) or Eq.(2-44) can also be expressed as

$$L_i = f(x, y, z, \&\&\& N_i) \quad (2-53)$$

where

- $x, y, z$  geocentric coordinates of satellite position
- $\&\&\&$  geocentric coordinates of satellite velocity

In Eq.(2-53) the tracking station coordinates are assumed to be known parameters. Eq.(2-53) shows that each observation has an extra parameter, the initial integer ambiguity. Fortunately, the number of parameters will not be increased if the observations are continuous. Therefore, the minimum number of parameters to be solved can be described.

$$n = 6 + m$$

where

$n$	total number of parameters to be solved
$6$	number of coordinate components of position and velocity of satellite
$m$	number of tracking stations

For example, if eight tracking stations are tracking one satellite at the same time, at least  $6+8=14$  parameters should be solved. For one epoch, only 8 observations are available. That means in order to solve the orbit determination problem using carrier-phase observations, from the theoretical point of view, at least two epochs of observation are necessary.

### 2.1.3.2 Error Budget

For dual frequency carrier phase observations, ionospheric error will be significantly decreased. Another advantage of carrier phase observations is that the receiver noise is much smaller due to high resolution of carrier phase measurement.

The carrier phase processed in the receiver is mainly affected by following error sources

- Observation resolution
- Variation of the antenna phase center
- Variation of phase delay in the receiver
- Instability of the oscillator
- Interchannel bias

Interchannel bias for each hardware channel can be of order of  $\pm 2.5$  mm r.m.s. Phase delay variations depend on the satellite signal strength. The influence can be reduced by processing observations from many satellites. Oscillator instabilities play only a minor role in carefully designed receivers if the timing signal is taken from the satellite clock or a well-behaved atomic clock. The phase center variation is minimized and reproducible for well-designed antenna. For a modern microstrip antenna the variation is a few mm (Seeber, 1993). Observation resolution depends on the signal to noise ratio from the satellite signals. Currently, the observation resolution is about 1% of the signal wavelength according to rule of thumb.

Using GPS as an example, the error budget of one-way carrier phase measurements are listed in Table 2-3.

Table 2-3 Error Budget of One-Way Carrier Phase Measurements (GPS, L1)

Error Source	Error (m)
Ionosphere	0.1
Troposphere	2.0*
Multipath	0.1
Satellite Clock	3.0*
Receiver Error	0.002
Total ( $1\sigma$ )	3.6

\* based on Table 2-1

From Table 2-3, the accuracy of a carrier phase observation is not much better than that of a range observation. Usually a carrier phase observation is used in differential way. Under this situation, the accuracy of the carrier phase observation is much higher than that of the range observation. See Chapter 7 for details. Another problem for carrier phase observations are initial ambiguities. It is difficult to solve initial ambiguities in real-time applications such as navigation.

## 2.2 Two-Way System

In a two-way system, the signal is transmitted and received by the same station. A typical two-way system is satellite laser ranging (SLR). Supposing that the signal is transmitted by the ground station at  $t_{i-1}$  and is reflected by the satellite at  $t_i = t_{i-1} + \Delta t_1$ . The same signal is returned and received at the ground station at

$t_{i+1} = t_{i-1} + \Delta t_1 + \Delta t_2$ . Then  $\Delta t_1 + \Delta t_2$  will be converted to the range observation by multiplying with velocity of light.

For two-way microwave measurement system, the received signal is reconstructed in a coherent transponder and retransmitted. The advantage of a two-way system is that only frequency fluctuations that occur in the up-link and down-link travel time are uncompensated and for time transfer it is unnecessary to know the precise positions of satellite or ground stations. The disadvantage is that the propagation errors (ionosphere and troposphere error) are increased twice.

In the following section the basic observations such as ranging, range rates (Doppler), carrier phases and laser ranging used in two-way systems are discussed.

## 2.2.1 Range

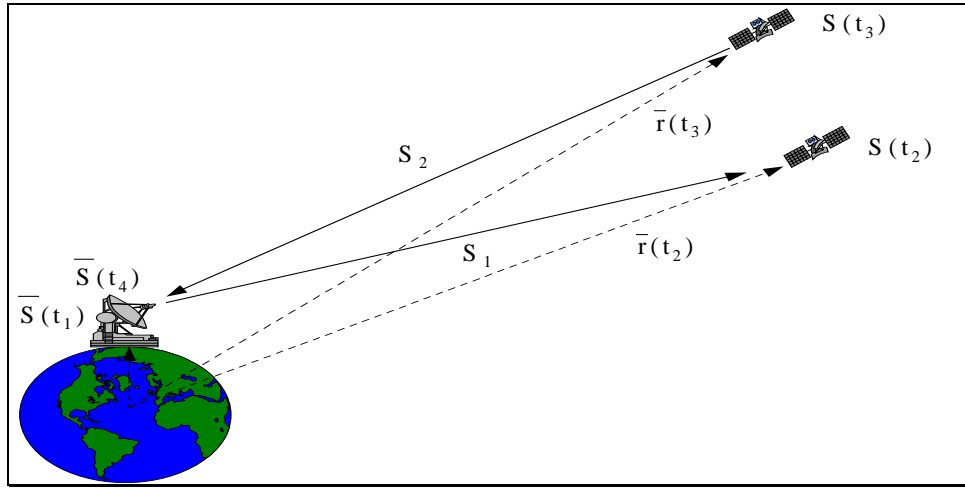


Figure 2-4 Two-Way Range Measurement

### 2.2.1.1 Basic Observation

In a two-way system, assuming the signal is transmitted from a receiver and returned to the receiver in some time later (see Figure 2-4), then two-way range observation can be expressed as

$$L = c(t_4 - t_1) = S_1 + S_2 + \varepsilon \quad (2-54)$$

where

$$S_1 = \|\bar{r}(t_2) - \bar{S}(t_1)\| = \{[\bar{r}(t_2) - \bar{S}(t_1)]^T [\bar{r}(t_2) - \bar{S}(t_1)]\}^{\frac{1}{2}} \quad (2-55)$$

$$S_2 = \|\bar{r}(t_3) - \bar{S}(t_4)\| = \{[\bar{r}(t_3) - \bar{S}(t_4)]^T [\bar{r}(t_3) - \bar{S}(t_4)]\}^{\frac{1}{2}} \quad (2-56)$$

and

$\bar{r}(t_2)$  satellite geocentric position vector at  $t_2$

$\bar{r}(t_3)$  satellite geocentric position vector at  $t_3$

$\bar{S}(t_1)$  geocentric vector of ground tracking station at  $t_1$

$\bar{S}(t_4)$  geocentric vector of ground tracking station at  $t_4$

The linear observation  $L$  is

$$L = L^0 + \delta L = S_1^0 + S_2^0 + \frac{\partial L}{\partial \bar{r}(t_2)} \delta \bar{r}(t_2) + \frac{\partial L}{\partial \bar{S}(t_1)} \delta \bar{S}(t_1) + \frac{\partial L}{\partial \bar{r}(t_3)} \delta \bar{r}(t_3) + \frac{\partial L}{\partial \bar{S}(t_4)} \delta \bar{S}(t_4) \quad (2-57)$$

where

$$\frac{\partial L}{\partial \bar{r}(t_2)} = \frac{\partial S_1}{\partial \bar{r}(t_2)} \quad (2-58)$$

$$\frac{\partial L}{\partial \bar{S}(t_1)} = \frac{\partial S_1}{\partial \bar{S}(t_1)} \quad (2-59)$$

$$\frac{\partial L}{\partial \bar{r}(t_3)} = \frac{\partial S_2}{\partial \bar{r}(t_3)} \quad (2-60)$$

$$\frac{\partial L}{\partial \bar{S}(t_4)} = \frac{\partial S_2}{\partial \bar{S}(t_4)} \quad (2-61)$$

$$\frac{\partial S_1}{\partial \bar{r}(t_2)} = \frac{[\bar{r}(t_2) - \bar{S}(t_1)]^T}{\|\bar{r}(t_2) - \bar{S}(t_1)\|} = \frac{[\bar{r}(t_2) - \bar{S}(t_1)]^T}{S_1} \quad (2-62)$$

$$\frac{\partial S_1}{\partial \bar{S}(t_1)} = -\frac{[\bar{r}(t_2) - \bar{S}(t_1)]^T}{\|\bar{r}(t_2) - \bar{S}(t_1)\|} = -\frac{[\bar{r}(t_2) - \bar{S}(t_1)]^T}{S_1} \quad (2-63)$$

$$\frac{\partial S_2}{\partial \bar{r}(t_3)} = \frac{[\bar{r}(t_3) - \bar{S}(t_4)]^T}{\|\bar{r}(t_3) - \bar{S}(t_4)\|} = \frac{[\bar{r}(t_3) - \bar{S}(t_4)]^T}{S_2} \quad (2-64)$$

$$\frac{\partial S_2}{\partial \bar{S}(t_4)} = \frac{[\bar{r}(t_3) - \bar{S}(t_4)]^T}{\|\bar{r}(t_3) - \bar{S}(t_4)\|} = \frac{[\bar{r}(t_3) - \bar{S}(t_4)]^T}{S_2} \quad (2-65)$$

$$\delta \bar{r}(t_2) = \frac{\partial \bar{r}(t_2)}{\partial \bar{r}(t_0)} \delta \bar{r}(t_0) + \frac{\partial \bar{r}(t_2)}{\partial \bar{p}(t_2)} \frac{\partial \bar{p}(t_2)}{\partial \bar{p}(t_0)} \delta \bar{p}(t_0) \quad (2-66)$$

$$\delta \bar{r}(t_3) = \frac{\partial \bar{r}(t_3)}{\partial \bar{r}(t_0)} \delta \bar{r}(t_0) + \frac{\partial \bar{r}(t_3)}{\partial \bar{p}(t_3)} \frac{\partial \bar{p}(t_3)}{\partial \bar{p}(t_0)} \delta \bar{p}(t_0) \quad (2-67)$$

### 2.2.1.2 Error Budget

In a two-way system, except multipath effects, all other propagation-related errors such as ionospheric and tropospheric errors have almost double influence on observations. Assuming these errors have the same order of magnitude on the signal. According to error propagation law, the standard error ( $1\sigma$ ) of two way range observation  $m_t$  is represented by

$$m_t = \sqrt{2m_{ion}^2 + 2m_{trop}^2 + m_{multi}^2 + 2m_s^2 + 2m_r^2 + 2m_{noise}^2} \approx \sqrt{2}m_o \quad (2-68)$$

where

- $m_{ion}$  ionospheric error
- $m_{trop}$  tropospheric error
- $m_{multi}$  multipath effect
- $m_s$  transponder related errors
- $m_r$  receiver related errors
- $m_{noise}$  random noises
- $m_o$  total error of the one-way observation

Two way range systems need only one clock. This is an advantage for two way systems. One way systems need two clocks, one for the receiver and another for the transmitter. These two clocks should be synchronized. The clock error is a major error source for one way range system.

## 2.2.2 Doppler

### 2.2.2.1 Basic Observation Equation

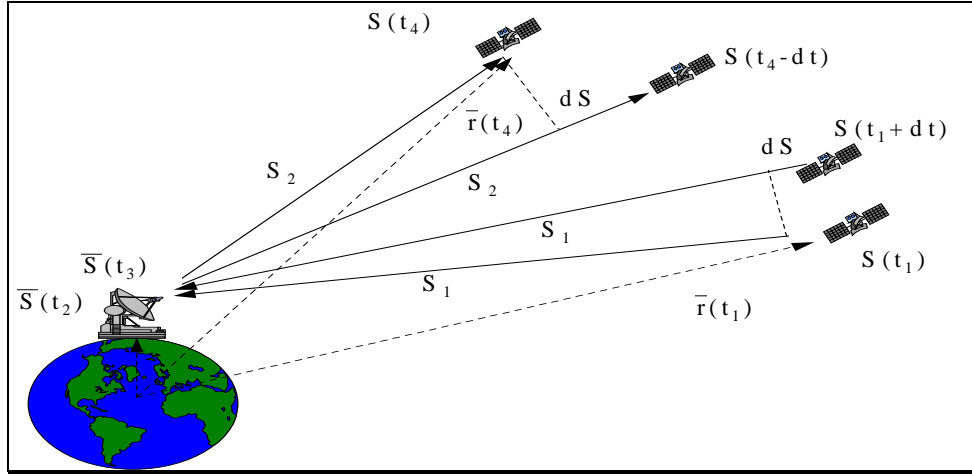


Figure 2-5 Two-Way Doppler Shift

One-way Doppler shift is expressed as

$$\frac{f_{r1}}{f_{t1}} = \left(1 - \frac{\dot{S}_1}{c}\right) \quad (2-69)$$

where

- $f_{r1}$  received frequency (downlink) at transponder
- $f_{t1} = f_t$  transmitted frequency at satellite
- $\dot{S}_1$  change rate of distance between satellite and ground station for downlink

When the transponder receives the signal and changes it to the coherent frequency  $f_{i2} = Kf_{r1}$ , then the signal is returned to the transmitter again. Doppler shift received by the satellite (the transponder) is written as

$$\frac{f_{r2}}{f_{t2}} = \left(1 - \frac{\dot{S}_2}{c}\right) \quad (2-70)$$

where

- $f_{r2} = f_r$  the received frequency (uplink) at the satellite
- $f_{t2}$  the transmitted frequency at the transponder
- $\dot{S}_2$  change rate of distance between satellite and ground station for uplink

From Figure 2-5,

$$S_1 = \|\bar{r}(t_1) - \bar{S}(t_2)\| = \{[\bar{r}(t_1) - \bar{S}(t_2)]^T [\bar{r}(t_1) - \bar{S}(t_2)]\}^{\frac{1}{2}} \quad (2-71)$$

$$S_2 = \|\bar{r}(t_4) - \bar{S}(t_3)\| = \{[\bar{r}(t_4) - \bar{S}(t_3)]^T [\bar{r}(t_4) - \bar{S}(t_3)]\}^{\frac{1}{2}} \quad (2-72)$$

$$\dot{S}_1 = \frac{dS_1}{dt} = \frac{[\bar{r}(t_1) - \bar{S}(t_2)]^T [\dot{\bar{r}}(t_1) - \dot{\bar{S}}(t_2)]}{S_1} \quad (2-73)$$

$$\dot{S}_2 = \frac{dS_2}{dt} = \frac{[\bar{r}(t_4) - \bar{S}(t_3)]^T [\dot{\bar{r}}(t_4) - \dot{\bar{S}}(t_3)]}{S_2} \quad (2-74)$$

Using Eq.(2-69), Eq.(2-70) becomes

$$f_{r2} = f_r = f_{t2} \left(1 - \frac{\dot{S}_2}{c}\right) = f_{r1} K \left(1 - \frac{\dot{S}_2}{c}\right) = f_t K \left(1 - \frac{\dot{S}_1}{c}\right) \left(1 - \frac{\dot{S}_2}{c}\right) \quad (2-75)$$

Eq.(2-75) can also be rewritten as

$$L = \Delta f = f_r - Kf_i = f_i K \left( \frac{S_1^{\&}}{c^2} - \frac{S_1^{\&}}{c} - \frac{S_2^{\&}}{c} \right) + \varepsilon \quad (2-76)$$

where

$K$  coherent frequency transpose factor, if uplink and downlink have different frequencies.

The linear observation  $L$  is given by

$$\begin{aligned} L = L_0 + \delta L = & f_i K \left( 1 - \frac{S_1^{\&}}{c} \right) \left( 1 - \frac{S_2^{\&}}{c} \right) + \frac{\partial L}{\partial \bar{r}(t_1)} \delta \bar{r}(t_1) + \frac{\partial L}{\partial \hat{r}(t_1)} \delta \hat{r}(t_1) + \frac{\partial L}{\partial \bar{S}(t_2)} \delta \bar{S}(t_2) + \\ & \frac{\partial L}{\partial \bar{r}(t_4)} \delta \bar{r}(t_4) + \frac{\partial L}{\partial \hat{r}(t_4)} \delta \hat{r}(t_4) + \frac{\partial L}{\partial \bar{S}(t_3)} \delta \bar{S}(t_3) \end{aligned} \quad (2-77)$$

From Eq.(2-76),

$$\frac{\partial L}{\partial \bar{r}(t_1)} = f_i K \left[ \frac{S_2^{\&}}{c^2} \frac{\partial S_1^{\&}}{\partial \bar{r}(t_1)} - \frac{1}{c} \frac{\partial S_1^{\&}}{\partial \bar{r}(t_1)} \right] = f_i K \left( \frac{S_2^{\&}}{c^2} - \frac{1}{c} \right) \frac{\partial S_1^{\&}}{\partial \bar{r}(t_1)} \quad (2-78)$$

$$\frac{\partial L}{\partial \hat{r}(t_1)} = f_i K \left( \frac{S_2^{\&}}{c^2} - \frac{1}{c} \right) \frac{\partial S_1^{\&}}{\partial \hat{r}(t_1)} \quad (2-79)$$

$$\frac{\partial L}{\partial \bar{S}(t_2)} = f_i K \left( \frac{S_2^{\&}}{c^2} - \frac{1}{c} \right) \frac{\partial S_1^{\&}}{\partial \bar{S}(t_2)} \quad (2-80)$$

$$\frac{\partial L}{\partial \bar{r}(t_4)} = f_i K \left[ \frac{S_1^{\&}}{c^2} \frac{\partial S_2^{\&}}{\partial \bar{r}(t_4)} - \frac{1}{c} \frac{\partial S_2^{\&}}{\partial \bar{r}(t_4)} \right] = f_i K \left( \frac{S_1^{\&}}{c^2} - \frac{1}{c} \right) \frac{\partial S_2^{\&}}{\partial \bar{r}(t_4)} \quad (2-81)$$

$$\frac{\partial L}{\partial \hat{r}(t_4)} = f_i K \left( \frac{S_1^{\&}}{c^2} - \frac{1}{c} \right) \frac{\partial S_2^{\&}}{\partial \hat{r}(t_4)} \quad (2-82)$$

$$\frac{\partial L}{\partial \bar{S}(t_3)} = f_i K \left( \frac{S_1^{\&}}{c^2} - \frac{1}{c} \right) \frac{\partial S_2^{\&}}{\partial \bar{S}(t_3)} \quad (2-83)$$

$$\frac{\partial S_1^{\&}}{\partial \bar{r}(t_1)} = \frac{[\hat{r}(t_1) - \bar{S}(t_2)]^T}{S_1} - \frac{S_1^{\&}}{S_1^2} [\bar{r}(t_1) - \bar{S}(t_2)]^T \quad (2-84)$$

$$\frac{\partial S_1^{\&}}{\partial \hat{r}(t_1)} = \frac{[\bar{r}(t_1) - \bar{S}(t_2)]^T}{S_1} \quad (2-85)$$

$$\frac{\partial S_1^{\&}}{\partial \bar{S}(t_2)} = -\frac{[\hat{r}(t_1) - \bar{S}(t_2)]^T}{S_1} + \frac{S_1^{\&}}{S_1^2} [\bar{r}(t_1) - \bar{S}(t_2)]^T \quad (2-86)$$

$$\frac{\partial S_1^{\&}}{\partial \bar{S}(t_2)} = -\frac{[\bar{r}(t_1) - \bar{S}(t_2)]^T}{S_1} \quad (2-87)$$

$$\frac{\partial S_2^{\&}}{\partial \bar{r}(t_4)} = \frac{[\hat{r}(t_4) - \bar{S}(t_3)]^T}{S_2} - \frac{S_2^{\&}}{S_2^2} [\bar{r}(t_4) - \bar{S}(t_3)]^T \quad (2-88)$$

$$\frac{\partial S_2^{\&}}{\partial \hat{r}(t_4)} = \frac{[\bar{r}(t_4) - \bar{S}(t_3)]^T}{S_2} \quad (2-89)$$

$$\frac{\partial S_2^{\&}}{\partial \bar{S}(t_3)} = -\frac{[\hat{r}(t_4) - \bar{S}(t_3)]^T}{S_2} + \frac{S_2^{\&}}{S_2^2} [\bar{r}(t_4) - \bar{S}(t_3)]^T \quad (2-90)$$

$$\frac{\partial S_2^{\&}}{\partial \bar{S}(t_3)} = -\frac{[\bar{r}(t_4) - \bar{S}(t_3)]^T}{S_2} \quad (2-91)$$

and

$$\delta \bar{r}(t_1) = \frac{\partial \bar{r}(t_1)}{\partial \bar{r}(t_0)} \delta \bar{r}(t_0) + \frac{\partial \bar{r}(t_1)}{\partial \bar{p}(t_1)} \frac{\partial \bar{p}(t_1)}{\partial \bar{p}(t_0)} \delta \bar{p}(t_0) \quad (2-92)$$

$$\delta\bar{r}(t_4) = \frac{\partial\bar{r}(t_4)}{\partial\bar{r}(t_0)} \delta\bar{r}(t_0) + \frac{\partial\bar{r}(t_4)}{\partial\bar{p}(t_0)} \frac{\partial\bar{p}(t_4)}{\partial\bar{p}(t_0)} \delta\bar{p}(t_0) \quad (2-93)$$

$$\delta\bar{r}(t_1) = \frac{\partial\bar{r}(t_1)}{\partial\bar{r}(t_0)} \delta\bar{r}(t_0) \quad (2-94)$$

$$\delta\bar{r}(t_4) = \frac{\partial\bar{r}(t_4)}{\partial\bar{r}(t_0)} \delta\bar{r}(t_0) \quad (2-95)$$

$$\delta\bar{S}(t_2) = \frac{\partial\bar{S}(t_2)}{\partial\bar{S}(t_0)} \delta\bar{S}(t_0) \quad (2-96)$$

$$\delta\bar{S}(t_3) = \frac{\partial\bar{S}(t_3)}{\partial\bar{S}(t_0)} \delta\bar{S}(t_0) \quad (2-97)$$

where

$\bar{p}$  satellite dynamical model parameters

### 2.2.2.2 Error Budget

Like two way range observations, for the two-way Doppler observation, the atmosphere errors are increased twice. Using error propagation law, the accuracy of two-way Doppler observation can be given by

$$m_d = \sqrt{2m_{ion}^2 + 2m_{trop}^2 + m_{multi}^2 + 2m_r^2 + 2m_{noise}^2} \approx \sqrt{2}m_o \quad (2-98)$$

where

$m_d$  two way Doppler error

$m_o$  one way Doppler error

## 2.3 Conclusion

In this chapter the major observations of one-way and two-way systems such as ranges, range rates (Doppler), carrier phases and laser ranges were discussed. One-way observations require two clocks, one in the receiver and another on-board the satellite. This introduces clock synchronization errors to the observations. Two-way observations do not have such a problem. Another advantage of two-way observations is that for time transfer no accurate position coordinates of satellite and ground station are needed to compute the signal propagation delays of the mainly reciprocal paths and the clock offset respectively (Hahn, 1996). Significant drawbacks of two-way observations are that atmospheric errors are introduced twice due to the signal traveling around the propagation path.

As an orbit tracking system for GNSS-2, range observations are one of the best choices for orbit determination, because a range observation is simple in mathematical form, easily processed and well modeled for the various error sources. It is very important that range observations can be used in real time. If SLR is used for orbit determination of GNSS-2 satellites, in addition to the advantages mentioned above, there is another advantage, high accuracy. The disadvantage is that SLR is strongly dependent on the weather, which can not be used in routine operation.

Carrier phase observations are highly accurate measurements, but they are complicated to process due to initial ambiguity and cycle slips, especially in real-time applications. If two L-band frequencies just like the GPS system are used, it is difficult to determine GEO satellite orbits using carrier phase observations because the initial ambiguity is not sensitive to GEO satellite.

Doppler measurement is also a good choice due to its high accuracy. It can also be used in real time applications. For GEO satellite orbit determination, the problem is that the position change of GEO satellite related to the earth is so small that the accuracy of Doppler measurement will not be good.



## CHAPTER 3 ORBIT TRACKING SYSTEMS AND THEIR ERROR BUDGETS

Traditionally, the satellite orbit is determined by ground tracking stations over a region or continent using radio tracking and receiving equipment or optical instruments like laser and camera. These are all called satellite ground tracking systems. With the development of satellite technology, more types of satellite tracking systems have appeared such as space-borne tracking and inter-satellite-link systems. At present, there are many ground-based and space-borne orbit tracking systems used for orbit determination, for instance, Satellite Laser Ranging (SLR), S-Band, International GPS Service (IGS) tracking network, Doppler Orbitography and Radio Positioning Integrated by Satellite (DORIS) and Precise Range and Range rate Equipment (PRARE), etc.. In this chapter, the current satellite tracking systems and possible applications of satellite orbit determination for future satellite-based navigation systems will be evaluated.

### 3.1 Ground Tracking Systems

The ground tracking systems used for basic orbit determination have been used for a long time. Usually ground tracking stations are distributed over some region or the globe. All one-way and/or two-way types of observations discussed in Chapter 2 can be used in the ground tracking systems.

#### 3.1.1 Satellite Laser Ranging (SLR)

SLR is a typical two-way, ground-based tracking system that has successfully been used in many geodetic and geophysical applications, for example, for the determination of the earth rotation parameters (ERP), polar parameters and crustal movements, etc.

The first SLR was a pulsed laser system, which was developed in the USA as early as 1961/1962 for tracking of artificial satellites. The satellite which carried laser reflectors was launched into an orbit of about 1000 km altitude and 80° inclination on October 9, 1964 and an accuracy of a few meters had been obtained (Vonbun 1977). Since then, the further development of SLR went on fast, the accuracy of range measurements being improved from several meters to a few millimeters.

##### 3.1.1.1 Principle

For laser ranging measurements to satellites the time of travel of a laser pulse between a ground station and a satellite is observed. A short laser pulse is generated in the ground station and is transmitted through an optical system to satellite. The target satellite carries appropriate retro-reflectors. The reflected pulse is received at the ground station, detected, amplified, analyzed, and used to stop an electronic counter.

The basic observation equation can be simply written as follows

$$L = S_1 + S_2 + \varepsilon \quad (3-1)$$

where

$\varepsilon$  atmospheric propagation error, satellite mass center error, tracking station center error, timing error, and laser system drift

### 3.1.1.2 Error Budget

SLR is a highly precise range measurement. Centimeter or even millimeter accuracy of SLR measurements can be achieved. The SLR error sources are different from pseudocode range measurement. Tropospheric error is one of the fundamental errors of SLR. Major error sources can be classified as follows

1. Atmospheric propagation error
2. Satellite mass center error
3. Tracking Station Position error
4. Timing error
5. Laser system drift (Temporal error)

#### (1) Atmospheric Propagation Error

The accuracy of a satellite laser ranging system is limited by atmospheric refraction and turbulence. According to Gardner et al, 1984, the standard error of path deviation due to atmospheric turbulence can be up to a few centimeters when the satellite is at low elevation angles (about 10°). Under most conditions, the standard error of path deviation is a few millimeters or lesser.

Atmospheric refraction increases the optical path length to a satellite by 2 ½ meter when the satellite is near zenith and by more than 13 meter when the satellite is at 10° elevation. Using Murray-Marini model, atmospheric refraction can be corrected to better than centimeter level.

#### (2) Satellite Mass Center Correction

The range correction to satellite mass center can be analytically calculated and measured in the laboratory prior to launch. This correction will be as large as 1 mm and would be a long term fixed range bias (Seeber, 1993).

#### (3) Tracking Station Position Error

The laser system that occupies a site can not be placed exactly at the reference mark position. Therefore the system reference point must be surveyed with respect to the local geodetic reference marker. The error in this measurement will constitute a fixed offset in station position. This error can be corrected.

#### (4) Timing Error

The standard epoch reference used for laser ranging is usually UTC that is maintained by a local atomic clock and periodically checked using GPS and Loran. According to observations of LAGEOS satellite, a 1 microsec epoch error will introduce an error in station position of about 4 mm.

#### (5) Thermal Effect

The thermal effect produces uncompensated system drift (change in internal delay) during ranging operations. These would be due to changes in temperature, cycling of fans and compressors, changes in line voltage, etc. The counter readings are roughly proportional to the temperature (Leschiutta et al, 1984), which can be estimated within mm level.

The SLR error budget can be summarized as follows.

Table 3-1 The Error Budget of SLR (Seeber 1993, Schillak 1998)

Error Source	Error (mm)
Atmospheric Propagation Error	1.0
Satellite Mass Center Correction	1.0
Tracking Station Position	5.0
Timing Error	0.3
Thermal Effect	5.0
Total (1 $\sigma$ )	8.2

SLR is the most accurate two-way ranging system to determine the satellite orbit, but SLR is strongly dependent on weather conditions and very expensive in building and maintaining the ground segment.

SLR is widely used for low earth satellites at an altitude of 1000 km from earth surface. According to results of GPS orbit determination using SLR, 5-8 centimeter accuracy in radial component can be achieved (Springer et al, 1999; Zhu et al, 1997), therefore for IGSO, GEO and MEO satellite orbit determination, about 10 cm accuracy level may be expected.

### 3.1.2 S-Band

S-Band systems are traditionally satellite tracking networks used by NASA and ESA for satellite orbit determination. S-Band systems are also two-way systems that determine and record the satellite range, range rate, and antenna gimbal angle positions. S-Band systems transmit continuous S-Band carrier signals with modulated pseudo random codes. These signals are demodulated on board satellite, remodulated to the down-link telemetry carrier signals with fixed ratio 221/240 of up-link to down-link frequency and retransmitted to the receiver at the ground station. The received signals at the ground station are compared to the transmitted signals in order to determine the distance between satellite and ground station (range observation). The precision of the measurement is within a few meters (Cappellari et al, 1976).

#### 3.1.2.1 Principle

For S-Band system the range measurement is made by means of an autocorrelation with a pseudo random code that is modulated onto the S-Band uplink carrier and coherently turned around by the transponder at the satellite. The local code generated at the ground station is delayed to allow comparison with the received code, which has undergone a two-way propagation delay. When the delay of the local code equals the two-way propagation delay, the autocorrelation function has a maximum value. The measured delay is converted to a double distance between the ground station and the satellite. After the signals are locked, the Doppler counter or range rate will be continuously observed. For the basic mathematical observation equations, see §2.2.1 and §2.2.2, Chapter 2.

#### 3.1.2.2 Error Budget

Table 3-2 Error Budget for S-Band\*

Error Source	Error		
	Range (m)	Doppler (mm/s)	Angles (°)
Ionosphere	5	Unknown	0.006
Troposphere	1	Unknown	0.003
Receiver Error	2	2	0.001
Total (1 $\sigma$ )	6	>2	0.007

\*Inter-Satellite-Link, Telespazio Inc, Italy, 1992

The accuracy of orbit determination of ERS1 and ERS2 satellites using S-band is shown in Figure 3-1.

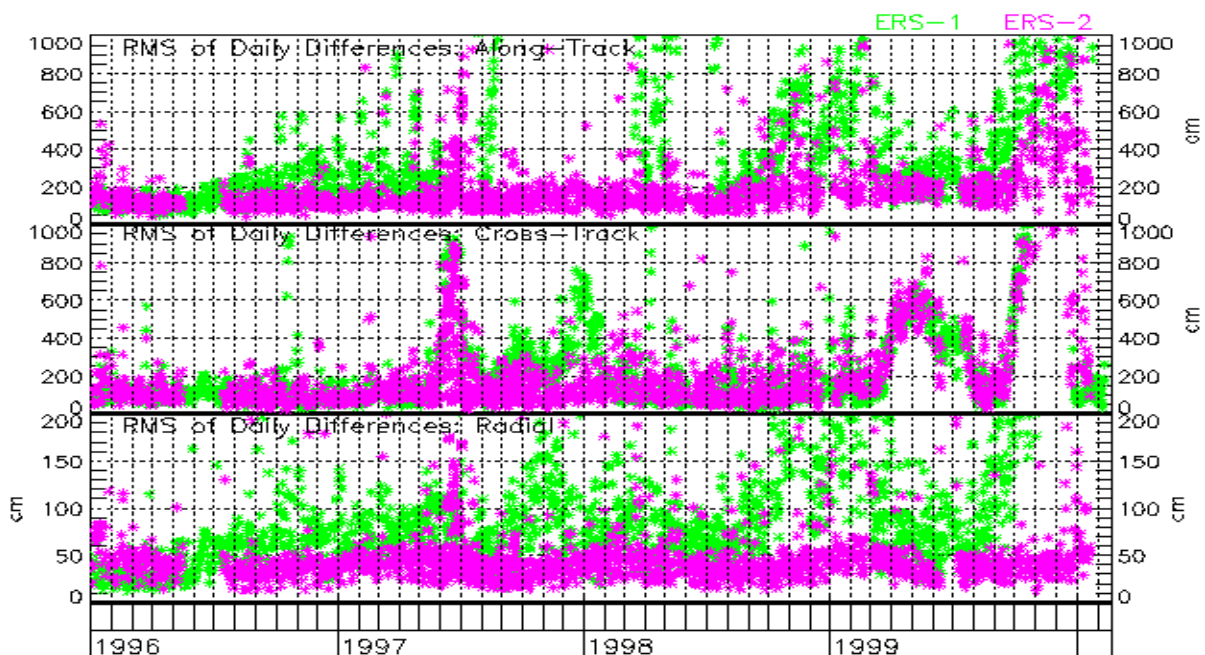


Figure 3-1 ERS Operational (S-Band) vs Precise Orbit Comparison  
(<http://nng.esoc.esa.de/ers/gifs/ocompo.gif>)

The S-Band orbit tracking systems are daily used by NASA and ESA for operational orbit determination of various types of satellites. The advantage is that there are many tracking stations currently available all over the world. If they are used for satellite orbit determination of the GNSS-2 system, the costs could be much reduced because current equipment and tracking stations could be used without significant modification. A disadvantage is the low accuracy.

### 3.1.3 IGS Tracking Station Network

IGS Tracking Station Network was officially established in January 1, 1994 by the International Association of Geodesy (IAG) (Beutler et al, 1996). The early objective of the IGS is to provide highly accurate orbits, earth rotation parameters, and station coordinates derived from GPS observations to support geodetic and geophysical research activities. Now the IGS products are not only used for geodetic and geodynamic research activities, but also support applications of atmospheric sciences, accurate time and frequency transfer.

IGS tracking stations are equipped with high accuracy, dual frequency, P-code geodetic GPS receivers operating at a thirty-second sampling rate (Noll et al, 1996). At present, the IGS tracking station network is composed of 229 stations (March, 2000) distributed over the world (see Figure 3-2), which provides capacity of continuous tracking GPS satellites. The observations from each tracking station are transmitted through phone lines, network, or satellite connections on a daily basis to regional and global data centers. GPS observations are processed by five IGS Analysis Centers to generate the precise GPS ephemerides, IGS Tracking Station and related Earth Rotation Parameter (ERP). The IGS official orbit is available about 11 days later after the observations. Its accuracy is of the order of 3-5 cm. IGS rapid combined orbits are produced within a delay of 22 hours (Beutler et al, 1996; Kouba et al, 1998).

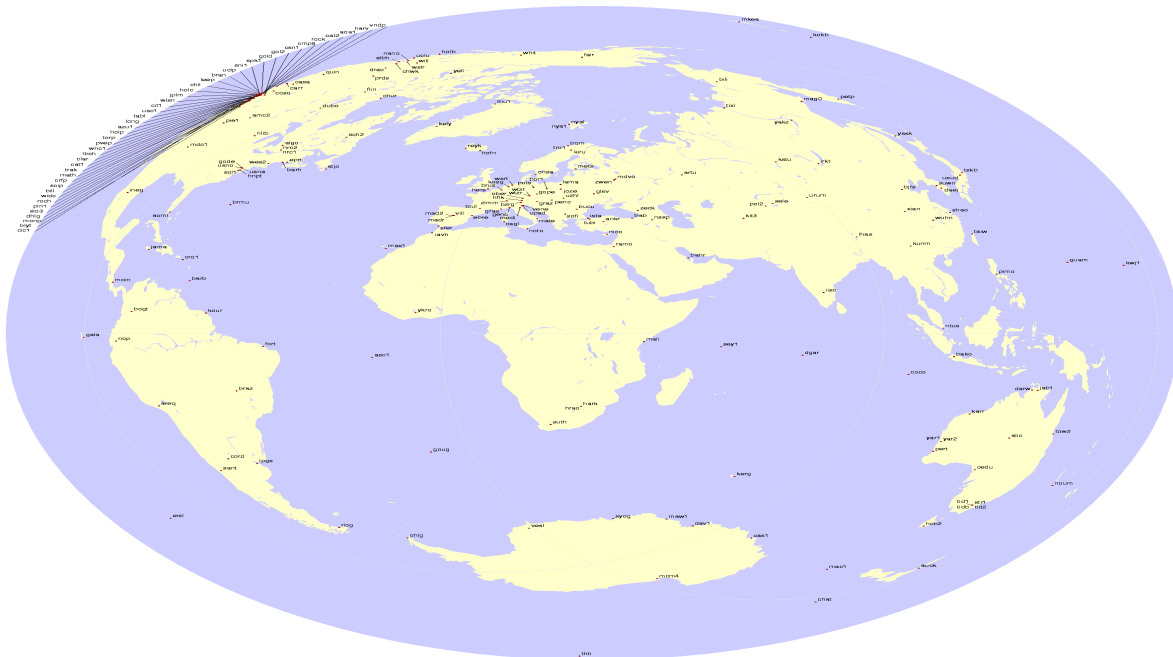


Figure 3-2 IGS Tracking Station Network in 2000 (from IGS Central Bureau <http://igsb.jpl.nasa.gov/network/map.html>)

#### 3.1.3.1 Principle

IGS is mainly composed of tracking stations, data centers and analysis centers.

IGS tracking stations are divided into three categories: global, regional, and local. Global stations are those whose data are analyzed by at least two IGS analysis centers (located on different continents) and are used for daily estimation of satellite orbits, Earth rotation parameters, and station positions and velocities. Local stations are utilized to augment the network of global and regional stations and could be episodically occupied.

IGS data centers are also divided into three levels, operational, regional and global data centers. Operational data centers are responsible for the direct interface to GPS receivers, connecting to the remote site daily and downloading and archiving the raw receiver data. Regional data centers gather data from various operational

data centers and maintain an archive for users interested in stations of a particular region. These data centers forward data from global sites to the global data centers within at most 24 hours of receipt. IGS global data centers are responsible for providing an on-line archive of at least 150 days of GPS data in RINEX. The global data centers are also required to provide an on-line archive of derived products, generated by the seven IGS analysis centers.

The seven IGS analysis centers retrieve the IGS tracking data from the global data centers on a daily basis and produce orbit products, Earth rotation parameters and station position solutions.

Observations of carrier phase and pseudorange from tracking stations are transferred to analysis centers through data centers. The observations gathered some days before are processed every day. In data processing, most of the modeled observations are undifferenced or double differenced carrier phases. The perturbation models include geopotential, Sun and Moon attraction (as point masses), solar radiation pressure and the solid earth tides and so on. GPS ephemerides, station coordinates, earth rotation parameters, etc are produced at each Analysis Center (AC). These products are then sent to the Analysis Center Coordinator who uses an orbit combination technique to produce the official IGS orbits.

### 3.1.3.2 Error Budget

Before observation processing, the GPS error budget for IGS should be the same as Table 2-1 and Table 2-3. Due to the great amount of observations, optimum global tracking network and refined mathematical processing models, the high accuracy of IGS orbit determination can be achieved.

As far as orbit determination for the GNSS-2 system is concerned, use of a IGS-like global tracking network would significantly enhance the accuracy of orbit determination of IGSO, GEO and MEO satellites. If the GNSS-2 signals are compatible with GPS, the current IGS global tracking network can also be used for precise orbit determination of the GNSS-2 system, which will greatly save time and cost.

## 3.2 Space-borne Tracking Systems

Space borne technology for orbit determination has been developing very quickly in recent years. DORIS (Doppler Orbitography and Radio Positioning Integrated by Satellite), PRARE (Precise Range and Range rate Equipment), Inter-Satellite-Links and GPS/GLONASS space borne navigation systems have been all successfully used for ERS (European Remote Sensing satellite) and TOPEX/POSEIDON (The Ocean Topography Experiment/ Poseidon, named for the Greek god of the sea.) that would use a satellite altimeter to measure the surface of the world's oceans satellite applications by JPL (Jet Propulsion Laboratory) and CNES (the French space agency). The major advantage of space-borne systems over ground-based systems is that the signal is received onboard the satellite, thus reducing costs and increasing accuracy of orbit determination.

### 3.2.1 DORIS (Doppler Orbitography and Radio Positioning Integrated by Satellite)

DORIS is a satellite tracking system which uses range-rate measurements of signals from a dense network of ground-based beacons. The data is processed on ground providing the satellite orbit with an accuracy in the order of centimeters. They are also processed on board to provide real time satellite positions with an accuracy of some tens of centimeters.

The DORIS system is developed by French Space Institutions and is based on the one-way measurement of Doppler shifts. The signal is transmitted by ground beacons and received by the DORIS onboard package when the satellite transits over the sky above the ground beacons (Seeber, 1993).

DORIS was originally designed to perform very precise orbit determination of low earth orbiting satellites, in support of POSEIDON ocean altimeter experiment, providing an orbit altitude reference for radar altimeter data processing, with an accuracy goal of 10 cm or less on the radial component of the orbit (Lefebvre, 1989; Willis 1995).

### 3.2.1.1 Principle

Doppler measurement is made at two frequencies, 2036.25 MHz and 401.25 MHz. The later frequency is used for ionospheric correction of signal propagation through the ionosphere and for measurement time-tagging and auxiliary data transmission. The measurement data onboard would be received and processed by the ground control station in the short time when satellite passes over.

The orbit determination beacons are distributed on a global network. Installation and maintenance of the network are performed by the IGN (French national geographic institute). The time reference of the system is provided by the master beacons, located in Toulouse, France and in Kourou, French Guyana, which are connected to atomic clocks.

### 3.2.1.2 Error Budget

The major error budget is summarized in Table 3-3.

Table 3-3 Error Budget for DORIS (Willis, 1997; Murielle 1997)

Error Source	Errors (mm/s)
Ionosphere	0.1
Troposphere	0.3
Multipath	0
Satellite Clock	0.3
Receiver Error	0.3
Total ( $1\sigma$ )	0.5

DORIS is a very precise orbit determination system for low orbit satellites and has been successfully used for SPOT2, TOPEX and SPOT3 satellite orbit determination missions. The selection of a one-way system (uplink) allows fully automated operation of the beacons and easy communication links for the overall system. DORIS can also determine the position of the ground beacons. Another advantage is that the one-way measurement of Doppler shift does not require a pointing antenna on board and is less sensitive to multipath effect and insensitive to transit time.

A disadvantage is that DORIS onboard receiver has only two receiving channels. The onboard receiver can only simultaneously track two ground beacons. This limits the accuracy of orbit determination for DORIS.

DORIS is not suitable for high altitude satellites such as IGSO, GEO and MEO satellites, because range-rate or Doppler shift is not accurate enough for high altitude satellite, especially for GEO satellites as the range rates remain very small.

## 3.2.2 PRARE (Precise Range and Range rate Equipment)

The PRARE System is developed and manufactured by the Institute of Navigation, Stuttgart; Kayser Threde GmbH, Munich; Dornier Satellite System GmbH, Friedrichshafen and the Geo-Forschungszentrum (GFZ), Potsdam (Flechtner et al, 1990; Seeber, 1993; Reigber et al, 1997).

PRARE is an autonomous space-borne two-way, dual frequency microwave-tracking system with its own telemetry, telecommand, data storage, timing and data transmission capability. It allows precise range and range rate at a sub-decimeter level of accuracy with the assistance of up to four transportable, dedicated ground station transponders at the same time in a code multiplexing method. It can be used for various applications in the fields of orbit determination, geodesy, geophysics and atmospheric sciences (Reigber et al, 1997).

### 3.2.2.1 Principle

The PRARE system consists of three components (Reigber et al, 1997):

(1) the space segment, a small self-contained hardware unit of dimensions 400x250x180 mm with a mass of 20 kg, a power consumption of 32 W and host satellite independent communication links,

(2) the ground segment, a network of 29 small autonomously transportable operating ground tracking stations, which can be installed at any site that is connected to a power line, for generation of tracking data,

(3) the control segment consisting of a command station (Stuttgart), which is responsible for space segment control and data dumping; a master station (Oberpfaffenhofen) which is responsible for station network management, user support, and data preprocessing, quality control and distribution; and a calibration station (Potsdam), where a third generation laser system is operated to produce simultaneous laser ranging observations for periodic system calibration.

Two PRARE signals (X and S-Bands) are emitted from space segment to earth. Both signals are modulated with PN-codes (10 MChips/s for X band and 1 Mchips/s for S-Band) and spread-spectrum binary data. They are all generated inside the space segment derived from its central ultra-stable oscillator and permanently disseminated by two dipole antennas.

As PRARE has four independent receiver channels, up to four preselected stations can be handled simultaneously. The transportable and automatically operating ground stations receive the X-band downlink signal and demodulate the PN-code. Then the PN-sequence is remodulated on the X-band that is retransmitted to the space segment (regenerative transponders) containing ground station measurement data used for the preprocessing of the data. The PRARE space segment measures both two-way range and the received two-way Doppler-shifted signals very precisely by comparing the phase of the received signal to the phase of the on-board clock. The overall accuracy stems mainly from this two-way configuration of the system that eliminates the most clock errors of one-way systems.

Ranging data is acquired by determination of the signal delay between outgoing and incoming signal (PN-code correlation method, 91 averaged measurements per second), range-rate by counting of the microwave cycles and the phase shift of the return signal (1 measurement per second). The high data precision is based on the full coherent two-way principle of the system, the high signal frequencies, and the appropriate resolution of the space segment receiver counters.

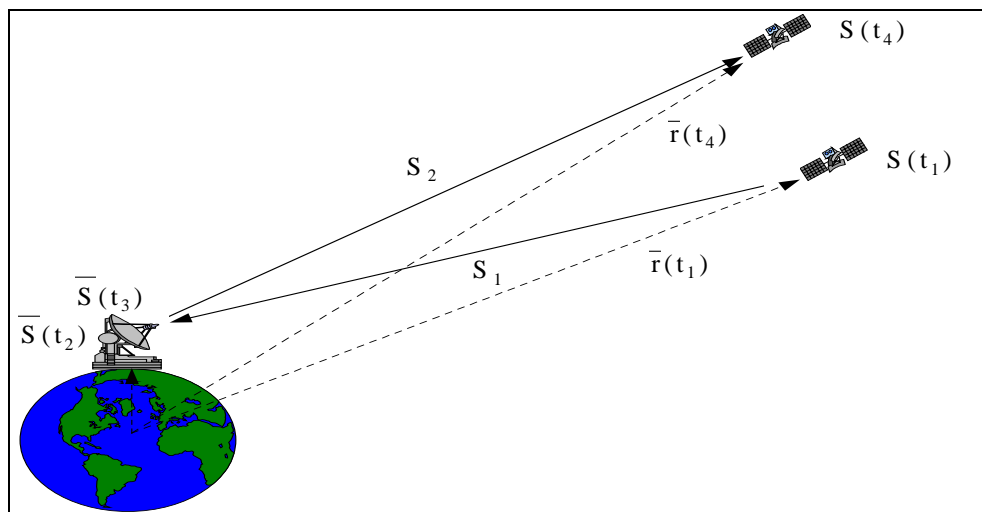


Figure 3-3 PRARE Two-Way Range Measurement

The basic observation can be written as follows

(1) Two-way range observation:

Assuming the signal is transmitted from the satellite. From Figure 3-3, two-way range observation is

$$L = cF(t_4 - t_1) = S_1 + S_2 + \varepsilon \quad (3-2)$$

where

$c$  speed of light in vacuum.

$F$  conversion factor from seconds of PRARE time to UTC units

$$\varepsilon = c(\Delta\tau_{91} + \Delta\tau_{sa} - \Delta\tau_{xx} + \Delta\tau_{ga} + \Delta\tau_{mc} + \Delta\tau_{pc} - \Delta\tau_{tr} - \Delta\tau_{io} + \Delta\tau_{ex} + \Delta\tau_{temp} + \Delta\tau_{agc} + \Delta\tau_{dop})$$

- $\Delta\tau_{91}$  91-value range correction  
 $\Delta\tau_{sa}$  satellite internal calibration correction  
 $\Delta\tau_{xx}$  ground station internal calibration correction  
 $\Delta\tau_{ga}$  ground station mechanical center correction  
 $\Delta\tau_{mc}$  satellite center of mass correction  
 $\Delta\tau_{pc}$  satellite phase center correction  
 $\Delta\tau_{tr}$  tropospheric correction  
 $\Delta\tau_{io}$  ionospheric correction  
 $\Delta\tau_{ex}$  external calibration correction  
 $\Delta\tau_{temp}$  correction due to mean temperature of space segment  
 $\Delta\tau_{agc}$  correction due to AGC (Automatic Gain Control)  
 $\Delta\tau_{dop}$  correction due to Doppler dependency

From Figure 3-3,

$$S_1 = \|\bar{r}(t_1) - \bar{S}(t_2)\| = \{[\bar{r}(t_1) - \bar{S}(t_2)]^T [\bar{r}(t_1) - \bar{S}(t_2)]\}^{\frac{1}{2}} \quad (3-3)$$

$$S_2 = \|\bar{r}(t_4) - \bar{S}(t_3)\| = \{[\bar{r}(t_4) - \bar{S}(t_3)]^T [\bar{r}(t_4) - \bar{S}(t_3)]\}^{\frac{1}{2}} \quad (3-4)$$

Using Taylor expression of  $\bar{r}, \bar{S}$  backwards in time, following relation holds

$$i) \bar{r}(t_1) \cong \bar{r}(t_4) - \dot{\bar{r}}(t_4)\Delta t_{14} + \frac{1}{2}\ddot{\bar{r}}(t_4)\Delta t_{14}^2 \quad (3-5)$$

$$ii) \bar{S}(t_2) \cong \bar{S}(t_3) - \dot{\bar{S}}(t_3)\Delta t_{23} + \frac{1}{2}\ddot{\bar{S}}(t_3)\Delta t_{23}^2 \quad (3-6)$$

where

$$\Delta t_{14} = t_4 - t_1 \cong \frac{S_1 + S_2}{c}, \quad \Delta t_{23} = t_3 - t_2 \quad \text{and} \quad \Delta t_{14} > \Delta t_{23} \quad (3-7)$$

Using Taylor expansion,

$$S_1 = S_2 + \frac{[\bar{r}(t_4) - \bar{S}(t_3)]^T}{S_2} \bar{\Delta} \quad (3-8)$$

two-way range measurements can be obtained:

$$\begin{aligned}
 L &= c(t_1 - t_4) = S_1 + S_2 = 2S_2 - \frac{[\bar{r}(t_4) - \bar{S}(t_3)]^T}{S_2} \dot{\bar{r}}(t_4)\Delta t_{14} \\
 &= 2\|\bar{r}(t_4) - \bar{S}(t_3)\| - \frac{[\bar{r}(t_4) - \bar{S}(t_3)]^T}{S_2} \dot{\bar{r}}(t_4)\Delta t_{14}
 \end{aligned} \quad (3-9)$$

letting

$$\frac{\Delta t_{14}}{S_2} \cong \frac{S_1 + S_2}{cS_2} \cong \frac{2S_2}{cS_2} = \frac{2}{c} \quad (3-10)$$

The linear observation equation can be expressed as

$$\delta L = \frac{\partial L}{\partial \bar{r}(t_4)} \delta \bar{r}(t_4) + \frac{\partial L}{\partial \dot{\bar{r}}(t_4)} \delta \dot{\bar{r}}(t_4) \quad (3-11)$$

where

$$\frac{\partial L}{\partial \bar{r}(t_4)} = 2 \frac{\partial \|\bar{r}(t_4) - \bar{S}(t_3)\|}{\partial \bar{r}(t_4)} - 2 \frac{\dot{\bar{r}}(t_4)}{c} \frac{\partial [\bar{r}(t_4) - \bar{S}(t_3)]}{\partial \bar{r}(t_4)} \quad (3-12)$$

$$\frac{\partial \|\bar{r}(t_4) - \bar{S}(t_3)\|}{\partial \bar{r}(t_4)} = \frac{[\bar{r}(t_4) - \bar{S}(t_3)]^T}{S_2} \quad (3-13)$$



$$\frac{\partial[\bar{r}(t_4) - \bar{S}(t_3)]}{\partial \bar{r}(t_4)} = \bar{I} \quad (3-14)$$

$$\frac{\partial L}{\partial \dot{\bar{r}}(t_4)} = 2 \frac{\partial \|\bar{r}(t_4) - \bar{S}(t_3)\|}{\partial \dot{\bar{r}}(t_4)} - 2 \frac{[\bar{r}(t_4) - \bar{S}(t_3)]^T}{c} \frac{\partial \dot{\bar{r}}(t_4)}{\partial \dot{\bar{r}}(t_4)} \quad (3-15)$$

$$\frac{\partial \|\bar{r}(t_4) - \bar{S}(t_3)\|}{\partial \dot{\bar{r}}(t_4)} = 0^T \quad (3-16)$$

$$\frac{\partial \dot{\bar{r}}(t_4)}{\partial \dot{\bar{r}}(t_4)} = \bar{I} \quad (3-17)$$

$\bar{I}$  identity matrix

and

$$\frac{\partial L}{\partial \bar{r}(t_4)} = 2 \frac{[\bar{r}(t_4) - \bar{S}(t_3)]^T}{S_2} - 2 \frac{\dot{\bar{r}}(t_4)}{c} \quad (3-18)$$

$$\frac{\partial L}{\partial \dot{\bar{r}}(t_4)} = -2 \frac{[\bar{r}(t_4) - \bar{S}(t_3)]^T}{c} \quad (3-19)$$

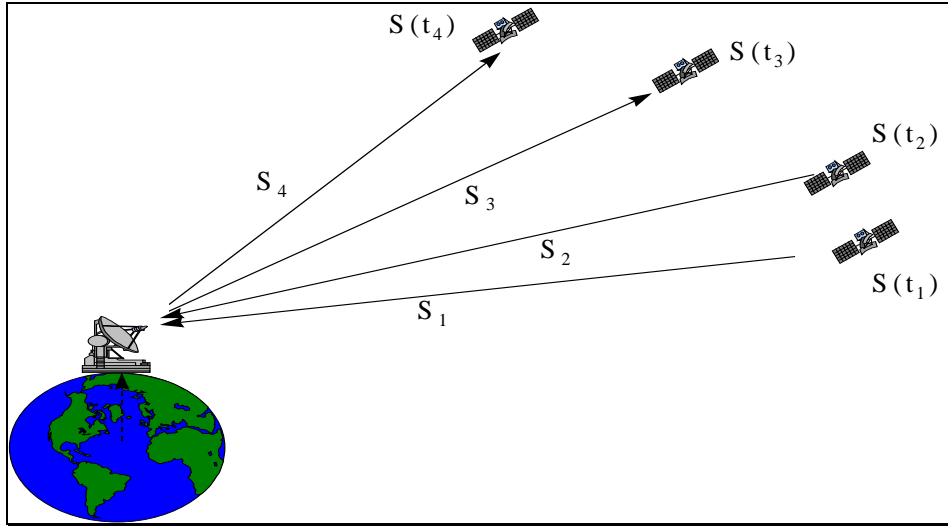


Figure 3-4 PRARE Two-Way Range Rate (Doppler Shift) Measurement

(2) PRARE two-way range rate (Doppler shift) observation equation is

$$L = N = \frac{kf_{id}}{c} [(S_2 - S_1) + (S_4 - S_3)] - \frac{kf_{id}}{c} [(\Delta S_2 - \Delta S_1) + (\Delta S_4 - \Delta S_3)] \quad (3-20)$$

The first term of above equation represents the number of cycles due to the geometrical Doppler shift, and the last one represents the corrections.

Full PRARE Doppler correction in cycles can be written as:

$$\Delta N = \Delta N_{sa} + \Delta N_{xx} + \Delta N_{ga} + \Delta N_{mc} + \Delta N_{pc} + \Delta N_{tr} + \Delta N_{io} + \Delta N_{ex} \quad (3-21)$$

where

$\Delta N_{sa}$  satellite internal calibration correction

$\Delta N_{xx}$  ground station internal calibration correction

$\Delta N_{ga}$  ground station mechanical correction

$\Delta N_{mc}$  satellite center of mass correction

$\Delta N_{pc}$  satellite phase center correction  
 $\Delta N_{tr}$  tropospheric correction  
 $\Delta N_{io}$  ionospheric correction  
 $\Delta N_{ex}$  external calibration correction.

The full correction  $\Delta N$  is added to the observed number of cycles  $N$ . The delivered measured two-way Doppler cycles are already corrected for the  $\Delta N_{xx}$  and  $\Delta N_{sa}$  by the PRARE Master Station. The values of these two corrections are not known from the data files. For orbit determination purposes the only corrections to be considered are  $\Delta N_{ga}$ ,  $\Delta N_{pc}$ ,  $\Delta N_{mc}$ ,  $\Delta N_{tr}$ ,  $\Delta N_{io}$  and  $\Delta N_{ex}$ .

### 3.2.2.2 Error Budget

The error budget of PRARE for range measurement is listed in Table 3-4. Actual accuracy of orbit determination of ERS satellite using PRARE is drawn in Figure 3-5 and Figure 3-6.

Table 3-4 Error Budget for PRARE (Reigber et al, 1989, 1997; Flechtner, 2000)

ERROR SOURCE	ERROR (cm)
Ionosphere	1.0
Troposphere	2.0-5.0
Calibration	1.5-2.0
Phase and Mass Center	1.0
Total ( $1\sigma$ )	6.5

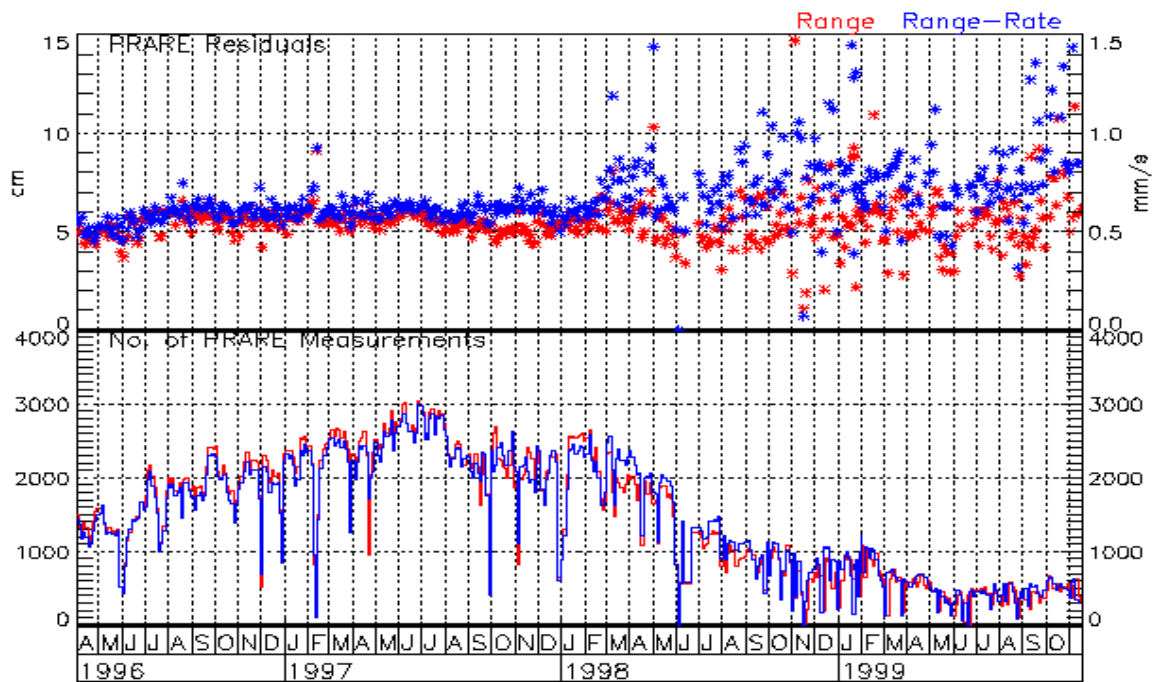


Figure 3-5 PRARE Measurement residual (From ESOC Homepage: <http://nng.esoc.esa.de/ers/prare/resip.html>)

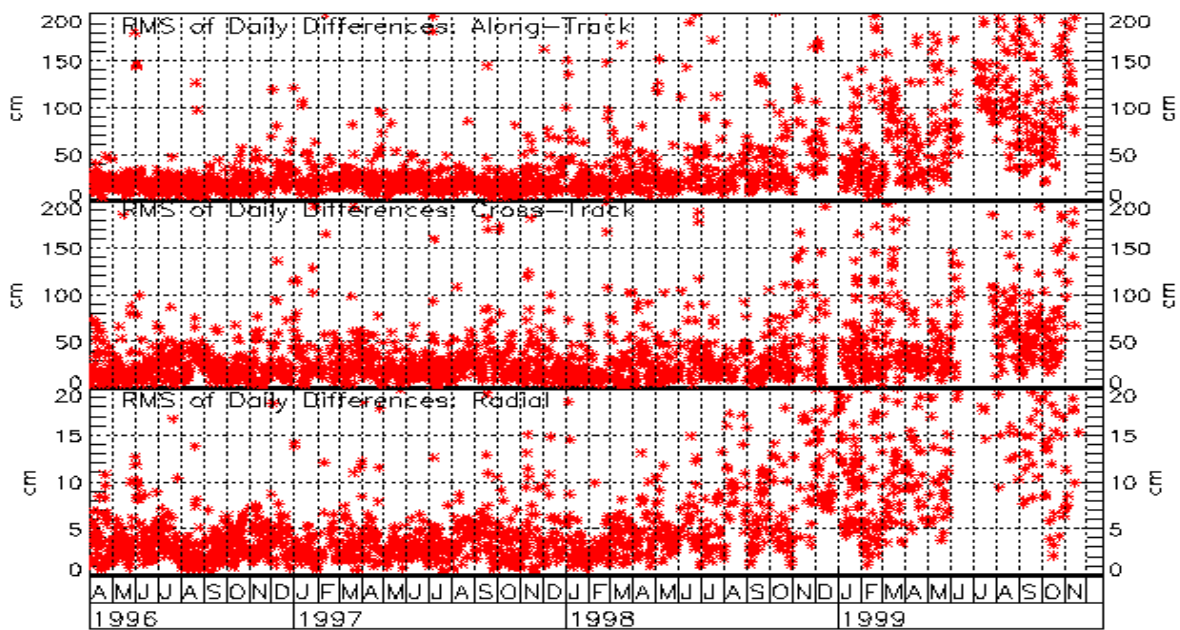


Figure 3-6 ERS PRARE vs Precise Orbit Comparison (From ESOC Homepage:  
<http://nng.esoc.esa.de/ers/prare/ocompo.html>)

PRARE is an autonomous, space-borne, all-weather, dual frequency, two-way microwave system with ranging and ranging rate measurements for application of high-precision orbit determination. The ground station network is operated continuously and is fully automatic. The time errors are significantly reduced using two way measurements. The most part of the ionospheric error can be eliminated using dual frequency measurements. In addition, PRARE can also determine the position of the ground stations.

A disadvantage is, that the use of two-way measurements can also increase the propagation errors. The principle error sources limiting accuracy of PRARE system is the error produced by the atmospheric refraction effects and internal delays.

In principle, PRARE can be used for orbit determination of GNSS-2 satellites, but has some problems like DORIS, i.e. low accuracy of Doppler measurements for GEO and IGSO satellites.

### 3.2.3 Inter-Satellite-Links (ISL)

#### 3.2.3.1 Principle

Inter-Satellite-Links require at least two satellites. One satellite is called orbiting platform, for which the orbit should be determined using other tracking systems, usually ground-based tracking systems. Another is user satellite the orbit of which will be determined by orbiting platform satellite. One- and/or two-way observations among satellites have been used so far to measure their relative position and velocity. At present, two models of ISL exist, a low-low model and a high-low model. The low-low model is used for satellites flying at low altitude, i.e. a few hundred of kilometers apart. The main satellite (the orbiting platform) tracks two or more user satellites. The high-low model describes the situation, where a high orbiting satellite carries an intersatellite measurement device that tracks a low orbiting satellite. The coverage for the high-low model is substantially smaller than that for the low-low model, only about 1/5 of the coverage of a low-low configuration (Mueller et al, 1988, Blaha 1991, Feltman 1999).

The first application of high-low intersatellite links between two satellites in orbit around the Earth started in April 1975 with a tracking experiment between the geostationary ATS-6 satellite and GEOS-3 at an altitude of 840 kilometer (Schmid et al., 1975). The ISL data has been used for the orbit computation of the low altitude satellites. During this experiment both one-way and two-way range and range-rate data were obtained over the

link ground station/ATS-6/GEOS-3. The specially processed range-rate measurements had a precision of about 0.3 mm/s. Now ISL has been used for many scientific research projects, for examples, GRACE (Gravity Recovery and Climate Experiment) and CHAMP (Challenging Mini-Satellite Payload).

The major observation of ISL is the one-way range, range rate and two-way range and range rate.

### 3.2.3.2 Error Budget

According to the discussions in the sections before, ISL error budget could be estimated as follows.

Table 3-5 Error Budget for Possible ISL\*

Error Source	Error	
	Range (cm)	Range Rate (mm/s)
Ionosphere	0.0	0.0
Troposphere	0.0	0.0
Multipath	0.3	0.0
Satellite Clock	<9.0	0.3
Receiver Error	3.0-9.0	0.3-9.0
Total (1 $\sigma$ )	>9.5	>0.5

\*Assuming satellites orbiting in more than 1000 km altitude

If ISL is used for GNSS-2 system, the advantage would be that atmospheric errors (ionosphere and troposphere) do not exist because IGSO, GEO and MEO satellites are far above the ionosphere and troposphere. The accuracy of the range rates (Doppler) will be very accurate and thus high accuracy of relative orbit determination can be achieved. Using ISL the onboard autonomous orbit determination is possible. The disadvantage is that frequency band of onboard receiver should be broader than that of the receiver on the ground, therefore the receiver errors are also significantly increased in ISL application. Another disadvantage is that the major satellite (orbiting platform) should be determined by the ground based tracking systems, therefore the absolute accuracy is still affected by atmosphere errors.

### 3.2.3 Navigation System (GPS/GLONASS)

GPS and GLONASS are satellite-based navigation systems that can be used in high precise positioning, navigation and time transfer applications. It can also be used for precise orbit determination of other earth orbit satellites, because on-board GPS/GLONASS receiver can track a number of GPS/GLONASS satellites.

The GPS system consists of 28 satellite (March 2000) with 20200 km altitude above the earth's surface and at least 4 satellites will be available anywhere on the earth, 24 hour a day. GPS satellite transmits signals at two frequencies L1=1575.42 MHz and L2=1227.6 MHz with C/A-code and P-code and navigation messages.

GLONASS was developed by former Soviet Union and now consists of 22 satellites (March 2000). Its function is like GPS, which can also provide all-weather, continuous, real time and precise navigation capacity. The satellites transmit signals at two frequencies L1=1602 -1615 MHz and L2=1246 - 1256 MHz.

The characteristics of two types of systems are listed in Table 3-6

Table 3-6 Characteristics of GPS and GLONASS (Seeber 1993, Leick 1995, Teunissen et al, 1998)

Feature	GPS	GLONASS
Orbit height	20200 km	19100 km
Period	12 h	11 h 15 m
Frequencies	1575.42 MHz 1227.60 MHz	1602-1615 MHz 1246-1256 MHz
Navigation Data	4D: x,y,z, t Velocity	4D: x,y,z, t Velocity
Availability	Continuous	Continuous
Coordinate system	WGS 84	PZ 90
Satellite signal division	Code division	Frequency division
Code type	PRN sequence	Gold code
Accuracy	15 m (P-code without SA)	10 m (P-code)

### 3.2.3.1 Principle

A GPS/GLONASS receiver can be installed on-board a satellite for orbit determination using pseudorange, Doppler (range and range rate) and carrier phase to GPS/GLONASS satellites.

The basic observation equations are just like one-way range, range rate and carrier phase ( see §2.1.1, §2.1.2 and §2.1.3 in Chapter 2).

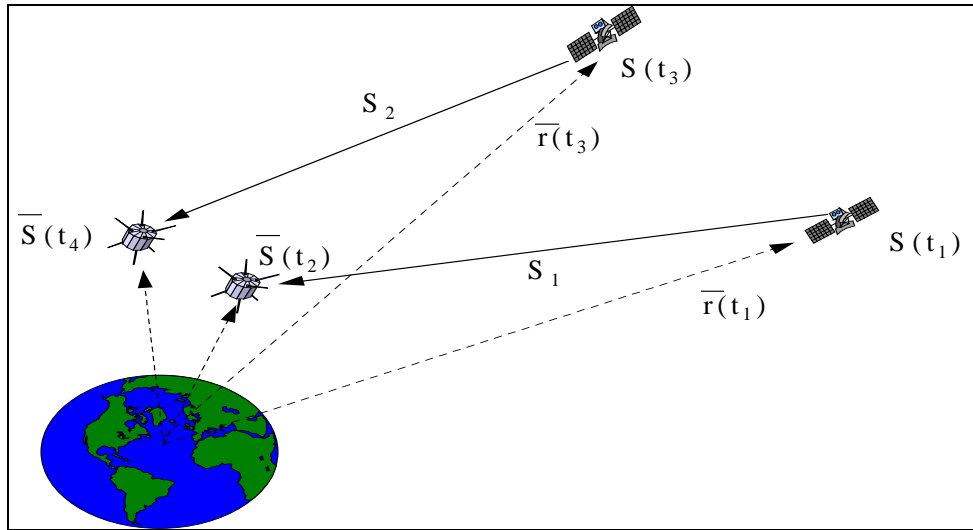


Figure 3-7 GPS Navigation System

### 3.2.3.2 Error Budget

The error budget of space-borne GPS orbit determination is the same as ground-based GPS navigation application except the atmosphere effects.

Table 3-7 Error Budget of Space-borne GPS One-Way Ranging

Error Source	Random (m)
Ionosphere	0.0
Troposphere	0.0
Multipath	1.2
Satellite Clock	3.0
Receiver Error	1-10
Total ( $1\sigma$ )	>4

One of the significant advantage of space-borne GPS/GLONASS navigation systems for orbit determination is that the ground tracking networks are not necessary. The atmosphere errors do not affect space-borne GPS/GLONASS orbit determination, but the receiver noise is significantly increased, which is related to the bandwidth of the receiver frequency, and becomes the major error source of orbit determination, as for space-borne GPS/GLOANSS application usually high kinematic models of receivers with broad frequency bandwidth are required to lock the signal from GPS/GLONASS satellites.

The use of space-borne GPS navigation systems for orbit determination of low and medium orbiting satellites will be a standard method in near future. It can provide small size, low cost hardware, global coverage and high performance of tracking and operation. These satellites normally fly below the GPS satellites. For GNSS-2 systems like Galileo, the orbital altitude of IGSO and GEO satellites are of course above the GPS satellite constellations. Since the antenna of the GPS satellites are toward to earth in order to assure global coverage, it is generally not possible to receive GPS signals for IGSO and GEO satellites. Only when GPS satellites approach the vanishing point behind the earth, the GPS signal will be accessed by space borne GPS receivers. This problem will be solved as GPS IIF satellites are launched into orbit.

### 3.3 Conclusion

There are still many other systems which can be used for GNSS-2 satellite orbit determination, for examples, DGPS or TOPEX/POSEIDON systems etc, but these systems are all dependent on GPS and are not discussed further here.

In this chapter, the major current tracking systems of orbit determination were briefly discussed and evaluated. From this discussion it can be seen that the range, range rate and carrier phase are the major types of observations for the orbit determination systems. The ground based tracking systems are still widely used for tracking satellites, for example, IGS global tracking network. For GNSS-2 satellite navigation system using IGSO, GEO and MEO satellites, some special factors should be considered. IGSO and GEO satellites are high altitude satellites about 42000 km from the earth surface, which will lead to following results, (1) radial change between satellite and ground tracking stations or ground beacons is slow, and thus, the Doppler shift which is based on radial changes is not significantly sensitive to IGSO and GEO satellites, and (2) there will be worse influence of geometrical distribution of the tracking station network on the accuracy of IGSO and GEO satellite orbit determination than on any other satellites. From (1), Doppler shift-based systems such as S-Band, DORIS and the Doppler measurement part of PRARE cannot achieve high accuracy of orbit determination for IGSO and GEO satellites. The remaining observations available are range and carrier phase. From (2), it is best that wide spaced ground tracking stations could be used for IGSO, GEO and MEO satellite orbit determination. According to §3.2.3 it can be seen that the current space-borne GPS/GLONASS navigation systems may not be suitable for IGSO and GEO satellite orbit determination, because the GPS/GLONASS signals are transmitting towards earth surface in order to assure global coverage. It is generally not possible for the onboard receiver to receive GPS/GLONASS signals at a geostationary and geosynchronous orbits, and even though the signal may be received at some special conditions, there is still a small chance of more than 4 satellites available for a fixed point at geostationary orbit over one day. Therefore the use of space-borne GPS/GLONASS navigation systems alone for orbit determination of IGSO and GEO satellites is still very difficult, but onboard orbit determination of GNSS-2 satellites could be possible due to successful launching of German space mission Equator-S and new type of GPS satellites (IIF) (Balbach et al, 1998). The Equator-S satellite used ground tracking stations and onboard GPS receiver to determine the Equator-S orbit. Using inter-satellite-links (see §3.2.3) would be also very promising.

According to the discussion above, a ground-based tracking system with range (including laser ranging) and carrier phase observations for IGSO, GEO and MEO satellite orbit determination may be a best choice for GNSS-2 systems.

## CHAPTER 4 MAJOR ERROR SOURCES OF SATELLITE OBSERVATIONS

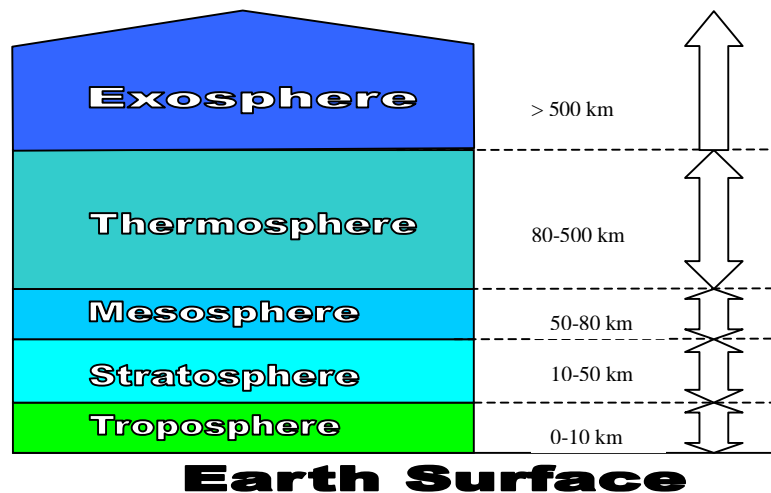
The accuracy of observations, further the accuracy of orbit determination will be affected by many error sources. The major error sources of the observations are tropospheric and ionospheric errors, multipath effects, satellite and receiver clock errors, etc. In this chapter the influences of these error sources on the accuracy of orbit determination using the ground tracking network will be discussed.

### 4.1 Atmospheric Errors

The atmosphere is a mixture of gases that surround the Earth. The atmosphere is held to the surface of the Earth by gravity. The atmosphere has no definite outer boundary. As it extends outward from Earth, it becomes thinner and blends with particles of interplanetary space.

The atmosphere is composed of 5 regions based on temperature trends. In the order of increasing height these are the troposphere, the stratosphere, the mesosphere, the thermosphere and exosphere. In the troposphere, as altitude increases, air temperature decreases. The temperature stops dropping at the tropopause, which is the boundary between the troposphere and the stratosphere.

In the upper stratosphere is the ozone layer ( $O_3$  molecules), which absorbs harmful ultraviolet radiation from the sun. The absorption of the solar energy explains the increase in temperature in this region.



Part of the upper atmosphere is composed of charged particles (ions and electrons). This region is known as the ionosphere. Ionosphere can be further divided into the different ionospheric layers or regions (D, E, and F) which are capable of reflecting high frequency radio waves. Notice that the electron concentration of the ionosphere is much greater during the day than at night, and in fact the D region disappears at night. This is because the ionospheric layers are produced by the action of solar extreme ultraviolet radiation, which is not present at night. An overview over structure of the atmosphere is given in Table 4-1 (Wild, 1994)

Table 4-1 Nomenclature of the Atmosphere

Name	Height above Surface (km)	Electron Density ( $cm^{-3}$ )	
		Night	Day
Troposphere	0-10	---	---
Stratosphere	10-50	---	---
Mesosphere	50-80	$10^3$	$10^3$
Thermosphere	80-500	$10^5$	$10^6$
Exosphere	>500	$10^4$	$10^5$

The effects of the atmosphere on radio signal propagation are mainly from two parts of the atmosphere, one is called troposphere and another is ionosphere.

### 4.1.1 Tropospheric Error

The troposphere is composed of dry gases and water vapor. Water vapor exists only below altitude of 12 km above sea level. Water vapor density varies widely with position and time and is much more difficult to predict than dry gases. Fortunately, however, water vapor effects represent only a relatively small fraction ( $\approx 1/10$ ) of total tropospheric error (Spiker, 1996). Dry gases are relatively uniform in its constituents. For L-band frequencies, oxygen, which is part of dry gases, is the dominant source of attenuation. Tropospheric errors cause the radio signal delay.

The signal from the satellite is refracted by the troposphere as it travels to the users on or near the Earth's surface. Tropospheric refraction causes a delay that depends upon the actual path of the ray and the refractive index of the gases along that path. For troposphere symmetric in azimuth about the user antenna, the delay depends only upon the vertical profile of the troposphere and elevation angle to the satellite.

There are several empirical models for computation of signal delay due to the tropospheric effects. Among them, Saastamoinen total delay model, Hopfield two quartic models and Black and Eisner model are more popularly used (Hofmann-Wellenhof et al 1992, Leick 1995, Spiker, 1996).

#### 1) Saastamoinen model (Spiker, 1996)

Tropospheric error which produces a signal delay and thus causes an increase in the observed range can be calculated by using Saastamoinen standard model as follows

$$\Delta S_{trop} = 0.002277(1 + D) \sec \psi_0 [P_0 + (\frac{1255}{T_0} + 0.005)e_0 - B \tan^2 \psi_0] + \delta_R m \quad (4-1)$$

where  $\Delta S_{trop}$  is the delay correction in meters;  $P_0, e_0$  are the atmospheric pressure and the partial pressure of water vapor at sea level in millibars;  $T_0$  is the absolute temperature at sea level in °Kelvin; The correction term  $B$  and  $\delta_R$  are given in Table 4-2 (Spilker, 1996) for various tracking station heights  $h$ . The apparent zenith angle  $\psi_0 = 90^\circ - E$  in which  $E$  is the elevation of satellite related to the tracking station; the value  $D$  is  $D = 0.0026 \cos 2\varphi + 0.00028h$ , where  $\varphi$  is the local latitude, and  $h$  is the tracking station height in km.

Table 4-2 Correction Terms for Saastamoinen Standard Model

Apparent Zenith Angle		Tracking Station Height Above Sea Level							
		0 km	0.5 km	1 km	1.5 km	2 km	3 km	4 km	5 km
$\delta_R$ m	60°00'	0.003	0.003	0.002	0.002	0.002	0.002	0.001	0.001
	66°00'	0.006	0.006	0.005	0.005	0.004	0.003	0.003	0.002
	70°00'	0.012	0.011	0.010	0.009	0.008	0.006	0.005	0.004
	73°00'	0.020	0.018	0.017	0.015	0.013	0.011	0.009	0.007
	75°00'	0.031	0.028	0.025	0.023	0.021	0.017	0.014	0.011
	76°00'	0.039	0.035	0.032	0.029	0.026	0.021	0.017	0.014
	77°00'	0.050	0.045	0.041	0.037	0.033	0.027	0.022	0.018
	78°00'	0.065	0.059	0.054	0.049	0.044	0.036	0.030	0.024
	78°30'	0.075	0.068	0.062	0.056	0.051	0.042	0.034	0.028
	79°00'	0.087	0.079	0.072	0.065	0.059	0.049	0.040	0.033
	79°30'	0.102	0.093	0.085	0.077	0.070	0.058	0.047	0.039
	79°45'	0.111	0.101	0.092	0.083	0.076	0.063	0.052	0.043
	80°00'	0.121	0.110	0.100	0.091	0.083	0.068	0.056	0.047
$B_{mb}$		1.156	1.079	1.006	0.938	0.874	0.757	0.654	0.563

#### 2) Hopfield Model (Hofmann-Wellenhof et al 1992)

Hopfield's empirical representation of the dry refractivity as a function of the height  $h$  above the surface can be written as

$$N_d(h) = N_{d,0} \left[ \frac{h_d - h}{h_d} \right]^4 \quad \text{for } h \leq h_d = 43 \text{ km} \quad (4-2)$$



The tropospheric path delay is given by

$$\Delta S_d = 10^{-6} N_{d,0} \int \left[ \frac{h_d - h}{h_d} \right]^4 dh \quad (4-3)$$

For observation site on the earth surface, Eq.(4-3) can be written as

$$\Delta S_d = \frac{10^{-6}}{5} N_{d,0} h_d \quad (4-4)$$

The wet part is much more difficult to be modeled. Hopfield used the same assumption as dry part. Therefore wet part delay can be expressed as

$$\Delta S_w = \frac{10^{-6}}{5} N_{w,0} h_w \quad h_w = 12 \text{ km} \quad (4-5)$$

where  $N_{d,0}$ ,  $N_{w,0}$  are the respective dry and wet refractive indices at the surface.

According to (Hofmann-Wellenhof et al, 1992),  $N_{d,0}$ ,  $N_{w,0}$  can be described as follows.

$$N_{d,0} = c_1 \frac{p}{T}, \quad c_1 = 77.64 \text{ k/mb} \quad (4-6)$$

$$N_{w,0} = c_2 \frac{e}{T} + c_3 \frac{e}{T^2} \quad (4-7)$$

$$c_2 = -12.96 \text{ k/mb} \quad (4-8)$$

$$c_3 = 3.718 \times 10^5 \text{ k}^2/\text{mb} \quad (4-9)$$

where

$p$  atmospheric pressure in millibars (mb)

$T$  temperature in Kelvin (K)

$e$  partial pressure of water vapor in mb

The magnitudes of tropospheric error of range measurements are listed in Table 4-3

Table 4-3 Influence of the Tropospheric Refraction on Range Measurement (Seeber, 1993)

Elevation angle	90°	20°	15°	10°	5°
Tropospheric Error (m)	2.51	7.29	9.58	14.04	25.82

### 4.1.2 Ionospheric Effect

The ionosphere is that part of the upper atmosphere where free electrons occur in sufficient density to have an appreciable influence on the propagation of radio frequency electromagnetic waves. This ionization depends primarily on the Sun and its activity. Ionospheric structures and peak densities in the ionosphere vary greatly with time (sunspot cycle, seasonally, and diurnally), with geographical location (polar, auroral zones, mid-latitudes, and equatorial regions), and with certain solar-related ionospheric disturbances.

The major part of the ionization is produced by solar X-ray and ultraviolet radiation, and by corpuscular radiation from the Sun. The most noticeable effect is seen as the Earth rotates with respect to the Sun; ionization increases in the sunlit atmosphere and decreases on the shadowed side. Although the Sun is the largest contributor toward the ionization, cosmic rays make a small contribution. Any atmospheric disturbance affects the distribution of the ionization.

Longer wavelength radio signals can be "bounced" off the ionosphere allowing radio signal transmission "over the horizon". This is how the long, medium and short wave radio broadcasts reach receivers over long distances. Because the ionosphere is not a nice smooth "mirror" the signal can be scattered in many directions causing loss of signal strength and interference from other transmitters. The ionosphere is particularly disturbed in the auroral regions, and during magnetic sub-storms.

Shorter wavelength radio signals pass through the ionosphere but are affected by it. These shorter wavelengths are used by satellites for communication and navigation purpose, and the ionosphere affects the signals rather like the way the atmosphere causes "twinkling" of the stars.

Considerable efforts have, therefore, been concentrated on modeling this ionospheric parameter. Several models are available including the Chiu model (Chiu, 1975), the Bent model (Bent et al. 1972) that has been used extensively for satellite tracking, the semi-empirical SLIM model (Anderson et al, 1987) based on theoretically obtained grid values, and the FAIM model (Anderson et al, 1989) that uses the Chiu formalism together with the SLIM results. The International Reference Ionosphere (IRI) is probably the most mature of these models, having undergone more than two decades of scrutiny and improvement.

At present, almost all empirical models of ionospheric parameters are limited to non-auroral, magnetically quiet conditions. Major efforts are underway to extend ionospheric predictability beyond these limitations. A promising venue seems to be the inclusion of real-time data from the newly developed automatic recording and scaling ionosondes.

Following Hofmann-Wellenhof (1992), Klobuchar (1996), Seeber (1993) and Wild (1994), the phase and range refractive indices can be written as

$$n_p = 1 + \frac{a}{f^2} \quad (4-10)$$

$$n_r = 1 - \frac{a}{f^2} \quad (4-11)$$

Then first orders of ionospheric group and phase delays for range and phase observations are proportional to the integrated number of free electrons along the propagation path and inversely proportional to the square of transmission frequency and can be written as

$$\Delta S_p^{ion} = \frac{40.3}{f^2} \int Ndl \quad (4-12)$$

$$\Delta S_r^{ion} = -\frac{40.3}{f^2} \int Ndl \quad (4-13)$$

where  $f$  is the carrier frequency and  $\int Ndl$  is Total Electron Content (TEC), integrated along the path from ground tracking station to satellite.

From Eq.(4-12) and Eq.(4-13) it can be seen that changes of range and phase caused by the ionospheric refraction may be restricted to the determination of the total electron content (TEC). TEC itself is dependent on sunspot activities, seasonal and diurnal variations, the line of sight which includes elevation and azimuth of the satellite and the position of the observation site.

Usually TEC can be measured using dual frequency observations forming wide-lane linear combination (L4). In the case of code observations the total electron content is proportional to the difference of the ionospheric refraction on the two frequencies. Ionospheric error can also be removed by ionosphere-free linear combination (L3). For single frequency users, some mathematical models, for examples, Klobuchar model (Klobuchar, 1996) and single-layer model (Wild 1994) may be used.

Following Wild (1994), a simple and widely used mathematic model, single-layer model (SLM) will be discussed here.

SLM is based on the assumption that all free electrons are concentrated in a spherical layer of infinitesimal thickness (single layer) at a height  $H$  above the earth's surface. From Eq.(4-12) and Eq.(4-13), ionospheric correction can be written as

$$\Delta S^{ion} = \pm \frac{40.3}{f^2} \frac{TVEC}{\cos z'} \quad (4-14)$$

where

$z'$  zenith distance at the intersection  $P$  of the actual signal with the single-layer

*TVEC* surface density of the electrons in the single-layer at point *P*; *TVEC* is also called the total vertical electron content

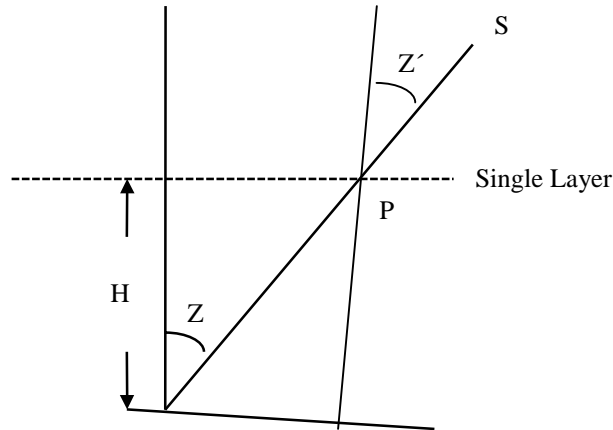


Figure 4-1 Single-Layer Model of the Ionosphere

SLM reduces the complicated layer structure of the ionosphere to a single layer. The height of this idealized layer is usually set to about 300-400 km.

In Eq.(4-14), *TVEC* can be developed as a function of Taylor series with latitude  $\varphi$  and the hour angle  $s$  of the Sun as independent variables, i.e.

$$TVEC(\varphi, s) = \sum_{i=0}^n \sum_{k=0}^m E_{ik} (\varphi - \varphi_0)^i (s - s_0)^k \quad (4-15)$$

where

$\varphi_0, s_0$  origin point of Taylor series development

$$E_{ik} = \frac{1}{i!k!} \left. \frac{\partial^{i+k} TVEC}{\partial \varphi^i \partial s^k} \right|_{\varphi_0 s_0}, \quad i = 0, 1, 2, \Lambda; k = 0, 1, \Lambda \quad (4-16)$$

The hour angle of the Sun is defined as the angle between the Sun and the local meridian (positive to the west). The local solar time  $t$  is related to the hour angle of the Sun by

$$t = s + 12^h$$

Usually,  $s_0$  is selected to be the hour angle corresponding to the middle of the observation interval,  $\varphi_0$  is defined as the mean value of the latitudes of all stations used to compute the model.

Eq.(4-14) and the coefficients in Eq.(4-15) are introduced as unknown parameters in observation equations and estimated together with the other unknowns during data processing.

Table 4-4 shows the maximum range errors of GPS dual frequencies due to ionosphere errors.

Table 4-4 Maximum vertical ionospheric range error (Seeber, 1993)

Frequency	1st order effect ( $1/f^2$ )	2nd order effect ( $1/f^3$ )	3rd order effect ( $1/f^4$ )
L1	32.5 (m)	0.036 (m)	0.002 (m)
L2	53.5 (m)	0.076 (m)	0.007 (m)
L1/L2	0.0 (m)	0.026 (m)	0.006 (m)

## 4.2 Multipath Effect

Multipath error is one of the dominant error sources for satellite-based navigation systems. Although this phenomenon has been known for many years, but since 1990' multipath effect is very interesting and hot topic in

navigation community. Many literatures are contributed to this topic and most parts of these papers focus on the correlator designs as well as signal processing in receiver hardware.

Van Nee (1991) analyzed the influence of multipath error on code measurements from the point of view of the GPS receiver hardware and concluded that multipath error may not be removed by long averaging time because there are mean range errors existing due to the nonlinearity in the code measurements. Braasch (1992) also analyzed the multipath effect from hardware point of view. Since then many advances related to GPS receiver hardware have been achieved, such as Narrow Correlators (Van Dierendonck et al 1993), Multipath Estimating Delay Lock Loop (MEDLL) (Townsend et al 1995), SNR-based method (Breivik et al 1997, Comp et al 1996, Sleewaegen 1997), Multiple Closely-Spaced Antennas (J.K. Ray et al 1998) and Dual-Depth Dual-Frequency Choke Ring (Filippov et al 1998) etc. Some authors presented pure algorithm-related methods such as Maximum Likelihood Estimator for Multipath (Weill 1995), Autocovariance Function of Pseudorange Multipath Error (El-Rabbany 1995), Uniform Geometrical Theory of Diffraction (GTD) to model and verify the differential carrier phase errors due to multipath (Gomez et al 1995). Raquet (1996) presented a unique method by using network adjustment to reduce the multipath error in the reference stations.

### 4.2.1 Multipath Envelopes

The incoming signals from satellites plus reflected incoming signals from nearby objects are received by satellite receivers. The locally generated replicas are aligned with these signals in the Phase and Delay Lock Loop (PLL and DLL) to make correlation function between the local replica and the incoming signals maximum. The reflected incoming signals are called multipath signals and their effects will distort the correlation functions and introduce code and phase tracking errors that are defined as multipath effects. Multipath effects appear to be the dominant error source in high precision navigation, influencing also fast ambiguity resolution.

Assuming input signals directly from satellite plus a multipath signal are given by

$$S(t) = AC(t - \tau) \cos \omega(t - \tau) + \alpha AC(t - \tau - \delta) \cos[\omega(t - \tau) - \theta_m] \quad (4-17)$$

where

- $A$  signal amplitude
- $C$  Code series
- $\omega$  carrier frequency
- $\alpha$  multipath relative amplitude coefficient < 1;
- $\tau$  time delay from the satellite to the receiver (line-of-sight);
- $\theta_m$  multipath relative phase;
- $\delta$  multipath relative time delay;

According to Van Dierendonck (1996), Eissfeller (1997) and Sleewaegen (1997), the outputs from receiver correlators are

$$I_P = AR(\tau') \cos(\Delta\varphi) + \alpha AR(\tau' - \delta) \cos(\Delta\varphi - \theta_m) \quad (4-18)$$

$$Q_P = AR(\tau') \sin(\Delta\varphi) + \alpha AR(\tau' - \delta) \sin(\Delta\varphi - \theta_m) \quad (4-19)$$

$$I_D = A[R(\tau' + dT/2) - R(\tau' - dT/2)] \cos(\Delta\varphi) \quad (4-20)$$

$$+ \alpha A[R(\tau' - \delta + dT/2) - R(\tau' - \delta - dT/2)] \cos(\Delta\varphi - \theta_m) \quad (4-21)$$

$$Q_D = A[R(\tau' + dT/2) - R(\tau' - dT/2)] \sin(\Delta\varphi) \quad (4-22)$$

$$+ \alpha A[R(\tau' - \delta + dT/2) - R(\tau' - \delta - dT/2)] \sin(\Delta\varphi - \theta_m) \quad (4-23)$$

where

- $\tau'$  synchronous delay time error produced by the receiver
- $\Delta\varphi$  difference between the local phase in PLL and the incoming carrier phase
- $T$  signal period
- $d$  early - late spacing between correlators in chips;  $d$  is between 0 and 1.  $d=1$  standard 1 chip spacing;  $d<1$  narrow spacing

If incoming phase is locked by local phase,  $Q_P = 0$ ; if incoming code is locked by local code,  $I_D = 0$ , i.e.

$$Q_P = AR(\tau') \sin(\Delta\varphi) + \alpha AR(\tau' - \delta) \sin(\Delta\varphi - \theta_m) = 0 \quad (4-24)$$

$$I_D = A[R(\tau' + dT/2) - R(\tau' - dT/2)]\cos(\Delta\varphi) + \alpha A[R(\tau' - \delta + dT/2) - R(\tau' - \delta - dT/2)]\cos(\Delta\varphi - \theta_m) = 0 \quad (4-25)$$

The problem is how the multipath signal delay time  $\delta$  affects correlation time  $\tau'$ . If multipath effects do not exist, i.e.  $\alpha = 0$ , Eq.(4-24) and Eq.(4-25) hold only and only if  $\tau' = \tau$ . Due to multipath effects, Eq.(4-24) and Eq.(4-25) will hold when  $\tau' \neq \tau$ , i.e. zero-crossing point is distorted.

The envelopes of influence of multipath signal time delay  $\delta$  on  $\tau'$  from Eq.(4-25) can be developed as follows.

Suppose

$$R(\tau') = \begin{cases} 1 - \frac{|\tau'|}{T} & |\tau'| \leq T \\ 0 & \tau' > T \end{cases} \quad (4-26)$$

and  $d=1$ ,  $\cos(\Delta\varphi) = 1$ ,  $\cos(\Delta\varphi - \theta_m) = 1$ .

If  $\delta - \tau' \leq \frac{T}{2}$ , Eq.(4-25) becomes

$$-\frac{|\tau' + T/2|}{T} + \frac{|\tau' - T/2|}{T} = -\alpha \left( -\frac{|\tau' + T/2 - \delta|}{T} + \frac{|\tau' - T/2 - \delta|}{T} \right)$$

i.e.

$$\tau' = \delta \frac{\alpha}{1 + \alpha} \quad (4-27)$$

If  $\delta - \tau' > \frac{T}{2}$ , then  $R(\tau' - T/2 - \delta) = 0$ ,

Eq.(4-25) becomes

$$-\frac{|\tau' + T/2|}{T} + \frac{|\tau' - T/2|}{T} = -\alpha \left( 1 - \frac{|\tau' + T/2 - \delta|}{T} \right) \\ \tau' = \left( \frac{3}{2}T - \delta \right) \frac{\alpha}{2 - \alpha} \quad (4-28)$$

Assuming  $\cos(\theta_c) = -1$ ,  $\cos(\theta_m - \theta_c) = -1$ , Eq.(4-27) and Eq.(4-28) become

$$\tau' = -\delta \frac{\alpha}{1 - \alpha} \quad (4-29)$$

$$\tau' = -\left( \frac{3}{2}T - \delta \right) \frac{\alpha}{2 + \alpha} \quad (4-30)$$

According to Eq.(4-27), Eq.(4-28), Eq.(4-29) and Eq.(4-30) and assuming  $\alpha = 0.5$ , the multipath error envelopes of code pseudoranges are drawn in Figure 4-2 and Figure 4-3 respectively.

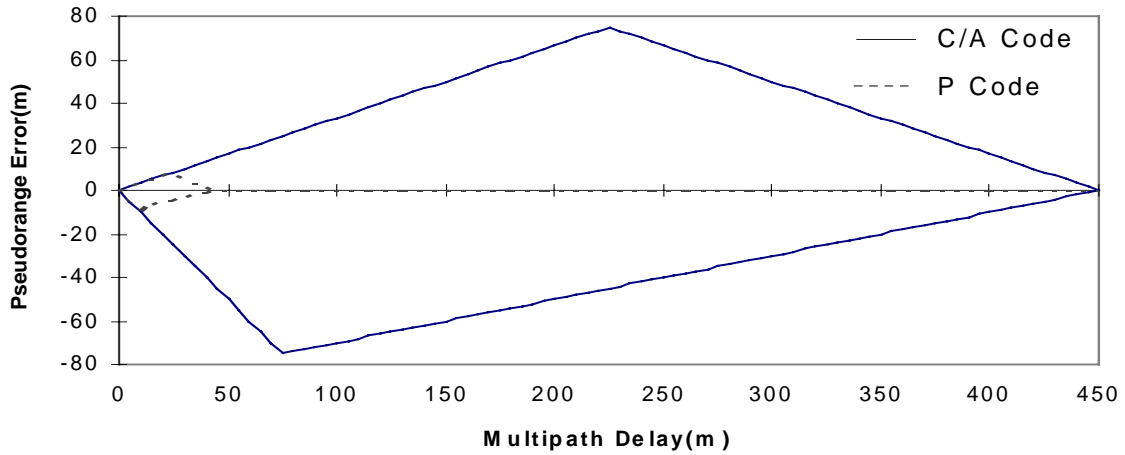


Figure 4-2 Multipath Error Envelope for GPS Code Pseudoranges

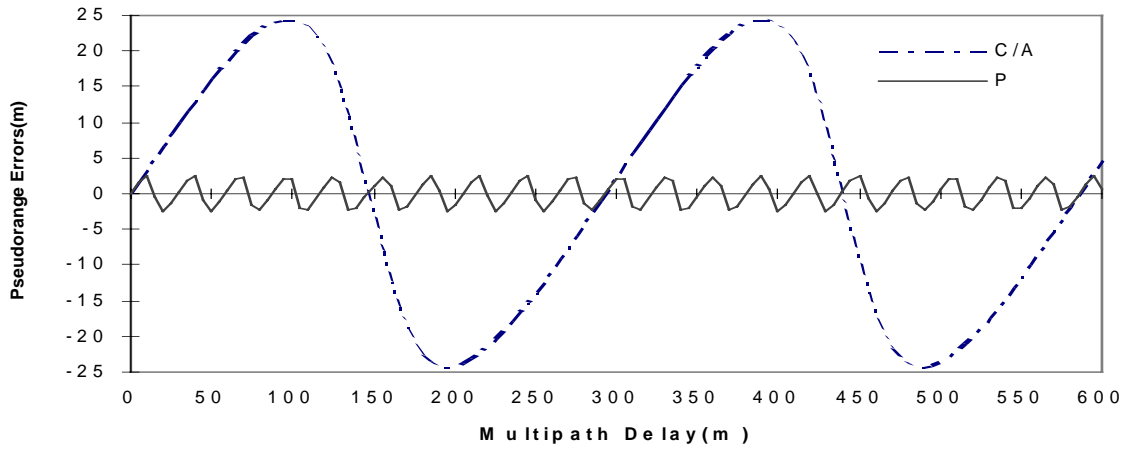


Figure 4-3 Periodic Function of Multipath Error

### 4.2.2 Influence of Multipath Errors on Range and Phase Observations

From the mathematical point-of-view, the influence of multipath delay  $\delta$  on correlation time  $\tau'$  can be directly derived from auto-correlation function  $R(\tau)$ .

Using very simple signal equation, suppose the arrived signal from satellite is

$$S_d = A \cos \omega(t - \tau) \tag{4-31}$$

where

$\tau$  time delay from the satellite to the receiver

One multipath signal reflected from near object is:

$$\begin{aligned} S_m &= \alpha A \cos[\omega(t - \tau - \delta)] \\ &= \alpha A \cos[\omega(t - \tau) + \theta_m] \end{aligned} \tag{4-32}$$

where

$\alpha$  multipath relative amplitude coefficient  $< 1$ ;

$\theta_m$  multipath relative phase ( $\theta_m = \omega\delta$ )

The signals received by satellite receiver are

$$\begin{aligned} S_r &= S_d + S_m = A \cos \omega(t - \tau) + \alpha A \cos[\omega(t - \tau) + \theta_m] \\ &= A \cos \omega(t - \tau) + \alpha A \cos \omega(t - \tau) \cos \theta_m - \alpha A \sin \omega(t - \tau) \sin \theta_m \\ &= A_r \left[ \frac{1 + \alpha \cos \theta_m}{A_r} \cos \omega(t - \tau) - \frac{\alpha \sin \theta_m}{A_r} \sin \omega(t - \tau) \right] \end{aligned} \quad (4-33)$$

where

$$A_r = \sqrt{A^2(1 + \alpha \cos \theta_m)^2 + \alpha^2 A^2 \sin^2 \theta_m} = A \sqrt{1 + 2\alpha \cos \theta_m + \alpha^2}$$

Finally Eq.(4-33) becomes

$$\begin{aligned} S_r &= A_r [\cos \phi \cos \omega(t - \tau) - \sin \phi \sin \omega(t - \tau)] \\ &= A_r \cos[\omega(t - \tau) + \phi] \end{aligned} \quad (4-34)$$

where

$$\phi = \tan^{-1} \left( \frac{\alpha \sin \theta_m}{1 + \alpha \cos \theta_m} \right) + n\pi$$

$\phi$  is the phase error caused by multipath effects

From Eq.(4-34), it is clear that the received signals are distorted by the multipath effects. The amplitude of the received signal  $A$  becomes  $A_r$  and the phase of the signals introduces phase shift  $\phi$ .

Suppose the local receiver produces a synchronous signal

$$S_l = A \cos \omega(t - \tau') \quad (4-35)$$

where

$\tau'$  correlation time error between replica and incoming signal produced by the receiver

The auto-correlation function of the receiver may be written as follows:

$$\begin{aligned} R(\tau') &= \int S_r(\tau) S_l(\tau') dt \\ &= \int A_r \cos[\omega(t - \tau) + \phi] A \cos \omega(t - \tau') dt = A_r A \int \cos[\omega(t - \tau) + \phi] \cos \omega(t - \tau') dt \end{aligned} \quad (4-36)$$

For simplicity, the time error, propagation errors and receiver errors (PLL track errors etc.) are not considered and assuming  $\alpha$  is a constant.

In order to make Eq.(4-36) maximum, let

$$\omega(t - \tau) + \phi = \omega(t - \tau')$$

i.e.

$$\tau = \tau' + \Delta\tau \quad (4-37)$$

and

$$\begin{aligned} \Delta\tau &= \frac{\phi}{\omega} = \frac{1}{2\pi f} \left[ \tan^{-1} \left( \frac{\alpha \sin \theta_m}{1 + \alpha \cos \theta_m} \right) + n\pi \right] \\ &\approx \frac{1}{2\pi f} \left[ \frac{\alpha \sin \theta_m}{1 + \alpha \cos \theta_m} - \frac{1}{3} \left( \frac{\alpha \sin \theta_m}{1 + \alpha \cos \theta_m} \right)^3 + \dots + n\pi \right] \end{aligned} \quad (4-38)$$

where

$$\phi = \left[ \frac{\alpha \sin \theta_m}{1 + \alpha \cos \theta_m} - \frac{1}{3} \left( \frac{\alpha \sin \theta_m}{1 + \alpha \cos \theta_m} \right)^3 + \dots + n\pi \right]$$

From Eq.(4-38), we can obtain

$$\Delta\rho = \pm \frac{M}{f} \quad (4-39)$$

where

$\Delta\rho$  multipath errors of pseudorange

$$M = \frac{c}{2\pi} \left[ \frac{\alpha \sin \theta_m}{1 + \alpha \cos \theta_m} - \frac{1}{3} \left( \frac{\alpha \sin \theta_m}{1 + \alpha \cos \theta_m} \right)^3 + \dots + n\pi \right]$$

$c$  light velocity

Actually, there are many reflected multipath signals, therefore Eq.(4-39) can also be written as

$$\Delta\rho \approx \pm \frac{\sum M}{f}$$

From Eq.(4-38), it can be shown that  $\Delta\tau$  is an error of time delay caused by multipath effects.  $n\pi$  is of the periodic term.  $\phi$  is a phase error.

Clearly, Eq. (4-37) can also be obtained from Eq.(4-24) and Eq.(4-25). Eq.(4-37) shows under the ideal situation, the multipath error is of a periodic term that can be removed by using the averaging method or filtering (Sennott et al 1987). Actually, code delay (distance between satellite and GPS receiver) is measured by the so-called DLL discriminator, which is based on the approach that the incoming signals are mixed with early and late codes produced by local GPS receiver. The mixed signals then enter the Low-Pass Filters (LPF). The output signals with early and late mixed codes from LPF are subtracted each other to form the DLL discriminator. The signals from DLL discriminator are zero if incoming signals are locked by local signals.

Theoretically, if the output of the discriminator is zero, the related autocorrelation function Eq.(4-36) reaches maximum, which means Eq.(4-37) holds. But actually in a GPS receiver, early and late local signals are not strictly symmetrically generated due to variety of the errors such as thermal noise, timing error and frequency drift, etc., i.e. that the output of the discriminator is zero doesn't mean that corresponding autocorrelation function Eq.(4-36) reaches maximum, and vice versa. Therefore a mean error exists, which is not zero if using DLL to track satellite signals under influence of multipath effect. Therefore the multipath errors can not be completely removed by averaging or filtering methods (van Nee 1991, Eissfeller 1997).

From discussion above and Eq.(4-38) and Eq.(4-39), the following conclusions about multipath effects can be reached.

1. Theoretically, the multipath errors shows a period property. The period is dependent on the signal frequency and in principle is equal to the signal period. Actually because early and late codes are not symmetrically produced by the local receiver, the multipath errors are not strictly periodic functions, there are mean errors existing,
2. The influence of multipath errors on code pseudorange is inversely proportional to the signal frequency. Periods of phase errors caused by multipath effects are dependent on the signal frequency,
3. The multipath error is dependent on receiver design,
4. The multipath error is independent of the length of baseline. It is related to the observation site.

According to these properties and the conclusion discussed above, the system part of multipath errors could be removed using linear combinations for the dual frequencies of the observations from the same site, the remaining random part of multipath errors might be eliminated by using averaging method for static measurements.



### 4.3 Clock Errors

Clock errors are divided into two parts, one is the satellite clock error and another is receiver clock error. Usually the satellite clock error is independent of the satellite direction and is a fundamental error for one-way ranging measurements. According to modern clock technology, atomic clocks such as cesium and rubidium clocks have the stability of about 1 part in  $10^{13}$  over a day or about 3.5 m in ranging (Parkinson et al, 1996) and can be used on board the satellite. Also the errors introduced as additional parameters with other orbit parameters in orbit determination processing can be determined. Generally because the ground tracking stations are equipped with very stable and high accuracy atom clocks, the receiver clock errors in these stations can be removed before data processing or it is so small that it can be neglected.

According to Chadwell (1995), satellite clock and receiver clock can be related by

$$\tau_s = \tau + \frac{\tau}{c^2} \left( \frac{GM}{r_t} + \frac{1}{2} \Omega^2 (x_t^2 + y_t^2) - \frac{3}{2} \frac{GM}{a} \right) - \frac{2}{c^2} (\mathbf{x}^s \cdot \mathbf{v}^s) \quad (4-44)$$

where

$\tau_s$	satellite clock time
$\tau$	ground receiver clock
$r_t$	geocenter position vector of ground receiver
$\Omega$	rotation rate of the Earth
$x_t$	x component of geocenter position vector of ground receiver
$y_t$	y component of geocenter position vector of ground receiver
$a$	semi-major axis of satellite orbit
$\mathbf{x}^s$	position vector of satellite in geocenter coordinate system
$\mathbf{v}^s$	velocity vector of satellite in geocenter coordinate system

Second term in Eq.(4-44) causes a secular offset that can be corrected by setting the satellite clock frequency lower by  $4.4 \times 10^{-10}$  MHz from the nominal frequency (Spilker, 1978). The third term (relativistic effects) causes a periodic variation that has a maximum magnitude of 14 m for single point positioning, but cancels out with between-station differences (Zhu and Groten, 1988).



## CHAPTER 5 PERTURBATION MODELS OF IGSO, GEO and MEO SATELLITE ORBITS

The performances of IGSO, GEO and MEO satellite orbits will be affected by many perturbations such as the non-central part of the Earth's gravitational potential, gravitational effects of Sun and Moon, solid earth tidal effects, solar radiation pressure, Albedo radiation pressure, gravitational effects of ocean tides, gravitational effects of the planets, relativistic corrections, thermal emission of the satellite etc. Because IGSO, GEO and MEO satellite orbits are far away from the earth, the effects of earth tides, ocean tides and earth radiation are much smaller. Hence the non-central part of the Earth, the gravitational effects of Sun and Moon and solar radiation pressure play a major role in the perturbations on IGSO, GEO and MEO satellite orbits. In this chapter, the computations of these three perturbation models will be discussed. The major literatures on this topic are referred to Soop (1994), Tscherning (1976, 1977).

### 5.1 The Earth Gravitational Perturbation

The earth geopotential is represented as a point mass and an expansion of spherical harmonics to represent the nonspherical effect of the Earth mass. The geopotential can be expressed by (Rothacher, 1992)

$$U = \frac{GM}{r} + GM \sum_{n=2}^N \sum_{m=0}^n \frac{a_e^n}{r^{n+1}} P_{nm}(\sin \varphi) (C_{nm} \cos m\lambda + S_{nm} \sin m\lambda) \quad (5-1)$$

where

$G$	Newtonian Gravitational Constant
$M$	the Earth's mass ( $GM=398.600415 \times 10^{12} \text{ m}^3 \text{ s}^{-2}$ )
$P_{nm}(\sin \varphi)$	associated Legendre function
$\lambda, \varphi$	geographic longitude and latitude of satellite
$C_{nm}, S_{nm}$	spherical harmonic coefficients.

In the equation above, the first term is the point mass part. The other terms are an expansion of spherical harmonics to represent the nonspherical effects of the earth mass, i.e. the Earth gravitational perturbation.

The forces produced by the geopotential are computed by

$$\text{grad}(U) = \left( \frac{\partial U}{\partial x}, \frac{\partial U}{\partial y}, \frac{\partial U}{\partial z} \right) = \text{grad} \left( \frac{GM}{r} \right) + GM \sum_{n=2}^N \sum_{m=0}^n \text{grad} \left\{ \frac{a_e^n}{r^{n+m+1}} P_n^{(m)}(\sin \varphi) (C_{nm} \xi_m + S_{nm} \eta_m) \right\} \quad (5-2)$$

#### 5.1.1 Computation of Legendre Polynomials

From Eq.(5-1) it can be seen that in order to compute the geopotential, the first step is computation of the Legendre polynomials.

The Legendre polynomials  $P_n$  as a function of the independent variable  $x$  can be defined by:

$$P_n(x) = \frac{1}{2^n n!} \frac{d^n}{dx^n} (x^2 - 1)^n \quad (5-3)$$

For a given value of  $x$ , the Legendre polynomials Eq.(5-3) can be calculated by the following recursive formula with starting values:

$$P_0(x) = 1; \quad P_1(x) = x$$

$$P_n(x) = \frac{2n-1}{n} x P_{n-1}(x) - \frac{n-1}{n} P_{n-2}(x) \quad \text{if } n \geq 2 \quad (5-4)$$

The associated Legendre function for a given order  $m$  and degree  $n$  is defined by:

$$P_{nm}(x) = (1-x^2)^{m/2} \frac{d^m P_n(x)}{dx^m} \quad (5-5)$$

With these definitions the spherical harmonics are not normalized. In order to normalize them, spherical harmonics needs to be multiplied by

$$\sqrt{(2n+1)} \quad \text{if } m=0; \quad (5-6)$$

$$\sqrt{2(2n+1) \frac{(n-m)!}{(n+m)!}} \quad \text{if } m \geq 1 \quad (5-7)$$

Assuming that

$$P_n^{(m)}(x) = \frac{d^m P_n(x)}{dx^m} \quad (5-8)$$

Eq.(5-8) can be calculated by the following recursive formula in  $n$  for given value of  $x$  and  $m \geq 1$  with starting values:

$$P_n^{(m)}(x) = 0 \quad \text{if } n < m \quad (5-9)$$

$$P_n^{(m)}(x) = 1 \times 3 \times \dots \times (2m-1) \quad \text{if } n = m \quad (5-10)$$

$$P_n^{(m)}(x) = \frac{2n-1}{n-m} x P_{n-1}^{(m)}(x) - \frac{n+m-1}{n-m} P_{n-2}^{(m)}(x) \quad \text{if } n > m \quad (5-11)$$

First, using the equations above to obtain  $P_n^{(m)}(x)$ , then using Eq.(5-5) to calculate the associated Legendre function  $P_{nm}$ ; at last using Eq.(5-4) to compute Legendre polynomials.

After Legendre polynomials have been computed, the coefficients should be normalized using Eq.(5-6) and Eq.(5-7).

### 5.1.2 Computation of Geopotential Perturbation

According to Eq.(5-5) and Eq.(5-8), Eq.(5-1) can be expressed by

$$\begin{aligned} U &= \frac{GM}{r} + GM \sum_{n=2}^N \sum_{m=0}^n \frac{a_e^n}{r^{n+1}} \cos^m \varphi P_n^{(m)}(\sin \varphi) (C_{nm} \cos m\lambda + S_{nm} \sin m\lambda) \\ &= \frac{GM}{r} + GM \sum_{n=2}^N \sum_{m=0}^n \frac{a_e^n}{r^{n+m+1}} P_n^{(m)}(\sin \varphi) (C_{nm} r^m \cos^m \varphi \cos m\lambda + S_{nm} r^m \cos^m \varphi \sin m\lambda) \end{aligned} \quad (5-12)$$

Assuming

$$\left. \begin{aligned} x &= r \cos \varphi \cos \lambda \\ y &= r \cos \varphi \sin \lambda \\ z &= r \sin \varphi \end{aligned} \right\} \quad (5-13)$$

and

$$\left. \begin{aligned} \xi_m &= r^m \cos^m \varphi \cos m\lambda \\ \eta_m &= r^m \cos^m \varphi \sin m\lambda \end{aligned} \right\} \quad (5-14)$$

$\xi_m, \eta_m$  can be calculated by the following recursive formulas:

$$\left. \begin{aligned} \xi_m &= \xi_{m-1} x - \eta_{m-1} y \\ \eta_m &= \xi_{m-1} y + \eta_{m-1} x \end{aligned} \right\} \quad (5-15)$$

Eq.(5-15) starts with  $\xi_0 = 1$  and  $\eta_0 = 0$ .

Rewrite Eq.(5-2) as follows

$$\text{grad}(U) = \left( \frac{\partial U}{\partial x}, \frac{\partial U}{\partial y}, \frac{\partial U}{\partial z} \right) = \text{grad} \left( \frac{GM}{r} \right) + GM \sum_{n=2}^N \sum_{m=0}^n \text{grad} \left\{ \frac{a_e^n}{r^{n+m+1}} P_n^{(m)}(\sin \varphi) (C_{nm} \xi_m + S_{nm} \eta_m) \right\} \quad (5-16)$$

where

$$\frac{\partial}{\partial x} \left\{ \frac{a_e^n}{r^{n+m+1}} \right\} = -(n+m+1) \frac{a_e^n}{r^{n+m+3}} x \quad (5-17)$$

$$\frac{\partial}{\partial y} \left\{ \frac{a_e^n}{r^{n+m+1}} \right\} = -(n+m+1) \frac{a_e^n}{r^{n+m+3}} y \quad (5-18)$$

$$\frac{\partial}{\partial z} \left\{ \frac{a_e^n}{r^{n+m+1}} \right\} = -(n+m+1) \frac{a_e^n}{r^{n+m+3}} z \quad (5-19)$$

$$\frac{\partial}{\partial x} [P_n^{(m)}(\sin \varphi)] = -\frac{zx}{r^3} P_n^{(m+1)}(\sin \varphi) \quad (5-20)$$

$$\frac{\partial}{\partial y} [P_n^{(m)}(\sin \varphi)] = -\frac{zy}{r^3} P_n^{(m+1)}(\sin \varphi) \quad (5-21)$$

$$\frac{\partial}{\partial z} [P_n^{(m)}(\sin \varphi)] = \frac{1}{r} - \frac{z^2}{r^3} P_n^{(m+1)}(\sin \varphi) \quad (5-22)$$

According to Eq.(5-13) and Eq.(5-14), the derivatives of  $\xi_m, \eta_m$  to coordinate components  $x, y, z$  are expressed by

$$\frac{\partial \xi_m}{\partial x} = \frac{m}{r} \left[ \frac{x}{r} \xi_m + \tan \varphi \cos \lambda \sin \varphi \xi_m + \eta_m \frac{\sin \lambda}{\cos \varphi} \right] = m \xi_{m-1} \quad (5-23)$$

$$\frac{\partial \xi_m}{\partial y} = \frac{m}{r} \left[ \frac{y}{r} \xi_m + \tan \varphi \sin \lambda \sin \varphi \xi_m - \eta_m \frac{\cos \lambda}{\cos \varphi} \right] = -m \eta_{m-1} \quad (5-24)$$

$$\frac{\partial \xi_m}{\partial z} = \frac{m}{r} \left[ \frac{z}{r} \xi_m - \tan \varphi \cos \varphi \xi_m \right] = 0 \quad (5-25)$$

$$\frac{\partial \eta_m}{\partial x} = \frac{m}{r} \left[ \frac{x}{r} \eta_m + \tan \varphi \cos \lambda \sin \varphi \eta_m - \xi_m \frac{\sin \lambda}{\cos \varphi} \right] = m \eta_{m-1} \quad (5-26)$$

$$\frac{\partial \eta_m}{\partial y} = \frac{m}{r} \left[ \frac{y}{r} \eta_m + \tan \varphi \sin \lambda \sin \varphi \eta_m + \xi_m \frac{\cos \lambda}{\cos \varphi} \right] = m \xi_{m-1} \quad (5-27)$$

$$\frac{\partial \eta_m}{\partial z} = \frac{m}{r} \left[ \frac{z}{r} \eta_m - \tan \varphi \cos \varphi \eta_m \right] = 0 \quad (5-28)$$

From Eq.(5-12) to Eq.(5-28), the geopotential perturbation can be computed.

### 5.1.3 The Effect of Geopotential Perturbation

The effects of geopotential perturbation on IGSO and GEO satellite orbits were computed according to discussion above. In the computation, GEM-T2 Earth model is used. The results are listed in Table 5-1 to Table 5-2 for IGSO satellite and in Table 5-3 to Table 5-4 for GEO satellite.

## 5.1.3.1 Influence of Geopotential on IGSO Satellites

Table 5-1 The Effect of Geopotential Perturbation on IGSO Satellite Orbit

(Zonal Part)

(Satellite Parameters:  $a=42164.174\text{km}$ , starting point  $\lambda=20^\circ$ ,  $i=63^\circ$ )

Perturbation Force	Acceleration ( $\text{m/sec}^2$ )	Orbit Errors (m)	
		One Day	Ten Days
$J_2$	$8 \times 10^{-6}$	8.90 (km)	88.7 (km)
$J_3$	$3 \times 10^{-9}$	0.03	0.25
$J_4$	$3 \times 10^{-10}$	0.18	1.83
$J_5$	$7 \times 10^{-12}$	0.00	0.03
$J_6$	$3 \times 10^{-12}$	0.00	0.03
$J_7$	$3 \times 10^{-13}$	0.00	0.00
$J_8$	$3 \times 10^{-14}$	0.00	0.00
$J_9$	$3 \times 10^{-15}$	0.00	0.00
$J_{10}$	$9 \times 10^{-16}$	0.00	0.00

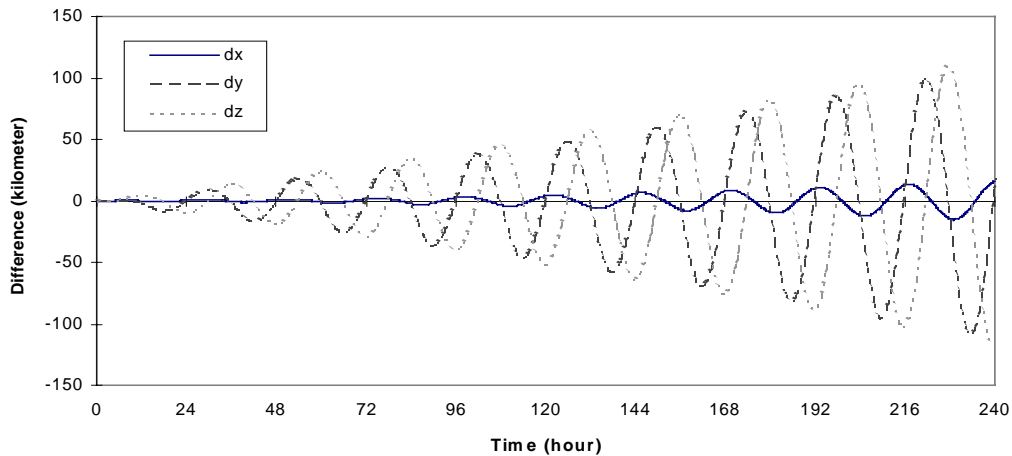
Table 5-2 The Effect of Geopotential Perturbation on IGSO Satellite Orbit

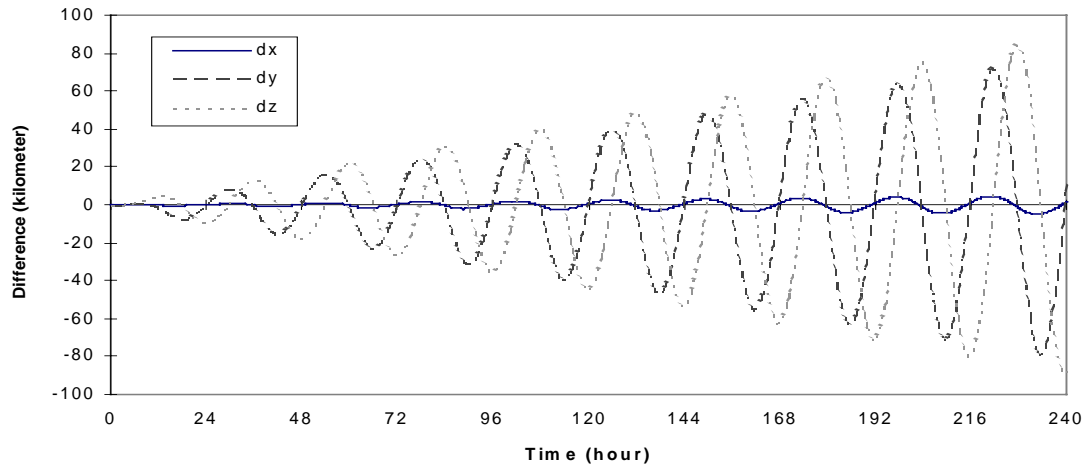
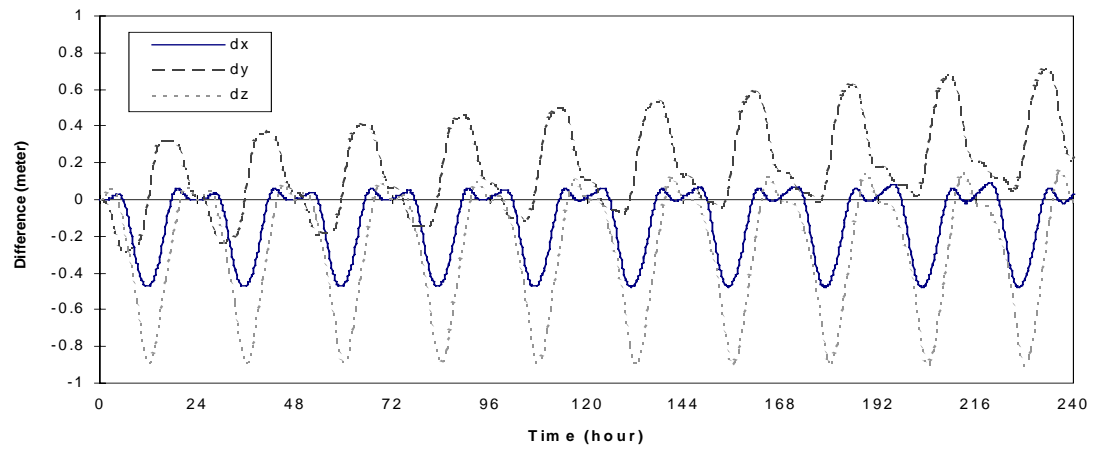
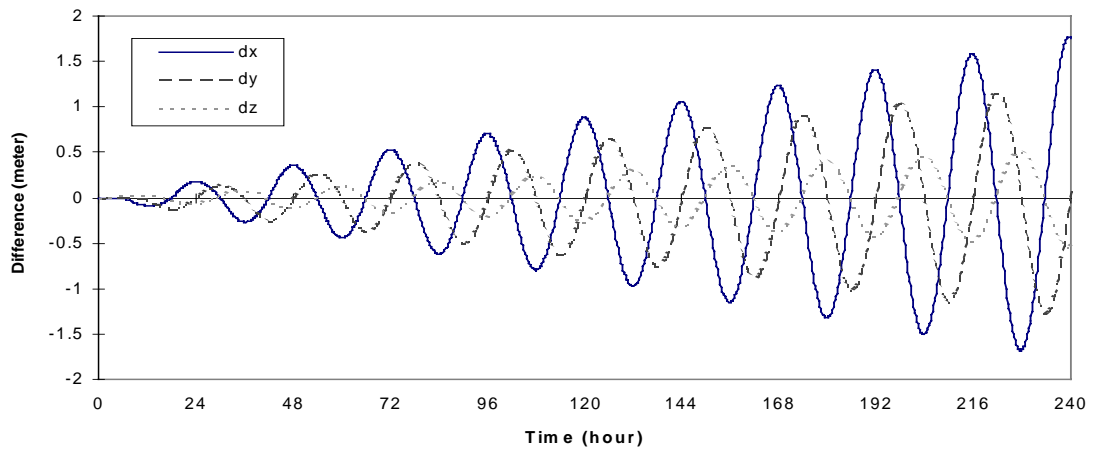
(Sectorial and Tesseral Part)

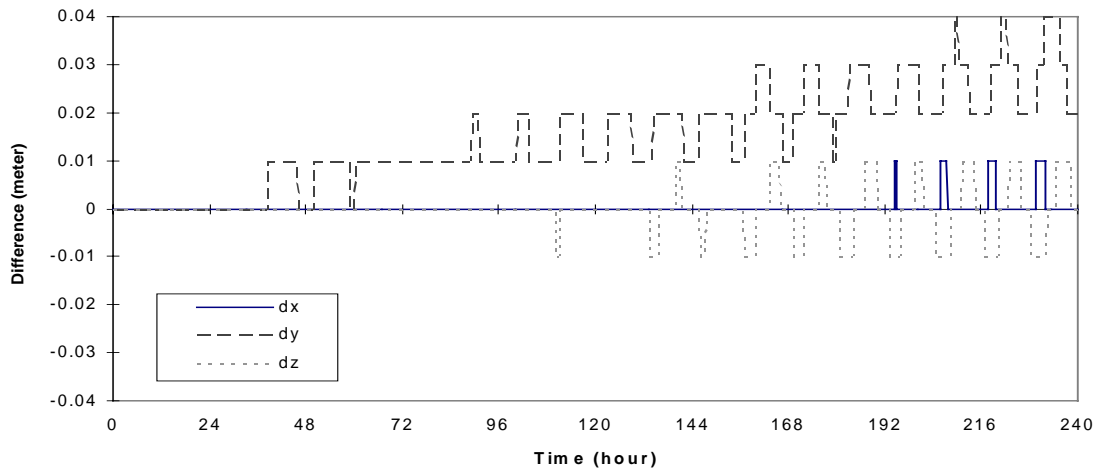
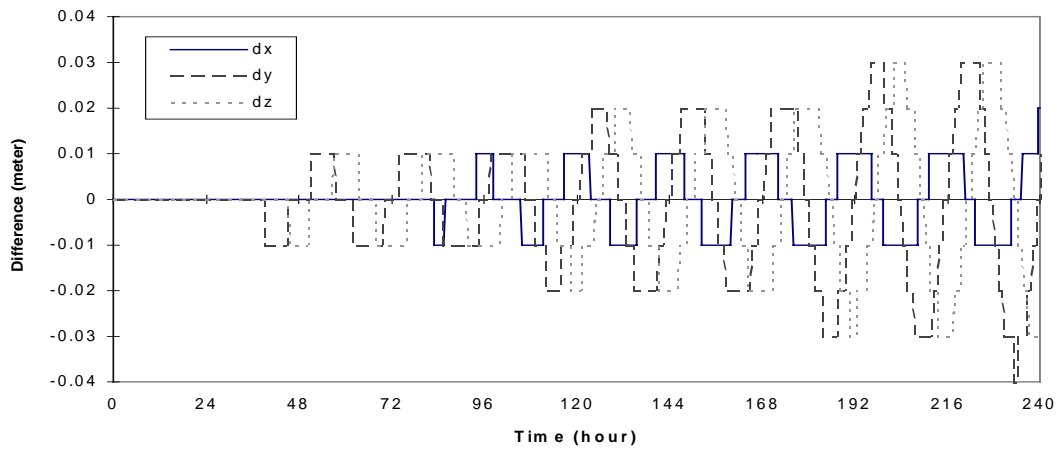
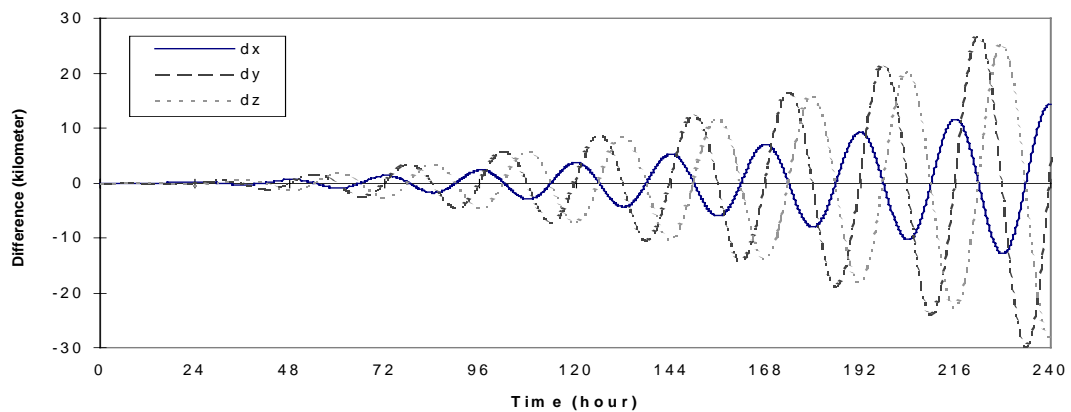
(Satellite Parameters:  $a=42164.174\text{km}$ ,  $\lambda=20^\circ$ ,  $i=63^\circ$ )

Perturbation Force	Acceleration ( $\text{m/sec}^2$ )	Orbit Errors (m)	
		One Day	Ten Days
$2 \leq n \leq 10, 1 \leq m \leq n$	$6 \times 10^{-8}$	371	31.6(km)
$3 \leq n \leq 10, 1 \leq m \leq n$	$2 \times 10^{-9}$	21.2	205.4
$4 \leq n \leq 10, 1 \leq m \leq n$	$9 \times 10^{-10}$	0.65	109.7
$5 \leq n \leq 10, 1 \leq m \leq n$	$1 \times 10^{-10}$	0.09	2.21
$6 \leq n \leq 10, 1 \leq m \leq n$	$1 \times 10^{-11}$	0.02	0.62
$7 \leq n \leq 10, 1 \leq m \leq n$	$4 \times 10^{-12}$	0.00	0.21
$8 \leq n \leq 10, 1 \leq m \leq n$	$2 \times 10^{-13}$	0.00	0.03
$9 \leq n \leq 10, 1 \leq m \leq n$	$7 \times 10^{-14}$	0.00	0.00
$n=10, 1 \leq m \leq n$	$3 \times 10^{-15}$	0.00	0.00

The detailed results on the effect of geopotential perturbation on IGSO satellite orbit are shown by the following figures.

Figure 5-1 The Effect of Geopotential Perturbation Model with  $2 \leq n \leq 10, 0 \leq m \leq n$

Figure 5-2 The Effect of Geopotential Perturbation  $J_2$  TermFigure 5-3 The Effect of Geopotential Perturbation  $J_3$  TermFigure 5-4 The Effect of Geopotential Perturbation  $J_4$  Term

Figure 5-5 The Effect of Geopotential Perturbation  $J_5$  TermFigure 5-6 The Effect of Geopotential Perturbation  $J_6$  TermFigure 5-7 The Effect of Geopotential Perturbation Sectorial and Tesseral Terms,  $2 \leq n \leq 10$ ,  $1 \leq m \leq n$



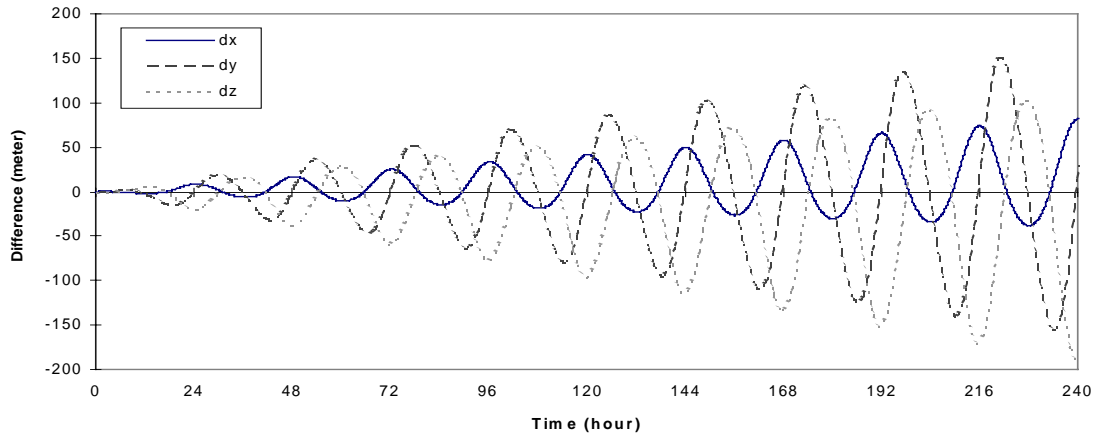


Figure 5-8 The Effect of Geopotential Perturbation Sectorial and Tesseral Terms,  $3 \leq n \leq 10, 1 \leq m \leq n$

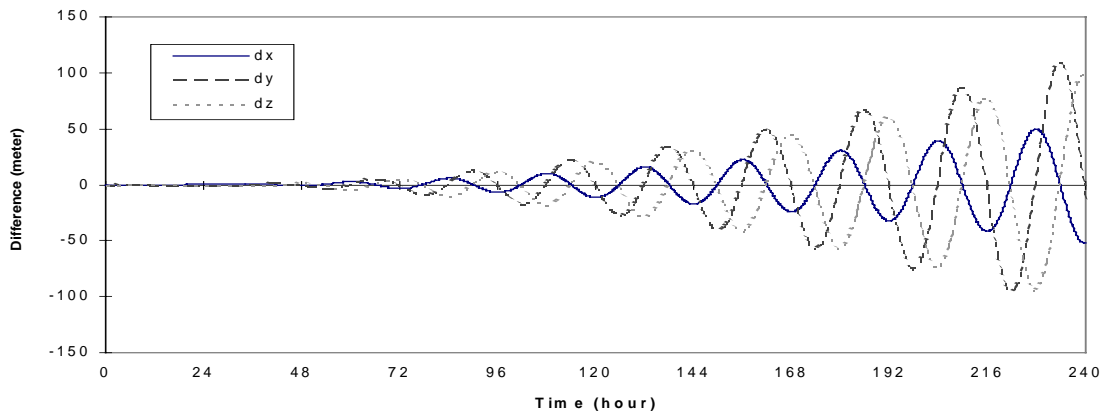


Figure 5-9 The Effect of Geopotential Perturbation Sectorial and Tesseral Terms,  $4 \leq n \leq 10, 1 \leq m \leq n$

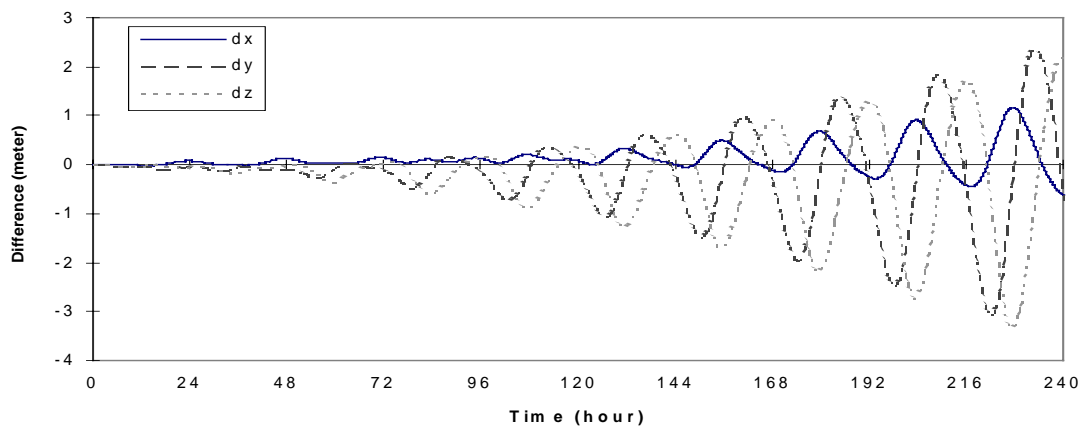


Figure 5-10 The Effect of Geopotential Perturbation Sectorial and Tesseral Terms,  $5 \leq n \leq 10, 1 \leq m \leq n$

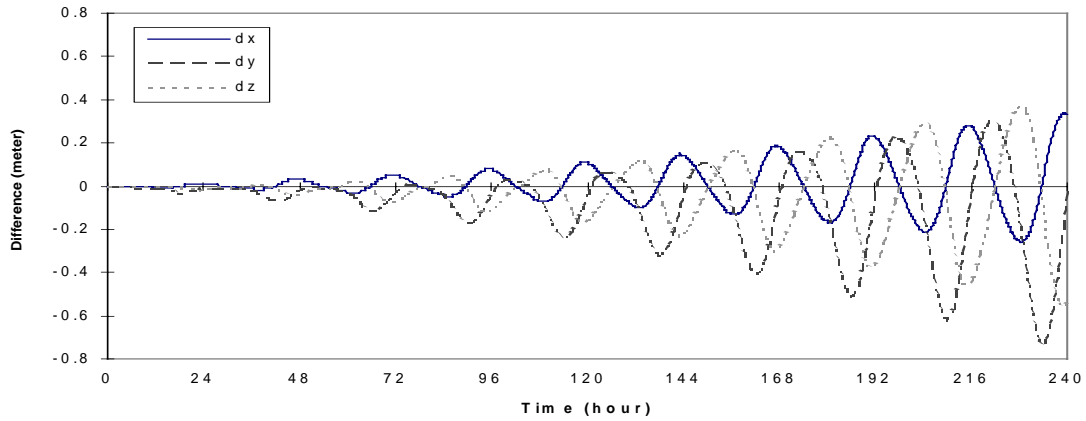


Figure 5-11 The Effect of Geopotential Perturbation Sectorial and Tesseral Terms,  $6 \leq n \leq 10$ ,  $1 \leq m \leq n$

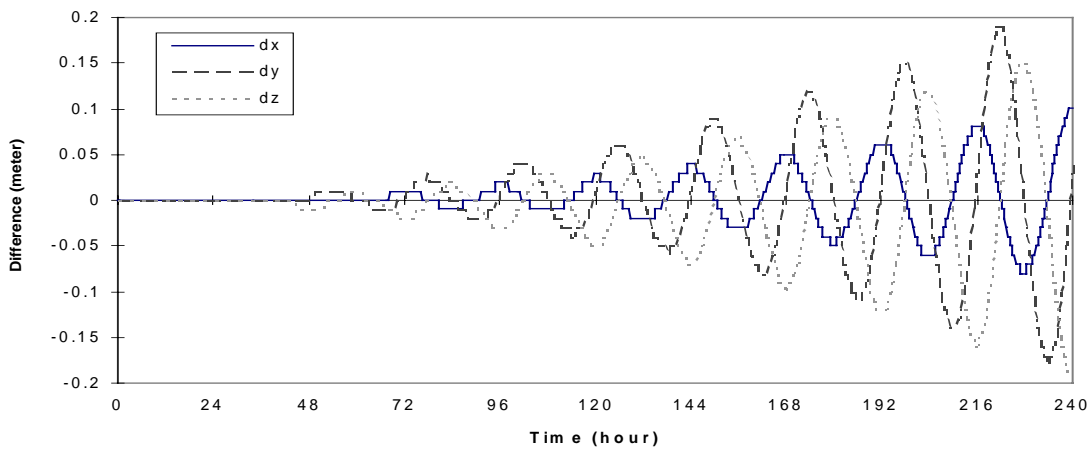
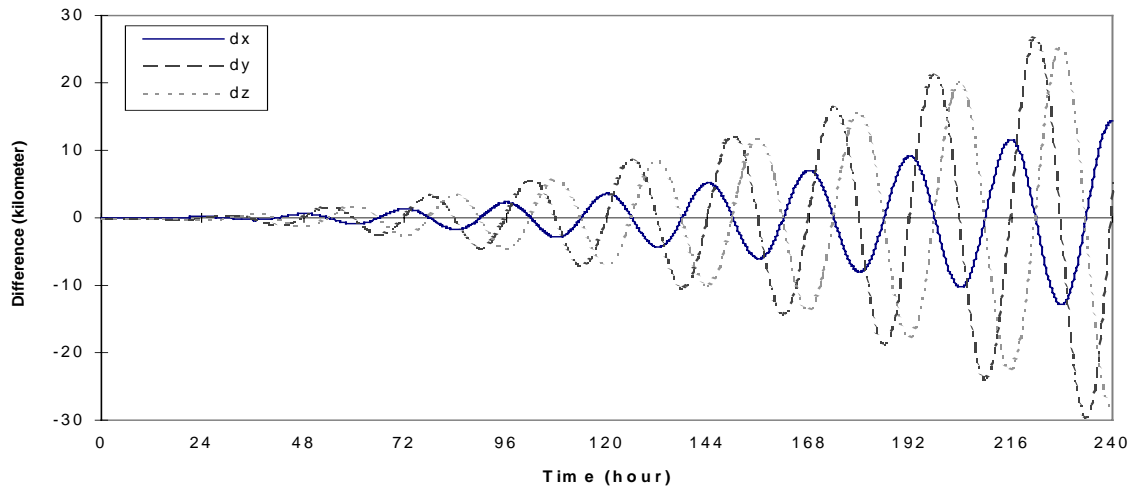


Figure 5-12 The Effect of Geopotential Perturbation Sectorial and Tesseral Terms,  $7 \leq n \leq 10$ ,  $1 \leq m \leq n$

Figure 5-1 shows total effects of geopotential perturbation with degree and order from 2 to 10 ( $2 \leq n \leq 10$ ,  $0 \leq m \leq n$ ). Figure 5-2 to Figure 5-6 show effects of geopotential perturbation of zonal terms ( $J_2$  to  $J_6$ ). Figure 5-7 to Figure 5-12 illustrate the effects of geopotential perturbation of sectorial and tesseral parts. Comparing Figure 5-1 with Figure 5-2 it can be seen that there are almost same change phases and periods in these two figures, which means that in total geopotential perturbation, zonal term  $J_2$  plays a major role (see Fig. 5-2). Interesting is that the even order terms have the same change phases and periods as the total perturbation effects, odd order terms have reverse phases that act as reducing the effects of the even order terms.

From Table 5-1 and Table 5-2 and Figure 5-12, it can be found that the geopotential model whose degree and order are more than 6 has an effect of max. 3 cm on IGSO satellite after ten days, thus the effect of geopotential model with degree more than 6 may be neglected in the satellite dynamic model if the accuracy of orbit determination to be within one meter is required.

Also from Figure 5-7 and Figure 5-8 there are some resonant phenomenon existing. According to Blitzer (1966), the coefficients of geopotential  $C_{22}$ ,  $S_{22}$  are resonant terms for 24 hour satellite. The resonant term means that if the force frequency is equal to the natural frequency of the satellite orbital motion, a dynamical resonance occurs. In other words, the influence of geopotential perturbations from these two coefficients on 24-hour satellite like GEO and IGSO are significantly increased. Figure 5-13 shows the effects of these two resonant terms on IGSO satellite. Although there are other resonant terms, for example,  $C_{31}$ ,  $S_{31}$ ,  $C_{32}$ ,  $S_{32}$ ,  $C_{33}$ ,  $S_{33}$ ,  $C_{41}$ ,  $S_{41}$ ,  $C_{42}$ ,  $S_{42}$ , etc., but compared to  $C_{22}$ ,  $S_{22}$ , the effects from these terms are very small.

Figure 5-13 The Effect of Geopotential Perturbation Model  $C_{22},S_{22}$ 

### 5.1.3.2 Geopotential Influence on GEO Satellite

The following results are for geostationary (GEO) satellites. A GEO orbit is one where the orbit has the same period as IGSO satellite (24 hour), but remains at a fixed point in the sky at all times and stationary over a single point on the Earth's surface. Obviously, a GEO satellite is a special case of IGSO satellite with inclination of orbit  $i=0$ .

The effects of geopotential on GEO satellite orbit are shown in Table 5-3 and Table 5-4.

Table 5-3 The Effect of Geopotential Perturbation on Geostationary Satellite Orbit

(Zonal Part )

(Satellite Parameters:  $a=42164.174km$ ,  $\lambda=20^\circ$ ,  $i=0^\circ$ )

Perturbation Force	Acceleration ( $m/sec^2$ )	Orbit Errors (m)	
		One Day	Ten Days
$J_2$	$8 \times 10^{-6}$	19.7 (km)	196 (km)
$J_3$	$3 \times 10^{-9}$	0.00	0.02
$J_4$	$3 \times 10^{-10}$	0.84	8.42
$J_5$	$7 \times 10^{-12}$	0.00	0.00
$J_6$	$3 \times 10^{-12}$	0.01	0.07
$J_7$	$3 \times 10^{-13}$	0.00	0.00
$J_8$	$3 \times 10^{-14}$	0.00	0.01
$J_9$	$3 \times 10^{-15}$	0.00	0.00
$J_{10}$	$9 \times 10^{-16}$	0.00	0.00

Table 5-4 The Effect of Geopotential Perturbation on Geostationary Satellite Orbit  
 (Sectorial and Tesseral Part)  
 (Satellite Parameters:  $a=42164.174km$ ,  $\lambda=20^\circ$ ,  $i=0^\circ$ )

Perturbation Force	Acceleration ( $m/sec^2$ )	Orbit Errors (m)	
		One Day	Ten Days
$2 \leq n \leq 10, 1 \leq m \leq n$	$6 \times 10^{-8}$	656	58.3 (km)
$3 \leq n \leq 10, 1 \leq m \leq n$	$2 \times 10^{-9}$	12.6	1200
$4 \leq n \leq 10, 1 \leq m \leq n$	$9 \times 10^{-10}$	2.15	121.9
$5 \leq n \leq 10, 1 \leq m \leq n$	$1 \times 10^{-10}$	0.18	40.1
$6 \leq n \leq 10, 1 \leq m \leq n$	$1 \times 10^{-11}$	0.01	0.72
$7 \leq n \leq 10, 1 \leq m \leq n$	$4 \times 10^{-12}$	0.00	0.77
$8 \leq n \leq 10, 1 \leq m \leq n$	$2 \times 10^{-13}$	0.00	0.05
$9 \leq n \leq 10, 1 \leq m \leq n$	$7 \times 10^{-14}$	0.00	0.05
$n=10, 1 \leq m \leq n$	$3 \times 10^{-15}$	0.00	0.00

The detailed information on the effects of geopotential perturbation on the geostationary satellite orbit can be seen in the following figures.

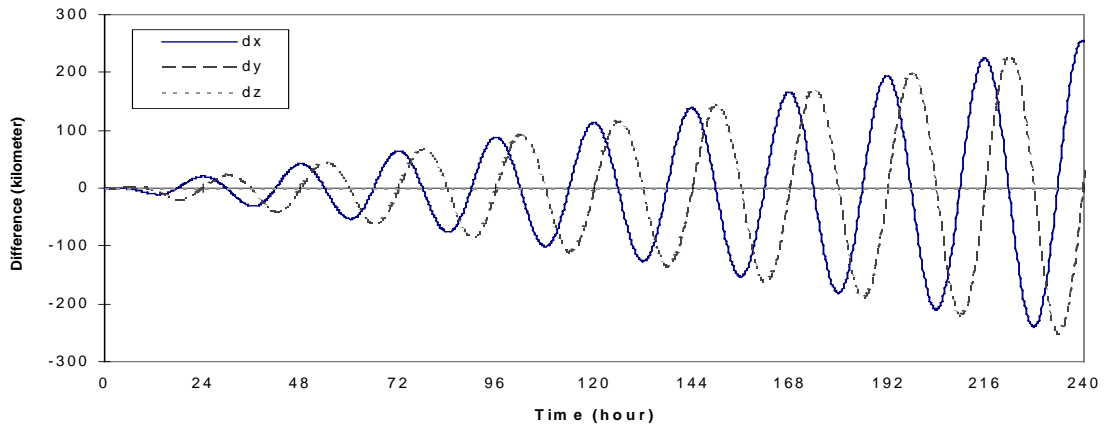


Figure 5-14 The Effect of Geopotential Perturbation Model with  $2 \leq n \leq 10, 0 \leq m \leq n$

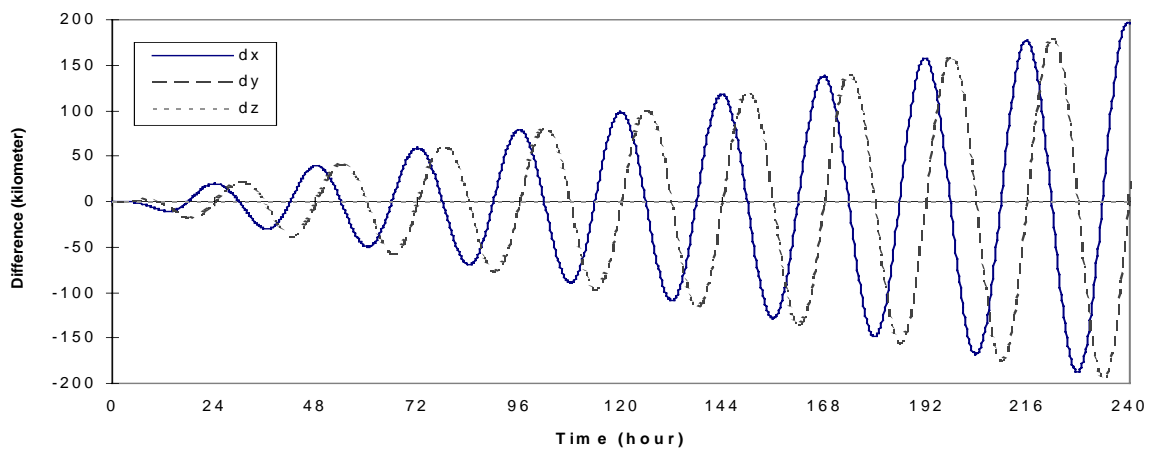


Figure 5-15 The Effect of Geopotential Perturbation  $J_2$  Term

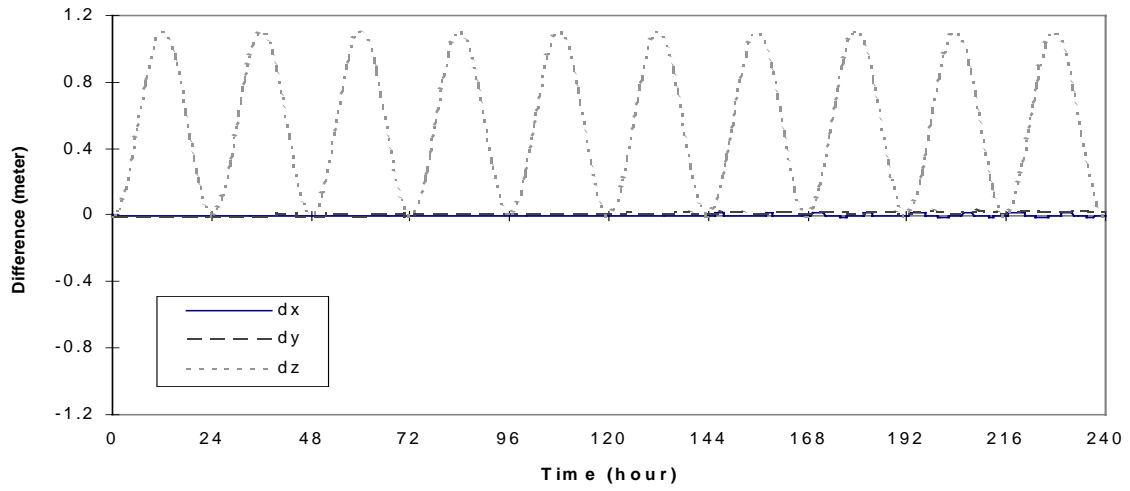


Figure 5-16 The Effect of Geopotential Perturbation  $J_3$  Term

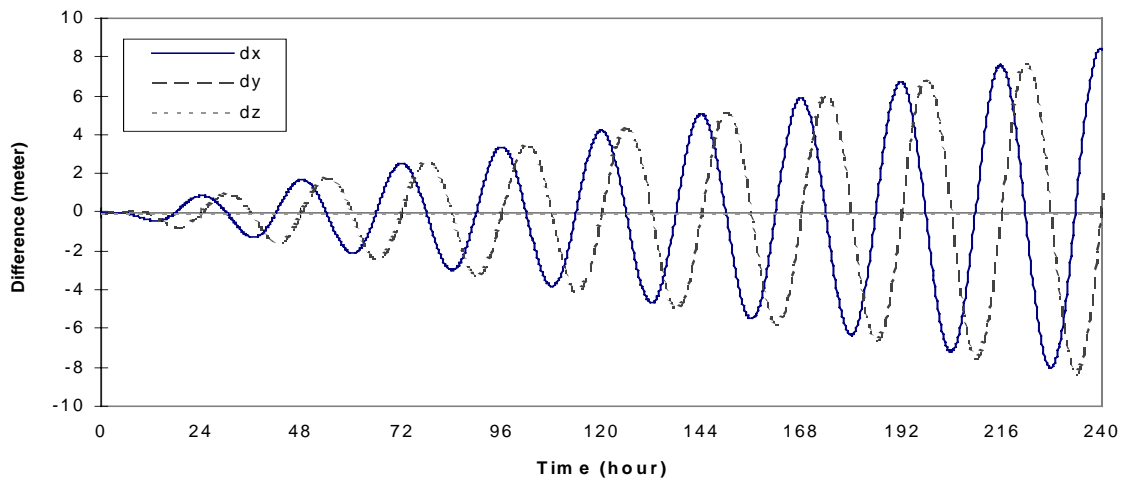


Figure 5-17 The Effect of Geopotential Perturbation  $J_4$  Term

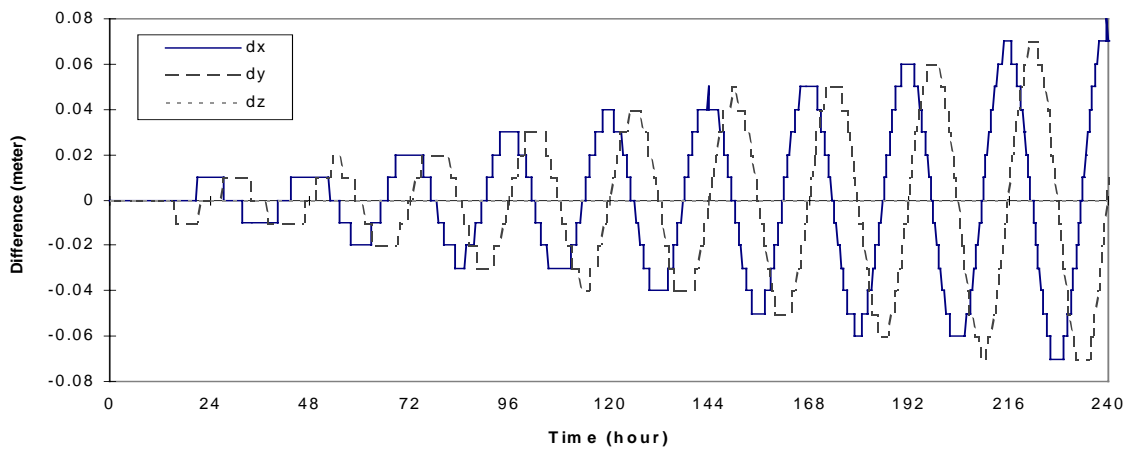


Figure 5-18 The Effect of Geopotential Perturbation  $J_6$  Term

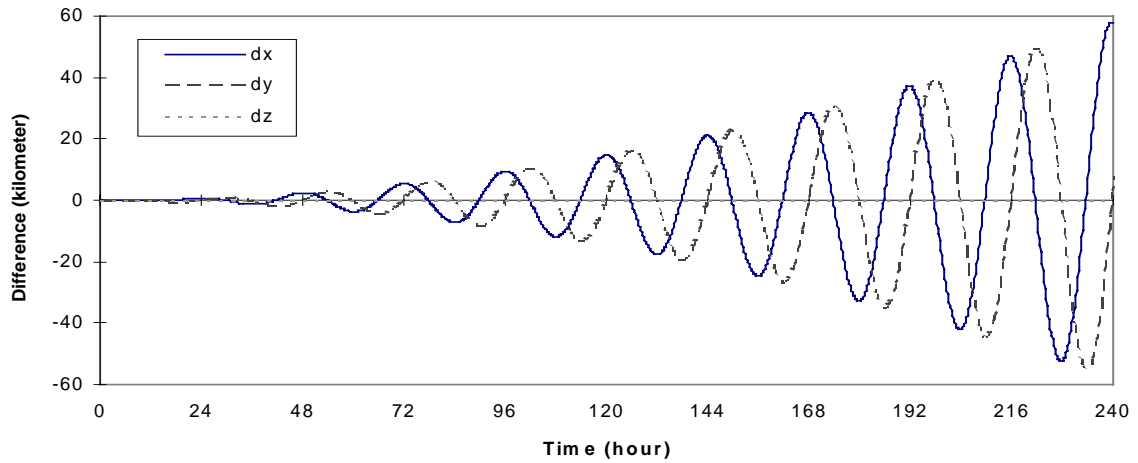


Figure 5-19 The Effect of Geopotential Perturbation Sectorial and Tesseral Terms,  $2 \leq n \leq 10$ ,  $1 \leq m \leq n$

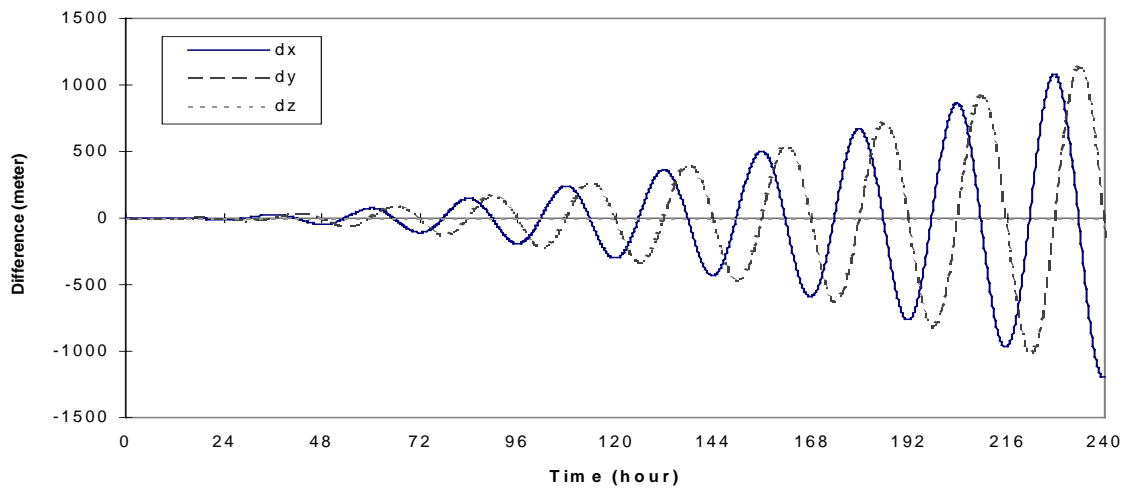


Figure 5-20 The Effect of Geopotential Perturbation Sectorial and Tesseral Terms,  $3 \leq n \leq 10$ ,  $1 \leq m \leq n$

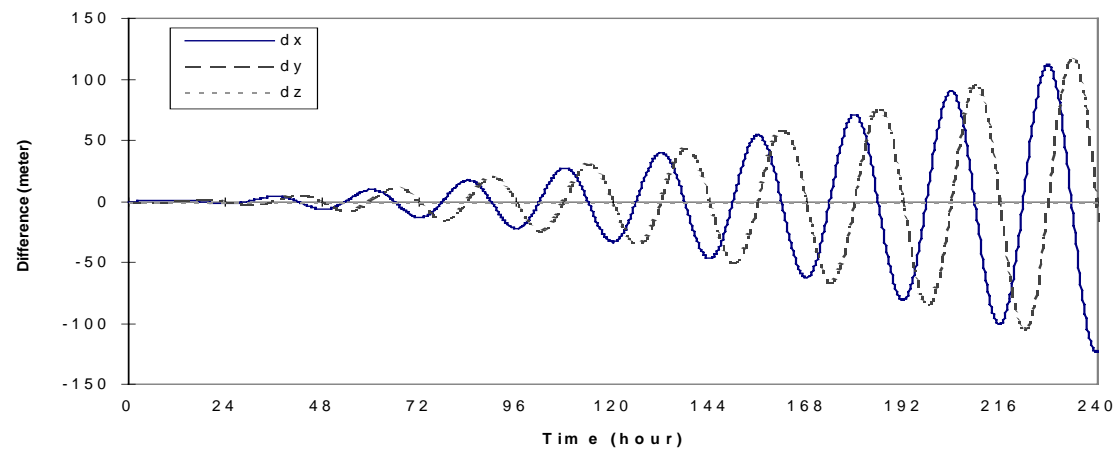


Figure 5-21 The Effect of Geopotential Perturbation Sectorial and Tesseral Terms,  $4 \leq n \leq 10$ ,  $1 \leq m \leq n$

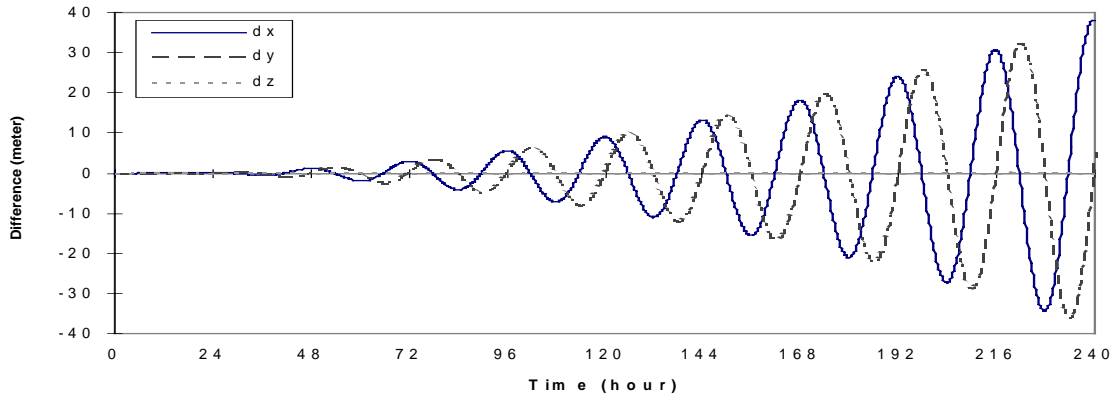


Figure 5-22 The Effect of Geopotential Perturbation Sectorial and Tesseral Terms,  $5 \leq n \leq 10, 1 \leq m \leq n$

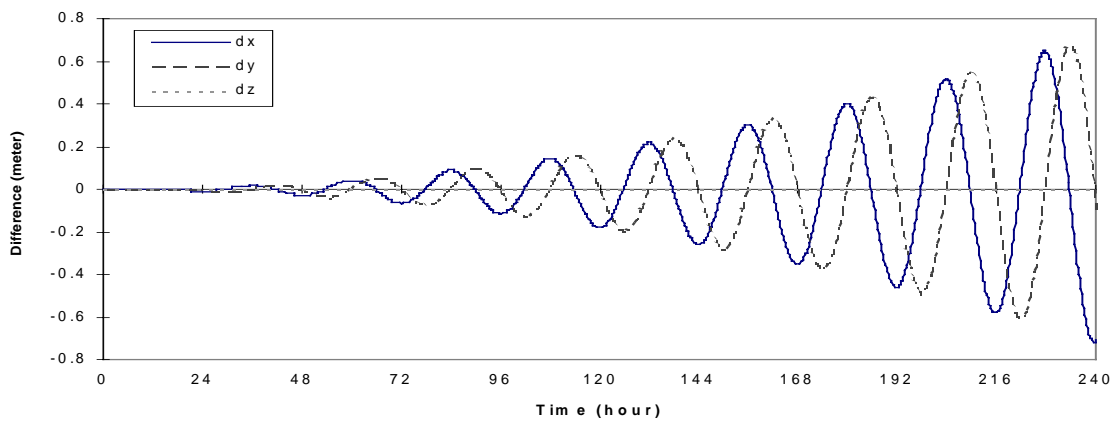


Figure 5-23 The Effect of Geopotential Perturbation Sectorial and Tesseral Terms,  $6 \leq n \leq 10, 1 \leq m \leq n$

From figures above it is clear that the influence of geopotential perturbation on GEO satellites is much larger than that on IGSO satellites. Also very interesting is that for zonal terms, the effects from the odd terms are almost zero, for example, from Eq.(5-1) geopotential  $J_3$  can be written by

$$U_3 = GM \frac{a_e^2}{r^3} J_3 \sin \varphi \left( \frac{5}{2} \sin^2 \varphi - \frac{1}{6} \right) \tag{5-22}$$

for GEO satellite  $\varphi = 0$ , the effect of  $J_3$  becomes zero. Other odd terms of the zonal part show the same property. Due to this reason, the effects of total geopotential perturbation are mainly from the even terms. Actually  $\varphi$  will not be zero for GEO satellites, therefore the effects of odd zonal terms are not totally zero, but very small like  $J_3$  in Figure 5-16.

### 5.1.3.3 Geopotential Influence on MEO (GPS)

Influence of geopotential perturbation on MEO(GPS) satellite is listed in Table 5-5 (Landau,1988).

Table 5-5 The Effect of Geopotential Perturbation on MEO(GPS) Satellite

Perturbation Force	Acceleration ( $m/sec^2$ )	Orbit Errors (m)	
		One Day	7 Days
$J_2$	$5 \times 10^{-5}$	10(km)	100(km)
$C_{nm}, S_{nm}(n,m < 8)$ without $C_{20}$	$3 \times 10^{-7}$	200	3.4(km)
$C_{nm}, S_{nm}(n,m > 8)$	$< 1 \times 10^{-8}$	0.03	0.1

## 5.2 The Solar and Lunar Attractions

Due to the great distance between the Earth and the Sun and between the Earth and Moon, it is unnecessary to take the nonspherical part of the Sun and Moon into account. For this reason, in the perturbation models the Sun and Moon are considered as point mass. The solar and lunar attractions on the satellite may be expressed in the inertial coordinate system as follows

(Kovalevsky 1967, Beutler 1996)

$$\frac{d^2 \vec{r}}{dt^2} = -\frac{\mu}{r^3} \vec{r} + \sum_{i=s,m} \mu_i \left[ \frac{\vec{r}_i - \vec{r}}{|\vec{r}_i - \vec{r}|^3} - \frac{\vec{r}_i}{r_i^3} \right] \quad (5-23)$$

where

$\vec{r}$  position vector of satellite

$\vec{r}_s$  position vector of Sun

$\vec{r}_m$  position vector of Moon

$\mu, \mu_s, \mu_m$  gravity constants of the Earth, Sun and Moon respectively.

In order to evaluate the influences of Sun and Moon on IGSO, GEO and MEO satellites, the accelerations produced by the solar and lunar attractions on IGSO and GEO satellites are computed using JPL Planetary Ephemeris DE200 and Eq.(5-23). The quantities of the accelerations and orbit errors by these two perturbation forces are listed in Table 5-6, Table 5-7 and Table 5-8 as well as are drawn in Figures 5-24, 5-25, 5-26 and 5-27.

Table 5-6 The Effect of Solar and Lunar Attraction on IGSO Satellite

(Satellite Parameters:  $a=42164.174\text{km}$ ,  $\lambda=20^\circ$ ,  $i=63^\circ$ )

Perturbation Force	Acceleration (m/sec <sup>2</sup> )	Orbit Errors (m)	
		One Day	Ten Days
Solar Attraction	$3 \times 10^{-6}$	945	8915
Lunar Attraction	$6 \times 10^{-6}$	2590	77 (km)

Table 5-7 The Effect of Solar and Lunar Attraction on GEO Satellite

(Satellite Parameters:  $a=42164.174\text{km}$ ,  $\lambda=20^\circ$ ,  $i=0^\circ$ )

Perturbation Force	Acceleration (m/sec <sup>2</sup> )	Orbit Errors (m)	
		One Day	Ten Days
Solar Attraction	$3 \times 10^{-6}$	2263	23183
Lunar Attraction	$6 \times 10^{-6}$	2311	14 (km)

Table 5-8 The Effect of Solar and Lunar Attraction on MEO (GPS) Satellite\*

Perturbation Force	Acceleration (m/sec <sup>2</sup> )	Orbit Errors (m)	
		One Day	Ten Days
Solar Attraction	$2 \times 10^{-6}$	800	3500
Lunar Attraction	$5 \times 10^{-6}$	3000	8000

\*Feltens, 1991; Landau, 1988



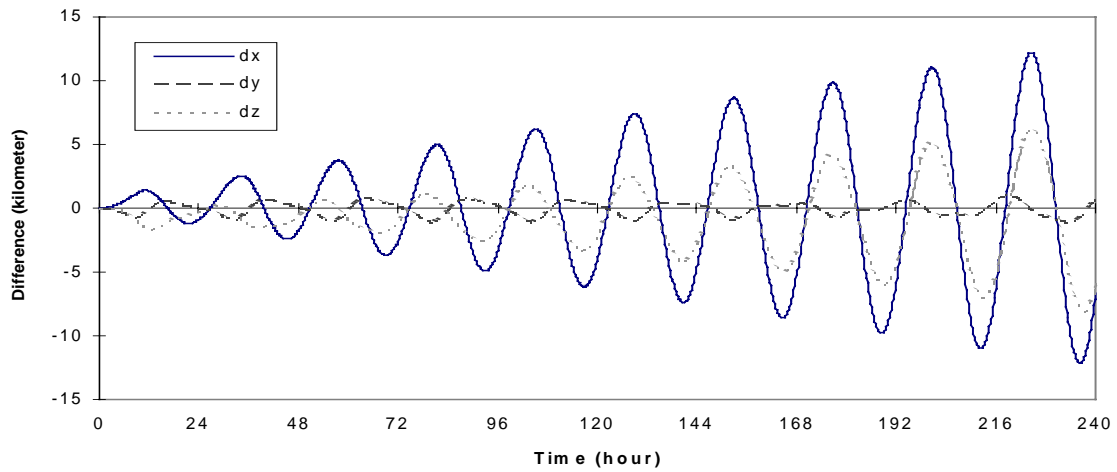


Figure 5-24 The Effect of the Solar Attraction on IGSO Satellite

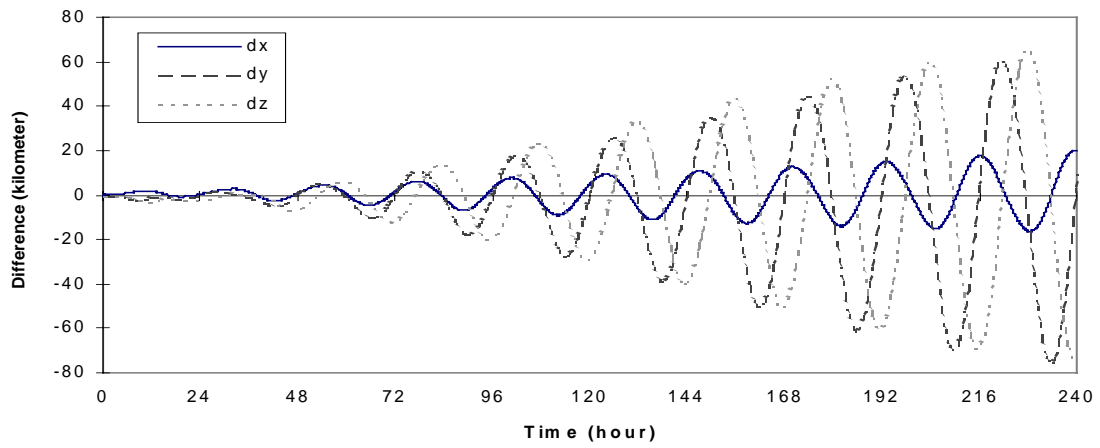


Figure 5-25 The Effect of the Lunar Attraction on IGSO Satellite

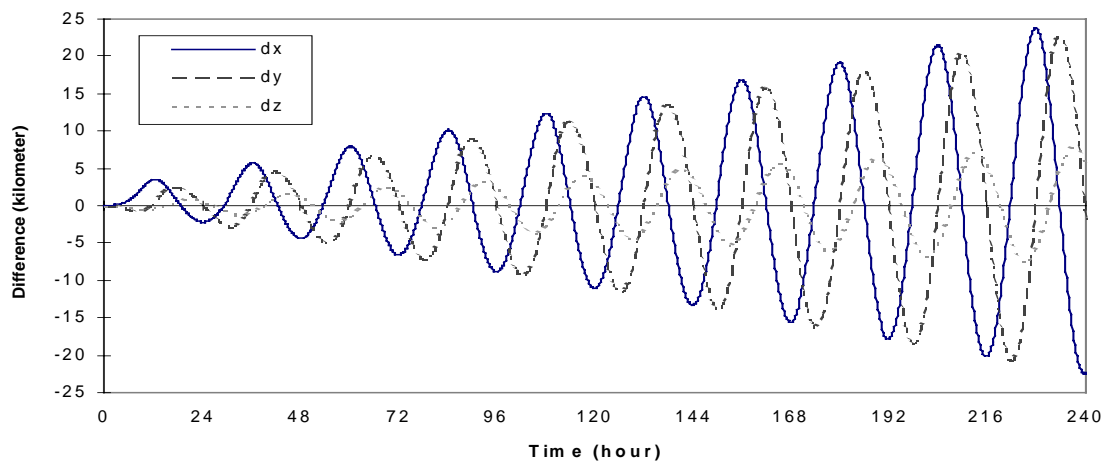


Figure 5-26 The Effect of the Solar Attraction on GEO Satellite

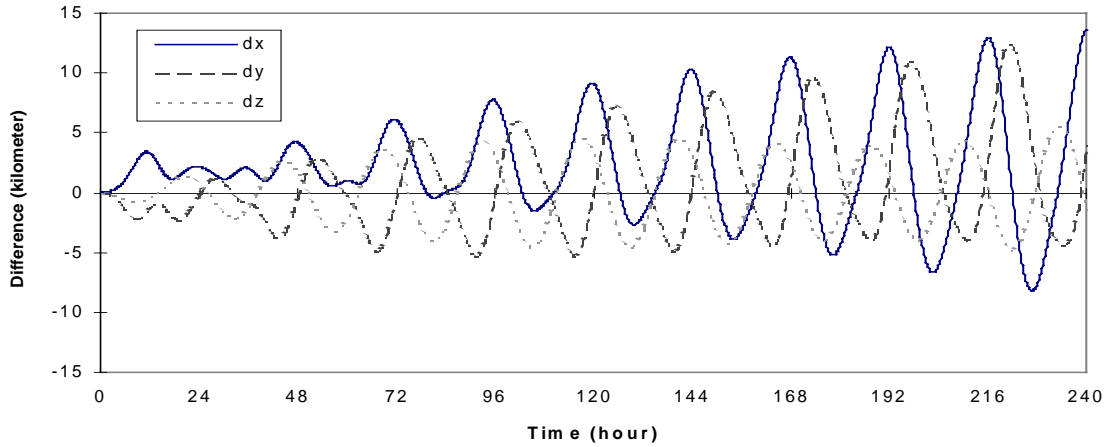


Figure 5-27 The Effect of the Lunar Attraction on GEO Satellite

### 5.3 The Solar Radiation Pressure Model

The effect of solar radiation pressure on satellite orbit can be divided into two categories, i.e. direct radiation and earth albedo radiation. Because IGSO, GEO and MEO satellites are much far away from the earth surface, the earth albedo radiation has small influence on these types of satellites and can be neglected. Therefore only the direct radiation pressure should be considered in the satellite dynamic models.

#### 5.3.1 Direct Radiation Pressure

For the direct radiation it means the satellite absorbs the entire solar radiation. If assuming the satellite is a perfect sphere, the perturbing acceleration of direct radiation pressure may be written by (Beutler 1996)

$$\vec{a}_d = \mu \left\{ P_s C_r \frac{A}{m} a_s^2 \frac{\vec{r} - \vec{r}_s}{|\vec{r} - \vec{r}_s|^3} \right\} \quad (5-24)$$

where

$\vec{a}_d$  acceleration due to the direct radiation pressure,

$\mu$  eclipse factor (=1 if the satellite is in sunlight,  
=0 if the satellite is in the Earth shadow,  
 $0 < \mu < 1$  if the satellite is in the Penumbra),

$A/m$  cross-section area of the satellite as seen from the Sun divided by its mass,

$a_s$  astronomical unit(AU)

$P_s = E / c$  radiation pressure for a completely absorbing object with  $A/m=1$  at the distance of one astronomical unit. ( $E$  is the solar constant,  $c$  the velocity of light),

$C_r$  reflection coefficient,

$\vec{r}, \vec{r}_s$  geocentric coordinates of satellite and Sun respectively.

If the GEO, IGSO and MEO satellites are assumed like GPS to be composed of a number of flat or cylindrical surfaces, each of which absorbs and reflects the solar light. Following Fliegel et al(1992), for the flat surfaces the components of the acceleration due to radiation pressure are expressed by

Normal

$$F_{1,N} = -\left(A \frac{E}{c}\right)(1 + \mu\nu) \cos^2 \theta \quad (5-25)$$

Shear

$$F_{1,S} = -\left(A \frac{E}{c}\right)(1 - \mu\nu) \sin \theta \cos \theta \quad (5-26)$$

Diffuse

$$F_{1,D} = -\frac{2}{3} \left( A \frac{E}{c} \right) \nu (1 - \mu) \cos \theta \quad (5-27)$$

where

- $\nu$  reflectivity, ranging from 0 (black) to 1 (white),
  - $\mu$  specularity, ranging from 0 (diffuse) to 1 (specular),
  - $\theta$  angle between the incoming solar ray and the normal to the flat surface,
- other symbols are the same as Eq.(5-24).

For the cylindrical surfaces the component of the acceleration due to radiation pressure can be written by Normal

$$F_{2,N} = -\left( A \frac{E}{c} \right) \left( 1 + \frac{\mu \nu}{3} \right) \cos^2 \theta \quad (5-28)$$

Shear

$$F_{2,S} = -\left( A \frac{E}{c} \right) (1 - \mu \nu) \sin \theta \cos \theta \quad (5-29)$$

Diffuse

$$F_{2,D} = -\frac{\pi}{6} \left( A \frac{E}{c} \right) \nu (1 - \mu) \cos \theta \quad (5-30)$$

For total acceleration, the accelerations from each surface are summed as

$$F_{N,\Sigma} = \sum_{i=1}^K F_{N,i} \quad (5-31)$$

$$F_{S,\Sigma} = \sum_{i=1}^K F_{S,i} \quad (5-32)$$

$$F_{D,\Sigma} = \sum_{i=1}^K F_{D,i} \quad (5-33)$$

The parameters in Eq.(5-28) to Eq.(5-30) are dependent on satellite profile. Fliegel et al (1992) give a simple formula for GPS components of total radiation accelerations in SV-body coordinate system, i.e.

$$\left. \begin{aligned} X &= -4.55 \sin(B) + 0.08 \sin(2B + 0.9) - 0.06 \cos(4B + 0.08) + 0.08 \\ Z &= -4.54 \cos(B) + 0.20 \sin(2B - 0.3) - 0.03 \sin(4B) \end{aligned} \right\} \quad (5-34)$$

where

$B$  the angle between the Sun and +Z axis.

All above formulas must be divided by satellite mass  $m_s$ . SV-body coordinate system is defined as follows: the +Z direction is toward the Earth and therefore along the SV antennas. The +X direction is positive toward the half plane that contains the Sun, and +Y completes a right-handed system and points along one of the solar panel center beams. Assuming  $\vec{r}$  represents a position vector of the satellite in the inertial system,  $\vec{r}_s$  a position vector of the Sun, also in the inertial system, then SV-body unit vector in the inertial system can be written as

$$\vec{u}_y = \frac{\vec{r} \times (\vec{r} - \vec{r}_s)}{|\vec{r} \times (\vec{r} - \vec{r}_s)|} \quad (5-35)$$

$$\vec{u}_z = -\frac{\vec{r}}{|\vec{r}|} \quad (5-36)$$

$$\vec{u}_x = \vec{u}_y \times \vec{u}_z \quad (5-37)$$

The acceleration due to direct radiation pressure according to Fliegel model which is also in the inertial coordinate system may be written by

$$\vec{a}_d = \mu \frac{a_s^2}{|\vec{r} - \vec{r}_s|^2 m} (X \vec{u}_x + Z \vec{u}_z) \times 10^{-5} \quad (5-38)$$

For actual orbit determination, the imperfect of the direct radiation model should be considered, therefore some unmodeled direct radiation errors are estimated during orbit determination. Rewriting Eq.(5-24) as follows

$$\frac{\ddot{\omega}}{a_d} = \mu \left\{ P_s (1 + \alpha + \alpha \Delta t) \frac{A}{m} a_s^2 \frac{\frac{\omega}{r-r_s} \frac{\omega}{r-r_s}}{|\frac{\omega}{r-r_s}|^3} \right\} \quad (5-39)$$

$\alpha$  can be considered as unmodeled errors of reflection coefficient  $C_r$ , which changes with time.  $C_r$  in Eq.(5-24) can be written as

$$C_r = C_r^0 + C_r^1 \quad (5-40)$$

where

$$C_r^0 = 1 + \alpha$$

$$C_r^1 = \alpha \Delta t$$

i.e. Eq.(5-24) becomes

$$\begin{aligned} \frac{\ddot{\omega}}{a_d} &= \mu \left\{ P_s C_r \frac{A}{m} a_s^2 \frac{\frac{\omega}{r-r_s} \frac{\omega}{r-r_s}}{|\frac{\omega}{r-r_s}|^3} \right\} \\ &= \mu \left\{ P_s C_r^0 \frac{A}{m} a_s^2 \frac{\frac{\omega}{r-r_s} \frac{\omega}{r-r_s}}{|\frac{\omega}{r-r_s}|^3} \right\} + \mu \left\{ P_s \alpha \Delta t \frac{A}{m} a_s^2 \frac{\frac{\omega}{r-r_s} \frac{\omega}{r-r_s}}{|\frac{\omega}{r-r_s}|^3} \right\} \end{aligned} \quad (5-41)$$

In Eq.(5-41), the first term can be calculated by mathematic model like Rock4 (Fliegel et al 1992, McCarthy 1992), the second term is solved during data processing of orbit determination.

### 5.3.2 Effect of Eclipses

In order to process the solar direct radiation, another problem, the sun eclipse, should be considered, i.e. how to process the satellite orbit when satellite is inside the shadow of the Earth. The effect of the eclipse is a difficult problem for satellite orbit determination, especially when satellite is in the penumbra. For the eclipse problem, the simple cylinder model can be used for computation of the shadow of the Earth. According to this simple model, for MEO (GPS) satellite, when the angle between the Sun and the +Z direction of the SV-body system of the satellite, is less than about  $14^\circ$ , the Sun is eclipsed, i.e. the satellite is inside the shadow of the Earth; for IGSO and GEO satellites with about 36000 km altitude from the surface of the Earth, the eclipse angle is about  $8.6^\circ$ , i.e. when the angle between the Sun and the +Z direction of the SV-body system of the satellite is less than about  $8.6^\circ$ , the satellite is inside the shadow of the Earth, see Figure 5-28.

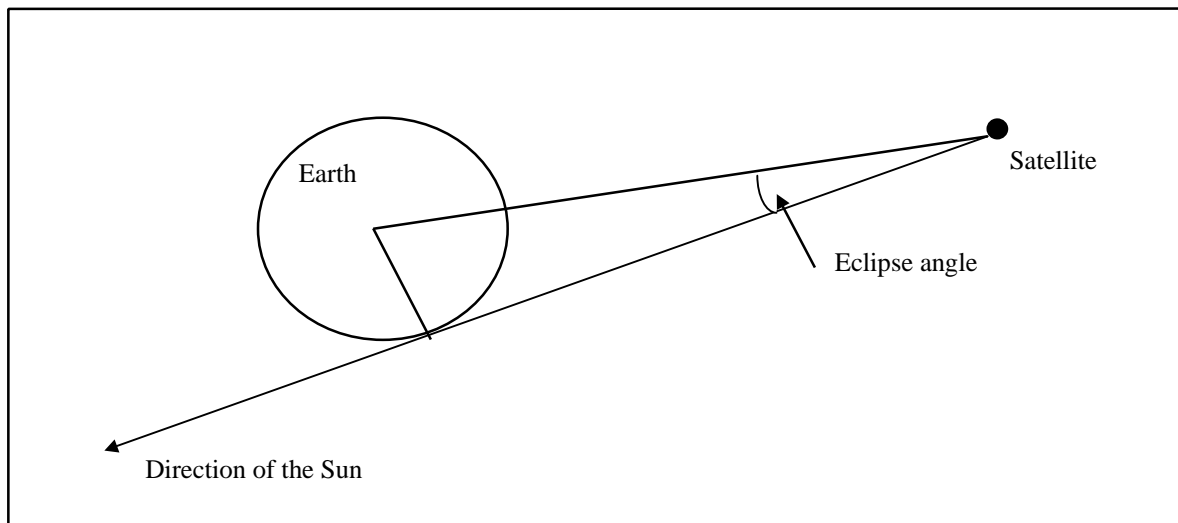


Figure 5-28 The Eclipse Angle of IGSO and GEO Satellites

Although this simple model can be used to check if the satellite is in the shadow of the Earth, the non-continuity of the solar radiation in force model due to the satellite entering the shadow of the earth will have problem in the orbit integration. During an eclipse, the satellite passes continuously from sunlight to shadow of the Earth, but

for orbit integration, continuous property may not be kept due to the size of integration step. The simple method to solve this problem is to use tuning parameters, which constructs transition status smoothly from sunlight to shadow. The shadow problem, however, still needs to be further improved for IGSO, GEO and MEO satellites, but this is dependent on actual design and profile of GNSS-2 satellites.

The effects of solar direct radiation on IGSO, GEO and MEO satellites are listed in Table 5-9, Table 5-10 and Table 5-11 as well as drawn in Figures 5-29 and 5-30.

Table 5-9 The Effect of Solar Radiation Pressure on IGSO Satellite

(Satellite Parameters:  $a=42164.174\text{km}$ ,  $\lambda=20^\circ$ ,  $i=63^\circ$ )

Perturbation Force	Acceleration ( $\text{m}/\text{sec}^2$ )	Orbit Errors (m)	
		One Day	Ten Days
Solar Radiation	$1 \times 10^{-7}$	317	3227

Table 5-10 The Effect of Solar Radiation Pressure on GEO Satellite

(Satellite Parameters:  $a=42164.174\text{km}$ ,  $\lambda=20^\circ$ ,  $i=0^\circ$ )

Perturbation Force	Acceleration ( $\text{m}/\text{sec}^2$ )	Orbit Errors (m)	
		One Day	Ten Days
Solar Radiation	$1 \times 10^{-7}$	317	3253

Table 5-11 The Effect of Solar Radiation Pressure on MEO Satellite

Perturbation Force	Acceleration ( $\text{m}/\text{sec}^2$ )	Orbit Errors (m)	
		One Day	Ten Days
Solar Radiation	$6 \times 10^{-8}$	200	1000

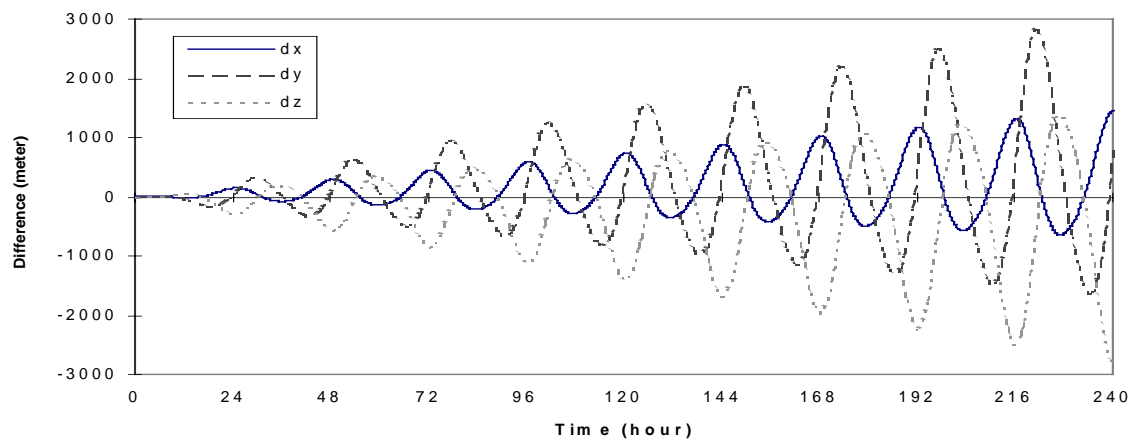


Figure 5-29 Effect of the Solar Radiation on Inclined Geosynchronous Satellite

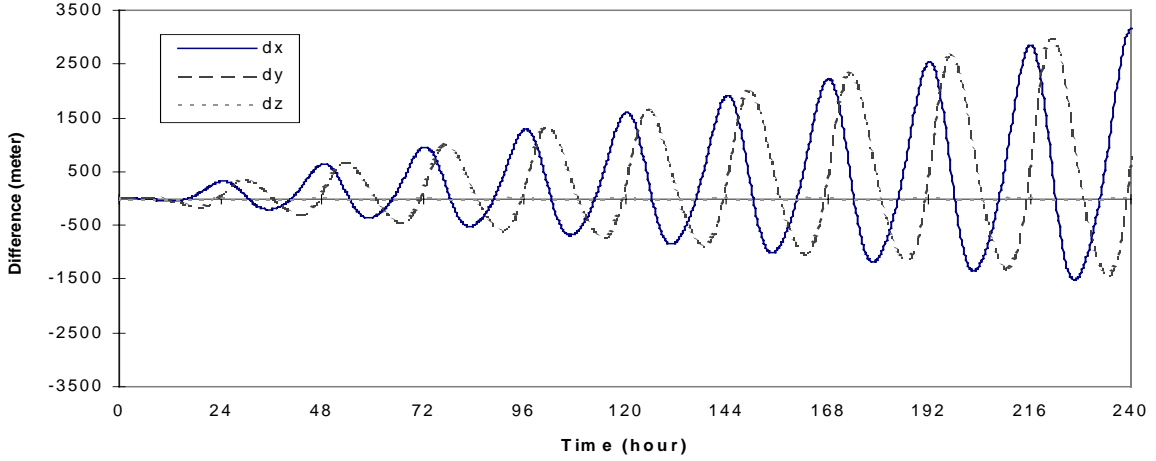


Figure 5-30 Effect of the Solar Radiation on Inclined Geostationary Satellite

## 5.4 Other Perturbations

Other important perturbations such as ocean tide, solid earth tide, permanent tide, station displacement due to Pole tide and solid earth tide, ocean loading and so on have very small influences on IGSO and GEO satellites compared to the perturbations discussed above, but to MEO satellite (like GPS) some of these perturbations may be considered.

### 5.4.1 Solid Earth Tides

Actually the earth can be considered as the elastic one, the attraction of the Sun and Moon on the earth will cause the earth mass to respond periodically by deforming and thus changing the earth's geopotential and displacing the tracking station positions. This phenomenon is called solid earth tides. According to McCarthy (1992), solid earth tides are most easily modeled as variations in the standard geopotential coefficients  $C_{nm}$  and  $S_{nm}$ , and can be calculated by two steps. First step uses a frequency independent Love number  $\kappa_2$  (assuming  $\kappa_2 = 0.3$ ) and an evaluation of the tidal potential in the time domain from a lunar and solar ephemeris. The changes in normalized second degree geopotential coefficients for this step can be describes as follows

$$\Delta \bar{C}_{20} = \frac{1}{\sqrt{5}} \kappa_2 \frac{R_e^3}{GM_\oplus} \sum_{j=2}^3 \frac{GM_j}{r_j^3} P_{20}(\sin \phi_j) \quad (5-42)$$

$$\Delta \bar{C}_{21} = \frac{1}{3} \sqrt{\frac{3}{5}} \kappa_2 \frac{R_e^3}{GM_\oplus} \sum_{j=2}^3 \frac{GM_j}{r_j^3} P_{21}(\sin \phi_j) \cos \lambda_j \quad (5-43)$$

$$\Delta \bar{S}_{21} = \frac{1}{3} \sqrt{\frac{3}{5}} \kappa_2 \frac{R_e^3}{GM_\oplus} \sum_{j=2}^3 \frac{GM_j}{r_j^3} P_{21}(\sin \phi_j) \sin \lambda_j \quad (5-44)$$

$$\Delta \bar{C}_{22} = \frac{1}{12} \sqrt{\frac{12}{5}} \kappa_2 \frac{R_e^3}{GM_\oplus} \sum_{j=2}^3 \frac{GM_j}{r_j^3} P_{22}(\sin \phi_j) \cos \lambda_j \quad (5-45)$$

$$\Delta \bar{S}_{22} = \frac{1}{12} \sqrt{\frac{12}{5}} \kappa_2 \frac{R_e^3}{GM_\oplus} \sum_{j=2}^3 \frac{GM_j}{r_j^3} P_{22}(\sin \phi_j) \sin \lambda_j \quad (5-46)$$

where

$\kappa_2$  nominal second degree Love number

$R_e$  equatorial radius of the Earth

$GM_\oplus$  gravitational parameter for the Earth

$GM_j$  gravitational parameter for the Moon ( $j=2$ ) and Sun ( $j=3$ )

- $r_j$  distance from geocenter to Moon or Sun  
 $\phi_j$  body fixed geocentric latitude of Moon or Sun  
 $\lambda_j$  body fixed east longitude (from Greenwich) of Sun or Moon

$r_j, \phi_j$  and  $\lambda_j$  can be calculated by using JPL Planetary Ephemeris DE200.

But Love number  $\kappa_2$  is not constant according to Wahr model (Wahr, 1981) and dependent on the frequency. Thus the second step corrects the geopotential change computed in the first step by using the frequency dependent Love numbers. The changes in normalized coefficients from step 2 are

$$\Delta\bar{C}_{nm} - i\Delta\bar{S}_{nm} = A_m \sum_{s(n,m)} \delta\kappa_s H_s \begin{pmatrix} 1 \\ -i \end{pmatrix} \begin{matrix} n+m & \text{even} \\ n+m & \text{odd} \end{matrix} e^{i\theta_s} \quad (5-47)$$

where

$$A_m = \frac{(-1)^m}{R_e \sqrt{4\pi(2 - \delta_{om})}}, \quad \delta_{om} = \begin{cases} 1 & m=0 \\ 0 & m \neq 0 \end{cases}$$

- $\delta\kappa_s$  difference between Wahr model for  $\kappa$  at frequency  $s$  and the nominal value  $\kappa_2$  in the sense  $\kappa_s - \kappa_2$   
 $H_s$  amplitude (m) of term at frequency  $s$  from the Cartwright and Tayler (1971) and Cartwright and Edden (1973) harmonic expansion of the tide generating potential.

The accelerations of IGSO and GEO satellite caused by solid earth tides are about  $4.0 \times 10^{-10} \text{ m/s}^2$ ; the acceleration of MEO (GPS) satellite is about  $3 \times 10^{-9} \text{ m/s}^2$  (Landau, 1988, Feltens 1991). From Table 5-1 to Table 5-4 we can conclude that the solid earth tides will cause the orbit errors of IGSO and GEO satellite about 0.10 m after one day arc; for MEO satellite the orbit error about 0.3 m (Landau, 1988), therefore this perturbation effect can be neglected from the satellite dynamical model for real-time orbit determination, because usually update step in orbit determination is short than 10 minutes and the influence from solid earth tides is very small; but for long period of orbit prediction or batch processing for post-processing, the solid earth tides should be included in the satellite dynamical models.

The solid earth tides also displace the tracking station coordinates. According to Chadwell (1995, pp.30), the correction has a maximum at  $\varphi = 45^\circ$  and is 0.013 m. Therefore this correction can also be neglected in the orbit determination of GNSS-2 satellites.

## 5.4.2 Ocean Tides

Ocean tides are also caused by the attraction of the Sun and Moon on the Earth's ocean that make the distribution of Earth's mass changes periodically. The exact modeling of ocean tides of the earth is a difficult problem due to the complex hydrodynamic response to the tidal forces. Approximately the same as the solid earth tides, the dynamical effect of ocean tides is most easily described as periodic variations in the normalized geopotential coefficients. The variations can be written as (Eanes, et al., 1983)

$$\Delta\bar{C}_{nm} - i\Delta\bar{S}_{nm} = F_{nm} \sum_{s(n,m)} \sum_{+} (C_{snm}^{\pm} \pm iS_{snm}^{\pm}) e^{\pm i\theta_s} \quad (5-48)$$

where

$$F_{nm} = \frac{4\pi G \rho_w}{g} \sqrt{\frac{(n+m)!}{(n-m)!(2n+1)(2-\delta_{om})}} \frac{1 + \kappa'_n}{2n+1}$$

$$g = 9.798261 \text{ ms}^{-2}$$

$$G = 6.673 \times 10^{-11} \text{ m}^3 \text{ kg}^{-1} \text{ s}^{-2} \quad \text{the gravitational constant}$$

$$\rho_w = 1025 \text{ kgm}^{-3}$$

$\kappa'_n$  load deformation coefficients

$$(\kappa'_2 = -0.3075, \kappa'_3 = -0.195, \kappa'_4 = -0.132, \kappa'_5 = -0.1032, \kappa'_6 = -0.0892)$$

$C_{snm}^{\pm}, S_{snm}^{\pm}$  ocean tide coefficients in  $m$  for the tide constituent  $s$

The computation detail is referred to McCarthy (1992).

The accelerations of IGSO and GEO satellite produced by ocean tides are about  $1 \times 10^{-10} \text{ m/s}^2$ ; for MEO (GPS) satellite is about  $5 \times 10^{-10} \text{ m/s}^2$  (Landau, 1988), i.e. after one day orbit arc computation, the maximum errors of IGSO and GEO is less than 0.01 meter, for MEO (GPS) satellite is less than 0.04 meter, therefore for real-time orbit determination the ocean tide terms can be neglected in the satellite dynamic model, but for long period of orbit prediction and batch processing, the ocean tide effects should be included in the satellite dynamic model.

### **5.4.3 Ocean Tide Loading**

Ocean tides by attraction of Sun and Moon also cause a periodic deformation of the crust. This phenomenon is called ocean tide loading. The displacements of tracking stations will be produced by the deformation of the crust, which can be described by three components of radial, east-west, north-south. The resulting displacements were computed by Scherneck (1991) using Schwiderski tide model, Green function for an elastic earth and Green function for a visco-elastic structure for stations on continental shelves. The displacement due to ocean loading is about 0.05 meter (Chadwell, 1995) and can be considered as tracking station error. The 0.05 meter of displacements of tracking stations will lead to 0.05 meter of orbit error, which is independent of the satellite type. In precise orbit determination, the effect of ocean loading should be included.



## CHAPTER 6      ALGORITHMS OF ORBIT DETERMINATION FOR IGSO, GEO & MEO SATELLITES

### 6.1 Numerical Integration

According to Newton's gravitational law, the satellite movement equation can be written as (Escobal, 1976)

$$\ddot{\mathbf{r}} = -\mu \frac{\mathbf{r}}{r^3} \quad (6-1)$$

where,

$\ddot{\mathbf{r}}$       satellite acceleration vector in inertial coordinate system  
 $\mathbf{r}$       satellite position vector in the same coordinate system  
 $\mu$       the earth's gravitational constant

Practically, the satellite is affected by various factors such as nonspherical earth gravitation, solar and lunar attractions, solar radiation, etc. Therefore the satellite movement equation can be more accurately expressed as

$$\ddot{\mathbf{r}} = -\mu \frac{\mathbf{r}}{r^3} + \frac{\partial \mathbf{R}}{\partial t} \quad (6-2)$$

where  $R$  is a perturbation function of the sum of various perturbation sources mentioned above.

Usually, there are two kinds of methods to solve this equation, analysis solution and numerical integration. The analysis method is complicated and the solution is low accuracy. The numerical integration is widely used and very rigorous, but time consuming for computation, especially for computation of complicated perturbation models. Two common algorithms of numerical integrations are Runge-Kutta and Adams-Cowell (Cappellari et al 1976, Xu 1989 and Engeln-Müllges et al, 1996).

#### 6.1.1 Runge-Kutta Integration

The solution of satellite movement equation can be considered as solution of the initial value problem of the following differential equation, i.e.

$$\left. \begin{aligned} \dot{\mathbf{y}}(t) &= f(\mathbf{y}, t) \\ \mathbf{y}(t_0) &= \mathbf{y}_0 \end{aligned} \right\} \quad (6-3)$$

Please note in Eq.(6-3),  $\mathbf{y}=(y_1, y_2, y_3, y_4, y_5, y_6)$ , which can be expressed as six Kepler orbital parameters.

The differential equation (6-3) can be solved by explicit Runge-Kutta algorithm as follows (Cappellari et al 1976, Xu 1989)

$$\left. \begin{aligned} y_{n+1} &= y_n + \sum_{i=1}^m w_i k_i \\ k_i &= f(t_n + c_i h, y_n + h \sum_{j=1}^{i-1} a_{ij} k_j) \end{aligned} \right\} \quad (6-4)$$

where

$h$               step length of integration  
 $f()$             the right function of satellite movement equation  
 $m$               order of Runge-Kutta method  
 $w_i$             weighted coefficients  
 $c_i, k_i, a_{ij}$     coefficients

In precise orbit determination, 8-order of Runge-Kutta integration algorithm should be used, which is given by (Cappellari et al 1976, Engeln-Müllges et al, 1996, Xu 1989)

$$\left. \begin{aligned}
k_1 &= f(t_n, y_n) \\
k_2 &= f\left(t_n + \frac{4}{27}h, y_n + \frac{4h}{27}k_1\right) \\
k_3 &= f\left[t_n + \frac{2}{9}h, y_n + \frac{h}{18}(k_1 + 3k_2)\right] \\
k_4 &= f\left[t_n + \frac{1}{3}h, y_n + \frac{h}{12}(k_1 + 3k_3)\right] \\
k_5 &= f\left[t_n + \frac{1}{2}h, y_n + \frac{h}{8}(k_1 + 3k_4)\right] \\
k_6 &= f\left[t_n + \frac{2}{3}h, y_n + \frac{h}{54}(13k_1 - 27k_3 + 42k_4 + 8k_5)\right] \\
k_7 &= f\left[t_n + \frac{1}{6}h, y_n + \frac{h}{4320}(389k_1 - 54k_3 + 966k_4 - 824k_5 + 243k_6)\right] \\
k_8 &= f\left[t_n + h, y_n + \frac{h}{20}(-231k_1 + 81k_3 - 1164k_4 + 656k_5 - 122k_6 + 800k_7)\right] \\
k_9 &= f\left[t_n + \frac{5}{6}h, y_n + \frac{h}{288}(-127k_1 + 18k_3 - 678k_4 + 456k_5 - 9k_6 + 576k_7 + 4k_8)\right] \\
k_{10} &= f\left[t_n + h, y_n + \frac{h}{820}(1481k_1 - 81k_3 + 7104k_4 - 3376k_5 + 72k_6 - 5040k_7 - 60k_8 + 720k_9)\right] \\
y_{n+1} &= y_n + \frac{h}{840}(41k_1 + 27k_4 + 272k_5 + 27k_6 + 216k_7 + 216k_9 + 41k_{10})
\end{aligned} \right\} \quad (6-5)$$

The right function  $f$  in Eq.(6-5) must be repeatedly computed several times for each integration step. The satellite movement equation is solved step by step, i.e. from known initial state  $y_0$ ,  $y_1$  can be computed; from  $y_1$ ,  $y_2$  can be computed, the rest is done similarly until  $y_n$  is obtained. Hence Runge-Kutta algorithm is also called one step method. Because Runge-Kutta algorithm has such a low computation efficiency, normally, it is used during the starting phase of orbit integration. Afterwards, the so-called multi-step algorithm will be used for subsequent integration of satellite movement equation.

### 6.1.2 Adams-Cowell Algorithm

Adams-Cowell's algorithm is a multi-step numerical integration, which can solve the following form of differential equation

$$\left. \begin{aligned}
\dot{x}(t) &= f(t, y) \\
y(t_0) &= y_0
\end{aligned} \right\} \quad (6-6)$$

Adams' integration algorithm can be divided into two types, Adams-Moulton (calibration) and Adams-Bashforth (prediction). Using Adams-Moulton algorithm to integrate the differential equation, the solution is given by (Cappellari et al 1976 and Xu 1989)

$$\left. \begin{aligned}
y_{n+1} &= y_n + h \sum_{k=0}^q \beta_k^* f_{n-k+1} \\
\beta_k^* &= \sum_{m=k}^q (-1)^k \gamma_m^* \binom{m}{k} \\
\gamma_m^* + \frac{1}{2} \gamma_{m-1}^* + \frac{1}{3} \gamma_{m-2}^* + \dots + \frac{1}{m+1} \gamma_{m-m}^* &= \begin{cases} 1 & m=0 \\ 0 & m \neq 0 \end{cases} \\
\binom{m}{k} &= \frac{k(k-1)(k-2)\dots[k-(m-1)]}{m!}
\end{aligned} \right\} \quad (6-7)$$

When  $y_{n+1}$  is computed from  $y_n$ , the right function is computed only once, the other right functions  $f_{n-1}, f_{n-2}, \dots, f_{n-9}$ , have been already computed before this step, therefore Adams' algorithm can integrate much faster than

Runge-Kutta algorithm does, but it can not integrate the differential equation directly from initial condition  $y_0$ , it needs  $y_0, y_1, y_2, \dots, y_q$  that can be provided by Runge-Kutta algorithm.

### 6.1.3 Cowell Algorithm

Cowell integration algorithm can solve following form of differential equations:

$$\left. \begin{aligned} \dot{\mathbf{x}}(t) &= f(t, \mathbf{y}) \\ \mathbf{x}(t_0) &= \mathbf{x}_0 \\ y(t_0) &= y_0 \end{aligned} \right\} \quad (6-8)$$

There are also two kinds of algorithms, prediction and calibration. The Cowell prediction algorithm is: (Cappellari et al 1976 and Xu 1989)

$$\left. \begin{aligned} y_{n+1} &= 2y_n - y_{n-1} + h^2 \sum_{k=0}^q \beta_k f_{n-k} \\ \beta_k &= \sum_{m=k}^q (-1)^k \binom{m}{k} \sigma_m \\ \sigma_m &= 1 - \sum_{j=0}^{m-1} \frac{2}{j+2} c_j \sigma_{m-j} \\ c_j &= \sum_{i=1}^j \frac{1}{i} \\ \sigma_0 &= 1 \end{aligned} \right\} \quad (6-9)$$

and Cowell calibration algorithm can be written as (Cappellari et al 1976 and Xu 1989)

$$\left. \begin{aligned} y_{n+1} &= 2y_n - y_{n-1} + h^2 \sum_{k=0}^q \beta_k^* f_{n-k+1} \\ \beta_k^* &= \sum_{m=k}^q \binom{m}{k} \sigma_m^* \\ \sigma_m^* &= - \sum_{j=0}^{m-1} \frac{2}{j+2} c_j \sigma_{m-j}^* \\ c_j &= \sum_{i=1}^j \frac{1}{i} \\ \sigma_0 &= 1 \end{aligned} \right\} \quad (6-10)$$

In practice, the prediction and calibration are combined to integrate the differential equation, first using prediction to compute the approximate  $y_{n+1}$  and also compute the right function with a certain accuracy and then using calibration to solve more precise  $y_{n+1}$ .

### 6.1.4 Numerical Integration of Satellite Dynamic Movement Equation

The satellite movement equation Eq.(6-2) can be equally written as follows

$$\left. \begin{aligned} \frac{dx}{dt} &= \dot{x} \\ \frac{dy}{dt} &= \dot{y} \\ \frac{dz}{dt} &= \dot{z} \\ \frac{d\dot{x}}{dt} &= -\frac{\mu}{r^3}x + \frac{\partial R_x}{\partial t} = \frac{\partial U}{\partial x} \\ \frac{d\dot{y}}{dt} &= -\frac{\mu}{r^3}y + \frac{\partial R_y}{\partial t} = \frac{\partial U}{\partial y} \\ \frac{d\dot{z}}{dt} &= -\frac{\mu}{r^3}z + \frac{\partial R_z}{\partial t} = \frac{\partial U}{\partial z} \end{aligned} \right\} \quad (6-11)$$

Assuming  $\dot{x} = v_x$ ,  $\dot{y} = v_y$ ,  $\dot{z} = v_z$ , Eq.(6-11) becomes

$$\left. \begin{aligned} v_x &= v_x \\ v_y &= v_y \\ v_z &= v_z \end{aligned} \right\} \quad (6-12)$$

and

$$\left. \begin{aligned} \dot{x} &= \frac{\partial U}{\partial x} \\ \dot{y} &= \frac{\partial U}{\partial y} \\ \dot{z} &= \frac{\partial U}{\partial z} \end{aligned} \right\} \quad (6-13)$$

Comparing Eq.(6-11), Eq.(6-12) and Eq.(6-13) with Eq.(6-3), it can be found that if  $x_0, y_0, z_0, \dot{x}_0, \dot{y}_0, \dot{z}_0$ , called initial orbit parameters, are known, Eq.(6-11) or Eq.(6-12) and Eq.(6-13) can be integrated using Runge-Kutta algorithm according to Eq.(6-4). First Eq.(6-13) is computed to obtain  $v_x, v_y, v_z$  and then Eq.(6-12) is solved to obtain  $x, y, z$ . Usually, Runge-Kutta algorithm is used to provide enough initial values and the right function computation, after that, Adams-Cowell integration algorithms will be used to perform further integration.

Using Cowell prediction and calibration algorithm Eq.(6-9) and Eq.(6-10) to integrate Eq.(6-13), the satellite position  $x, y, z$  can be solved and then using Adams-Moulton algorithm Eq.(6-7) to integrate Eq.(6-13), satellite velocity  $\dot{x}, \dot{y}, \dot{z}$  will be solved, i.e. the satellite movement equation Eq.(6-2) or Eq.(6-11) have been fully solved using numerical integration method.

## 6.2 Orbit Determination Methods

Usually orbit determination methods can be divided into two processing modes: sequential and all-observation-together processing (batch). Sequential processing means that satellite orbit will be updated when each or each set of observations are available. In this way, orbit can be determined in both real- and post-time. Batch (all-observation-together) processing implies that orbit will be determined after all observations arrive, usually batch processing is used in post-time. For satellite-based navigation system, real-time orbit determination is very important, as navigation users need orbit ephemeris updated in real-time to compute their positions.

In this chapter my focus is on sequential processing method of orbit determination.

### 6.2.1 Kalman Filter for Orbit Determination

Sequential processing usually uses Kalman filter for orbit determination which can be generally described as follows

Supposing that the satellite system state equation is

$$\overset{\omega}{x}_k = \Phi_{k,k-1} \overset{\omega}{x}_{k-1} + \Gamma_{k,k-1} \overset{\omega}{w}_{k-1} \quad (6-14)$$

The observation equation is

$$\overset{\omega}{y}_k = H_k \overset{\omega}{x}_k + G_k \overset{\omega}{z}_k + \mathcal{E}_k \quad (6-15)$$

where

$\overset{\omega}{x}_k$   $n$  dimensional signal state vector such as satellite orbit and dynamic parameters

$\overset{\omega}{y}_k$   $m$  dimensional observation vector

$\overset{\omega}{z}_k$   $p$  dimensional systematic parameter vector like tracking station coordinates, etc.

$\Phi_{k,k-1}$   $n \times n$  dimensional state transition matrix

$\overset{\omega}{w}_k$  dynamic system noise vector

$\mathcal{E}_k$  observation noise vector

$G_k$   $m \times p$  dimensional coefficient matrix of non-random parameters

$\Gamma_{k,k-1}$  coefficient matrix of dynamic system noise vector

$H_k$   $m \times n$  dimensional observation coefficient matrix

The a priori statistic information of  $\overset{\omega}{x}_0$  is given by the expectancy  $E\{\overset{\omega}{x}_0\}$  and the covariance  $D\{\overset{\omega}{x}_0\} = P_0$ .

Obviously, according to the assumption in Eq.(6-14) and (6-15),  $\overset{\omega}{x}_k$  is a random parameter vector and  $\overset{\omega}{z}_k$  is a non-random parameter vector. In order to solve the problem, Eq.(6-14) and Eq.(6-15) can be rewritten in the following matrix form:

$$\begin{bmatrix} \overset{\omega}{y}_k \\ \overset{\omega}{z}_k \\ \overset{\omega}{x}_k \end{bmatrix} = \begin{bmatrix} H_k & G_k \\ I_x & 0 \end{bmatrix} \begin{bmatrix} \overset{\omega}{x}_k \\ \overset{\omega}{z}_k \end{bmatrix} + \begin{bmatrix} \mathcal{E}_k \\ \overset{\omega}{z}_k \\ \mathcal{E}_{x_k} \end{bmatrix} \quad (6-16)$$

where  $\overset{\omega}{x}_k$  is assumed to be pseudo-observation,  $\mathcal{E}_{x_k}$  is the pseudo-observation noise.

The a priori values  $\overset{\omega}{x}_k$  and covariance matrix  $P'_{x_k}$  can be approximated from Eq.(6-14). The results are

$$\overset{\omega}{x}_k = \Phi_{k,k-1} \overset{\omega}{x}_{k-1} \quad (6-17)$$

$$P'_{x_k} = \Phi_{k,k-1} P_{x_{k-1}} \Phi_{k,k-1}^T + \Gamma_{k,k-1} Q_{k-1} \Gamma_{k,k-1}^T \quad (6-18)$$

where  $\overset{\omega}{x}_{k-1}$  is the estimator of  $\overset{\omega}{x}_{k-1}$  at the epoch of  $k-1$ ;  $P_{x_{k-1}}$  is the covariance matrix of  $\overset{\omega}{x}_{k-1}$ .

$Q_{k-1} = \text{cov}(\overset{\omega}{w}_{k-1}, \overset{\omega}{w}_{k-1})$  is the system state noise covariance at  $k-1$ .

Covariance matrix of the observation is

$$R = \begin{bmatrix} R_k & 0 \\ 0 & P'_{x_k} \end{bmatrix}$$

where  $R_k$  is the covariance matrix of observation vector  $\overset{\omega}{y}_k$ ;  $P'_{x_k}$  represents a priori information of system parameters.

Using the least squares method, we can obtain

$$\begin{aligned} \begin{bmatrix} \overset{\omega}{x}_k \\ \overset{\omega}{z}_k \end{bmatrix} &= \left\{ \begin{bmatrix} H_k^T & I_{x_k} \\ G_k^T & 0 \end{bmatrix} \begin{bmatrix} R_k^{-1} & 0 \\ 0 & P'^{-1}_{x_k} \end{bmatrix} \begin{bmatrix} H_k & G_k \\ I_{x_k} & 0 \end{bmatrix} \right\}^{-1} \begin{bmatrix} H_k^T & I_{x_k} \\ G_k^T & 0 \end{bmatrix} \begin{bmatrix} R_k^{-1} & 0 \\ 0 & P'^{-1}_{x_k} \end{bmatrix} \begin{bmatrix} \overset{\omega}{y}_k \\ \overset{\omega}{z}_k \\ \overset{\omega}{x}_k \end{bmatrix} \\ &= \begin{bmatrix} H_k^T R_k^{-1} H_k + P'^{-1}_{x_k} & H_k^T R_k^{-1} G_k \\ G_k^T R_k^{-1} H_k & G_k^T R_k^{-1} G_k \end{bmatrix}^{-1} \begin{bmatrix} H_k^T & I_{x_k} \\ G_k^T & 0 \end{bmatrix} \begin{bmatrix} R_k^{-1} & 0 \\ 0 & P'^{-1}_{x_k} \end{bmatrix} \begin{bmatrix} \overset{\omega}{y}_k \\ \overset{\omega}{z}_k \\ \overset{\omega}{x}_k \end{bmatrix} \\ &= \begin{bmatrix} H_k^T R_k^{-1} H_k + P'^{-1}_{x_k} & H_k^T R_k^{-1} G_k \\ G_k^T R_k^{-1} H_k & G_k^T R_k^{-1} G_k \end{bmatrix}^{-1} \begin{bmatrix} H_k^T R_k^{-1} \overset{\omega}{y}_k + P'^{-1}_{x_k} \overset{\omega}{x}_k \\ G_k^T R_k^{-1} \overset{\omega}{y}_k \end{bmatrix} \end{aligned} \quad (6-19)$$

Here,  $\overset{\omega}{x}_k, \overset{\omega}{z}_k$  are a priori unbiased estimates of  $\overset{\omega}{x}_k, \overset{\omega}{z}_k$  respectively.

If assuming

$$A_{11} = H_k^T R_k^{-1} H_k + P'_{x_k}{}^{-1}$$

$$A_{12} = H_k^T R_k^{-1} G_k$$

$$A_{21} = G_k^T R_k^{-1} H_k$$

$$A_{22} = G_k^T R_k^{-1} G_k$$

$$b_1 = H_k^T R_k^{-1} \bar{\mathbb{O}} y_k + P'_{x_k}{}^{-1} \bar{\mathbb{O}} x_k$$

$$b_2 = G_k^T R_k^{-1} \bar{\mathbb{O}} y_k,$$

we can get

$$\bar{\mathbb{O}} x_k = \bar{A}_{11}^{-1} b_1 - \bar{A}_{11}^{-1} A_{12} A_{22}^{-1} b_2 \quad (6-20)$$

$$\bar{\mathbb{O}} z_k = -A_{22}^{-1} A_{21} \bar{A}_{11}^{-1} b_1 + (A_{22}^{-1} + A_{22}^{-1} A_{21} \bar{A}_{11}^{-1} A_{12} A_{22}^{-1}) b_2 \quad (6-21)$$

where

$$\bar{A}_{11}^{-1} = (A_{11} - A_{12} A_{22}^{-1} A_{21})^{-1} \quad (6-22)$$

If matrices  $D$  and  $C$  are positive definite and others are arbitrary matrices, following relation holds

$$(ACB + D)^{-1} = D^{-1} - D^{-1} A (BD^{-1} A + C^{-1}) BD^{-1} \quad (6-23)$$

From Eq.(6-23),  $\bar{A}_{11}^{-1}$  becomes

$$\begin{aligned} \bar{A}_{11}^{-1} &= [H_k^T R_k^{-1} H_k + P'_{x_k}{}^{-1} - H_k^T R_k^{-1} G_k (G_k^T R_k^{-1} G_k)^{-1} G_k^T R_k^{-1} H_k]^{-1} \\ &= \{P'_{x_k}{}^{-1} + H_k^T [R_k^{-1} - R_k^{-1} G_k (G_k^T R_k^{-1} G_k)^{-1} G_k^T R_k^{-1}] H_k\}^{-1} \\ &= P'_{x_k} - P'_{x_k} H_k^T \{ [R_k^{-1} - R_k^{-1} G_k (G_k^T R_k^{-1} G_k)^{-1} G_k^T R_k^{-1}]^{-1} + H_k P'_{x_k} H_k^T \}^{-1} H_k P'_{x_k} \\ &= P'_{x_k} - P'_{x_k} H_k^T \{ H_k P'_{x_k} H_k^T + R_k [I_k - G_k (G_k^T R_k^{-1} G_k)^{-1} G_k^T R_k^{-1}]^{-1} \}^{-1} H_k P'_{x_k} \end{aligned} \quad (6-24)$$

The gain matrix is defined as

$$K_k = P'_{x_k} H_k^T \{ H_k P'_{x_k} H_k^T + R_k [I_k - G_k (G_k^T R_k^{-1} G_k)^{-1} G_k^T R_k^{-1}]^{-1} \}^{-1} \quad (6-25)$$

Substituting Eq.(6-22) into Eq.(6-20), taking into account Eq.(6-27) yields

$$\bar{\mathbb{O}} x_k = \bar{\mathbb{O}} x_k - K_k H_k \bar{\mathbb{O}} x_k + (I - K_k H_k) P'_{x_k} H_k^T R_k^{-1} [I - G_k (G_k^T R_k^{-1} G_k)^{-1} G_k^T R_k^{-1}] \bar{\mathbb{O}} y_k \quad (6-26)$$

Assuming

$$R_k^{-1} [I - G_k (G_k^T R_k^{-1} G_k)^{-1} G_k^T R_k^{-1}] = [R_k^{-1} - R_k^{-1} G_k (G_k^T R_k^{-1} G_k)^{-1} G_k^T R_k^{-1}] = W^{-1}$$

then

$$\begin{aligned} &(I - K_k H_k) P'_{x_k} H_k^T R_k^{-1} [I - G_k (G_k^T R_k^{-1} G_k)^{-1} G_k^T R_k^{-1}] \\ &= (I - K_k H_k) P'_{x_k} H_k^T W^{-1} \\ &= \{P'_{x_k} - P'_{x_k} H_k^T [H_k P'_{x_k} H_k^T + W]^{-1} H_k P'_{x_k}\} H_k^T W^{-1} \end{aligned} \quad (6-27)$$

From Eq.(6-23), the equation above becomes

$$= [P'_{x_k}{}^{-1} + H_k^T W^{-1} H_k]^{-1} H_k^T W^{-1} \quad (6-28)$$

According to the relation ( $D$  and  $C$  should be positive definite)

$$CB(ACB + D)^{-1} = (C^{-1} + BD^{-1}A)BD^{-1} \quad (6-29)$$

then Eq.(6-28) becomes

$$\begin{aligned} &= P'_{x_k} H_k^T (H_k P'_{x_k} H_k^T + W)^{-1} \\ &= P'_{x_k} H_k^T \{ H_k P'_{x_k} H_k^T + R_k [I - G_k (G_k^T R_k^{-1} G_k)^{-1} G_k^T R_k^{-1}]^{-1} \}^{-1} = K_k \end{aligned} \quad (6-30)$$

Therefore

$$\begin{aligned}\bar{x}_k &= \bar{x}_k - K_k H_k \bar{x}_k + K_k y_k \\ &= \bar{x}_k + K_k (y_k - H_k \bar{x}_k)\end{aligned}\quad (6-31)$$

Eq.(6-21) will be written as

$$\begin{aligned}\bar{z}_k &= -(G_k^T R_k^{-1} G_k)^{-1} G_k^T R_k^{-1} [(H_k K_k - I) \bar{y}_k + H_k (I - K_k H_k) \bar{x}_k] \\ &= -(G_k^T R_k^{-1} G_k)^{-1} G_k^T R_k^{-1} (H_k K_k - I) (\bar{y}_k - H_k \bar{x}_k)\end{aligned}\quad (6-32)$$

From Eq.(6-19), the covariance matrix  $P_{x_k}$  of  $\bar{x}_k$  is

$$P_{x_k} = \bar{A}_{11}^{-1} = (I - K_k H_k) P'_{x_k} \quad (6-33)$$

and the covariance matrix  $P_{z_k}$  of  $\bar{z}_k$  is in the following form:

$$\begin{aligned}P_{z_k} &= A_{22}^{-1} + A_{22}^{-1} A_{21} \bar{A}_{11}^{-1} A_{12} A_{22}^{-1} \\ &= (G_k^T R_k^{-1} G_k)^{-1} \left[ I + G_k^T R_k^{-1} H_k (I - K_k H_k) P'_{x_k} H_k^T R_k^{-1} G_k (G_k^T R_k^{-1} G_k)^{-1} \right]\end{aligned}\quad (6-34)$$

The summary of the Kalman filter algorithm just developed for orbit determination is as follows. First, the a priori unbiased estimate  $\bar{x}_k$  of state vector  $x_k$  is computed at epoch  $k$ , that is

$$\bar{x}_k = \Phi_{k,k-1} \bar{x}_{k-1} \quad (6-35)$$

The  $\bar{x}_k$  covariance matrix is

$$P'_{x_k} = \Phi_{k,k-1} P_{x_{k-1}} \Phi_{k,k-1}^T + \Gamma_{k,k-1} Q_{k-1} \Gamma_{k,k-1}^T \quad (6-36)$$

Then the gain matrix can be computed by Eq.(6-25).

Finally, the a posteriori state vector estimate  $\bar{x}_k$  and its error covariance matrix can be obtained by applying Eq.(6-31) and Eq.(6-33). The non-random parameter vector  $\bar{z}_k$  is estimated by Eq.(6-32), its variance matrix is obtained using Eq.(6-34).

## 6.2.2 Dynamic Orbit Determination Method

The satellite run around the Earth, which is affected by various factors such as the earth gravitation, solar and lunar attraction, solar radiation pressure and so on. Dynamical method requires modeling of the complete set of these factors acting on an orbiting satellite. These modeling have been discussed in Chapter 5.

Suppose that  $\bar{x} = \{x, y, z, \dot{x}, \dot{y}, \dot{z}\}$  is a state vector of satellite, the satellite equation has the following form

$$\frac{d\bar{x}}{dt} = f(\bar{x}(t), t) \quad (6-37)$$

The observation equation is given by

$$\bar{y} = O(\bar{x}(t), \bar{z}(t), t) + \bar{\varepsilon} \quad (6-38)$$

The satellite movement equation Eq.(6-37) can not be directly used by Kalman filter discussed above. Some changes should be made, and supposing that state vector of satellite  $\bar{x}_k$  is close enough to its true value  $\bar{x}_k$ , i.e.

$$|\Delta x_k| = |\bar{x}_k - x_k| < \varepsilon$$

then Eq.(6-37) and Eq.(6-38) are developed according to Taylor series as

$$\bar{x}_k = \bar{x}_k + \left(\frac{\partial f}{\partial x}\right)' \Delta x_k + \frac{1}{2} \left(\frac{\partial^2 f}{\partial x^2}\right)' (\Delta x_k)^2 + \dots \quad (6-39)$$

$$\bar{y}_k = \bar{y}_k + \left(\frac{\partial O}{\partial x}\right)'_k \Delta x_k + \left(\frac{\partial O}{\partial z}\right)'_k \Delta z_k + \frac{1}{2} \left(\frac{\partial^2 O}{\partial x^2}\right)'_k (\Delta x_k)^2 + \frac{1}{2} \left(\frac{\partial^2 O}{\partial z^2}\right)'_k (\Delta z_k)^2 + \dots \quad (6-40)$$

where „ ‘ “ means related terms are computed by approximate  $\bar{x}_k$  at epoch  $t_k$ .

Neglecting the second and higher order terms and supposing

$$\left. \begin{aligned} F_k &= \left(\frac{\partial f}{\partial x}\right)'_k, H_k = \left(\frac{\partial O}{\partial x}\right)'_k \\ \Delta x_k &= \bar{x}_k - x_k, \Delta z_k = \bar{z}_k - z_k \end{aligned} \right\} \quad (6-41)$$

the linear dynamic and observation equations can be expressed as

$$\left. \begin{aligned} \Delta \bar{x}_k &= F_k \Delta x_k + \bar{w}_k \\ \bar{y}_k &= H_k \Delta x_k + G_k \Delta z_k + \bar{\varepsilon}_k \end{aligned} \right\} \quad (6-42)$$

where  $\bar{w}_k$  is the dynamic noise and  $\bar{\varepsilon}_k$  is the measurement noise and we can further assume that  $E(\bar{w}_k) = 0, E(\bar{\varepsilon}_k) = 0$ .

The satellite dynamic system equation becomes

$$\Delta \bar{x}_k = \Phi_{k,k-1} \Delta \bar{x}_{k-1} + \Gamma_{k,k-1} \bar{w}_{k-1} \quad (6-43)$$

where  $\Phi_{k,k-1}$  is a solution of following differential equation

$$\frac{d\Phi}{dt} = F\Phi \quad (6-44)$$

Eq.(6-44) shows that if the dimension of state vector is 6, actually 36 differential equations in Eq.(6-44) must be solved. In the orbit computation, the dimension of state vector is more than 6, so the solution of Eq.(6-44) is a time-consuming task for computer. Eq.(6-44) can only be rigorously solved using numerical integration method. For actually application, some approximation approach may be used. From Kalman filter algorithm,  $\bar{x}_k$  should be first computed using numerical integration,  $\bar{x}_k$  is also called reference value (or  $\bar{x}_0, \bar{x}_1, \Lambda, \bar{x}_k$  series called reference orbit) and should be precisely computed, as the errors of the reference orbit will affect the accuracy of orbit determination; for computation of  $\Delta \bar{x}_k$  and  $P_{kk-1}$ ,  $\Phi_{k,k-1}$  may not be so precise as for the computation of  $\bar{x}_k$ . Therefore approximation approach can be used to compute  $\Phi_{k,k-1}$  for  $\Delta \bar{x}_k$  and  $P_{kk-1}$ . The computation burden will be significantly reduced and the accuracy of orbit determination will be kept.

The approximation approach of the solution of Eq.(6-44) in the stationary system can be expressed as

$$\Phi(t) = e^{Ft} \quad (6-45)$$

Supposing  $t=h$ ,  $\Phi$  is a system transition matrix, then according to Tarlor series

$$\Phi(h) = e^{Fh} = I + Fh + \frac{1}{2!} Fh * Fh + \frac{1}{3!} Fh * Fh * Fh + \dots \quad (6-46)$$

where

$I$  an identity matrix.

Referring to Eq.(6-11) to Eq.(6-13),  $F$  in Eq.(6-46) may be written as



$$F = \begin{bmatrix} \frac{\partial \&}{\partial x} & \frac{\partial \&}{\partial y} & \frac{\partial \&}{\partial z} & \frac{\partial \&}{\partial \&} & \frac{\partial \&}{\partial \&} & \frac{\partial \&}{\partial \&} \\ \frac{\partial \&}{\partial x} & \frac{\partial \&}{\partial y} & \frac{\partial \&}{\partial z} & \frac{\partial \&}{\partial \&} & \frac{\partial \&}{\partial \&} & \frac{\partial \&}{\partial \&} \\ \frac{\partial \&}{\partial x} & \frac{\partial \&}{\partial y} & \frac{\partial \&}{\partial z} & \frac{\partial \&}{\partial \&} & \frac{\partial \&}{\partial \&} & \frac{\partial \&}{\partial \&} \\ \frac{\partial \&}{\partial x} & \frac{\partial \&}{\partial y} & \frac{\partial \&}{\partial z} & \frac{\partial \&}{\partial \&} & \frac{\partial \&}{\partial \&} & \frac{\partial \&}{\partial \&} \\ \frac{\partial^2 U}{\partial x^2} & \frac{\partial^2 U}{\partial x \partial y} & \frac{\partial^2 U}{\partial x \partial z} & \frac{\partial^2 U}{\partial x \partial \&} & \frac{\partial^2 U}{\partial x \partial \&} & \frac{\partial^2 U}{\partial x \partial \&} \\ \frac{\partial^2 U}{\partial x \partial y} & \frac{\partial^2 U}{\partial y^2} & \frac{\partial^2 U}{\partial z \partial y} & \frac{\partial^2 U}{\partial \& \partial y} & \frac{\partial^2 U}{\partial \& \partial y} & \frac{\partial^2 U}{\partial \& \partial y} \\ \frac{\partial^2 U}{\partial x \partial z} & \frac{\partial^2 U}{\partial y \partial z} & \frac{\partial^2 U}{\partial z^2} & \frac{\partial^2 U}{\partial \& \partial z} & \frac{\partial^2 U}{\partial \& \partial z} & \frac{\partial^2 U}{\partial \& \partial z} \end{bmatrix}$$

i.e.

$$F = \begin{bmatrix} 0 & 0 & 0 & 1 & 0 & 0 \\ 0 & 0 & 0 & 0 & 1 & 0 \\ 0 & 0 & 0 & 0 & 0 & 1 \\ \frac{\partial^2 U}{\partial x^2} & \frac{\partial^2 U}{\partial y \partial x} & \frac{\partial^2 U}{\partial z \partial x} & 0 & 0 & 0 \\ \frac{\partial^2 U}{\partial x \partial y} & \frac{\partial^2 U}{\partial y^2} & \frac{\partial^2 U}{\partial z \partial y} & 0 & 0 & 0 \\ \frac{\partial^2 U}{\partial x \partial z} & \frac{\partial^2 U}{\partial y \partial z} & \frac{\partial^2 U}{\partial z^2} & 0 & 0 & 0 \end{bmatrix} \quad (6-47)$$

In Eq.(6-42),

$$\begin{aligned} \frac{\partial^2 U}{\partial x \partial y} &= \frac{\partial^2 U}{\partial y \partial x} \\ \frac{\partial^2 U}{\partial x \partial z} &= \frac{\partial^2 U}{\partial z \partial x} \\ \frac{\partial^2 U}{\partial y \partial z} &= \frac{\partial^2 U}{\partial z \partial y} \end{aligned}$$

Considering the various perturbations, the general derivatives in Eq.(6-47) are very difficult to be expressed. In the following, only the geopotential, solar and lunar influences are considered, then

$$U = U_e + U_s + U_m$$

where subscript  $e$  means the geopotential,  $s$  means Sun and  $m$  Moon.

### 1) Geopotential

Rewriting Eq.(5-1) as follows,

$$U_e = \frac{GM}{r} + GM \sum_{n=2}^N \sum_{m=0}^n \frac{a_e^n}{r^{n+1}} P_{nm}(\sin \varphi) (C_{nm} \cos m\lambda + S_{nm} \sin m\lambda) \quad (6-48)$$

where

- $G$  Newtonian gravitational constant
- $M$  the Earth's mass ( $GM=398.600415 \times 10^{12} \text{ m}^3 \text{ s}^{-2}$ )
- $P_{nm}(\sin \varphi)$  associated Legendre function
- $\lambda, \varphi$  geographic longitude and latitude of satellite
- $C_{nm}, S_{nm}$  spherical harmonic coefficients.

$U_e$  is in the earth-fixed coordinate system. Clearly, geopotential  $U_e$  is directly related to the spherical components  $r, \varphi, \lambda$ , not Cartesian components  $x, y, z$ . From relations,

$$\left. \begin{aligned} x &= r \cos \varphi \cos \lambda \\ y &= r \cos \varphi \sin \lambda \\ z &= r \sin \varphi \end{aligned} \right\} \quad (6-49)$$

we can obtain,

$$\left. \frac{\partial^2 U_e}{\partial x^2} \right|_e = \frac{\partial^2 U_e}{\partial r^2} \left( \frac{\partial r}{\partial x} \right)^2 + \frac{\partial U_e}{\partial r} \frac{\partial^2 r}{\partial x^2} \quad (6-50)$$

$$\left. \frac{\partial^2 U_e}{\partial x \partial y} \right|_e = \frac{\partial^2 U_e}{\partial r^2} \frac{\partial r}{\partial x} \frac{\partial r}{\partial y} + \frac{\partial U_e}{\partial r} \frac{\partial^2 r}{\partial x \partial y} \quad (6-51)$$

$$\left. \frac{\partial^2 U_e}{\partial x \partial z} \right|_e = \frac{\partial^2 U_e}{\partial r^2} \frac{\partial r}{\partial x} \frac{\partial r}{\partial z} + \frac{\partial U_e}{\partial r} \frac{\partial^2 r}{\partial x \partial z} \quad (6-52)$$

$$\left. \frac{\partial^2 U_e}{\partial y^2} \right|_e = \frac{\partial^2 U_e}{\partial r^2} \left( \frac{\partial r}{\partial y} \right)^2 + \frac{\partial U_e}{\partial r} \frac{\partial^2 r}{\partial y^2} \quad (6-53)$$

$$\left. \frac{\partial^2 U_e}{\partial y \partial z} \right|_e = \frac{\partial^2 U_e}{\partial r^2} \frac{\partial r}{\partial y} \frac{\partial r}{\partial z} + \frac{\partial U_e}{\partial r} \frac{\partial^2 r}{\partial y \partial z} \quad (6-54)$$

$$\left. \frac{\partial^2 U_e}{\partial z^2} \right|_e = \frac{\partial^2 U_e}{\partial r^2} \left( \frac{\partial r}{\partial z} \right)^2 + \frac{\partial U_e}{\partial r} \frac{\partial^2 r}{\partial z^2} \quad (6-55)$$

where, the symbol  $|_e$  means the derivatives in the earth-fixed coordinate system. These derivatives will be converted to the inertial coordinate system.

If only the  $J_2$  term in geopotential Eq.(6-48) is considered, the Eq.(6-50) to Eq.(6-55) become,

$$\begin{aligned} \left. \frac{\partial^2 U_e}{\partial x^2} \right|_e &= \left[ 2 \frac{GM}{r^3} - 6 \frac{GM}{r^3} J_2 \left( \frac{a_e}{r} \right)^2 (3 \sin^2 \varphi - 1) \right] \cos^2 \varphi \cos^2 \lambda - 6 \frac{GM}{r^3} J_2 \left( \frac{a_e}{r} \right)^2 \sin^2 2\varphi \cos^2 \lambda \\ &+ \left[ -\frac{GM}{r^3} + \frac{3}{2} \frac{GM}{r^3} J_2 \left( \frac{a_e}{r} \right)^2 (5 \sin^2 \varphi - 1) \right] \sin^2 \lambda \\ &+ \left[ -\frac{GM}{r^3} + 3 \frac{GM}{r^3} J_2 \left( \frac{a_e}{r} \right)^2 \left( -\frac{3}{2} + \frac{7}{2} \sin^2 \varphi \right) \right] \sin^2 \varphi \cos^2 \lambda \end{aligned} \quad (6-56)$$

$$\begin{aligned} \left. \frac{\partial^2 U_e}{\partial x \partial y} \right|_e &= \left[ \frac{GM}{r^3} - 3 \frac{GM}{r^3} J_2 \left( \frac{a_e}{r} \right)^2 (3 \sin^2 \varphi - 1) \right] \cos^2 \varphi \sin 2\lambda - 3 \frac{GM}{r^3} J_2 \left( \frac{a_e}{r} \right)^2 \sin 2\varphi \sin 2\varphi \sin 2\lambda \\ &- \left[ -\frac{GM}{r^3} + \frac{3}{2} \frac{GM}{r^3} J_2 \left( \frac{a_e}{r} \right)^2 (5 \sin^2 \varphi - 1) \right] \sin \lambda \cos \lambda \\ &+ \left[ -\frac{GM}{r^3} + 3 \frac{GM}{r^3} J_2 \left( \frac{a_e}{r} \right)^2 \left( -\frac{3}{2} + \frac{7}{2} \sin^2 \varphi \right) \right] \sin^2 \varphi \sin \lambda \cos \lambda \end{aligned} \quad (6-57)$$

$$\begin{aligned} \left. \frac{\partial^2 U_e}{\partial x \partial z} \right|_e &= \left[ \frac{GM}{r^3} - 3 \frac{GM}{r^3} J_2 \left( \frac{a_e}{r} \right)^2 (3 \sin^2 \varphi - 1) \right] \sin 2\varphi \cos \lambda + 6 \frac{GM}{r^3} J_2 \left( \frac{a_e}{r} \right)^2 \sin 2\varphi (\cos^2 \varphi - \sin^2 \varphi) \cos \lambda \\ &- \left[ -\frac{GM}{r^3} + 3 \frac{GM}{r^3} J_2 \left( \frac{a_e}{r} \right)^2 \left( -\frac{3}{2} + \frac{7}{2} \sin^2 \varphi \right) \right] \sin \varphi \cos \varphi \cos \lambda \end{aligned} \quad (6-58)$$

$$\begin{aligned} \left. \frac{\partial^2 U_e}{\partial y^2} \right|_e &= \left[ 2 \frac{GM}{r^3} - 6 \frac{GM}{r^3} J_2 \left( \frac{a_e}{r} \right)^2 (3 \sin^2 \varphi - 1) \right] \cos^2 \varphi \sin^2 \lambda - 6 \frac{GM}{r^3} J_2 \left( \frac{a_e}{r} \right)^2 \sin^2 2\varphi \sin^2 \lambda \\ &+ \left[ -\frac{GM}{r^3} + \frac{3}{2} \frac{GM}{r^3} J_2 \left( \frac{a_e}{r} \right)^2 (5 \sin^2 \varphi - 1) \right] \cos^2 \lambda \end{aligned}$$

$$+ \left[ -\frac{GM}{r^3} + 3\frac{GM}{r^3} J_2 \left(\frac{a_e}{r}\right)^2 \left(-\frac{3}{2} + \frac{7}{2} \sin^2 \varphi\right) \right] \sin^2 \varphi \sin^2 \lambda \quad (6-59)$$

$$\begin{aligned} \left. \frac{\partial^2 U_e}{\partial y \partial z} \right|_e &= \left[ \frac{GM}{r^3} - 3\frac{GM}{r^3} J_2 \left(\frac{a_e}{r}\right)^2 (3 \sin^2 \varphi - 1) \right] \sin 2\varphi \sin \lambda + 6\frac{GM}{r^3} J_2 \left(\frac{a_e}{r}\right)^2 \sin 2\varphi (\cos^2 \varphi - \sin^2 \varphi) \sin \lambda \\ &- \left[ -\frac{GM}{r^3} + 3\frac{GM}{r^3} J_2 \left(\frac{a_e}{r}\right)^2 \left(-\frac{3}{2} + \frac{7}{2} \sin^2 \varphi\right) \right] \sin \varphi \cos \varphi \sin \lambda \end{aligned} \quad (6-60)$$

$$\left. \frac{\partial^2 U_e}{\partial z^2} \right|_e = \left[ 2\frac{GM}{r^3} - 6\frac{GM}{r^3} J_2 \left(\frac{a_e}{r}\right)^2 (3 \sin^2 \varphi - 1) \right] \sin^2 \varphi - 6\frac{GM}{r^3} J_2 \left(\frac{a_e}{r}\right)^2 \sin^2 2\varphi \quad (6-61)$$

## 2) Solar and lunar Attractions

The solar and lunar attractions Eq.(5-23) may be rewritten in the following forms:

$$\mathbb{E} = -\mu \frac{x}{r^3} + \sum_{i=s,m} \mu_i \left[ \frac{x_i - x}{\sqrt{(x_i - x)^2 + (y_i - y)^2 + (z_i - z)^2}} - \frac{x_i}{r_i^3} \right] \quad (6-62)$$

$$\mathbb{E} = -\mu \frac{y}{r^3} + \sum_{i=s,m} \mu_i \left[ \frac{y_i - y}{\sqrt{(x_i - x)^2 + (y_i - y)^2 + (z_i - z)^2}} - \frac{y_i}{r_i^3} \right] \quad (6-63)$$

$$\mathbb{E} = -\mu \frac{z}{r^3} + \sum_{i=s,m} \mu_i \left[ \frac{z_i - z}{\sqrt{(x_i - x)^2 + (y_i - y)^2 + (z_i - z)^2}} - \frac{z_i}{r_i^3} \right] \quad (6-64)$$

From Eq.(6-62) to Eq.(6-64), we can get

$$\begin{aligned} \frac{\partial^2 U_{s,m}}{\partial x^2} &= -(1-3\frac{x^2}{r^2}) \frac{1}{r^3} - \sum_{i=s,m} \mu_i \left[ \frac{x_i - x}{\left(\sqrt{(x_i - x)^2 + (y_i - y)^2 + (z_i - z)^2}\right)^3} \right. \\ &\quad \left. + \frac{2(x_i - x)}{\left(\sqrt{(x_i - x)^2 + (y_i - y)^2 + (z_i - z)^2}\right)^3} - \frac{3(x_i - x)^3}{\left(\sqrt{(x_i - x)^2 + (y_i - y)^2 + (z_i - z)^2}\right)^5} \right] \end{aligned} \quad (6-65)$$

$$\frac{\partial^2 U_{s,m}}{\partial x \partial y} = 3\frac{xy}{r^5} - \sum_{i=s,m} \mu_i \left[ \frac{y_i - y}{\sqrt{(x_i - x)^2 + (y_i - y)^2 + (z_i - z)^2}} - \frac{(x_i - x)^2 (y_i - y)}{\left(\sqrt{(x_i - x)^2 + (y_i - y)^2 + (z_i - z)^2}\right)^5} \right] \quad (6-66)$$

$$\frac{\partial^2 U_{s,m}}{\partial x \partial z} = 3\frac{xz}{r^5} - \sum_{i=s,m} \mu_i \left[ \frac{z_i - z}{\sqrt{(x_i - x)^2 + (y_i - y)^2 + (z_i - z)^2}} - \frac{(x_i - x)^2 (z_i - z)}{\left(\sqrt{(x_i - x)^2 + (y_i - y)^2 + (z_i - z)^2}\right)^5} \right] \quad (6-67)$$

$$\frac{\partial^2 U_{s,m}}{\partial y^2} = -(1-3\frac{y^2}{r^2}) \frac{1}{r^3} - \sum_{i=s,m} \mu_i \left[ \frac{y_i - y}{\left(\sqrt{(x_i - x)^2 + (y_i - y)^2 + (z_i - z)^2}\right)^3} \right]$$

$$+ \left[ \frac{2(y_i - y)}{\left(\sqrt{(x_i - x)^2 + (y_i - y)^2 + (z_i - z)^2}\right)^3} - \frac{3(y_i - y)^3}{\left(\sqrt{(x_i - x)^2 + (y_i - y)^2 + (z_i - z)^2}\right)^5} \right] \quad (6-68)$$

$$\frac{\partial^2 U_{s,m}}{\partial y \partial z} = 3 \frac{xz}{r^5} - \sum_{i=s,m} \mu_i \left[ \frac{z_i - z}{\sqrt{(x_i - x)^2 + (y_i - y)^2 + (z_i - z)^2}} - \frac{(y_i - y)^2 (z_i - z)}{\left(\sqrt{(x_i - x)^2 + (y_i - y)^2 + (z_i - z)^2}\right)^5} \right] \quad (6-69)$$

$$\begin{aligned} \frac{\partial^2 U_{s,m}}{\partial z^2} = & -(1 - 3 \frac{z^2}{r^2}) \frac{1}{r^3} - \sum_{i=s,m} \mu_i \left[ \frac{z_i - z}{\left(\sqrt{(x_i - x)^2 + (y_i - y)^2 + (z_i - z)^2}\right)^3} \right. \\ & \left. + \frac{2(z_i - z)}{\left(\sqrt{(x_i - x)^2 + (y_i - y)^2 + (z_i - z)^2}\right)^3} - \frac{3(z_i - z)^3}{\left(\sqrt{(x_i - x)^2 + (y_i - y)^2 + (z_i - z)^2}\right)^5} \right] \end{aligned} \quad (6-70)$$

### 3) No Perturbations

If in the state transit matrix the perturbation influence on the satellite dynamic model is not considered, the derivative components in Eq.(6-47) may be written as

$$\frac{\partial^2 U}{\partial x^2} = -(1 - 3 \frac{x^2}{r^2}) \frac{1}{r^3} \quad (6-71)$$

$$\frac{\partial^2 U}{\partial x \partial y} = 3 \frac{xy}{r^5} \quad (6-72)$$

$$\frac{\partial^2 U}{\partial x \partial z} = 3 \frac{xz}{r^5} \quad (6-73)$$

$$\frac{\partial^2 U}{\partial y^2} = -(1 - 3 \frac{y^2}{r^2}) \frac{1}{r^3} \quad (6-74)$$

$$\frac{\partial^2 U}{\partial y \partial z} = 3 \frac{yz}{r^5} \quad (6-75)$$

$$\frac{\partial^2 U}{\partial z^2} = -(1 - 3 \frac{z^2}{r^2}) \frac{1}{r^3} \quad (6-76)$$

Now Kalman filter algorithm for dynamic orbit determination can be summarized as follows

$$\left. \begin{aligned} \bar{x}_k &= f(\bar{x}_k, t) \\ \bar{y}_k &= H_k \bar{x}_k + G_k \bar{z}_k \\ P'_k &= \Phi_{k,k-1} P_{k-1} \Phi_{k,k-1}^T + \Gamma_{k,k-1} Q_{k-1} \Gamma_{k,k-1}^T \\ K_k &= P'_k H_k^T \left\{ H_k P'_k H_k^T + R_k [I_k - G_k (G_k^T R_k^{-1} G_k)^{-1} G_k^T R_k^{-1}]^{-1} \right\}^{-1} \\ \bar{x}_k &= \bar{x}_k + K_k (y_k - H_k \bar{x}_k) \\ P_{x_k} &= (I - K_k H_k) P'_{x_k} \\ \bar{z}_k &= -(G_k^T R_k^{-1} G_k)^{-1} G_k^T R_k^{-1} (H_k K_k - I) (y_k - H_k \bar{x}_k) \\ P_{z_k} &= (G_k^T R_k^{-1} G_k)^{-1} \left[ I + G_k^T R_k^{-1} H_k (I - K_k H_k) P'_{x_k} H_k^T R_k^{-1} G_k (G_k^T R_k^{-1} G_k)^{-1} \right] \end{aligned} \right\} \quad (6-77)$$

Eq.(6-77) is also called Extended Kalman Filter (EKF).

### 6.2.3 Kinematic Orbit Determination

The kinematic method, which is traditionally used for ground navigation and positioning, can also be used for orbit determination. Kinematic orbit determination is independent of the satellite dynamic force model and is a geometrical method, which does not consider the dynamic property of moving objects. In other words the kinematic method does not consider the attractions from various sources on satellites. This property is especially beneficial for orbit determination during satellite maneuver, because the exact satellite maneuver force model is difficult to be constructed. The accuracy of the kinematic orbit determination is strongly dependent on the accuracy of observations. This is big difference from dynamic method. The accuracy of the dynamic orbit determination method is not only dependent on the observation, but also dependent on the satellite force models. The disadvantage of kinematic orbit determination is that the observation sample rate should be higher than that of dynamic orbit method, which results in huge observation volume. Another disadvantage is that it is not able to use the kinematic method to predict satellite orbit. This may be a serious problem for users of real-time navigation and positioning applications. Specifically, the kinematic orbit determination is used in such situations where the satellite dynamical forces are difficult to be precisely described by mathematical models, for example, during satellite maneuver. In addition, kinematic orbit determination can also be used to determine some dynamic parameters. Another interesting aspect of kinematic orbit determination is onboard satellite autonavigation. In this mode, high accuracy of orbit determination can be achieved. The satellite orbit integrity is enhanced by comparing the orbit results determined onboard with the results by the ground-based method.

It should be noted that kinematic orbit determination described here is different from other kinematic orbit applications (Byun et al 1998 and Balbach et al 1998). Byun et al used onboard GPS receivers to determine satellite orbit just like ground kinematic navigation and positioning. In our method, onboard GPS receivers are not necessary and the kinematic orbit determination is still based on ground-based tracking network.

For GEO satellite, the state vector may be written as

$$\mathbf{x} = \begin{bmatrix} x \\ y \\ z \\ \dot{x} \\ \dot{y} \\ \dot{z} \\ \ddot{x} \\ \ddot{y} \\ \ddot{z} \\ p_1 \\ p_2 \\ M \\ p_n \end{bmatrix} \quad (6-78)$$

where

- $x$        $x$  component of satellite position in the Earth-fixed system
- $y$        $y$  component of satellite position in the Earth-fixed system
- $z$        $z$  component of satellite position in the Earth-fixed system
- $\dot{x}$       $x$  component of satellite velocity in the Earth-fixed system
- $\dot{y}$       $y$  component of satellite velocity in the Earth-fixed system
- $\dot{z}$       $z$  component of satellite velocity in the Earth-fixed system
- $\ddot{x}$      $x$  component of satellite acceleration in the Earth-fixed system
- $\ddot{y}$      $y$  component of satellite acceleration in the Earth-fixed system
- $\ddot{z}$      $z$  component of satellite acceleration in the Earth-fixed system
- $p_i$     other parameters such as clock error, tropospheric correction etc.

Kinematic orbit determination can be used in the Earth-fixed coordinate system. This is different from dynamic orbit determination which is only used in an inertial coordinate system.

For state vector Eq.(6-78), state transition matrix is given by

$$\Phi_{k,k-1} = \begin{bmatrix} 1 & 0 & 0 & \Delta t & 0 & 0 & \frac{1}{2}\Delta t^2 & 0 & 0 & a_{1,10} & a_{1,11} & \Lambda & a_{1,n} \\ 0 & 1 & 0 & 0 & \Delta t & 0 & 0 & \frac{1}{2}\Delta t^2 & 0 & a_{2,10} & a_{2,11} & \Lambda & a_{2,n} \\ 0 & 0 & 1 & 0 & 0 & \Delta t & 0 & 0 & \frac{1}{2}\Delta t^2 & a_{3,10} & a_{3,11} & \Lambda & a_{3,n} \\ 0 & 0 & 0 & 1 & 0 & 0 & \Delta t & 0 & 0 & a_{4,10} & a_{4,11} & \Lambda & a_{4,n} \\ 0 & 0 & 0 & 0 & 1 & 0 & 0 & \Delta t & 0 & a_{5,10} & a_{5,11} & \Lambda & a_{5,n} \\ 0 & 0 & 0 & 0 & 0 & 1 & 0 & 0 & \Delta t & a_{6,10} & a_{6,11} & \Lambda & a_{6,n} \\ 0 & 0 & 0 & 0 & 0 & 0 & 1 & 0 & 0 & a_{7,10} & a_{7,11} & \Lambda & a_{7,n} \\ 0 & 0 & 0 & 0 & 0 & 0 & 0 & 1 & 0 & a_{8,10} & a_{8,11} & \Lambda & a_{8,n} \\ 0 & 0 & 0 & 0 & 0 & 0 & 0 & 0 & 1 & a_{9,10} & a_{9,11} & \Lambda & a_{9,n} \\ 0 & 0 & 0 & 0 & 0 & 0 & 0 & 0 & 0 & a_{10,10} & 0 & \Lambda & 0 \\ 0 & 0 & 0 & 0 & 0 & 0 & 0 & 0 & 0 & 0 & a_{11,11} & \Lambda & 0 \\ \Lambda & \Lambda & \Lambda & \Lambda & \Lambda & \Lambda & \Lambda & \Lambda & \Lambda & \Lambda & \Lambda & \Lambda & \Lambda \\ 0 & 0 & 0 & 0 & 0 & 0 & 0 & 0 & 0 & 0 & 0 & \Lambda & a_{n,n} \end{bmatrix} \quad (6-79)$$

where

$$\Delta t = t_k - t_{k-1}$$

$a_{1,10}, \Lambda, a_{nn}$  are coefficients of  $\Delta p_i$ .

The system and observation equations for Kalman filter are

$$\left. \begin{aligned} \overset{\omega}{x}_k &= \Phi_{k,k-1} \overset{\omega}{x}_{k-1} + \Gamma_{k,k-1} \overset{\omega}{w}_k \\ \overset{\omega}{y}_k &= H_k \overset{\omega}{x}_k + \overset{\omega}{\varepsilon}_k \end{aligned} \right\} \quad (6-80)$$

Then Kalman filter which can be used in kinematic orbit determination is

$$\left. \begin{aligned} \overset{\omega}{x}_k &= \Phi_{k,k-1} \overset{\omega}{x}_{k-1} \\ P'_k &= \Phi_{k,k-1} P_{k-1} \Phi_{k,k-1}^T + \Gamma_{k,k-1} Q_{k-1} \Gamma_{k,k-1}^T \\ K_k &= P'_k H_k^T (H_k P'_k H_k^T + R_k)^{-1} \\ \overset{\omega}{x}_k &= \overset{\omega}{x}_k + K_k (y_k - H_k \overset{\omega}{x}_k) \\ P_k &= (I - K_k H_k) P'_k \end{aligned} \right\} \quad (6-81)$$

where

- $\overset{\omega}{x}_k$  system status vector at epoch  $k$
- $\overset{\omega}{w}_k$  process noise at epoch  $k$
- $\overset{\omega}{y}_k$  vector of observations
- $\overset{\omega}{\varepsilon}_k$  measurement noise
- $\Phi_{k,k-1}$  state transition matrix between epochs  $k, k-1$
- $G_{k,k-1}$  system noise matrix between epochs  $k, k-1$
- $H_k$  design matrix
- $P'_k$  predicted covariance matrix at epoch  $k$
- $P_k$  improved covariance matrix at epoch  $k$
- $K_k$  Kalman filter gain matrix
- $\overset{\omega}{x}_k$  prediction of  $\overset{\omega}{x}_k$  at epoch  $k$
- $\overset{\omega}{x}_k$  estimation of  $\overset{\omega}{x}_k$  based on the measurements  $\overset{\omega}{y}_1$  to  $\overset{\omega}{y}_{k-1}$

Because geostationary satellite moves very slowly relative to the Earth, the polynomial with second order is precise enough to be used in the state transition matrix of Eq.(6-79).

The kinematic orbit determination can also be used with satellite dynamic models that are used to produce reference orbit, therefore Eq.(6-77) can be modified as follows

$$\left. \begin{aligned} \bar{\mathbf{x}}_k &= f(\bar{\mathbf{x}}_k, t) \\ P'_k &= \Phi_{k,k-1} P_{k-1} \Phi_{k,k-1}^T + \Gamma_{k,k-1} Q_{k-1} \Gamma_{k,k-1}^T \\ K_k &= P'_k H_k^T (H_k P'_k H_k^T + R_k)^{-1} \\ \bar{\mathbf{x}}_k &= \bar{\mathbf{x}}_k + K_k (y_k - H_k \bar{\mathbf{x}}_k) \\ P_k &= (I - K_k H_k) P'_k \end{aligned} \right\} \quad (6-82)$$

## 6.2.4 Reduced-Dynamic Method

Dynamic orbit determination is a very precise method, its accuracy, however, is strongly dependent on the satellite force models. The accuracy of orbit determination is significantly reduced if the satellite forces are mismodeled. The kinematic orbit determination is a purely geometric method. The accuracy of the orbit determination is completely dependant on the accuracy of observation. The errors of satellite force models do not affect the accuracy of kinematic orbit determination. The reduced dynamic method may be defined as the half dynamic and the half geometric method, in which the satellite force models are modeled as sum of deterministic and stochastic components. The stochastic force model is characterized by two selectable parameters: a correlation time constant  $T$  and a steady state variance  $V$ . In the Kalman filter, the stochastic force models are estimated at each step. When  $T$  is set to zero, and  $V$  is made large, orbit determination method will become geometric(kinematic) one, because deterministic components are not considered in Kalman filter; if  $T$  is large and  $V$  is zero, the orbit determination method becomes dynamic one, stochastic components are not estimated. That orbit is determined by adjusting  $T$  and  $V$  to balance dynamic, geometric and measurement errors is called the reduced dynamic method (Yunk et al, 1994). Reduced dynamic orbit determination was successfully used for the TOPEX/Poseidon mission. The results have been compared with flight GPS receiver and laser/DORIS dynamic solutions. About 3 cm RMS accuracy in altitude can be obtained (Yunk et al, 1994).

Kalman filter algorithm for reduced dynamic orbit determination may be written as follows

$$\left. \begin{aligned} \bar{\mathbf{x}}_k &= f'(\bar{\mathbf{x}}_k, t) \\ P'_k &= \Phi_{k,k-1} P_{k-1} \Phi_{k,k-1}^T + \Gamma_{k,k-1} Q_{k-1} \Gamma_{k,k-1}^T \\ K_k &= P'_k H_k^T (H_k P'_k H_k^T + R_k)^{-1} \\ \bar{\mathbf{x}}_k &= \bar{\mathbf{x}}_k + K_k (y_k - H_k \bar{\mathbf{x}}_k) \\ P_k &= (I - K_k H_k) P'_k \end{aligned} \right\} \quad (6-83)$$

where,  $Q_{k-1}$  is dependent on two adjustable parameters  $T$  and  $V$ ; force model  $f'(\bar{\mathbf{x}}_k, t)$  is imperfect and mainly composed of deterministic components. The parts of parameters of stochastic component are included in  $\bar{\mathbf{x}}_k$ .

In order to predict highly precise satellite orbits for a long arc, some imperfect dynamic parameters such as solar radiation coefficients should be included in the state vector to solve these parameters during orbit determination. The sample rate of observations for the reduced dynamic method should be higher than that for the dynamic method, but lower than that of kinematic method. In other words, the dynamic method needs less observations than the reduced dynamic and kinematic methods. In order to obtain high accuracy orbit, the kinematic method requires lots of observations in short time.

## 6.3 Data Processing

In the following, data processing for orbit determination and the difference between sequential and batch processing will be discussed.

### 6.3.1 Batch Processing

Precise satellite orbit determination is usually post-processed in batch mode, i.e. all observation data available in a tracking session is collected and processed together. Using this mode the highest accuracy of orbit determination can be achieved. The basic method can be briefly described as follows.

Assuming that the satellite state vector is  $\overset{w}{x} = \{x, y, z, \dot{x}, \dot{y}, \dot{z}\}$ , the state transition matrix is  $\Phi(t_i, t_{i-1})$  and the observation is  $\rho_i$ . If the observation set is available in the following forms,

$$L = \{\rho_1(t_1), \rho_2(t_1), \dots, \rho_n(t_1); \rho_1(t_2), \rho_2(t_2), \dots, \rho_n(t_2); \dots; \rho_1(t_k), \rho_2(t_k), \dots, \rho_n(t_k)\},$$

then

$$L_1 = \begin{bmatrix} \Delta\rho_1(t_1) \\ \Delta\rho_2(t_1) \\ \Lambda \\ \Delta\rho_n(t_1) \end{bmatrix} = H_1 \Phi(t_1, t_0) \overset{w}{x}_0 + \overset{w}{\varepsilon}_1 \quad (6-85)$$

$$L_2 = \begin{bmatrix} \Delta\rho_1(t_2) \\ \Delta\rho_2(t_2) \\ \Lambda \\ \Delta\rho_n(t_2) \end{bmatrix} = H_2 \Phi(t_2, t_0) \overset{w}{x}_0 + \overset{w}{\varepsilon}_2 \quad (6-86)$$

$$\dots\dots\dots$$

$$L_k = \begin{bmatrix} \Delta\rho_1(t_k) \\ \Delta\rho_2(t_k) \\ \Lambda \\ \Delta\rho_n(t_k) \end{bmatrix} = H_k \Phi(t_k, t_0) \overset{w}{x}_0 + \overset{w}{\varepsilon}_k \quad (6-87)$$

where

- $L_i$  the sub-observation matrix at epoch  $i$ ,
- $\Delta\rho_i(t_j)$  the difference between computation and observation at tracking station  $i$  and epoch  $t_j$ ,
- $H_i$  the observation coefficient at epoch  $i$ ,
- $\Phi(t_i, t_0)$  the state transition matrix between epoch  $t_i$  and  $t_0$ ,
- $\overset{w}{x}_0$  the initial state vector including initial orbit parameters and initial ambiguities.

$\overset{w}{x}_0$  can be solved using least-squares solution

$$\overset{w}{L} = \begin{bmatrix} L_1 \\ L_2 \\ \dots \\ L_k \end{bmatrix} = \begin{bmatrix} H_1 \Phi(t_1, t_0) \\ H_2 \Phi(t_2, t_0) \\ \dots \\ H_k \Phi(t_k, t_0) \end{bmatrix} \overset{w}{x}_0 + \overset{w}{\varepsilon}$$

$$\overset{w}{H}^T \overset{w}{P} \overset{w}{H} \overset{w}{x}_0 + \overset{w}{H}^T \overset{w}{P} \overset{w}{L} = 0 \quad (6-88)$$

$$\overset{w}{x}_0 = -(\overset{w}{H}^T \overset{w}{P} \overset{w}{H})^{-1} \overset{w}{H}^T \overset{w}{P} \overset{w}{L}$$

where

$$\overset{w}{H} = \begin{bmatrix} H_1 \Phi(t_1, t_0) \\ H_2 \Phi(t_2, t_0) \\ \dots \\ H_k \Phi(t_k, t_0) \end{bmatrix}$$



$P$  the weight matrix of all observations

### 6.3.2 Sequential Processing

According to discussion in section §6.2.1, sequential processing is used for both real-time and post-processing applications. Orbit determination will be updated when the new observations are available. The basic equations are Eq.(6-77), Eq.(6-81), Eq.(6-82) and Eq.(6-83).

### 6.3.3 Comparison Between Batch and Sequential Processing

From the mathematical point of view, the result of batch processing is different from sequential processing, only at the final epoch the results should be the same. This can be explained by the following figures

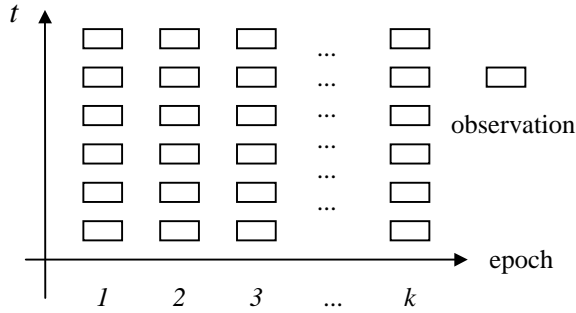


Figure 6-1 Batch Processing

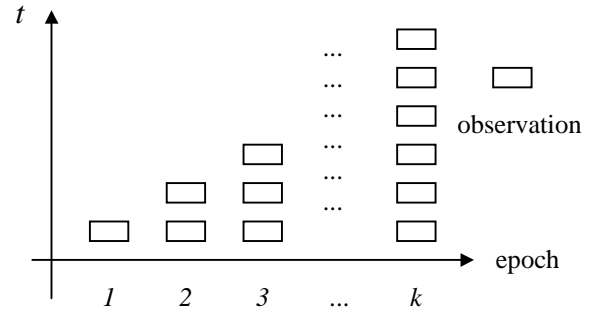


Figure 6-2 Sequential Processing

In Figure 6-1 and Figure 6-2, the box represents the observation, vertical axis represents the time in which observation has been made, horizontal axis stands for epoch at which observation has been processed by sequential or batch processing mode.

From Figure 6-1 and Figure 6-2 it can be seen that batch processing uses all observations during whole observation session to determine the satellite orbit. Sequential processing uses all observations available until the current to determine satellite orbit. From Figure 6-1, at epoch 1 the orbit results are produced by processing all observations. From epoch 2, epoch 3 ... until epoch  $k$ , the used observations are same for all epochs by batch processing. From Figure 6-2, procedures are different. At first epoch only observation at first epoch is used; at second epoch only first and second observations are used; at  $k$  epoch all observations from first epoch to  $k$ -th epoch are used. In other words, sequential processing only uses *past and current* observations and does not use *future* observations. From the description above we can see that the accuracy of orbit determination for the whole orbit arc length by batch processing is uniform, but the accuracy of orbit determination by sequential processing is not uniform. For sequential processing the accuracy of orbit determination will gradually become better and better as the new observations come and are processed.

The exact proof can be given as follows: starting from simple situation, only two observations at two epochs  $y_1, y_2$  are considered.

From batch processing

$$\begin{pmatrix} y_1 \\ y_2 \\ x_1 \end{pmatrix} = \begin{pmatrix} H_1 x'_1 \\ H_2 \Phi_{21} x'_1 \\ x'_1 \end{pmatrix} + \begin{pmatrix} \varepsilon_1 \\ \varepsilon_2 \\ \varepsilon_3 \end{pmatrix} \quad (6-88)$$

The solution

$$x_1 = \left[ (H_1^T R_1^{-1} H_1 + P_1^{-1}) + \Phi_{21}^T H_2^T R_2^{-1} H_2 \Phi_{21} \right]^{-1} \left[ (H_1^T R_1^{-1} y_1 + P_1^{-1} x'_1) + \Phi_{21}^T H_2^T R_2^{-1} y_2 \right] \quad (6-89)$$

and

$$x_2 = \Phi_{21} \left[ (H_1^T R_1^{-1} H_1 + P_1^{-1}) + \Phi_{21}^T H_2^T R_2^{-1} H_2 \Phi_{21} \right]^{-1} \left[ (H_1^T R_1^{-1} y_1 + P_1^{-1} x'_1) + \Phi_{21}^T H_2^T R_2^{-1} y_2 \right] \quad (6-90)$$

Eq.(6-89) and Eq.(6-90) are the results of batch processing.

From the sequential processing by using Kalman filter, the results are

$$x_1 = x'_1 + K_1(y_1 - H_1 x'_1) \quad (6-91)$$

$$x_2 = x'_2 + K_2(y_2 - H_2 x'_2) \quad (6-92)$$

$$x'_2 = \Phi_{21} x_1 = \Phi_{21} [x'_1 + K_1(y_1 - H_1 x'_1)] \quad (6-93)$$

$$K_1 = P'_1 H_1^T (H_1 P'_1 H_1^T + R_1)^{-1} \quad (6-94)$$

$$\begin{aligned} K_2 &= P'_2 H_2^T (H_2 P'_2 H_2^T + R_2)^{-1} = \Phi_{21} P_1 \Phi_{21}^T H_2^T (H_2 \Phi_{21} P_1 \Phi_{21}^T H_2^T + R_2)^{-1} \\ &= \Phi_{21} (I - K_1 H_1) P'_1 \Phi_{21}^T H_2^T [H_2 \Phi_{21} (I - K_1 H_1) P'_1 \Phi_{21}^T H_2^T + R_2]^{-1} \end{aligned} \quad (6-95)$$

According to Eq.(6-93) to Eq.(6-95), Eq.(6-92) becomes

$$\begin{aligned} x_2 &= \Phi_{21} [x'_1 + K_1(y_1 - H_1 x'_1)] + \Phi_{21} (I - K_1 H_1) P'_1 \Phi_{21}^T H_2^T [H_2 \Phi_{21} (I - K_1 H_1) P'_1 \Phi_{21}^T H_2^T + R_2]^{-1} \\ &\quad \times [y_2 - H_2 \Phi_{21} (x'_1 + K_1(y_1 - H_1 x'_1))] \end{aligned} \quad (6-96)$$

Considering Eq.(6-23) and Eq.(6-29),

$$(I - K_1 H_1) P'_1 = [P'_1 - P'_1 H_1^T (H_1 P'_1 H_1^T + R_1)^{-1} H_1 P'_1] = (H_1^T R_1^{-1} H_1 + P_1'^{-1})^{-1} \quad (6-97)$$

$$\begin{aligned} (I - K_1 H_1) P'_1 H_1^T R_1^{-1} &= (H_1^T R_1^{-1} H_1 + P_1'^{-1})^{-1} H_1^T R_1^{-1} \\ &= P'_1 H_1^T (H_1 P'_1 H_1^T + R_1)^{-1} = K_1 \end{aligned} \quad (6-98)$$

Therefore

$$\begin{aligned} &x'_1 + K_1(y_1 - H_1 x'_1) \\ &= K_1 y_1 + x'_1 - K_1 H_1 x'_1 \\ &= (I - K_1 H_1) P'_1 H_1^T R_1^{-1} y_1 + (I - K_1 H_1) P'_1 P_1'^{-1} x'_1 \\ &= (I - K_1 H_1) P'_1 (H_1^T R_1^{-1} y_1 + P_1'^{-1} x'_1) \\ &= (H_1^T R_1^{-1} H_1 + P_1'^{-1})^{-1} (H_1^T R_1^{-1} y_1 + P_1'^{-1} x'_1) \end{aligned} \quad (6-99)$$

Sequential result  $x_2$  can be written as

$$\begin{aligned} x_2 &= \Phi_{21} \left\{ (H_1^T R_1^{-1} H_1 + P_1'^{-1})^{-1} (H_1^T R_1^{-1} y_1 + P_1'^{-1} x'_1) \right. \\ &\quad \left. + (H_1^T R_1^{-1} H_1 + P_1'^{-1})^{-1} \Phi_{21}^T H_2^T [H_2 \Phi_{21} (H_1^T R_1^{-1} H_1 + P_1'^{-1})^{-1} \Phi_{21}^T H_2^T + R_2]^{-1} \right. \\ &\quad \left. \times [y_2 - H_2 \Phi_{21} (H_1^T R_1^{-1} H_1 + P_1'^{-1})^{-1} (H_1^T R_1^{-1} y_1 + P_1'^{-1} x'_1)] \right\} \\ &= \Phi_{21} \left\{ (H_1^T R_1^{-1} H_1 + P_1'^{-1})^{-1} (H_1^T R_1^{-1} y_1 + P_1'^{-1} x'_1) \right. \\ &\quad \left. + [(H_1^T R_1^{-1} H_1 + P_1'^{-1}) + \Phi_{21}^T H_2^T R_2^{-1} H_2 \Phi_{21}]^{-1} \Phi_{21}^T H_2^T R_2^{-1} \right. \\ &\quad \left. \times [y_2 - H_2 \Phi_{21} (H_1^T R_1^{-1} H_1 + P_1'^{-1})^{-1} (H_1^T R_1^{-1} y_1 + P_1'^{-1} x'_1)] \right\} \\ &= \Phi_{21} \left\{ [(H_1^T R_1^{-1} H_1 + P_1'^{-1}) + \Phi_{21}^T H_2^T R_2^{-1} H_2 \Phi_{21}]^{-1} \Phi_{21}^T H_2^T R_2^{-1} y_2 \right. \\ &\quad \left. + [(H_1^T R_1^{-1} H_1 + P_1'^{-1})^{-1} \right. \\ &\quad \left. - [(H_1^T R_1^{-1} H_1 + P_1'^{-1}) + \Phi_{21}^T H_2^T R_2^{-1} H_2 \Phi_{21}]^{-1} \Phi_{21}^T H_2^T R_2^{-1} H_2 \Phi_{21} (H_1^T R_1^{-1} H_1 + P_1'^{-1})^{-1}] (H_1^T R_1^{-1} y_1 + P_1'^{-1} x'_1) \right\} \\ &= \Phi_{21} \left\{ [(H_1^T R_1^{-1} H_1 + P_1'^{-1}) + \Phi_{21}^T H_2^T R_2^{-1} H_2 \Phi_{21}]^{-1} \Phi_{21}^T H_2^T R_2^{-1} y_2 \right. \\ &\quad \left. + [(H_1^T R_1^{-1} H_1 + P_1'^{-1}) + \Phi_{21}^T H_2^T R_2^{-1} H_2 \Phi_{21}]^{-1} [(H_1^T R_1^{-1} H_1 + P_1'^{-1})^{-1} \{ (H_1^T R_1^{-1} H_1 + P_1'^{-1}) + \Phi_{21}^T H_2^T R_2^{-1} H_2 \Phi_{21} \} \right. \\ &\quad \left. - \Phi_{21}^T H_2^T R_2^{-1} H_2 \Phi_{21} (H_1^T R_1^{-1} H_1 + P_1'^{-1})^{-1}] (H_1^T R_1^{-1} y_1 + P_1'^{-1} x'_1) \right\} \end{aligned} \quad (6-100)$$

In Eq.(6-100), because

$(H_1^T R_1^{-1} H_1 + P_1'^{-1})^{-1}$  and  $\Phi_{21}^T H_2^T R_2^{-1} H_2 \Phi_{21}$  are positive and symmetrical matrices, therefore

$$(H_1^T R_1^{-1} H_1 + P_1'^{-1})^{-1} \Phi_{21}^T H_2^T R_2^{-1} H_2 \Phi_{21} = \Phi_{21}^T H_2^T R_2^{-1} H_2 \Phi_{21} (H_1^T R_1^{-1} H_1 + P_1'^{-1})^{-1}$$

then Eq.(6-100) becomes

$$x_2 = \Phi_{21} \left[ (H_1^T R_1^{-1} H_1 + P_1'^{-1}) + \Phi_{21}^T H_2^T R_2^{-1} H_2 \Phi_{21} \right]^{-1} \left[ (H_1^T R_1^{-1} y_1 + P_1'^{-1} x_1') + \Phi_{21}^T H_2^T R_2^{-1} y_2 \right] \quad (6-101)$$

The sequential results are expressed by Eq.(6-99) and Eq.(6-101). Clearly Eq.(6-101) is the same as Eq.(6-90), i.e. both batch and sequential processing should have the same results at the final epoch. Eq.(6-99) is different from Eq.(6-89), which means except final epoch, the results of sequential processing at other epochs are different from batch processing. Similarly, for observations  $y_1, y_2, \dots, y_n$  the results of batch and sequential processing at the epoch  $n$  can be expressed as

$$x_n = \Phi_{n1} \left[ (H_1^T R_1^{-1} H_1 + P_1'^{-1}) + \sum_{i=2}^n \Phi_{i1}^T H_i^T R_i^{-1} H_i \Phi_{i1} \right]^{-1} \left[ (H_1^T R_1^{-1} y_1 + P_1'^{-1} x_1') + \sum_{i=2}^n \Phi_{i1}^T H_i^T R_i^{-1} y_i \right] \quad (6-102)$$

But actually, due to accuracy limit, after some steps of process the sequential processing has almost the same results as batch processing, referred to Figure 6-3 and Figure 6-4.

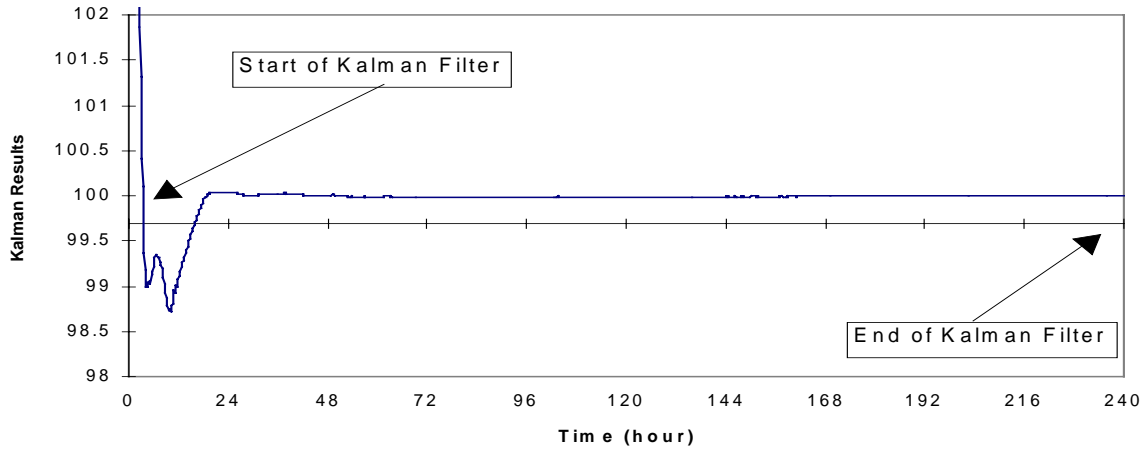


Figure 6-3 Sequential Processing

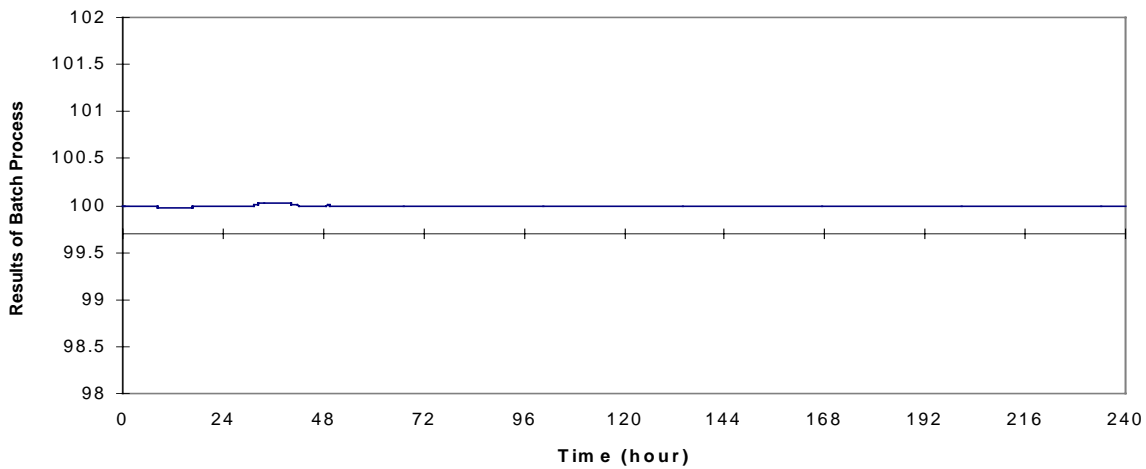


Figure 6-4 Batch Processing



## CHAPTER 7 ORBIT DETERMINATION USING CARRIER PHASE OBSERVATIONS

Highly precise orbit determination of IGSO, GEO and MEO satellites is a key issue for second generation of Global Navigation Satellite System (GNSS-2). According to research work (Hein et al, 1997), using pseudo-range observation the accuracy of orbit determination of IGSO and GEO satellites is about 1-2 meters. In order to obtain better accuracy of satellite orbits, one should use the carrier phase measurements that are the most accurate observations available at present. The carrier phase observable is biased by integer number of cycles called an initial ambiguity. If the initial ambiguities of carrier phase observations are solved, precise orbit determination with the accuracy of order of better than 1 meter level can be achieved.

In this chapter, the orbit determination of IGSO, GEO and MEO satellites using carrier phase observations are described. Some problems of carrier phase observations with IGSO, GEO and MEO orbit determination are presented. The initial ambiguity resolution which could be used for orbit determination are discussed. In order to overcome the influence of multipath effects on initial ambiguity resolution, a new and unique method for reduction of multipath effects is presented and discussed. The results of orbit determination using carrier phase observations based on simulation data are shown in §9.3, Chapter 9. The cycle slip problem in the carrier phase observations is not considered.

### 7.1 Mathematical Models for Carrier Phase Observations

#### 7.1.1 Carrier Phase

Orbit determination using carrier-phase observations is greatly different from that using range observations. Carrier phase observations are biased by integer number of cycles and oscillator frequency offsets between the transmitter and the receiver. In the observation equations, the initial ambiguities should be included as parameters and resolved with other parameters at the same time. From Eq.(2-43), Chapter 2, the carrier phase observation equation is rewritten as

$$L = \varphi_r(t) - \varphi_t(t) = \frac{2\pi}{\lambda_1} S_1 + \lambda N_1 + \varepsilon \quad (7-1)$$

where

- $\varphi_r$  receiver's phase,
- $\varphi_t$  received satellite phase at the nominal reception time  $t$ ,
- $N_1$  initial integer ambiguity,
- $\lambda_1$  wavelength of signal frequency
- $c$  speed of light in vacuum,
- $\varepsilon$  carrier-phase measurement noise including hardware delays of receiver and the satellite as well as multipath.
- $S_1$  line-of-sight between satellite and tracking station

#### 7.1.2 Doppler

Doppler measurements may also be used to determine the satellite orbit. The basic observation equation of integrated Doppler count measurement is given by (Figure 2-3)

$$L = (f_0 - f_t)(t_3 - t_1) + \frac{f_0}{c}(S_2 - S_1) \quad (7-2)$$

where

- $f_0$  the reference frequency of the receiver
- $f_t$  the transmitting frequency of satellite signal (not shifted by Doppler effect)
- $S_1, S_2$  line-of-sights between satellite and tracking station at different epochs

The observation equation Eq.(7-2) can be used with Kalman filter or batch processing to determine the satellite orbit. The advantage is that there are no initial ambiguities in Doppler measurements. Due to slow changes of the line-of-sight between tracking station and GEO satellite, it is difficult to determine a GEO satellite orbit using Doppler observations. This problem will be further shown in §7.2.2.

### 7.1.3 Effects of Initial Ambiguities on Orbit Determination

Initial ambiguities will affect the accuracy of satellite orbit determination, which can be evaluated below. Rewriting Eq.(7-1):

$$\rho_i = \sqrt{(x_i - x)^2 + (y_i - y)^2 + (z_i - z)^2} + \lambda N_i \quad (7-3)$$

Differentiating Eq.(7-3),

$$\Delta \rho_i = \frac{1}{\rho'} [(x_i - x)\Delta x + (y_i - y)\Delta y + (z_i - z)\Delta z] + \lambda \Delta N_i \quad (7-4)$$

where,

$$\rho' = \sqrt{(x_i - x)^2 + (y_i - y)^2 + (z_i - z)^2}$$

Assuming that the accuracy of  $\Delta x, \Delta y, \Delta z$  are equal and  $\Delta \rho = 0$ . The vectors  $\overset{w}{r}, \overset{w}{r}_i$  and  $\Delta \overset{w}{r}$  can be expressed as

$$\left. \begin{aligned} \overset{w}{r} &= x_i i + y_j j + z_k k \\ \overset{w}{r}_i &= x_i i + y_i j + z_i k \\ \Delta \overset{w}{r} &= \Delta x i + \Delta y j + \Delta z k \end{aligned} \right\} \quad (7-5)$$

Then Eq.(7-4) becomes

$$\lambda N_i = \frac{(\overset{w}{r} - \overset{w}{r}_i) \Delta \overset{w}{r}}{|\overset{w}{r} - \overset{w}{r}_i|} = \frac{|\overset{w}{r} - \overset{w}{r}_i| |\Delta \overset{w}{r}| \cos \theta}{|\overset{w}{r} - \overset{w}{r}_i|} \quad (7-6)$$

letting  $\theta=0$ , Eq.(7-6) can be written as

$$\lambda N_i = |\Delta \overset{w}{r}| \quad (7-7)$$

Eq.(7-7) shows the influence of initial ambiguity on the accuracy of orbit determination. Using GPS L1 frequency as an example, one cycle error in the initial ambiguity will cause 0.19 meter error in satellite orbit.

### 7.1.4 Kalman Filter for Orbit Determination using Carrier Phase Observation

Using the Kalman filter and carrier-phase observations to determine IGSO, GEO and MEO satellite orbits, the initial ambiguities should be included as system parameters in the satellite dynamical model or as non-random parameters in observation equations. The float solutions are obtained as Kalman filter processes the incoming observations. In order to fix the float ambiguities to integers, it is necessary to take special strategies such as bias optimizing (Blewitt, 1989), LAMBDA (Teunissen 1994 and Jonge et al, 1996), TCAR (Harris, 1996 and Forssell et al 1997), etc..

Assuming that the state variance is  $\overset{w}{x} = \{x, y, z, \lambda N_1, \lambda N_2, \lambda N_3, \dots, \lambda N_n\}$  in which  $n$  is the number of tracking stations, the satellite movement equation has a following form,

$$\frac{d\overset{w}{x}}{dt} = f[\overset{w}{x}(t), t] = \begin{bmatrix} f_1 \\ f_2 \\ \dots \\ f_n \end{bmatrix} \quad (7-8)$$

the state transition matrix  $\Phi$  can be written as follows

$$\frac{d\Phi}{dt} = F\Phi \quad (7-9)$$

where,

$$F = \begin{bmatrix} \frac{\partial f_1}{\partial x} & \frac{\partial f_1}{\partial y} & \frac{\partial f_1}{\partial z} & \frac{\partial f_1}{\partial \lambda} & \frac{\partial f_1}{\partial \lambda} & \frac{\partial f_1}{\partial \lambda} & \frac{\partial f_1}{\partial N_1} & \cdots & \frac{\partial f_1}{\partial N_n} \\ \frac{\partial f_2}{\partial x} & \frac{\partial f_2}{\partial y} & \frac{\partial f_2}{\partial z} & \frac{\partial f_2}{\partial \lambda} & \frac{\partial f_2}{\partial \lambda} & \frac{\partial f_2}{\partial \lambda} & \frac{\partial f_2}{\partial N_1} & \cdots & \frac{\partial f_2}{\partial N_n} \\ \frac{\partial f_3}{\partial x} & \frac{\partial f_3}{\partial y} & \frac{\partial f_3}{\partial z} & \frac{\partial f_3}{\partial \lambda} & \frac{\partial f_3}{\partial \lambda} & \frac{\partial f_3}{\partial \lambda} & \frac{\partial f_3}{\partial N_1} & \cdots & \frac{\partial f_3}{\partial N_n} \\ \frac{\partial f_4}{\partial x} & \frac{\partial f_4}{\partial y} & \frac{\partial f_4}{\partial z} & \frac{\partial f_4}{\partial \lambda} & \frac{\partial f_4}{\partial \lambda} & \frac{\partial f_4}{\partial \lambda} & \frac{\partial f_4}{\partial N_1} & \cdots & \frac{\partial f_4}{\partial N_n} \\ \cdots & \cdots & \cdots & \cdots & \cdots & \cdots & \cdots & \cdots & \cdots \\ \frac{\partial f_k}{\partial x} & \frac{\partial f_k}{\partial y} & \frac{\partial f_k}{\partial z} & \frac{\partial f_k}{\partial \lambda} & \frac{\partial f_k}{\partial \lambda} & \frac{\partial f_k}{\partial \lambda} & \frac{\partial f_k}{\partial N_1} & \cdots & \frac{\partial f_k}{\partial N_n} \\ \cdots & \cdots & \cdots & \cdots & \cdots & \cdots & \cdots & \cdots & \cdots \\ \frac{\partial f_n}{\partial x} & \frac{\partial f_n}{\partial y} & \frac{\partial f_n}{\partial z} & \frac{\partial f_n}{\partial \lambda} & \frac{\partial f_n}{\partial \lambda} & \frac{\partial f_n}{\partial \lambda} & \frac{\partial f_n}{\partial N_1} & \cdots & \frac{\partial f_n}{\partial N_n} \end{bmatrix} \quad (7-10)$$

The transition matrix  $\Phi$  with initial ambiguities as parameters is more complex than without initial ambiguities. The Kalman filter algorithms discussed in Chapter 6 can be used with carrier phase observation for satellite orbit determination.

According to Eq.(7-1), the carrier phase range equations can be written as

$$\rho_i = \sqrt{(x_i - x)^2 + (y_i - y)^2 + (z_i - z)^2} + \lambda N_i \quad (7-11)$$

linearizing Eq.(7-10),

$$\Delta \rho_i = \frac{1}{\rho'} [(x_i - x)\Delta x + (y_i - y)\Delta y + (z_i - z)\Delta z] + \lambda \Delta N_i \quad (7-12)$$

Then,

$$\overset{\omega}{y} = H\overset{\omega}{\Delta x} + \overset{\omega}{\varepsilon} \quad (7-13)$$

where,

$$\overset{\omega}{y} = \begin{bmatrix} \Delta \rho_1 \\ \Delta \rho_2 \\ \Delta \rho_3 \\ \cdots \\ \Delta \rho_m \end{bmatrix}, \quad H = \begin{bmatrix} \frac{\partial \rho_1}{\partial x} & \frac{\partial \rho_1}{\partial y} & \frac{\partial \rho_1}{\partial z} & \frac{\partial \rho_1}{\partial \lambda} & \frac{\partial \rho_1}{\partial \lambda} & \frac{\partial \rho_1}{\partial \lambda} & \frac{\partial \rho_1}{\partial N_1} & \cdots & \frac{\partial \rho_1}{\partial N_n} \\ \frac{\partial \rho_2}{\partial x} & \frac{\partial \rho_2}{\partial y} & \frac{\partial \rho_2}{\partial z} & \frac{\partial \rho_2}{\partial \lambda} & \frac{\partial \rho_2}{\partial \lambda} & \frac{\partial \rho_2}{\partial \lambda} & \frac{\partial \rho_2}{\partial N_1} & \cdots & \frac{\partial \rho_2}{\partial N_n} \\ \frac{\partial \rho_3}{\partial x} & \frac{\partial \rho_3}{\partial y} & \frac{\partial \rho_3}{\partial z} & \frac{\partial \rho_3}{\partial \lambda} & \frac{\partial \rho_3}{\partial \lambda} & \frac{\partial \rho_3}{\partial \lambda} & \frac{\partial \rho_3}{\partial N_1} & \cdots & \frac{\partial \rho_3}{\partial N_n} \\ \cdots & \cdots & \cdots & \cdots & \cdots & \cdots & \cdots & \cdots & \cdots \\ \frac{\partial \rho_m}{\partial x} & \frac{\partial \rho_m}{\partial y} & \frac{\partial \rho_m}{\partial z} & \frac{\partial \rho_m}{\partial \lambda} & \frac{\partial \rho_m}{\partial \lambda} & \frac{\partial \rho_m}{\partial \lambda} & \frac{\partial \rho_m}{\partial N_1} & \cdots & \frac{\partial \rho_m}{\partial N_n} \end{bmatrix}$$

$$\overset{\omega}{\Delta x} = \{\Delta x, \Delta y, \Delta z, \Delta \lambda, \Delta \lambda, \Delta \lambda, \Delta N_1, \dots, \Delta N_n\}$$

In developing the equations above it is assumed that all observations are continuous. If the cycle slips occur, there are two methods to solve it: first using cycle slip fixing strategies to repair the cycle slips at the observation preprocessing session, therefore the above equations will never be changed; secondly the new initial ambiguities

can be added as extra parameters in satellite state vector, but the satellite dynamic and observation equations will become complicated.

## 7.2. Problems of Carrier Phase Observation

### 7.2.1 Ambiguity Solution Convergence

Normally ambiguities as parameters are solved during orbit determination at the same time as the other parameters such as satellite positions, velocities and satellite dynamic parameters. Other ambiguity solution approaches will be discussed in a later section.

The probability of ambiguity solution is dependent on the satellite types and the empirical formular can be expressed as,

$$P(\text{Ambiguity}) = f(\&PDOP) = \kappa \frac{\&}{PDOP} \quad (7-14)$$

where

- $\kappa$  coefficient related to frequency, atmosphere and so on
- $P$  probability
- $\&$  change rate of line-of-sight between tracking station and satellite

The probability of ambiguity solution related to types of satellite orbits using GPS L1 frequency as an example is approximately shown in Figure 7-1.

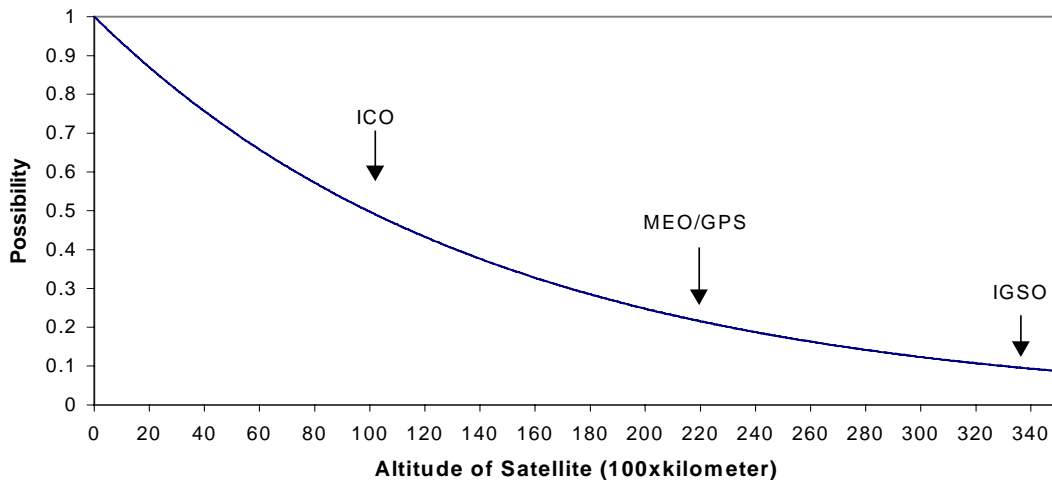


Figure 7-1 Ambiguity Solution Related to the Altitude of Satellite

In the figure above, ICO (Intermediate Circular Orbits) is a circular orbit at an altitude of around 10,000 km.

Based on mathematic point-of-view and simulation tests for various satellite constellations, the relations of ambiguity solution with ICO, MEO/GPS, IGSO and GEO satellites are listed in Table 7-1.

Table 7-1 Ambiguity Convergence

	NI	100%
ICO/(10000km)	7 <sup>m</sup>	1 <sup>h</sup>
MEO/GPS	20 <sup>m</sup>	4 <sup>h</sup>
IGSO	2 <sup>h</sup>	25 <sup>h</sup>
GEO	∞	∞



In Table 7-1, NI means that almost all of ambiguities are rounded to nearest integers. 100% means the exact integer ambiguities solved (possibly under simulation test).

From Eq.(7-14), Figure 7-1 and Table 7-1, it is obvious that the ambiguity solution is strongly dependent on the rate of change of line-of-sight between tracking station and satellite as well as PDOP. Hence, the lower the satellite orbit, the better for the ambiguity solution. For GEO satellite, if no special techniques such as wide band and multi-frequency are used, the initial ambiguity cannot be directly solved during orbit determination. This problem will be shown in the next section.

## 7.2.2 Geostationary Satellite Orbit Determination using Carrier Phase Observation

Due to the slow movement of geostationary satellite relative to the surface of the Earth, the initial ambiguities of carrier phase observations are very difficult to be solved (see Figure 7-2). For detailed information about the distribution of tracking stations, sample rate of observation, true initial ambiguities and orbital arc length are referred to Chapter 9, *Software and Simulation Results*.

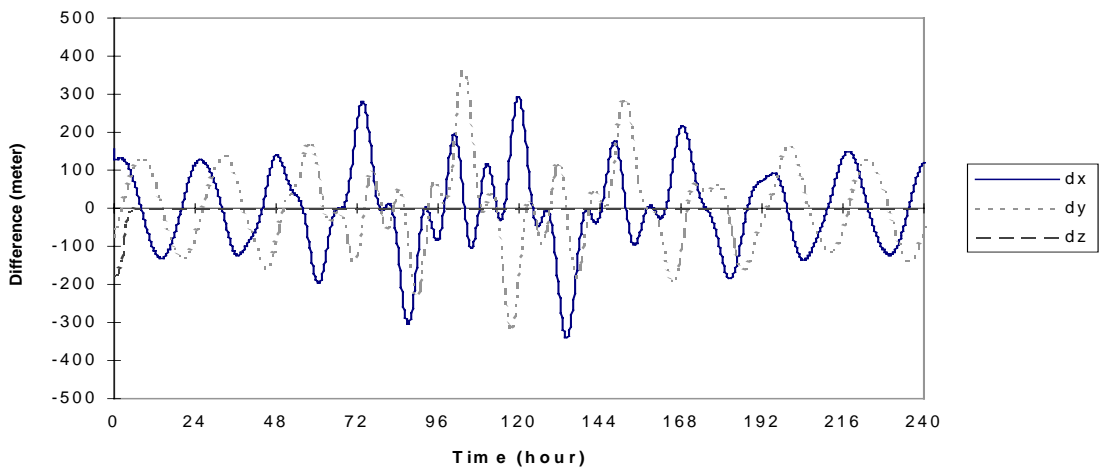


Figure 7-2 Results of Orbit Determination using Phase observation of GEO  $\lambda=-10^\circ$

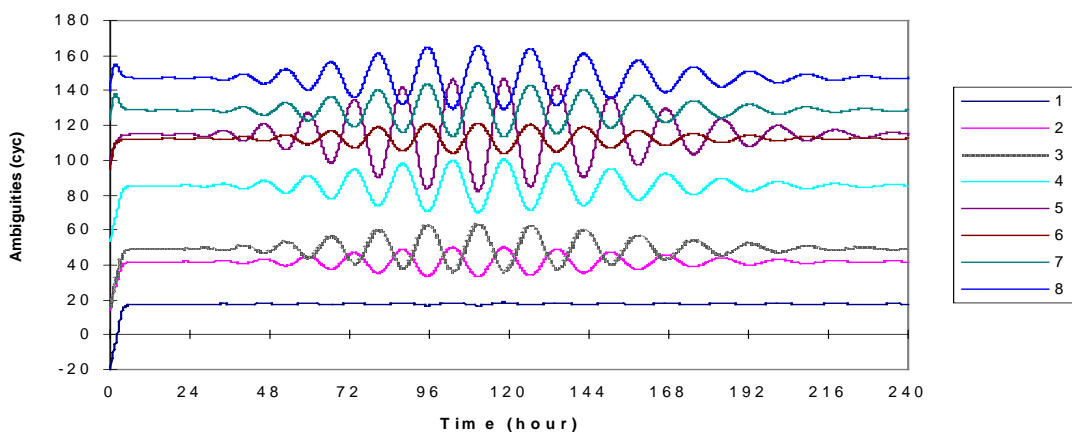


Figure 7-3 Ambiguities of GEO Orbit Determination

Figure 7-2 shows the results of GEO satellite orbit determination using carrier phase observations. Figure 7-3 shows the initial ambiguity solutions. The solution of the initial ambiguities is strongly dependent on the changes of geometry between satellites and tracking stations. GEO satellites move very slowly relative to the earth, which makes the initial ambiguities difficult to be distinguished from other parameters. The initial ambiguities for GEO satellite can be solved only before orbit determination, i.e. during observation preprocessing phase. In

order to use carrier phase observation for GEO satellite orbit determination, other independent methods such as CCD camera and SLR could be used in data preprocessing. Using these techniques, the precise distance between satellite and tracking station is obtained and the initial ambiguities of carrier phase observations can be computed. Because the tracking stations for orbit determination are located in the open area, the locked signals in the tracking stations will not be easily interrupted. Therefore initial ambiguities will not be easily changed.

### 7.3 Ambiguity Resolution Approaches

There are many ambiguity resolution approaches for GPS. Some typical methods may also be suitable for GNSS-2/Galileo orbit determination when using carrier phase measurements.

Following Teunissen (1994), the ambiguity approach can be described as follows.

The carrier phase measurement can be represented as

$$\Phi = \|\overset{w}{r} - \overset{w}{R}\| + c(dt - dT) + \lambda N + \varepsilon \quad (7-15)$$

where

$\overset{w}{r}$	unknown receiver antenna position vector at signal reception time
$\overset{w}{R}$	given satellite antenna position vector at signal transmission time
$c$	speed of light in vacuum
$cdt$	receiver clock range offset
$cdT$	satellite clock range offset
$\lambda$	carrier wavelength of the signal
$N$	carrier phase ambiguity

The term  $\varepsilon$  represents carrier phase measurement noise and biases such as satellite ephemeris errors, tropospheric and ionospheric delays, and ranging errors caused by multipath effects. In the processing of carrier phase data it is common to differentiate the carrier phase measurements between satellites and between receivers to eliminate some common errors. This gives the single and double differenced carrier phase observation equations

$$\nabla\Phi = \nabla\|r - R\| + c\nabla dt + \lambda\nabla N + \nabla\varepsilon \quad (7-16)$$

$$\Delta\nabla\Phi = \Delta\nabla\|r - R\| + \lambda\Delta\nabla N + \Delta\nabla\varepsilon \quad (7-17)$$

$\nabla$  and  $\Delta\nabla$  stand for the single and double difference operator. In the following discussion a two-receiver situation is assumed. The term  $\nabla dt$  then denotes the single differenced clock error between the reference receiver and the remote receiver. Because of double differencing this error vanishes in Eq.(7-17). In both equations the ambiguity-terms  $\nabla N$  and  $\Delta\nabla N$  are known to be integers.

Linearization of the observation equations with respect to the unknown parameters and a collection of these linearized equations into a linear system of equations gives:

$$\overset{w}{y} = A\overset{w}{a} + B\overset{w}{b} + \overset{w}{\varepsilon} \quad (7-18)$$

with  $E\{\overset{w}{\varepsilon}\} = 0$ ,  $D\{\overset{w}{\varepsilon}\} = D\{\overset{w}{y}\} = Q_y$

where

$\overset{w}{y}$	vector of observed minus computed differenced carrier phase observations
$\overset{w}{a}$	vector of unknown ambiguities
$\overset{w}{b}$	vector of unknown coordinates of baseline or satellite position, velocity and related dynamic parameters
$A, B$	design matrices for unknown ambiguities and parameters
$\overset{w}{\varepsilon}$	vector of unmodeled errors (in the following $\overset{w}{\varepsilon}$ is sufficiently small to be neglected)
$Q_y$	variance-covariance matrix of the observations $\overset{w}{y}$
$E\{.\}$	expectation operator
$D\{.\}$	dispersion operator

Because  $\overset{w}{a}$  should be integers, it can be shown, that Eq. (7-18) may be solved in three steps. Firstly, estimating a double difference float solution (real-valued ambiguities  $\overset{w}{a}$  with  $\overset{w}{b}$ ), i.e.

$$\min_{a,b} \|\overset{w}{y} - A\overset{w}{a} - B\overset{w}{b}\|_{Q_y}^2 \quad \text{with } \overset{w}{a}, \overset{w}{b} \in R^n \quad (7-19)$$

where

$$\|\cdot\|_{Q_y}^2 = (\cdot)^T Q_y^{-1} (\cdot)$$

$Q_y$  variance-covariance matrix of double-difference carrier phase observations

$R^n$   $n$ -dimensional space of reals

Secondly, solving the following minimization problem, integer ambiguity estimation:

$$\min_a (\hat{a} - a)^T Q_{\hat{a}}^{-1} (\hat{a} - a) \text{ with } a \in Z^m \quad (7-20)$$

where

$Z^m$   $m$ -dimensional space of integers

The final step is called fixed solution, once the integer least square ambiguity vector  $\hat{a} \in Z^m$  has been obtained, the residual  $(\hat{a} - a)$  is used to adjust the solution  $\hat{b}$ . As a result, the final solution is obtained as

$$\hat{b} = \hat{b} - Q_{\hat{b}\hat{a}} Q_{\hat{a}}^{-1} (\hat{a} - a) \quad (7-21)$$

The difficulty of integer ambiguity solution is in the second step, the integer ambiguity estimation. There are many ambiguity resolution approaches to solve this problem, two of them are LAMBDA and TCAR.

### 7.3.1 LAMBDA Method

LAMBDA stands for Least-squares AMBIGUITY Decorrelation Adjustment method. Its two main features are

- sequential conditional least squares estimation
- preceded by a decorrelation of the ambiguities

The method contains a strict extension of standard least-squares to the integer domain. The novelty of the method is a decorrelating reparametrization of the ambiguities, by which the integer least-squares estimates can be computed very fast and efficiently. This new method is proposed by Teunissen (1993, 1994).

The basic LAMBDA idea is that integer ambiguity solution will become easy once the confidence ellipsoid of the ambiguities equals a sphere. In the case of GPS, however, the confidence ellipsoid is usually rotated with respect to the coordinate axes and extremely elongated, particularly for short observational time-spans and without P-code data. Teunissen (1993, 1994, 1995) introduced a one-to-one transformation from the original set of ambiguities to a new set of ambiguities, of which the confidence ellipsoid has more sphere-like properties and therefore the ambiguities are more decorrelated.

LAMBDA method consists of two steps. The first, the ambiguity transformation, i.e. ambiguity decorrelation, and the second, ambiguity search based on transformed ambiguity space. The first step is unique for LAMBDA method. The second step may use any other ambiguity search approach (Hatch, 1990; Frei et al, 1990, 1993; Euler and Landau, 1992 etc). Therefore in the following we focus on the first step, ambiguity transformation used by LAMBDA.

Since in Eq.(7-20) the constraint is an integer-constraint  $a \in Z^m$ , it is also called integer least-squares estimation. The key problem is the minimization of Eq.(7-20). All possible ambiguity vectors with integer elements that can solve Eq.(7-20) belong to a confidence ellipsoid that is given by:

$$E = \left\{ \hat{a} \in R^m \mid Q(\hat{a}) = (\hat{a} - \hat{a})^T Q_{\hat{a}}^{-1} (\hat{a} - \hat{a}) \leq \chi_{m,1-\alpha}^2 \right\} \quad (7-22)$$

where,

$E$  ellipsoid set of points  $\hat{a}$  in  $R^m$

$Q(\hat{a})$  quadratic form in  $\hat{a}$

$\chi_{m,1-\alpha}^2$  chi-squares percentile for  $m$  degrees of freedom and confidence level  $1 - \alpha$

$\alpha$  error probability (significance level)

LAMBDA objective is to reparametrize Eq.(7-20) in such a way, that an equivalent formulation is obtained, but one that is easily solved. The simplest integer estimation method is "rounding to the nearest integer" and applied

to Eq.(7-20) means, that  $Q_{\bar{a}}$  has to be diagonal. In order to achieve this objective, the transformation matrix  $Z$  should be found, which will make covariance matrix of  $Z$  to be diagonal.

The covariance matrix of float ambiguity can be decomposed into

$$Q_{\bar{a}} = LDL^T \quad (7-23)$$

where

$D$  diagonal matrix  
 $L$  low or upper triangular matrix

If the elements of transformation matrix  $Z$  are integers and satisfies

$$Q_{\bar{z}} = ZQ_{\bar{a}}Z^T = ZLD(L^T)^{-1}(Z^T)^{-1} = D \quad (7-24)$$

where

$$Z = L^{-1} \quad (7-25)$$

Then  $Q_{\bar{z}}$  will be a diagonal matrix and original float ambiguity solution  $\bar{a}^{\oplus}$ , can be transformed to

$$\bar{z}^{\oplus} = Z\bar{a}^{\oplus} \quad (7-26)$$

Due to diagonal matrix  $Q_{\bar{z}}$ , integer ambiguity  $\bar{z}^{\oplus}$  can be obtained by using „rounding to the nearest integer“ to transformed ambiguity  $\bar{z}^{\oplus}$ .

Finally by inversion of Eq.(7-26), the original integer ambiguity solution can be obtained

$$\bar{a}^{\oplus} = Z^{-1}\bar{z}^{\oplus} \quad (7-27)$$

From Eq.(7-23) to Eq.(7-27), the transformation matrix  $Z$  should possess following properties

- the transformation must have integer elements
- the transformation must be volume preserving, and
- the transformation should aim at reducing the product of all the ambiguity variances.

If these three conditions are met, it is guaranteed that:

- the transformed ambiguities are again integer-valued, and
- the variance-covariance matrix of the transformed ambiguities is more diagonal than the original variance-covariance matrix.

Due to restrictions on  $Z$  it is generally not possible to get a complete diagonalization of variance-covariance matrix  $Q_{\bar{z}}$ . Nevertheless a decrease in correlation, although not complete, will be very helpful for ambiguity search approach.

According to Eq.(7-25), the matrix  $Z$  can be formed by letting the elements of matrix  $Z$  equal to the nearest integers of elements of matrix  $L^{-1}$ . Actually the matrix  $Z$  is formed by a concatenation of ambiguity transformations. In this sequence two kinds of transformation occur alternately, namely a Gauss-transformation that reduces the variances of the ambiguities to a certain level and a permutation that interchanges two ambiguities each time such that a further reduction of the variances is possible. Once the ambiguity transformation is applied, the Cholesky-decomposition of the transformed confidence ellipsoid provides a completion of squares, that allows an efficient computation of the integer least-squares estimates of the ambiguities. For detail of the procedure, refer to (Paul de Jonge et al 1996).

### 7.3.2 Three Carrier Ambiguity Resolution - TCAR

TCAR uses three frequencies to solve initial ambiguities. The signal structures for probable three frequencies (E1/E2/E3) are summarized in Table 7-4.

Table 7-4 Three Frequency Signal Structure

	Frequency [Mhz]	Chipping Rate [Mchip/s]	Carrier Wavelength [m]	Code Wavelength [m]
E1	1589.742	2.046	0.1886	146.53
E2	1561.098	2.046	0.1920	146.53
E3	1215.324	0.25575	0.2467	1172.2

A limiting factor for successful ambiguity resolution is the existence of unmodeled multipath errors in the carrier phase and code measurements. TCAR is a direct resolution method for initial integer ambiguity of carrier phase observation presented by (Harris 1997 and Forssell et al. 1997). The influence of the multipath effects on TCAR algorithm has been researched by (Werner et al. 1998).

TCAR approach may be written in the following three steps according to the different ambiguity solution phases.

Step 1:

From E1 code measurements,

$$\bar{\rho}_{(I)} = R_1 \quad (7-28)$$

*super widelane* float ambiguity of E1 and E2 phase measurement combination may be solved by

$$\bar{N}_{12} := \Phi_1 - \Phi_2 - \left(\frac{1}{\lambda_1} - \frac{1}{\lambda_2}\right) \bar{\rho}_{(I)} \quad (7-29)$$

where

$$N_{12} := N_1 - N_2$$

The accuracy of  $\bar{\rho}_{(I)}$  is less than  $\pm 10\text{m}$  if there are no adverse multipath effects. The wave length of linear combination of  $\Phi_1 - \Phi_2$  is about 10 m. Therefore *super widelane* integer ambiguity solution can easily be obtained from Eq.(7-29), i.e.

$$\bar{N}_{12} := [\bar{N}_{12}] \quad (7-30)$$

where

[ ] means rounding to nearest integer

Step 2:

From integer ambiguity  $\bar{N}_{12}$ , more precise phase range is solved by using narrow widelane linear combinations of E1 and E3 phase observations:

$$\bar{\rho}_{(II)} = \frac{\lambda_1 \lambda_2}{\lambda_2 - \lambda_1} (\Phi_1 - \Phi_2 - \bar{N}_{12}) \quad (7-31)$$

Hence new ambiguity  $\bar{N}_{13}$  with smaller wavelength can be solved by

$$\bar{N}_{13} := \Phi_1 - \Phi_3 - \left(\frac{1}{\lambda_1} - \frac{1}{\lambda_3}\right) \bar{\rho}_{(II)} \quad (7-32)$$

$$\bar{N}_{13} := [\bar{N}_{13}] \quad (7-33)$$

where,

$\bar{N}_{13}$  integer ambiguity

$\bar{N}_{13}$  float ambiguity and

$$N_{13} := N_1 - N_3$$

In Step 2, the wavelength of  $\Phi_1 - \Phi_2$  is 0.80 meter, the accuracy of  $\bar{\rho}_{(II)}$  is in centimeter level (see L4\* in Table 7-7) and better than  $\bar{\rho}_{(I)}$ , therefore, the ambiguity with smaller wavelength  $\bar{N}_{13}$  can be solved by rounding to the nearest integer.

Step 3:

Final integer ambiguities  $\bar{N}_1, \bar{N}_2$  and  $\bar{N}_3$  will be solved as follows

$$\bar{\rho}_{(III)} = \frac{\lambda_1 \lambda_3}{\lambda_3 - \lambda_1} (\Phi_1 - \Phi_3 - \bar{N}_{13}) \quad (7-34)$$

$$\bar{N}_1 = \Phi_1 - \frac{\bar{\rho}_{(III)}}{\lambda_1} \quad \bar{N}_2 = \Phi_2 - \frac{\bar{\rho}_{(III)}}{\lambda_2} \quad \bar{N}_3 = \Phi_3 - \frac{\bar{\rho}_{(III)}}{\lambda_3} \quad (7-35)$$

$$\bar{N}_1 := [\bar{N}_1] \quad \bar{N}_2 := [\bar{N}_2] \quad \bar{N}_3 := [\bar{N}_3] \quad (7-36)$$

The first step is very important for the successful solution of the initial integer ambiguities for TCAR algorithm. If under strong multipath environment, the error of  $\bar{\rho}_{(I)}$  is larger than  $\pm 10$  meter, it is impossible for  $N_{12}$  to get integer solution. Thus from the second step to the last step, a big bias will be introduced into all integer ambiguity solutions, which lead to ambiguity resolution failure.

The multipath effects may be reduced using linear combinations, which will be discussed in the next section. L3 is an ionospheric-free linear combination that is little affected by multipath effects as well (see Table 7-7). In order to eliminate the influence of multipath effects and ionospheric errors on TCAR algorithm, the ionosphere-free or multipath-free linear combination of E1/E3 code measurements should be formed as the first step for  $\rho_{(I)}$ , i.e. improved TCAR steps may be written as follows,

Step1:

Ionospheric-free linear combinations of E1 and E3 code pseudoranges should be produced by

$$\bar{\rho}_{(I)} = \frac{f_{E1}^2}{f_{E1}^2 - f_{E3}^2} \rho_{E1} - \frac{f_{E3}^2}{f_{E1}^2 - f_{E3}^2} \rho_{E3} \quad (7-37)$$

From Table 7-7, it is guaranteed that  $\bar{\rho}_{(I)}$  has much little influence from ionospheric errors and multipath effects. Thus the float ambiguity  $\bar{N}_{12}$  is solved by using widelane linear combinations of E1 and E2 phase observations and  $\bar{\rho}_{(I)}$

$$\bar{N}_{12} := \Phi_1 - \Phi_2 - \left( \frac{1}{\lambda_1} - \frac{1}{\lambda_2} \right) \bar{\rho}_{(I)} \quad (7-38)$$

Because the wave length of linear combination of  $\Phi_1 - \Phi_2$  is about 10 meter and the accuracy of  $\bar{\rho}_{(I)}$  is much better than 10 meter, integer ambiguity  $\bar{N}_{12}$  can easily be obtained by rounding  $\bar{N}_{12}$  to the nearest integer, i.e.

$$\bar{N}_{12} := [\bar{N}_{12}] \quad (7-39)$$

where

$\bar{N}_{12}$  integer ambiguity

$\bar{N}_{12}$  float ambiguity

$\bar{N}_{12} := N_1 - N_2$

Step 1 is a big difference from the original TCAR algorithm Eq.(7-28) and will significantly reduce the ionospheric errors and multipath effects. In Step 2 there is no influence from multipath effects, hence Step 2 does not need to be changed. Step 3 also remains without changes.

From the discussion above it is clear that TCAR still can not guarantee 100% success in the integer ambiguity resolution of original carrier phase observations. The key step is the last step. For example, if L1 is strongly affected by ionospheric and/or multipath errors, the last step will not be successful. In other words, the accuracy of  $\bar{\rho}_{(III)}$  in Eq.(7-34) and Eq.(7-35) should be better than 0.10 meter, otherwise, the last step may be a failure.

## CHAPTER 8 GEOSTATIONARY ORBIT DETERMINATION AND PREDICTION DURING SATELLITE MANEUVERS

Geostationary satellites (GEO) are important candidates for the GNSS-2 system. Theoretically, a geostationary orbit is one where the orbit has the same period as the earth's rotation period, and remains at a “fixed” point on the sky at all times and stationary over a single point on the Earth's surface. The orbit is a circle and the orbit must lie in the earth's equatorial plane.

Because of various perturbations such as nonspheric earth gravitation, solar and lunar attractions, once a satellite is placed in the proper position of geostationary orbit, it doesn't stay there, it tends to drift.

Geostationary satellite drifts can be divided into two parts, one is the in-plane drift and the other is the out-of-plane drift. The in-plane drift is caused by changes of the orbital parameter *longitude of the ascending node*,  $\Omega$ . The out-of-plane drift is produced by variation of the orbital parameter *inclination of orbit*,  $i$ .

When geostationary satellite drifts away from its “fixed” position, satellite maneuver or station keeping operation will be started. The operation frequency is dependent on the deadbands, normally 0.1 degree or larger. Regular weekly or two weekly longitude maneuvers may be preferred for simplicity, inclination maneuvers will be less frequent, larger and will normally have an in-plane component that will need to be corrected rapidly (Dow, 1999). For almost weekly maneuvers, geostationary satellite is very difficult to be used for navigation application purpose.

MEO and IGSO satellites also meet the maneuver problems, but it is not so serious as GEO satellites, because the frequencies of maneuver operation for MEO and IGSO are much lower than for GEO satellites. Therefore in this chapter, the emphasis is on GEO satellite maneuvers. The kinematic orbit determination method discussed in Chapter 6 will be used to solve this problem during GEO satellite maneuvers.

### 8.1 Perturbations of Geostationary Satellite

For geostationary satellite maneuvers or stationkeeping, the changes of orbital parameters *longitude of the ascending node*  $\Omega$  and *inclination of orbit*  $i$  under influence of the perturbations are very important. The changes of these two parameters are analyzed as follows.

The orbital elements and time are related to perturbation functions by the following system of differential equations, also called Lagrange equations:

$$\left. \begin{aligned} \frac{da}{dt} &= \frac{2}{na} \frac{\partial R}{\partial M} \\ \frac{de}{dt} &= \frac{1-e^2}{na^2 e} \frac{\partial R}{\partial M} - \frac{\sqrt{1-e^2}}{na^2 e} \frac{\partial R}{\partial \omega} \\ \frac{d\omega}{dt} &= -\frac{\cos i}{na^2 \sqrt{1-e^2} \sin i} \frac{\partial R}{\partial i} + \frac{\sqrt{1-e^2}}{na^2 e} \frac{\partial R}{\partial e} \\ \frac{di}{dt} &= \frac{-1}{na^2 \sqrt{1-e^2} \sin i} \frac{\partial R}{\partial \Omega} + \frac{\cos i}{na^2 \sqrt{1-e^2} \sin i} \frac{\partial R}{\partial \omega} \\ \frac{d\Omega}{dt} &= \frac{1}{na^2 \sqrt{1-e^2} \sin i} \frac{\partial R}{\partial i} \\ \frac{dM}{dt} &= n - \frac{1-e^2}{na^2 e} \frac{\partial R}{\partial e} - \frac{2}{na} \frac{\partial R}{\partial a} \end{aligned} \right\} \quad (8-1)$$

where

$a, e, i, \Omega, \omega$ , and  $M$  are the semimajor axis of the orbit, eccentricity, orbital inclination, longitude of the ascending node, argument of perigee and mean anomaly, respectively.  $M = n(t - T_0)$ , where  $n$  is called the mean motion, and  $T_0$  the time of perifocal passage;  $R$  is a perturbation function.

Clearly, due to the complexity of the perturbation function  $R$  in Eq.(8-1), it is impossible to obtain closed solutions, instead, an approximate solution will be obtained. The perturbations on the satellite can be classified as three types, first, the secular variations or the ever-increasing or the decreasing changes from the some epoch; second, the long periodic variations and third the short periodic variations. These can be expressed by (Escobal, 1965, pp. 362).

$$q = q_0 + \frac{q_1}{8}(t - t_0) + K_1 \cos(2\omega) + K_2 \sin(2v + 2\omega) \quad (8-2)$$

where,

$v$  true anomaly

In Eq.(8-2) above, the second term is the secular variation that is ever-increasing or decreasing, the third term is the long periodic variation that is related to the argument of perigee  $\omega$ .  $\omega$  changes slowly with the period  $2\pi$ . The last term is short periodic variation, caused by the trigonometric functions of linear combinations of  $M$  or  $v$  and  $\omega$ , in which the changes of true anomaly,  $v$ , are much more faster than the slow secular variations in the argument of perigee  $\omega$ .

For geostationary satellite maneuver or stationkeeping, the secular variations of  $\Omega, i$ , are more interesting, because the secular variation makes geostationary satellites drift away from their fixed position and never to return. This is different from the periodic terms. Therefore in the following section only the effects of the secular variation terms are discussed.

### 8.1.1 Nonspherical Earth Gravitation

The geopotential perturbation function can be written as

$$R = GM \sum_{n=2}^N \sum_{m=0}^n \frac{a_e^n}{r^{n+1}} P_{nm}(\sin \varphi) (C_{nm} \cos m\lambda + S_{nm} \sin m\lambda) \quad (8-3)$$

The secular terms are only related to the coefficients of zonal terms, thus Eq.(8-3) can be expressed as

$$R = GM \left[ \frac{3}{2} \frac{J_2}{r^2} (1 - 5 \sin^2 \varphi) + \frac{5}{2} \frac{J_3}{r^3} (3 - 7 \sin^2 \varphi) \sin \varphi - \frac{5}{8} \frac{J_4}{r^4} (3 - 42 \sin^2 \varphi + 63 \sin^4 \varphi) \right. \\ \left. - \frac{3}{8} \frac{J_5}{r^5} (35 - 210 \sin^2 \varphi + 231 \sin^4 \varphi) \sin \varphi + \frac{1}{16} \frac{J_6}{r^6} (35 - 945 \sin^2 \varphi + 3465 \sin^4 \varphi - 3003 \sin^6 \varphi) + \Lambda \right] \quad (8-4)$$

where

$$J_i = C_{i0}$$

Neglecting the high order terms in Eq.(8-4), considering  $\sin \varphi = \sin i \sin(v + \omega)$ , Eq.(8-4) becomes

$$R = GM \left[ \frac{3}{2} \frac{J_2}{a^3} \left(\frac{a}{r}\right)^3 \left\{ \frac{1}{3} - \frac{1}{2} \sin^2 i + \frac{1}{2} \sin^2 i \cos 2(v + \omega) \right\} - \frac{5}{4} \frac{J_3}{a^4} \left(\frac{a}{r}\right)^4 \left\{ \left( \frac{15}{8} \sin^2 i - \frac{3}{2} \right) \sin(v + \omega) \right. \right. \\ \left. \left. - \frac{5}{8} \sin^2 i \sin 3(v + \omega) \right\} \sin i - \frac{35}{8} \frac{J_4}{a^5} \left(\frac{a}{r}\right)^5 \left\{ \frac{3}{35} - \frac{3}{7} \sin^2 i + \frac{3}{8} \sin^4 i + \sin^2 i \left( \frac{3}{7} - \frac{1}{2} \sin^2 i \right) \cos 2(v + \omega) \right. \right. \\ \left. \left. + \frac{1}{8} \sin^4 i \cos 4(v + \omega) \right\} \right] \quad (8-5)$$

According to Eq.(8-2), the perturbation function with the secular variations in Eq.(8-5) can be expressed as



$$R_s = GM \left[ \frac{3}{2} \frac{J_2}{a^3} \left( \frac{a}{r} \right)^3 \left\{ \frac{1}{3} - \frac{1}{2} \sin^2 i \right\} - \frac{35}{8} \frac{J_4}{a^5} \left( \frac{a}{r} \right)^5 \left\{ \frac{3}{35} - \frac{3}{7} \sin^2 i + \frac{3}{8} \sin^4 i \right\} \right] \quad (8-6)$$

and the periodic variation perturbation function by

$$R_p = GM \left[ \frac{3}{2} \frac{J_2}{a^3} \left( \frac{a}{r} \right)^3 \left\{ \frac{1}{2} \sin^2 i \cos 2(v + \omega) \right\} - \frac{J_3}{a^4} \left( \frac{a}{r} \right)^4 \left\{ \left( \frac{15}{8} \sin^2 i - \frac{3}{2} \right) \sin(v + \omega) - \frac{5}{8} \sin^2 i \sin 3(v + \omega) \right\} \sin i \right. \\ \left. - \frac{35}{8} \frac{J_4}{a^5} \left( \frac{a}{r} \right)^5 \left\{ \sin^2 i \left( \frac{3}{7} - \frac{1}{2} \sin^2 i \right) \cos 2(v + \omega) + \frac{1}{8} \sin^4 i \cos 4(v + \omega) \right\} \right] \quad (8-7)$$

Inserting Eq.(8-6) and Eq.(8-7) into Eq.(8-1), the variations of  $\Omega$  and  $i$  due to perturbations Eq.(8-6) and Eq.(8-7) can be obtained as

$$\frac{d\Omega}{dt} = \frac{1}{na^2 \sqrt{1-e^2} \sin i} \frac{\partial R}{\partial i} \\ = \frac{n}{\sqrt{1-e^2}} \left[ \frac{3}{2} \frac{J_2}{a^2} \left( \frac{a}{r} \right)^3 (-\cos i) - \frac{35}{8} \frac{J_4}{a^4} \left( \frac{a}{r} \right)^5 \left\{ \frac{6}{7} \cos i + \frac{3}{2} \sin^2 i \cos i \right\} \right] \quad (8-8)$$

$$\frac{di}{dt} = \frac{\cos i}{na^2 \sqrt{1-e^2} \sin i} \frac{\partial R}{\partial \omega} \\ = \frac{n \cos i}{\sqrt{1-e^2}} \left[ \frac{3}{2} \frac{J_2}{a^2} \left( \frac{a}{r} \right)^3 \left\{ -\sin i \sin 2(v + \omega) \right\} - \frac{J_3}{a^3} \left( \frac{a}{r} \right)^4 \left\{ \left( \frac{15}{8} \sin^2 i - \frac{3}{2} \right) \cos(v + \omega) - \frac{15}{8} \sin^2 i \cos 3(v + \omega) \right\} \right. \\ \left. + \frac{35}{8} \frac{J_4}{a^4} \left( \frac{a}{r} \right)^5 \left\{ 2 \sin i \left( \frac{3}{7} - \frac{1}{2} \sin^2 i \right) \sin 2(v + \omega) + \frac{1}{2} \sin^3 i \sin 4(v + \omega) \right\} \right] \quad (8-9)$$

From two-body theory of satellite movement,

$$\left. \begin{aligned} r &= \frac{a(1-e^2)}{1+e \cos v} = a(1-e \cos E) \\ \sin v &= \frac{\sqrt{1-e^2} \sin E}{1-e \cos E} \\ M &= E - e \sin E = n(t - T_0) \\ dM &= ndt \\ dM &= (1-e \cos E)dE \\ \sin E dE &= \frac{a(1-e^2) \sin v dv}{(1+e \cos v)^2} \end{aligned} \right\} \quad (8-10)$$

where

$n$  unperturbed two-body mean motion  
 $E$  eccentric anomaly  
 $T_0$  time of perifocal passage

then the following equation can be obtained

$$\frac{dM}{dv} = \left( \frac{r}{a} \right)^2 \frac{1}{\sqrt{1-e^2}} \quad (8-11)$$

In order to evaluate  $\Omega$  and  $i$  variations under the influence of nonspherical earth gravitation, Eq.(8-8) and Eq.(8-9) are integrated over a revolution of geostationary satellite movement. The results are

$$\Delta \Omega_s = - \frac{1}{\sqrt{1-e^2}} \left[ \frac{3}{2} \frac{J_2}{a^2} \cos i \frac{1}{2\pi} \int_{t_s}^{t_e} \left( \frac{a}{r} \right)^3 ndt - \frac{35}{8} \frac{J_4}{a^4} \left\{ \frac{6}{7} \cos i + \frac{3}{2} \sin^2 i \cos i \right\} \frac{1}{2\pi} \int_{t_s}^{t_e} \left( \frac{a}{r} \right)^5 ndt \right] \\ = - \frac{1}{\sqrt{1-e^2}} \left[ \frac{3}{2} \frac{J_2}{a^2} \cos i \frac{1}{2\pi} \int_0^{2\pi} \left( \frac{a}{r} \right)^3 dM - \frac{35}{8} \frac{J_4}{a^4} \left\{ \frac{6}{7} \cos i + \frac{3}{2} \sin^2 i \cos i \right\} \frac{1}{2\pi} \int_0^{2\pi} \left( \frac{a}{r} \right)^5 dM \right] \quad (8-12)$$

$$\begin{aligned} \Delta i_s = & \frac{\cos i}{\sqrt{1-e^2}} \left[ -\frac{3}{2} \frac{J_2}{a^2} (\sin i) \frac{1}{2\pi} \int_0^{2\pi} \left(\frac{a}{r}\right)^3 \sin 2(v+\omega) dM - \frac{J_3}{a^3} \left\{ \left(\frac{15}{8} \sin^2 i - \frac{3}{2}\right) \frac{1}{2\pi} \int_0^{2\pi} \left(\frac{a}{r}\right)^4 \cos(v+\omega) dM \right. \right. \\ & \left. \left. - \frac{15}{8} \sin^2 i \frac{1}{2\pi} \int_0^{2\pi} \left(\frac{a}{r}\right)^4 \cos 3(v+\omega) dM \right\} + \frac{35}{8} \frac{J_4}{a^4} \left\{ 2 \sin i \left(\frac{3}{7} - \frac{1}{2} \sin^2 i\right) \frac{1}{2\pi} \int_0^{2\pi} \left(\frac{a}{r}\right)^5 \sin 2(v+\omega) dM \right. \right. \\ & \left. \left. + \frac{1}{2} \sin^3 i \frac{1}{2\pi} \int_0^{2\pi} \left(\frac{a}{r}\right)^5 \sin 4(v+\omega) dM \right\} \right] \end{aligned} \quad (8-13)$$

where  $t_s$  is the epoch of integrating start,  $t_e$  the epoch that the satellite takes a revolution and returns to the starting point that the integration begins.

Because

$$\frac{1}{2\pi} \int_0^{2\pi} \left(\frac{a}{r}\right)^3 dM = \frac{1}{2\pi} \int_0^{2\pi} \left(\frac{a}{r}\right)^3 \left(\frac{r}{a}\right)^2 \frac{1}{\sqrt{1-e^2}} dv = \frac{1}{2\pi} \int_0^{2\pi} \frac{1+e \cos v}{(1+e)^{3/2}} dv = (1-e^2)^{-3/2} \quad (8-14)$$

$$\frac{1}{2\pi} \int_0^{2\pi} \left(\frac{a}{r}\right)^4 dM = \frac{1}{2\pi} \int_0^{2\pi} \frac{(1+e \cos v)^2}{(1-e^2)^{5/2}} dv = (1-e^2)^{-5/2} \left[ 1 + \frac{e^2}{2} \right] \quad (8-15)$$

$$\frac{1}{2\pi} \int_0^{2\pi} \left(\frac{a}{r}\right)^5 dM = \frac{1}{2\pi} \int_0^{2\pi} \frac{(1+e \cos v)^3}{(1-e^2)^{7/2}} dv = (1-e^2)^{-7/2} \left[ 1 + \frac{3}{2} e^2 + \frac{1}{3} e^3 \right] \quad (8-16)$$

$$\frac{1}{2\pi} \int_0^{2\pi} \left(\frac{a}{r}\right)^3 \sin 2(v+\omega) dM = \frac{1}{2\pi} \int_0^{2\pi} \frac{1+e \cos v}{(1-e^2)^{3/2}} \sin 2(v+\omega) dv = 0 \quad (8-17)$$

$$\frac{1}{2\pi} \int_0^{2\pi} \left(\frac{a}{r}\right)^4 \cos(v+\omega) dM = \frac{1}{2\pi} \int_0^{2\pi} \frac{(1+e \cos v)^2}{(1-e^2)^{5/2}} \cos(v+\omega) dv = (1-e^2)^{-5/2} e \cos \omega \quad (8-18)$$

$$\frac{1}{2\pi} \int_0^{2\pi} \left(\frac{a}{r}\right)^4 \cos 3(v+\omega) dM = \frac{1}{2\pi} \int_0^{2\pi} \frac{(1+e \cos v)^2}{(1-e^2)^{5/2}} \cos 3(v+\omega) dv = 0 \quad (8-19)$$

$$\frac{1}{2\pi} \int_0^{2\pi} \left(\frac{a}{r}\right)^5 \sin 2(v+\omega) dM = \frac{1}{2\pi} \int_0^{2\pi} \frac{(1+e \cos v)^3}{(1-e^2)^{7/2}} \sin 2(v+\omega) dv = (1-e^2)^{-7/2} e^2 \frac{3}{4} \sin 2\omega \quad (8-20)$$

$$\frac{1}{2\pi} \int_0^{2\pi} \left(\frac{a}{r}\right)^5 \sin 4(v+\omega) dM = \frac{1}{2\pi} \int_0^{2\pi} \frac{(1+e \cos v)^3}{(1-e^2)^{7/2}} \sin 4(v+\omega) dv = (1-e^2)^{-7/2} e^2 \frac{3}{4} \sin 4\omega \quad (8-21)$$

Eq. (8-12) and Eq.(8-13) become

$$\begin{aligned} \Delta \Omega_s = & -\frac{1}{\sqrt{1-e^2}} \left[ \frac{3}{2} \frac{J_2}{a^2} \cos i (1-e^2)^{-3/2} - \frac{35}{8} \frac{J_4}{a^4} \left\{ \frac{6}{7} \cos i + \frac{3}{2} \sin^2 i \cos i \right\} (1-e^2)^{-7/2} \left( 1 + \frac{3}{2} e^2 + \frac{1}{3} e^3 \right) \right] \\ & = -\frac{1}{(1-e^2)^2} \left[ \frac{3}{2} \frac{J_2}{a^2} \cos i - \frac{35}{8} \frac{J_4}{a^4} \left\{ \frac{6}{7} \cos i + \frac{3}{2} \sin^2 i \cos i \right\} \frac{1}{(1-e^2)^2} \left( 1 + \frac{3}{2} e^2 + \frac{1}{3} e^3 \right) \right] \\ & = -\left[ \frac{3}{2} \frac{J_2}{p^2} \cos i - \frac{35}{8} \frac{J_4}{p^4} \left\{ \frac{6}{7} \cos i + \frac{3}{2} \sin^2 i \cos i \right\} \left( 1 + \frac{3}{2} e^2 + \frac{1}{3} e^3 \right) \right] \end{aligned} \quad (8-22)$$

$$\begin{aligned} \Delta i_s = & \frac{\cos i}{\sqrt{1-e^2}} \left[ -\frac{J_3}{a^3} \left\{ \left(\frac{15}{8} \sin^2 i - \frac{3}{2}\right) (1-e^2)^{-5/2} e \cos \omega \right\} + \frac{35}{8} \frac{J_4}{a^4} \left\{ 2 \sin i \left(\frac{3}{7} - \frac{1}{2} \sin^2 i\right) (1-e^2)^{-7/2} e^2 \frac{3}{4} \sin 2\omega \right\} \right. \\ & \left. + \frac{1}{2} \sin^3 i (1-e^2)^{-7/2} e^2 \frac{3}{4} \sin 4\omega \right] \\ & = \frac{\cos i}{(1-e^2)^3} \left[ -\frac{J_3}{a^3} \left\{ \left(\frac{15}{8} \sin^2 i - \frac{3}{2}\right) e \cos \omega \right\} + \frac{35}{8} \frac{J_4}{a^4} \left\{ 2 \sin i \left(\frac{3}{7} - \frac{1}{2} \sin^2 i\right) \frac{e^2}{(1-e^2)} \frac{3}{4} \sin 2\omega \right\} + \frac{1}{2} \sin^3 i \frac{e^2}{(1-e^2)} \frac{3}{4} \sin 4\omega \right] \\ & = \cos i \left[ -\frac{J_3}{p^3} \left\{ \left(\frac{15}{8} \sin^2 i - \frac{3}{2}\right) e \cos \omega \right\} + \frac{35}{8} \frac{J_4}{p^4} \left\{ \frac{3}{2} e^2 \sin i \left(\frac{3}{7} - \frac{1}{2} \sin^2 i\right) \sin 2\omega + \frac{3}{8} e^2 \sin^3 i \sin 4\omega \right\} \right] \end{aligned} \quad (8-23)$$

where  $p = a\sqrt{1-e^2}$

Clearly, from the results Eq.(8-22) and Eq.(8-23), the short periodic variations of the orbital parameters under the influence of the non-spherical earth gravitation are removed, the remaining is secular and long periodic variation terms, i.e.

$$\Delta\Omega_s = -\left[\frac{3}{2}\frac{J_2}{p^2}\cos i - \frac{35}{8}\frac{J_4}{p^4}\left\{\frac{6}{7}\cos i + \frac{3}{2}\sin^2 i \cos i\right\}\left(1 + \frac{3}{2}e^2 + \frac{1}{3}e^3\right)\right] \quad (8-24)$$

$$\Delta i_s = \cos i \left[ -\frac{J_3}{p^3}\left\{\left(\frac{15}{8}\sin^2 i - \frac{3}{2}\right)e \cos \omega\right\} + \frac{35}{8}\frac{J_4}{p^4}\left\{\frac{3}{2}e^2 \sin i\left(\frac{3}{7} - \frac{1}{2}\sin^2 i\right)\sin 2\omega + \frac{3}{8}e^2 \sin^3 i \sin 4\omega\right\}\right] \quad (8-25)$$

General forms of Eq. (8-24) and Eq.(8-25) can be written as,

$$\Delta\Omega_s = -\left[\frac{3}{2}\frac{J_2}{p^2}\cos i - \frac{35}{8}\frac{J_4}{p^4}\left\{\frac{6}{7}\cos i + \frac{3}{2}\sin^2 i \cos i\right\}\left(1 + \frac{3}{2}e^2 + \frac{1}{3}e^3\right)\right]\bar{n}(t - T_0) \quad (8-26)$$

$$\Delta i_s = \cos i \left[ -\frac{J_3}{p^3}\left\{\left(\frac{15}{8}\sin^2 i - \frac{3}{2}\right)e \cos \omega\right\} + \frac{35}{8}\frac{J_4}{p^4}\left\{\frac{3}{2}e^2 \sin i\left(\frac{3}{7} - \frac{1}{2}\sin^2 i\right)\sin 2\omega + \frac{3}{8}e^2 \sin^3 i \sin 4\omega\right\}\right]\bar{n}(t - T_0) \quad (8-27)$$

Since  $J_2=0.1083\times 10^{-2}$ ,  $J_3=0.2532\times 10^{-5}$ ,  $J_4=0.1620\times 10^{-5}$ ,  $J_3$  and  $J_4$  are much smaller than  $J_2$ , and for geostationary satellite,  $e\approx 0$  and  $i\approx 0$ , therefore in Eq. (8-26) and Eq.(8-27), the terms related to  $J_3$  and  $J_4$  can be neglected, Eq.(8-26) and Eq.(8-27) become

$$\Delta\Omega_s = -\left(\frac{3}{2}\frac{J_2}{p^2}\cos i\right)\bar{n}(t - T_0) \quad (8-28)$$

$$\Delta i_s = 0 \quad (8-29)$$

Eq.(8-28) shows the secular variations of the longitude of the ascending node  $\Omega$  of the satellite orbit are produced by geopotential zonal terms, especially  $J_2$ . This effect causes the ascending node to drift toward west if  $0^\circ \leq i \leq 90^\circ$ . From Eq.(8-29) the zonal terms have no direct influence on orbital inclination  $i$ .

### 8.1.2 Solar and Lunar Attractions

Because of the great distance between the Earth and the Sun and the Earth and the Moon, the non-spherical parts of the Sun and the Moon don't need to be taken into account. Due to this reason, in the perturbation models, the Sun and the Moon can be considered as point masses. The solar and lunar attractions on the satellite can be expressed in the inertial coordinate system (the center of the earth as the origin of the system) as follows

$$\frac{d^2\bar{r}}{dt^2} = -\frac{\mu}{r^3}\bar{r} + \sum_{i=1}^2 \mu_i \left[ \frac{\bar{r}_i \cdot \bar{r}}{|\bar{r}_i - \bar{r}|^3} - \frac{\bar{r}_i}{r_i^3} \right] \quad (8-30)$$

where

$\bar{r}$  position vector of satellite

$\bar{r}_1$  position vector of Sun

$\bar{r}_2$  position vector of Moon

$\mu, \mu_1, \mu_2$  the gravity constants of the Earth, the Sun and the Moon respectively.

According to Eq.(8-30) the perturbation functions of the Sun and the Moon on satellite can be respectively written as

$$\begin{aligned} R_s &= G_s M_s \left( \frac{1}{|\bar{r}_s - \bar{r}|} - \frac{\bar{r}_s \cdot \bar{r}}{r_s^3} \right) \\ &= G_s M_s \left( \frac{1}{\sqrt{(x_s - x)^2 + (y_s - y)^2 + (z_s - z)^2}} - \frac{x_s x + y_s y + z_s z}{(x_s^2 + y_s^2 + z_s^2)^{3/2}} \right) \end{aligned} \quad (8-31)$$

$$R_m = G_m M_m \left( \frac{1}{|\bar{r}_m - \bar{r}|} - \frac{\bar{r}_m \cdot \bar{r}}{r_m^3} \right)$$

$$= G_m M_m \left( \frac{1}{\sqrt{(x_m - x)^2 + (y_m - y)^2 + (z_m - z)^2}} - \frac{x_m x + y_m y + z_m z}{(x_m^2 + y_m^2 + z_m^2)^{3/2}} \right) \quad (8-32)$$

It is known that

$$|\bar{r}_i - \bar{r}|^2 = (x_i - x)^2 + (y_i - y)^2 + (z_i - z)^2 = r_i^2 - 2(x_i x + y_i y + z_i z) + r^2$$

and  $r_i \gg r$ , then

$$\frac{1}{|\bar{r}_i - \bar{r}|} = \frac{1}{r_i} \left[ 1 - \frac{2(x_i x + y_i y + z_i z)}{r_i^2} + \frac{r^2}{r_i^2} \right]^{-\frac{1}{2}}$$

and

$$\cos \delta = \frac{\bar{r}_i \cdot \bar{r}}{r_i r} = \frac{x_i x + y_i y + z_i z}{r_i r}$$

thus

$$\begin{aligned} \frac{1}{|\bar{r}_i - \bar{r}|} &= \frac{1}{r_i} \left[ 1 + \left\{ \frac{-2\bar{r}_i \cdot \bar{r}}{r_i^2} + \left( \frac{r}{r_i} \right)^2 \right\} \right]^{-\frac{1}{2}} \\ &= \frac{1}{r_i} \left[ 1 + \frac{\bar{r}_i \cdot \bar{r}}{r_i^2} + \left\{ \frac{3}{2} \left( \frac{\bar{r}_i \cdot \bar{r}}{r_i^2} \right)^2 - \frac{1}{2} \left( \frac{r}{r_i} \right)^2 \right\} + \Lambda \right] \\ &= \frac{1}{r_i} \left[ 1 + \frac{r}{r_i} \cos \delta + \frac{r^2}{r_i^2} \left( -\frac{1}{2} + \frac{3}{2} \cos^2 \delta \right) + \frac{r^3}{r_i^3} \left( -\frac{3}{2} \cos \delta + \frac{5}{2} \cos^2 \delta \right) + \Lambda \right] \\ R_i &= \frac{G_i M_i}{r_i} \left[ 1 + \frac{r^2}{r_i^2} \left( -\frac{1}{2} + \frac{3}{2} \cos^2 \delta \right) + \frac{r^3}{r_i^3} \left( -\frac{3}{2} \cos \delta + \frac{5}{2} \cos^3 \delta \right) + \Lambda \right] \end{aligned} \quad (8-33)$$

Removing the constant term in Eq.(8-33), Eq.(8-33) becomes

$$R_i = \frac{G_i M_i}{r_i} \left[ \frac{r^2}{r_i^2} \left( -\frac{1}{2} + \frac{3}{2} \cos^2 \delta \right) + \frac{r^3}{r_i^3} \left( -\frac{3}{2} \cos \delta + \frac{5}{2} \cos^3 \delta \right) + \Lambda \right] \quad (8-34)$$

In the equations above subscript  $i$  means  $s$  or  $m$ , i.e. the Sun and the Moon respectively. The relations between  $\delta$  and satellite orbit parameters are shown in the following figure.

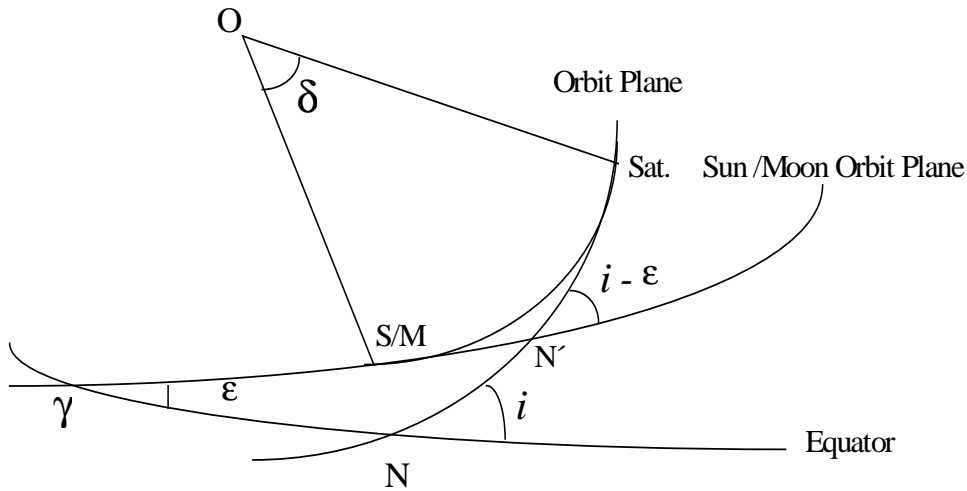


Figure 8-1 Relations between Satellite and Sun/Moon

In Figure 8-1  $\varepsilon$  is the obliquity of the ecliptic. The arc between  $\gamma$  and  $N'$  is defined as  $\Omega$ . The arc between satellite and  $N'$  as  $\nu + \omega$ . The arc between  $\gamma$  and Sun/Moon as  $\nu' + \omega'$ ,

From Figure 8-1,

$$\cos \delta = \cos(v + \omega) \cos(\Omega - v' - \omega') - \sin(v + \omega) \sin(\Omega - v' - \omega') \cos(i - \varepsilon)$$

In Eq.(8-34) if only the first term is considered, Eq.(8-34) becomes

$$\begin{aligned} R_i = G_i M_i \frac{r^2}{r_i^3} & \left[ -\frac{1}{2} + \frac{3}{2} \cos^2(v + \omega) \cos^2(\Omega - v' - \omega') \right. \\ & - 3 \cos(v + \omega) \cos(\Omega - v' - \omega') \sin(v + \omega) \sin(\Omega - v' - \omega') \cos(i - \varepsilon) \\ & \left. + \frac{3}{2} \sin^2(v + \omega) \sin^2(\Omega - v' - \omega') \cos^2(i - \varepsilon) \right] \end{aligned} \quad (8-35)$$

$$\begin{aligned} R_i = \frac{G_i M_i}{r_i} \frac{a^2}{r_i^2} (1 - e^2)^2 & \left[ -\frac{1}{2} \frac{1}{(1 + e \cos v)^2} + \frac{3}{2} \frac{\cos^2(v + \omega)}{(1 + e \cos v)^2} \cos^2(\Omega - v' - \omega') \right. \\ & \left. - \frac{3}{4} \frac{\sin 2(v + \omega)}{(1 + e \cos v)^2} \sin 2(\Omega - v' - \omega') \cos(i - \varepsilon) + \frac{3}{2} \frac{\sin^2(v + \omega)}{(1 + e \cos v)^2} \sin^2(\Omega - v' - \omega') \cos^2(i - \varepsilon) \right] \end{aligned} \quad (8-36)$$

Inserting Eq.(8-36) into Eq.(8-1), the following differential equations can be obtained

$$\begin{aligned} \frac{di}{dt} = \frac{n}{n^2 \sin(i - \varepsilon)} \frac{G_i M_i}{r_i^3} (1 - e^2)^{3/2} & \left[ \cos(i - \varepsilon) \left\{ -\frac{3}{2} \frac{\sin 2(v + \omega)}{(1 + e \cos v)^2} \cos^2(\Omega - v' - \omega') \right. \right. \\ & - \frac{3}{2} \frac{\cos 2(v + \omega)}{(1 + e \cos v)^2} \sin 2(\Omega - v' - \omega') \cos(i - \varepsilon) + \frac{3}{2} \frac{\sin 2(v + \omega)}{(1 + e \cos v)^2} \sin^2(\Omega - v' - \omega') \cos^2(i - \varepsilon) \left. \right\} \\ & - \left\{ -\frac{3}{2} \frac{\cos^2(v + \omega)}{(1 + e \cos v)^2} \sin 2(\Omega - v' - \omega') - \frac{3}{2} \frac{\sin 2(v + \omega)}{(1 + e \cos v)^2} \cos 2(\Omega - v' - \omega') \cos(i - \varepsilon) \right. \\ & \left. \left. + \frac{3}{2} \frac{\sin^2(v + \omega)}{(1 + e \cos v)^2} \sin 2(\Omega - v' - \omega') \cos^2(i - \varepsilon) \right\} \right] \end{aligned} \quad (8-37)$$

$$\begin{aligned} \frac{d\Omega}{dt} = \frac{n}{n^2 \sin(i - \varepsilon)} \frac{G_i M_i}{r_i^3} (1 - e^2)^{3/2} & \left[ \frac{3}{4} \frac{\sin 2(v + \omega)}{(1 + e \cos v)^2} \sin 2(\Omega - v' - \omega') \sin(i - \varepsilon) \right. \\ & \left. - \frac{3}{2} \frac{\sin^2(v + \omega)}{(1 + e \cos v)^2} \sin^2(\Omega - v' - \omega') \sin 2(i - \varepsilon) \right] \end{aligned} \quad (8-38)$$

Before solving Eq.(8-37) and Eq.(8-38), the following integrations should be solved first, considering

$$\frac{dM}{dv} = \left(\frac{r}{a}\right)^2 \frac{1}{\sqrt{1 - e^2}}$$

$$\int_{t_s}^{t_e} \frac{\sin 2(v + \omega)}{(1 + e \cos v)^2} n dt = \int_0^{2\pi} \frac{\sin 2(v + \omega)}{(1 + e \cos v)^2} dM = \int_0^{2\pi} \frac{\sin 2(v + \omega)}{(1 + e \cos v)^2} \left(\frac{r}{a}\right)^2 \frac{1}{\sqrt{1 - e^2}} dv = (1 - e^2)^{3/2} \int_0^{2\pi} \frac{\sin 2(v + \omega)}{(1 + e \cos v)^4} dv \quad (8-39)$$

$$\int_{t_s}^{t_e} \frac{\cos 2(v + \omega)}{(1 + e \cos v)^2} n dt = (1 - e^2)^{3/2} \int_0^{2\pi} \frac{\cos 2(v + \omega)}{(1 + e \cos v)^4} dv \quad (8-40)$$

$$\int_{t_s}^{t_e} \frac{\sin^2(v + \omega)}{(1 + e \cos v)^2} n dt = (1 - e^2)^{3/2} \int_0^{2\pi} \frac{\sin^2(v + \omega)}{(1 + e \cos v)^4} dv \quad (8-41)$$

$$\int_{t_s}^{t_e} \frac{\cos^2(v + \omega)}{(1 + e \cos v)^2} n dt = (1 - e^2)^{3/2} \int_0^{2\pi} \frac{\cos^2(v + \omega)}{(1 + e \cos v)^4} dv \quad (8-42)$$

Eq. (8-39) to Eq.(8-42) are difficult to integrate, but for geostationary satellite,  $e \approx 0$ , then Eq.(8-39) to Eq.(8-42) become

$$\int_{t_s}^{t_e} \frac{\sin 2(v + \omega)}{(1 + e \cos v)^2} n dt = \int_0^{2\pi} \sin 2(v + \omega) dv = 0 \quad (8-43)$$

$$\int_{t_s}^{t_e} \frac{\cos 2(v + \omega)}{(1 + e \cos v)^2} n dt = \int_0^{2\pi} \cos 2(v + \omega) dv = 0 \quad (8-44)$$

$$\int_{t_s}^{t_e} \frac{\sin^2(v + \omega)}{(1 + e \cos v)^2} n dt = \int_0^{2\pi} \sin^2(v + \omega) dv = \pi \quad (8-45)$$

$$\int_{t_s}^{t_e} \frac{\cos^2(v + \omega)}{(1 + e \cos v)^2} n dt = \int_0^{2\pi} \cos^2(v + \omega) dv = \pi \quad (8-46)$$

From Eq.(8-43) to Eq.(8-46), the solutions of Eq.(8-37) and Eq.(8-38) are given by

$$\begin{aligned} \Delta i_i &= \frac{1}{n^2 \sin(i - \varepsilon)} \frac{G_i M_i}{r_i^3} \left[ \frac{3}{2} \pi \sin 2(\Omega - v' - \omega') - \frac{3}{2} \pi \sin 2(\Omega - v' - \omega') \cos^2(i - \varepsilon) \right] \\ &= \frac{\pi}{n^2 \sin(i - \varepsilon)} \frac{G_i M_i}{r_i^3} \frac{3}{2} \left[ \sin 2(\Omega - v' - \omega') - \sin 2(\Omega - v' - \omega') \cos^2(i - \varepsilon) \right] \end{aligned} \quad (8-47)$$

$$\Delta \Omega_i = -\frac{3\pi}{n^2} \frac{G_i M_i}{r_i^3} \sin^2(\Omega - v' - \omega') \cos(i - \varepsilon) \quad (8-48)$$

Considering the effects of the Sun and the Moon on the geostationary satellite respectively and inclinations of the Sun and the Moon with equator as  $23.442^\circ$  and  $28.6^\circ$  (Soop, 1994), Eq.(8-47) and Eq.(8-48) can be written as

$$\Delta i_s = \frac{\pi}{n^2 \sin(-23^\circ.442)} \frac{G_s M_s}{r_s^3} \frac{3}{2} \left[ \sin 2(-v_s - \omega_s) - \sin 2(-v_s - \omega_s) \cos^2(-23^\circ.442) \right] \quad (8-49)$$

$$\Delta \Omega_s = -\frac{3\pi}{n^2} \frac{G_s M_s}{r_s^3} \sin^2(-v_s - \omega_s) \cos(-23^\circ.442) \quad (8-50)$$

$$\Delta i_m = \frac{\pi}{n^2 \sin(-5^\circ.14)} \frac{G_m M_m}{r_m^3} \frac{3}{2} \left[ \sin 2(-v_m - \omega_m) - \sin 2(-v_m - \omega_m) \cos^2(-5^\circ.14) \right] \quad (8-51)$$

$$\Delta \Omega_m = -\frac{3\pi}{n^2} \frac{G_m M_m}{r_m^3} \sin^2(-v_m - \omega_m) \cos(-5^\circ.14) \quad (8-52)$$

According to Eq.(8-49) to Eq.(8-52), the secular variations of the inclination  $i$  and the longitude of the ascending node,  $\Omega$ , of the geostationary satellite due to the Sun and the Moon attractions are drawn in Figure 8-2 and Figure 8-3. In the figures, assuming the Sun and the Moon move along the Sun/Moon orbits from  $0^\circ$  to  $360^\circ$ . For the Sun it takes one year, for the Moon it only needs about one month.

From Eq.(8-28) and Eq.(8-29), and the discussion above it is clear that the secular variations of the inclination  $i$  and the longitude of the ascending node,  $\Omega$ , of geostationary satellite are mainly caused by Sun and Moon attractions. Although the secular variations are produced by the  $J_2$  term of non-spherical gravitation as well, comparing to the Sun and the Moon, the variations caused by  $J_2$  are very small. Therefore the major effects that are considered for GEO satellite maneuvers are the Sun and the Moon attractions.

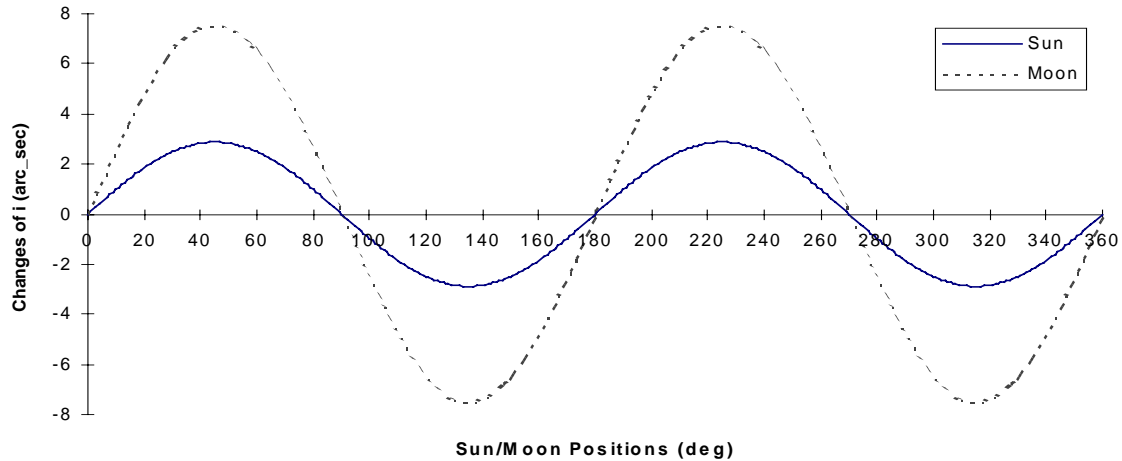


Figure 8-2 Secular Variations of Inclination of GEO Satellite due to Sun/Moon Position Changing

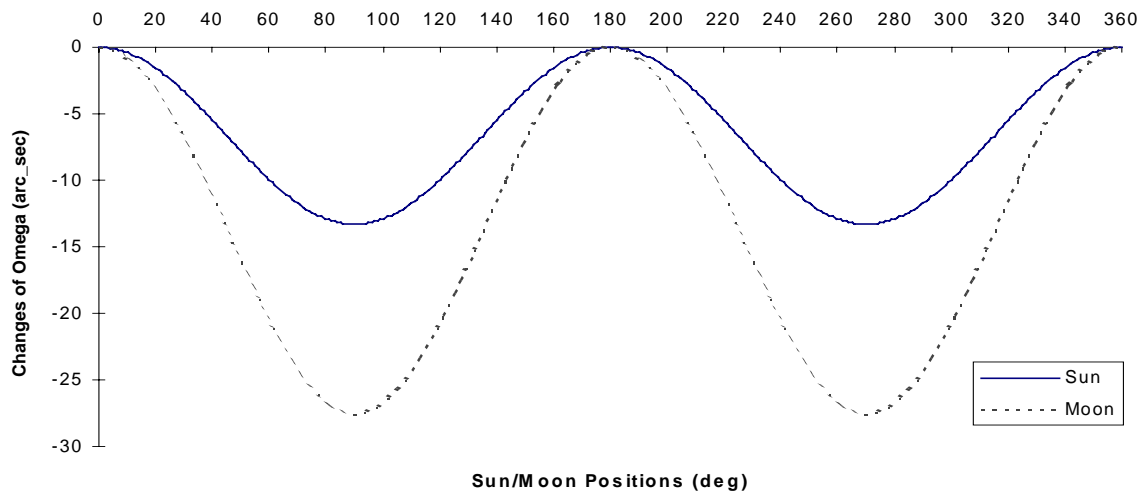


Figure 8-3 Secular Variations of Longitude of Ascending Node of GEO Satellite due to Sun/Moon Position Changes

Figure 8-2 and Figure 8-3 show that the gravitational attractions of the Sun and the Moon pull the geostationary satellites out of equatorial orbit plane, gradually increasing satellite's orbital inclination. In addition, the noncircular shape of the earth's equator causes these satellites to be slowly driven to one of two stable equilibrium points along the equator, resulting in an east-west liberation (drifting back and forth) about these points.

The secular variation from the Moon attraction is about twice as strong as from the Sun's attraction. This is because the distance from the Sun is much larger than the Moon and the attraction from the Sun decreases with the cube of the distance from the Sun to the Earth. For the secular variation of inclination  $i$  from the Sun attraction, the maximum variations will be reached four times each year, two times for positive changes and two times for negative changes. For the secular variation of inclination  $i$  from the Moon attraction, the maximum variations will be reached four times each lunar month, also two times for positive changes and two times for negative changes. For the secular variation of the longitude of the ascending node,  $\Omega$ , from the Sun attraction, the maximum variations occur at midsummer and midwinter. At the beginning of spring and autumn, the secular variation of  $\Omega$  is zero. The effect of the lunar perturbation on the orbital inclination is the same as that of the solar perturbation. The variations are maximum twice per lunar month and passes through zero in between.

Due to non-spherical geopotential gravitation, the Sun and the Moon attractions, the inclination and longitude of the ascending node of the geostationary satellite will gradually drift away from the original position.

To counteract these drifts due to perturbations, sufficient fuel is loaded into the maneuver rockets onboard of all geostationary satellites to periodically correct any changes over the planned lifetime of the satellite. These periodic corrections are known as stationkeeping or satellite maneuvers. North-south stationkeeping corrects the slowly increasing inclination back to zero and east-west stationkeeping keeps the satellite at its assigned position within the geostationary belt. These maneuvers are planned to maintain the geostationary satellite within a small distance of its ideal location (both north-south and east-west). This tolerance is normally designed to ensure the satellite remains within the ground antenna beamwidth without tracking.

In Germany, Deutsche Telekom owns and operates three geostationary telecommunication and direct broadcasting satellites. The Telekom DFS-Kopernikus satellites are maneuvered in longitude (EW) on a weekly and in inclination (NS) on a two week basis. TVSAT-2 is operated in EW and NS on a two week cycle. It results that the Flight Dynamics System has to cope with 11 maneuvers on a fortnight basis (Bisten, M.& Damiano, A. 1996)

## 8.2 Orbit Determination During Satellite Maneuvers

If a geostationary satellite is used for navigation purpose, the orbit information (ephemeris) should be continually broadcasted to the users for their navigation and positioning computation. Due to the large orbit errors during satellite maneuvers, the orbit information at that time can not be used. During this period, users have to stop their navigation and positioning applications. Normally, the geostationary satellite maneuver is operated weekly, which makes a big problem for navigation users to get correct orbit information in real-time. In order to overcome this problem, the precise orbit determination and prediction methods during satellite maneuver should be considered.

The situation of satellite orbit changes during the satellite maneuver can be shown in Figure 8-4.

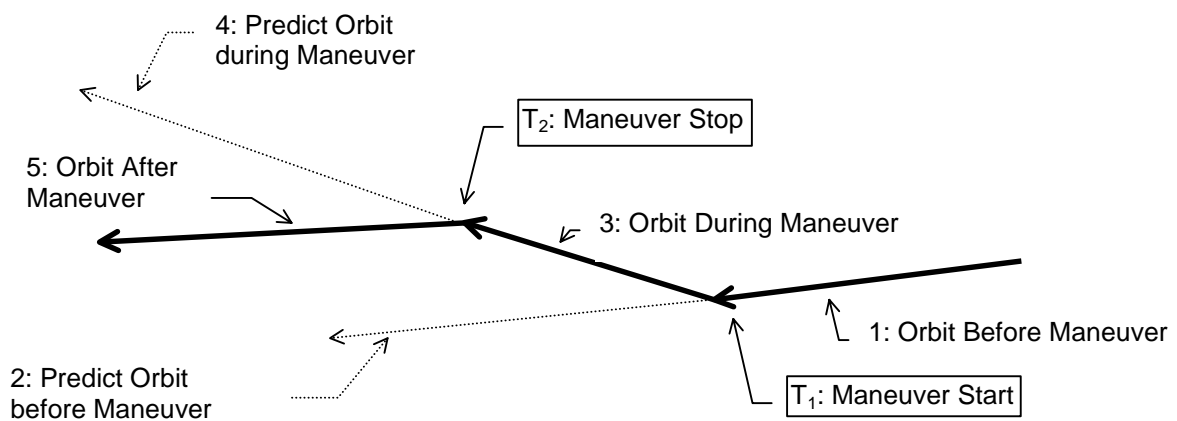


Figure 8-4 Three Phases of GEO Satellite Tracks during Maneuver

Figure 8-4 shows five tracks of GEO satellite orbit. Track 1 is an orbit track before maneuver; Track 2 is the predicted orbit before maneuver; Track 3 is the track of GEO satellite during maneuver; Track 4 is the predicted orbit during maneuver; Track 5 is a satellite orbit after maneuver. Tracks 1, 3 and 5 are actually GEO satellite orbits. Without maneuver operation, actual GEO satellite tracks should be Track 1 and Track 2. Normally GEO satellite orbit is determined and predicted using precise satellite dynamic models which include geopotential, solar and lunar attractions, solar radiation pressure etc., but no satellite maneuver force model is included due to difficulties to model the maneuver force. Currently, the most of the GEO satellites are used for communication purposes, people are more concerned about GEO satellite drift, they are not so interested in the actual satellite orbit. But for navigation application, the actual orbit of GEO satellite is very important. Users need the actual position and velocity of GEO satellite as references to compute their own positions and velocities.

There are two phases that are big problems for satellite navigation application during satellite maneuver. The first phase: satellite maneuver begins at  $T_1$  (see Figure 8-4); navigation users use the predicted orbit Track 2 (predicted before maneuver), but the actual orbit is Track 3. This will introduce a big orbit error for the navigation users in their navigation computation. The second phase is that the satellite maneuver stops at  $T_2$ , the



predicted orbit is Track 4, the actual orbit is Track 5, but the navigation users still use predicted orbit Track 4. This will also introduce a big orbit error for the navigation users.

In order to solve the problems discussed above, other two problems should be solved before. First, the orbit determination during maneuver; second, the precise satellite maneuver force model that can be used for orbit prediction. Because navigation users can only use predicted orbit for their navigation application, the precise maneuver force model is very important for GEO orbit prediction during satellite maneuver.

In the following, the orbit determination of the GEO satellite during maneuver and the maneuver force model will be discussed.

### 8.2.1 Orbit Determination Without Maneuver Operation

In order to compare the accuracy, the simulation results of kinematic and dynamic orbit determination methods without maneuver operation are presented (see Figure 8-5 and Figure 8-6). Observations are ranges with 1 m random noises and the sample rate is 1 min. Eight ESA tracking stations (see Chapter 9) are used in simulations. A geostationary satellite is supposed to be located in the sky at ground  $\lambda = 0^\circ$  above. The results of orbit determination are shown in Figure 8-5 and Figure 8-6.

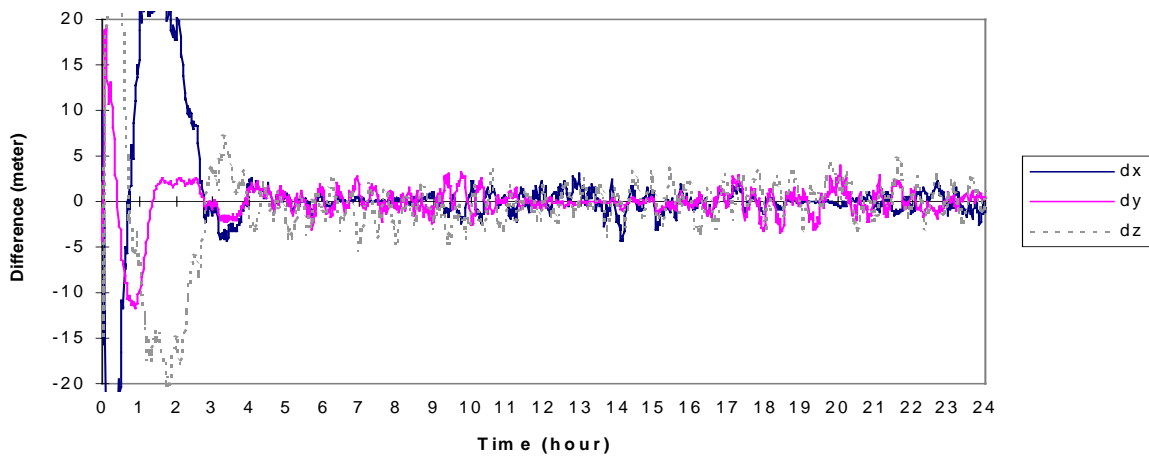


Figure 8-5 Kinematic Orbit Determination of Geostationary Satellite

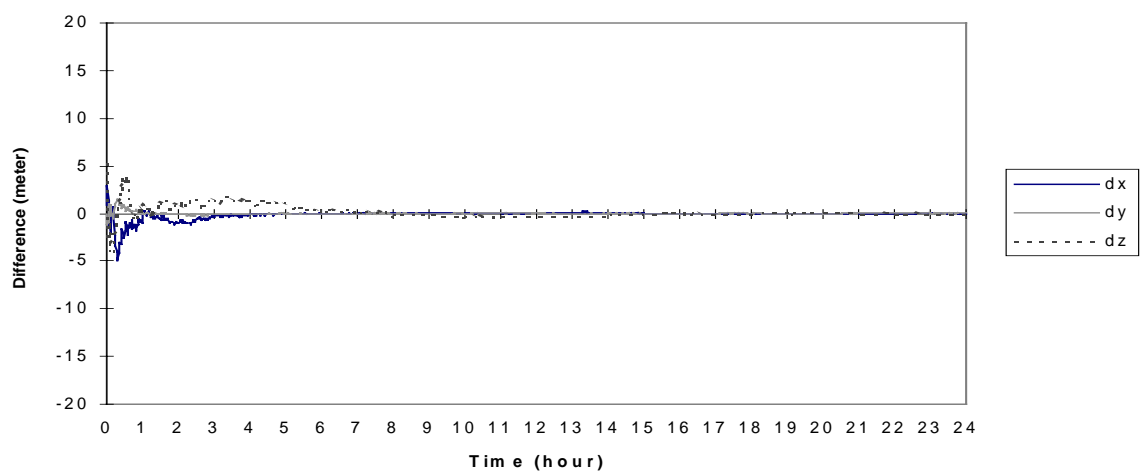


Figure 8-6 Dynamic Orbit Determination of Geostationary Satellite

From Figure 8-5 and Figure 8-6, the accuracy of dynamic orbit determination is better than kinematic orbit determination. In the simulation test above, the satellite dynamic force models are assumed to include all necessary perturbations, therefore the highest accuracy can be achieved for dynamic orbit determination. This also shows that the accuracy of dynamic orbit determination is strongly dependent on the dynamic force models.

On the other side, the accuracy of kinematic orbit determination is not related to the dynamic force models, it only depends on the observation noise and geometrical distribution of the ground tracking stations. The lower the noise of observation, the better the accuracy of the kinematic orbit determination. Figure 8-7, that shows the results of kinematic orbit determination using carrier phase observation, verifies the conclusion above.

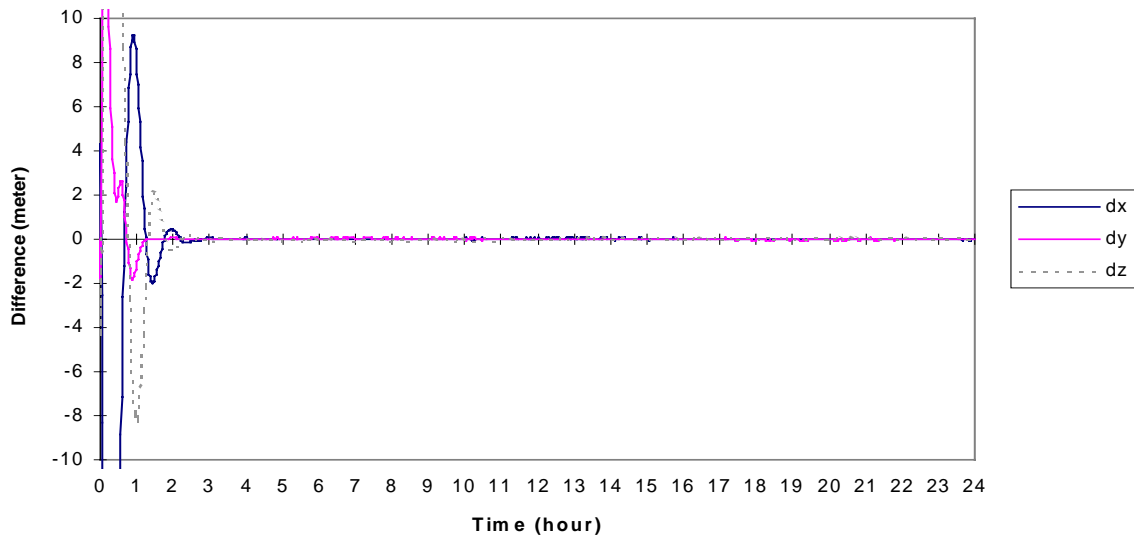


Figure 8-7 Kinematic Orbit Determination of Geostationary Satellite using Carrier Phase Observation

### 8.2.2 Orbit Determination With Maneuver Operation

Following are the results of orbit determination during satellite maneuvers using the kinematic and the dynamic methods. The observations are still ranges with 1 m random noise. The satellite maneuver starts at 5<sup>h</sup>00<sup>m</sup> and stops at 10<sup>h</sup>00<sup>m</sup>. The maneuver lasts 5 hours. The maneuver accelerations are assumed as follows

$$\left. \begin{aligned} \ddot{x} &= \ddot{y} = 8 \times 10^{-7} \text{ m/s}^2 \\ \ddot{z} &= 0 \end{aligned} \right\} \quad (8-53)$$

Eq. (8-53) means the satellite maneuver force push the satellite to move in the east direction in the in-plane of the orbit.

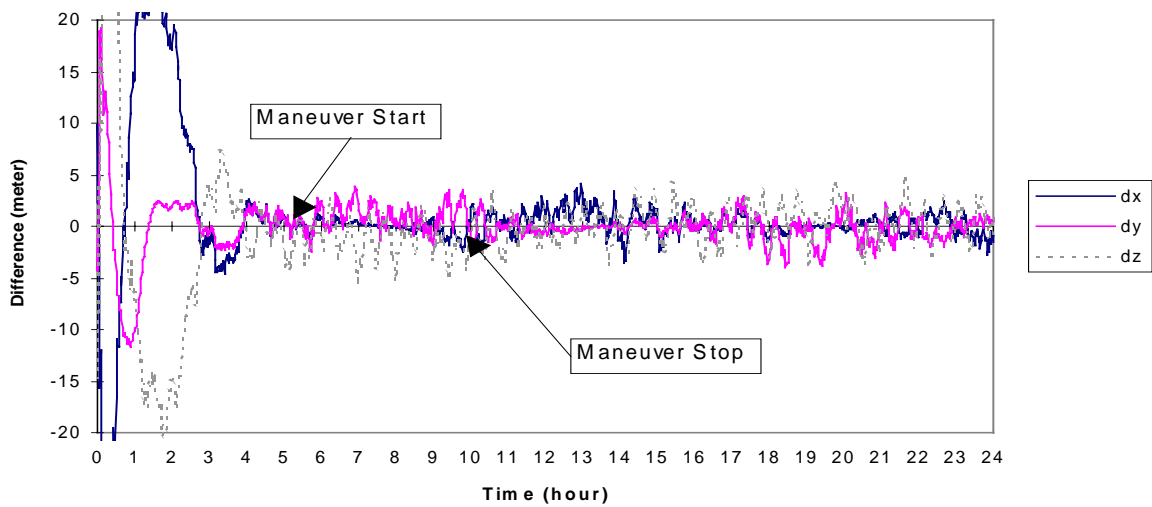


Figure 8-8 Kinematic Orbit Determination of Geostationary Satellite during Maneuver

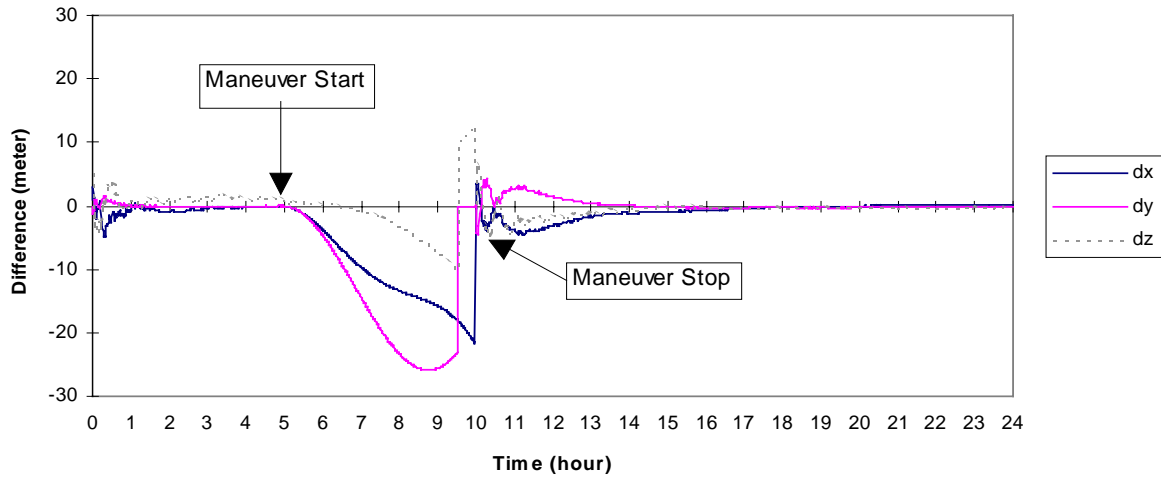


Figure 8-9 Dynamic Orbit Determination of Geostationary Satellite during Maneuver

Comparing Figure 8-5 with Figure 8-8, it shows that there are no great differences found for orbit determination using kinematic method with or without maneuver operations. This property can be used for improving maneuver force model. Comparing Figure 8-6 with Figure 8-9 it is obvious that during satellite maneuver, the accuracy of the dynamic orbit determination is significantly degraded. For some larger maneuver force, the accuracy of dynamic orbit determination would be worse. This is because in the dynamic method, no precise maneuver force models are included. Even if the maneuver force models were included, but there were some unmodeled or mismodeled errors, the accuracy of the dynamic orbit determination would also be reduced.

### 8.3 Maneuver Force Model

For post-processing, it is sufficient to use the kinematic method for orbit determination during satellite maneuver. For real-time navigation application, users usually need the so-called satellite ephemeris, i.e. predicted orbit, as a reference to compute their positions and velocities. The kinematic method can be used to determine the satellite orbit during satellite maneuver, but it cannot be used to predict orbit. For orbit prediction, the dynamic method is still needed and the maneuver force should be included in the satellite dynamic force models.

First let us see the accuracy of orbit prediction using current dynamic models without satellite maneuver force model included.

Figure 8-10 and Figure 8-11 show the accuracy of orbit prediction due to the maneuver accelerations expressed by Eq.(8-53). The maneuver operation lasts about 5 hours. Figure 8-12 shows the accuracy of orbit prediction due to the maneuver accelerations written below and the maneuver operation lasts about 48 minutes

$$\left. \begin{array}{l} \ddot{x} = \ddot{y} = 8 \times 10^{-5} \text{ m/s}^2 \\ \ddot{z} = 0 \end{array} \right\} \quad (8-54)$$

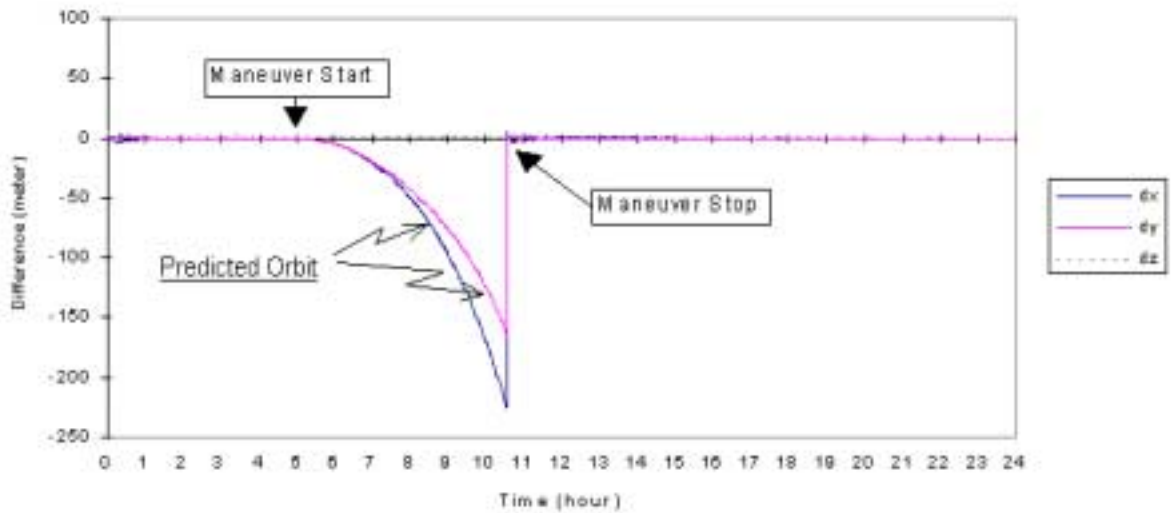


Figure 8-10 Dynamic Orbit Prediction during Satellite Maneuver

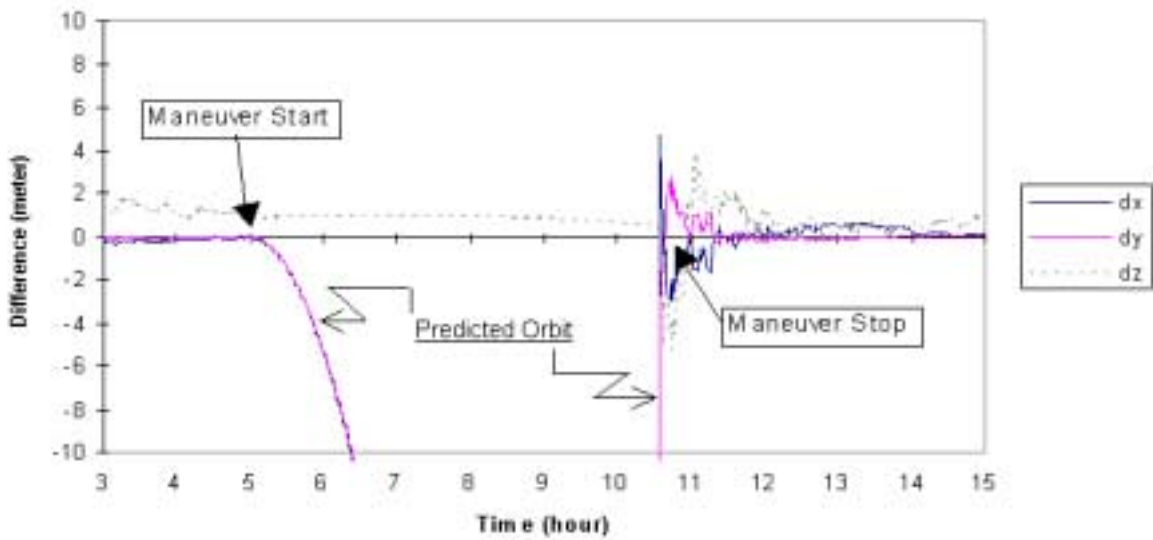


Figure 8-11 Enlarged Part of Figure 8-10

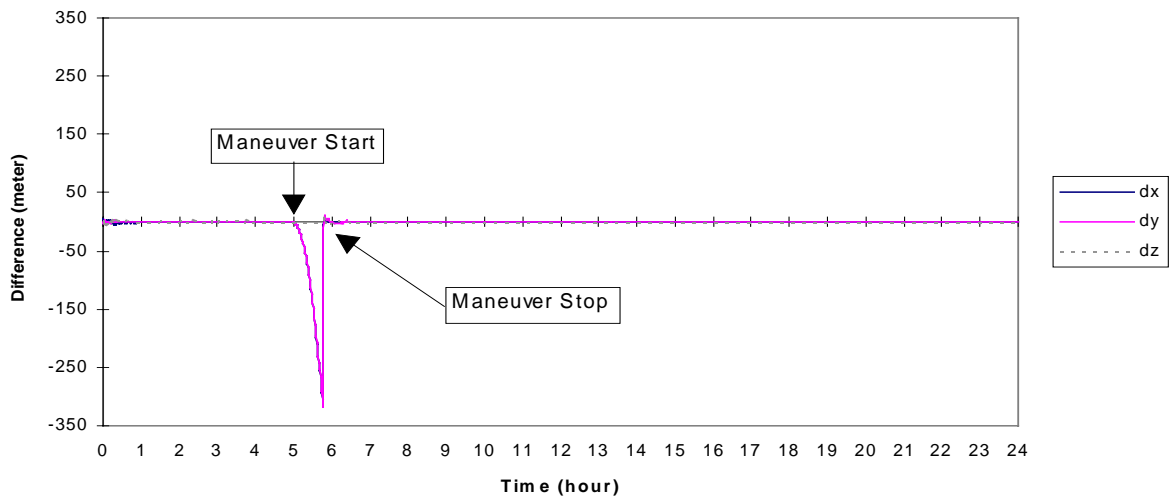


Figure 8-12 Dynamic Orbit Prediction during Satellite Maneuver

After one hour from maneuver starting at maneuver accelerations described in Eq.(8-53), the orbit prediction error will reach about 5 meter (see Figure 8-10 and Figure 8-11), which may be tolerable for the navigation

users. But for the larger maneuver accelerations, see Eq.(8-54), after 5 minutes from maneuver starting, the prediction error will reach about 5 meter, maximum about 330 meter. Obviously the larger the maneuver acceleration, the worse the accuracy of orbit prediction. Also it can be inferred that the shorter the time of maneuver operation, the better the accuracy of orbit prediction.

From the discussion above it can be concluded that for about 5 meter orbit accuracy required by navigation users, if maneuver force model is not included in dynamic model for orbit determination, the time of maneuver operation for maneuver acceleration like Eq.(8-53) should not exceed one hour; for maneuver acceleration like Eq.(8-54), maneuver operation time should not exceed 5 minutes. For longer maneuver operation, proper maneuver force model should be included into the dynamic models of orbit determination and prediction.

### 8.3.1 Nominal Model

When onboard rocket is fired during the satellite maneuver operation, the rocket thrust is slightly higher than its normal value, short time later it will be kept constant. Therefore the nominal maneuver force model can be written by (Gill et al, 1993)

$$\vec{a}_t(t) = \frac{T(t)}{m(t)} \vec{e}(t) \quad (8-55)$$

$$T(t) = \begin{cases} 0 & t < t_0 \\ T_0 - (T_0 - T_{ss})(t - t_0)/(t_d - t_0) & t_0 \leq t < t_d \\ T_{ss} & t_d \leq t < t_e \\ 0 & t_e \leq t \end{cases} \quad (8-56)$$

where

- $T(t)$  thrust magnitude
- $T_0$  initial value of thruster at firing start  $t_0$
- $T_{ss}$  constant thrust after  $t_d$
- $t_0$  epoch of firing start
- $t_d$  epoch of thrust becoming constant
- $t_e$  epoch of maneuver end
- $m(t)$  satellite mass
- $\vec{e}(t)$  thrust direction unit vector in inertial space

In Eq.(8-56), it is assumed that the thrust linearly decreases from its initial value  $T_0$  to a value  $T_{ss}$  that remains constant during the following steady state thrust phase up to the maneuver end.

### 8.3.2 Approximation using Kinematic Orbit Determination

The values of  $T(t)$  and  $m(t)$  in Eq.(8-55) and Eq.(8-56) depend on the force profile of the onboard rocket. The difference between nominal and actual thrusts can be given by

$$\left. \begin{aligned} \Delta a_x &= a_0^x(t_0) + a_1^x(t - t_0) + a_2^x(t - t_0)^2 + \Lambda \\ \Delta a_y &= a_0^y(t_0) + a_1^y(t - t_0) + a_2^y(t - t_0)^2 + \Lambda \\ \Delta a_z &= a_0^z(t_0) + a_1^z(t - t_0) + a_2^z(t - t_0)^2 + \Lambda \end{aligned} \right\} \quad (8-57)$$

From dynamic orbit determination, the acceleration of the GEO satellite can be obtained by dynamic model computation. From kinematic orbit determination, Eq.(6-79), GEO satellite acceleration is also solved, therefore  $\Delta a_x, \Delta a_y, \Delta a_z$  in Eq.(8-57) can be obtained by making difference of these two types of accelerations.

By solving the least square problem in Eq.(8-57), the parameters of  $a_0^x, a_1^x, \Lambda, a_0^y, a_1^y, \Lambda, a_0^z, a_1^z, \Lambda$ , can be obtained. Then these parameters as well as nominal maneuver force model Eq.(8-55) and Eq.(8-56) can be included in satellite dynamic model to predict the satellite orbit. For real-time application, Kalman filter or sequential least-squares methods can be used to solve Eq.(8-57) to get update values of these parameters.

Clearly from Eq.(8-57), the acceleration is in the earth-fixed system, which cannot be directly compared with the acceleration from the dynamic model. The coordinate system conversion should be made before. The transformation can be done as follows.

Assuming  $[N]$  is the nutation transformation matrix,  $[P]$  the precession matrix,  $[C]$  the polar motion matrix and  $[G]$  the sidereal time transformation matrix, then transformations from the earth-fixed coordinate system to inertial coordinate system are

$$\overset{w}{r}_i = [N][P][C][G]\overset{w}{r}_e \tag{8-58}$$

$$\overset{w}{v}_i = [N][P][C]\{[G]\overset{w}{v}_e + [\mathcal{G}]\overset{w}{r}_e\} \tag{8-59}$$

$$\overset{w}{a}_i = [N][P][C]\{[G]\overset{w}{a}_e + 2[\mathcal{G}]\overset{w}{v}_e\} \tag{8-60}$$

where

$\overset{w}{r}_i, \overset{w}{r}_e$  position vectors of satellite in the inertial and the earth-fixed systems, respectively

$\overset{w}{v}_i, \overset{w}{v}_e$  velocity vectors of satellite in the inertial and the earth-fixed systems, respectively

$\overset{w}{a}_i, \overset{w}{a}_e$  acceleration vectors of satellite in the inertial and the earth-fixed systems, respectively

Normally  $\mathcal{E}$  and  $[\mathcal{G}]$  are very small, therefore the product of  $[\mathcal{G}]\overset{w}{r}_e$  can be neglected.

According to the method described above, using simulation data, the results of orbit prediction during satellite maneuvers are shown in Figure 8-13 and Figure 8-14.

For the maneuver operated at the acceleration of Eq.(8-53), the orbit prediction during satellite maneuver is drawn as in Figure 8-13; for the maneuver acceleration of Eq.(8-54), the orbit prediction is drawn in Figure 8-14. In the orbit prediction, it is assumed that 50% of maneuver acceleration is modeled by nominal maneuver force model, Eq.(8-55) and Eq.(8-56); 20% of maneuver acceleration were corrected by Eq.(8-57), which was updated at the rate of about 60 minutes for Figure 8-13 and 10-15 minutes for Figure 8-14 by kinematic orbit determination results, the remaining 30% were unmodeled maneuver force errors that were not corrected during orbit prediction.

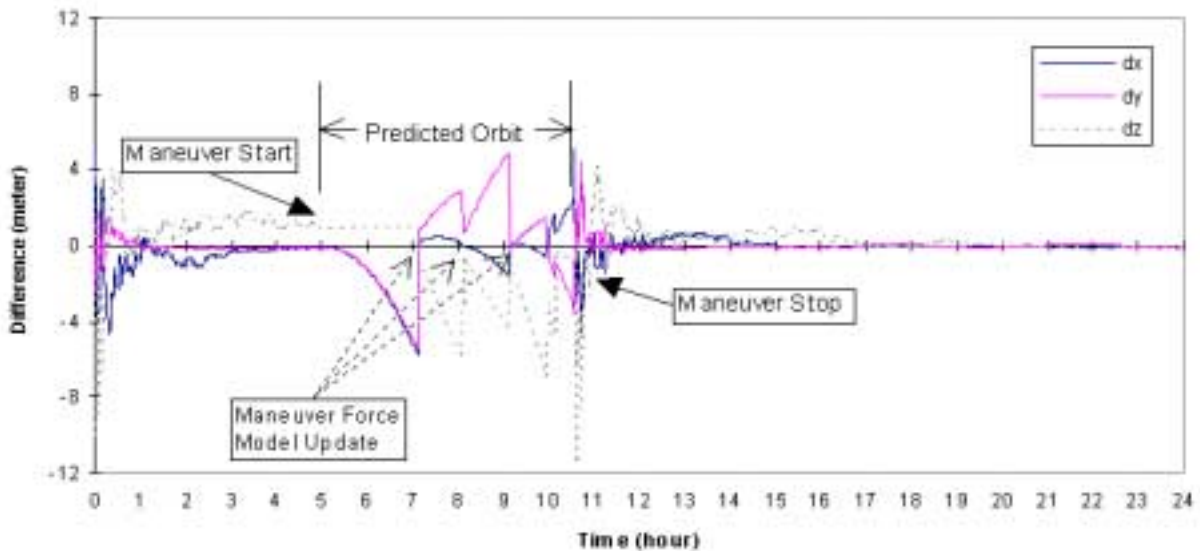


Figure 8-13 Orbit Prediction during Satellite Maneuver

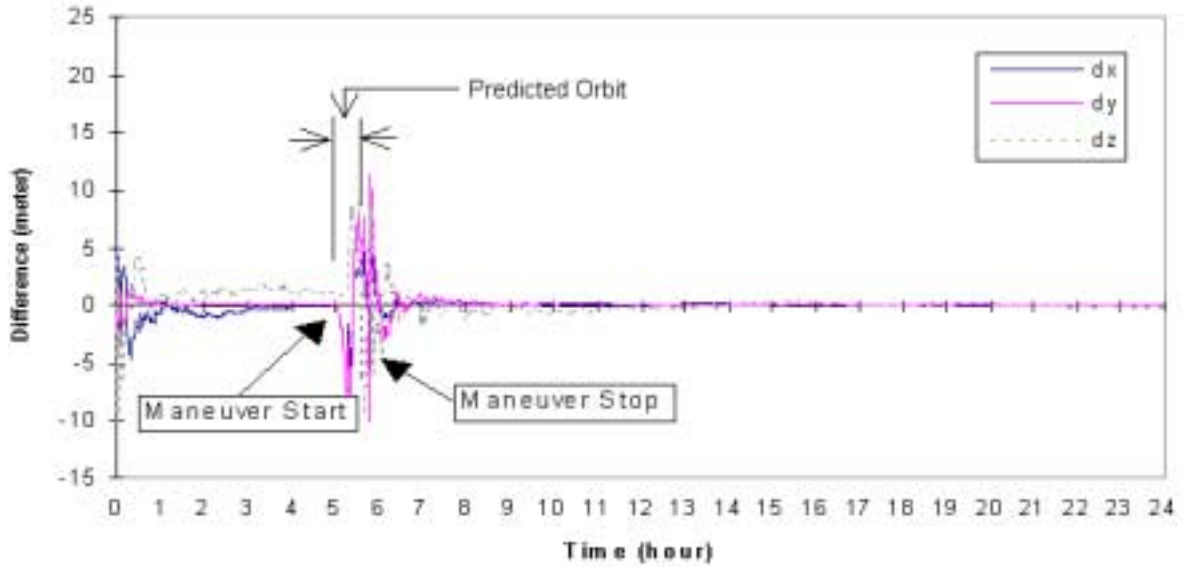


Figure 8-14 Orbit Prediction during Satellite Maneuver

Comparing Figure 8-10 with Figure 8-13 and Figure 8-12 with Figure 8-14, it can be seen that the accuracies of predicted orbit are significantly enhanced by the maneuver force models that are updated by kinematic orbit determination. In Figure 8-11, the accuracy of prediction orbit is about 300 meters for 5 hours of maneuver operation, but in Figure 8-13, the accuracy of prediction orbit is about 5 meters for 5 hours of maneuver operation. In Figure 8-12, the accuracy of prediction orbit is about 300 meters after 48 minutes of maneuver operation, but in Figure 8-14, the accuracy of prediction orbit is about 5-10 meters after 48 minutes of maneuver operation. It should be noted again that in the results above, 30% unmodeled maneuver force errors are assumed, which were not corrected during orbit determination and prediction. If maneuver force model is more accurately or the accuracy of observation is increased, the time of orbit prediction will be longer.





## CHAPTER 9 SOFTWARE AND SIMULATION RESULTS

### 9.1 Software

According to the discussions and algorithms in the previous chapters, I have written the software for IGSO and GEO orbit determination using extended Kalman filter, called GEOKAL (GEO/IGSO orbit determination using KALman filter). At present in the software, GEOKAL, the major perturbations such as geopotential perturbation, solar and lunar attractions and solar radiation force are included in the satellite dynamic models. Observations which can be processed are ranges and carrier phases. The major flow chart of software GEOKAL is as follows:

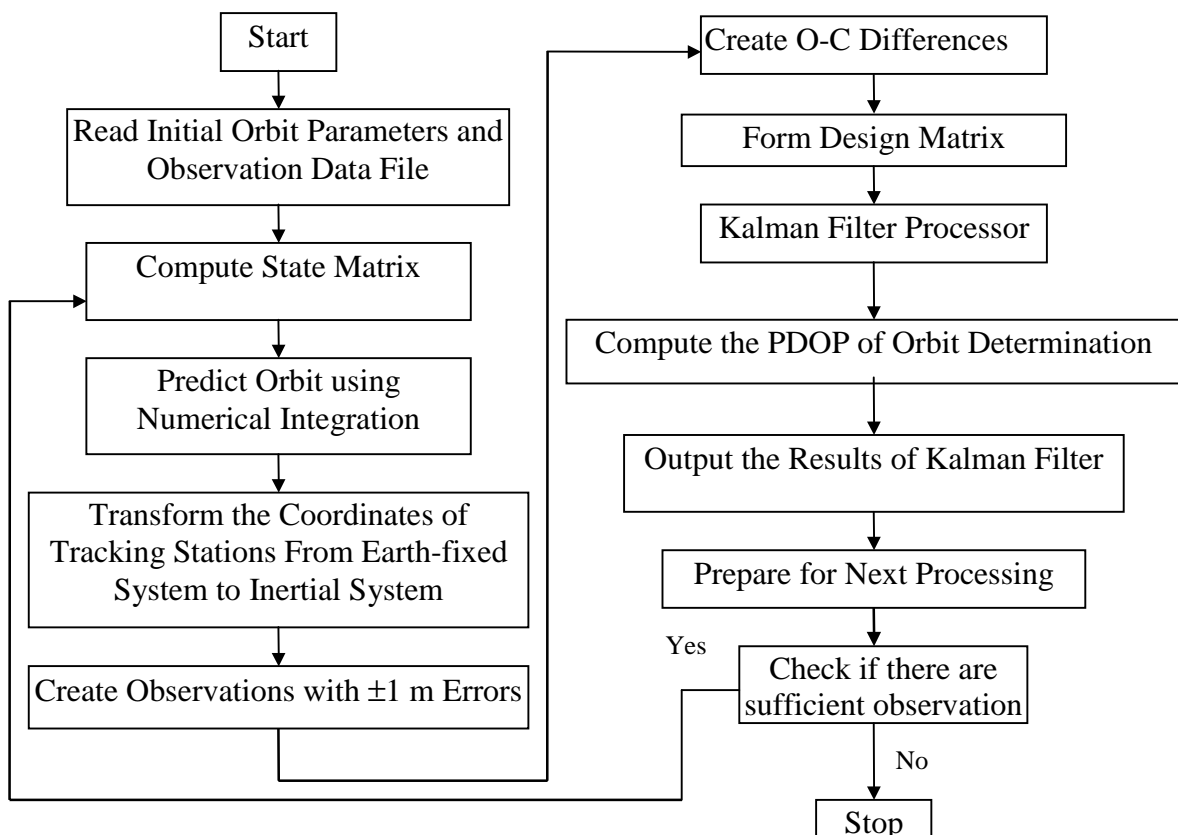


Figure 9-1 The flowchart of Program GEOKAL

#### 9.1.1 Coordinate System

In the software, GEOKAL, there are two coordinate systems used, i.e. the earth-fixed geocentric coordinate WGS84 which is defined and maintained by National Imagery and Mapping Agency (NIMA), USA and inertial coordinate FK5 in which polar axis points in the direction of the mean pole at J2000.0 as defined by the IAU conventional models of precession and nutation.

### 9.1.2 Distribution of Tracking Stations

The following eight ESA satellite tracking stations are used for GNSS-2/Galileo satellite orbit determination in the simulation study.

Table 9-1 The Distribution of ESA Tracking Stations

Index	Tracking Station	Latitude	Longitude
(1)	Herstmonceux	52°00′	00°00′
(2)	Azoren	38°30′	-28°00′
(3)	Kreta	35°00′	25°00′
(4)	Maspalomas	27°20′	-15°00′
(5)	Kourou	05°05′	-52°23′
(6)	Libreville	00°23′	09°27′
(7)	Hartebeesthoek	-25°30′	25°00′
(8)	Perth	-31°33′	115°30′

The distribution of the tracking stations and ground tracks of IGSO, GEO and MEO satellites for a possible GNSS-2/Galileo constellation are shown in Figure 9-2, Figure 9-3 and Figure 9-4 respectively. The longitude of subpoints of IGSO and GEO satellites are located at  $\lambda = -10^\circ, 20^\circ$  and  $60^\circ$  respectively.

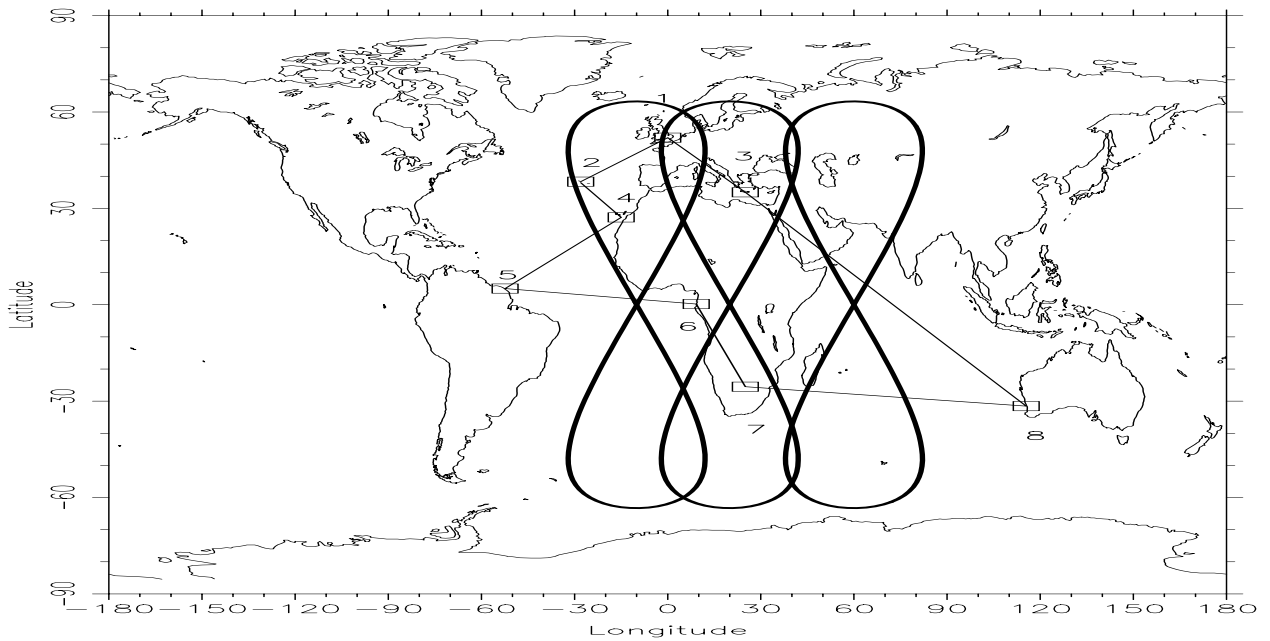


Figure 9-2 Distribution of Assumed Tracking Stations and IGSO Satellite Ground Tracks of GNSS2

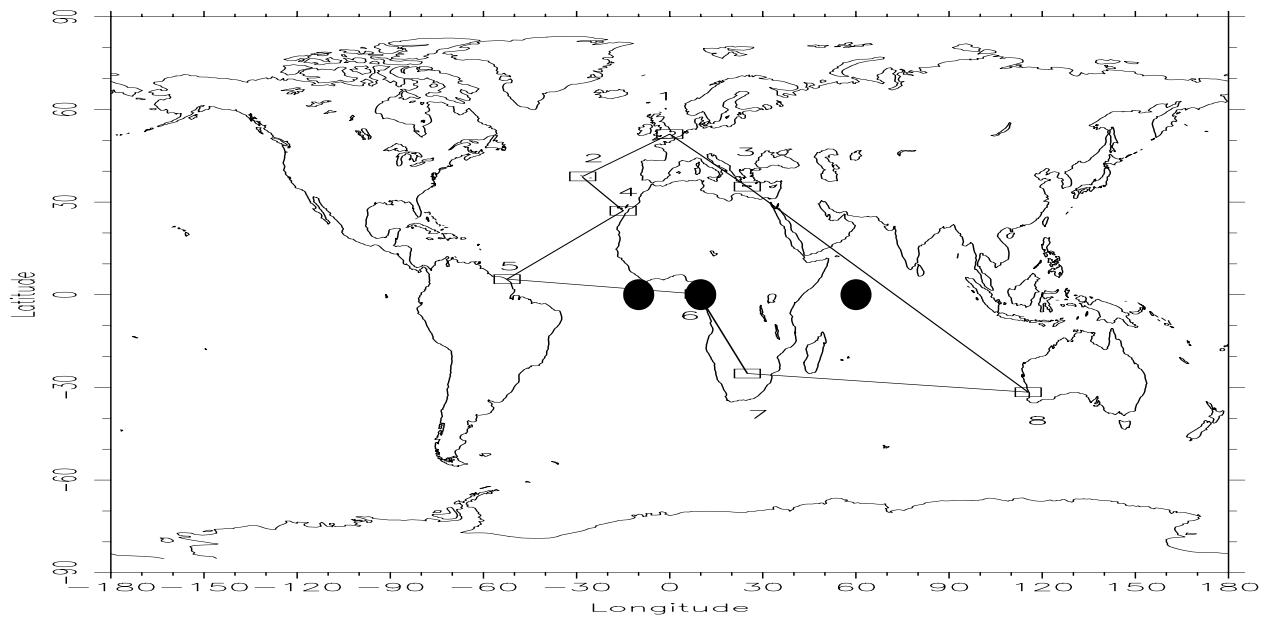


Figure 9-3 Distribution of Assumed Tracking Stations and GEO Satellite Ground Tracks of GNSS2

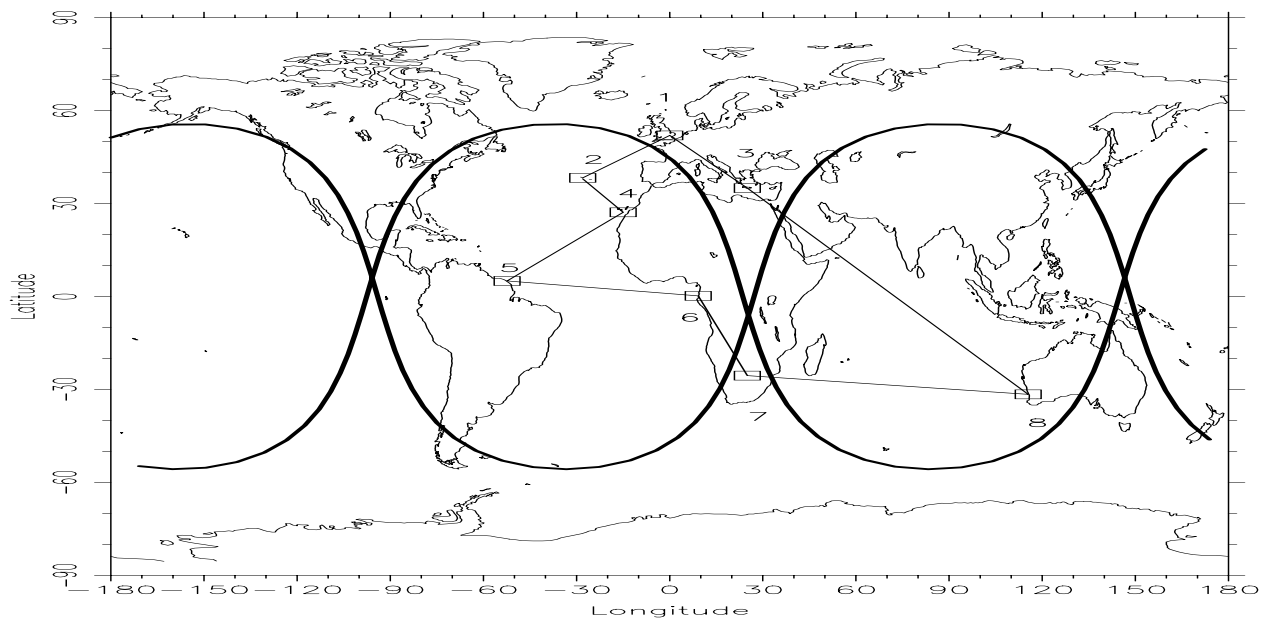


Figure 9-4 Distribution of Assumed Tracking Stations and MEO Satellite Ground Tracks of GNSS2

### 9.1.3 Satellite Visibility

The satellite visibility means the satellite will be seen when the satellite passes over the tracking station. The visibility can be measured with the elevation of the satellite related to the local coordinate system of the tracking station.

The satellite visibilities of IGSO and GEO satellites located at  $\lambda = -10^\circ, 20^\circ$  and  $60^\circ$  for the assumed tracking stations are drawn as follows.

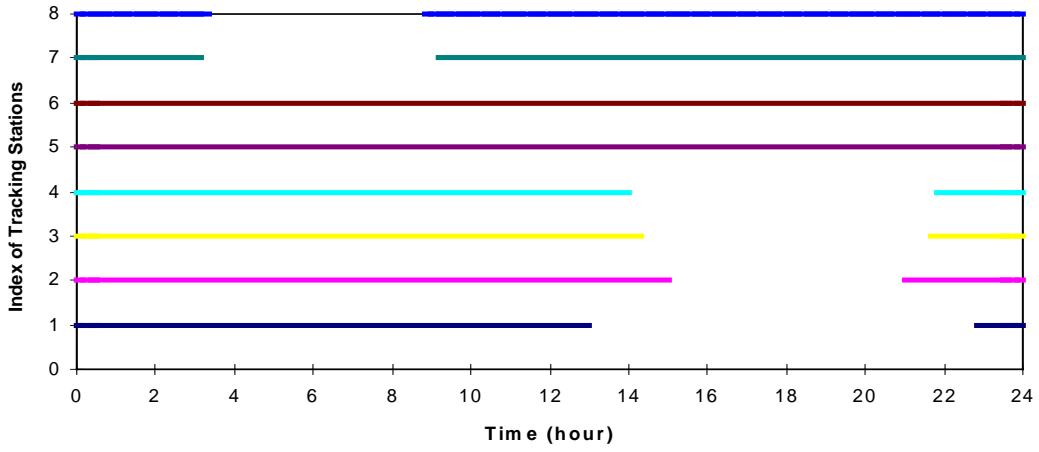


Figure 9-5 Visibility of an IGSO Satellite at  $\lambda = -10^\circ$

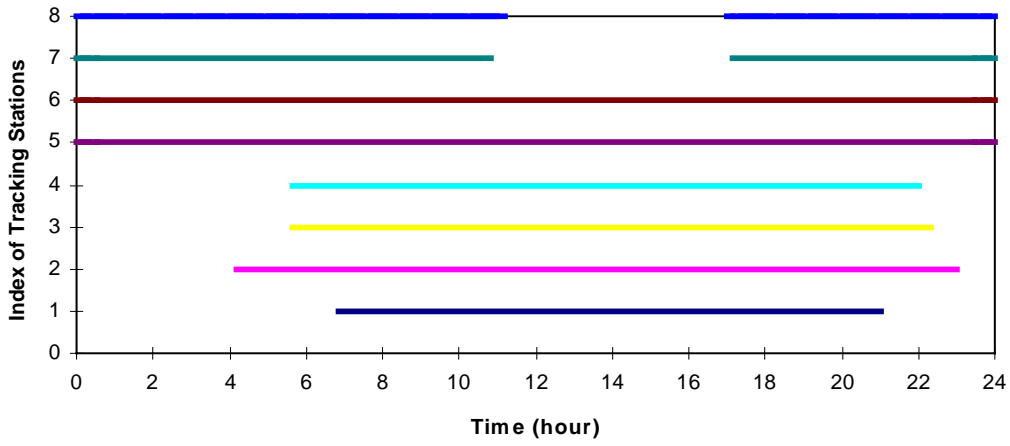


Figure 9-6 Visibility of an IGSO Satellite at  $\lambda = 20^\circ$

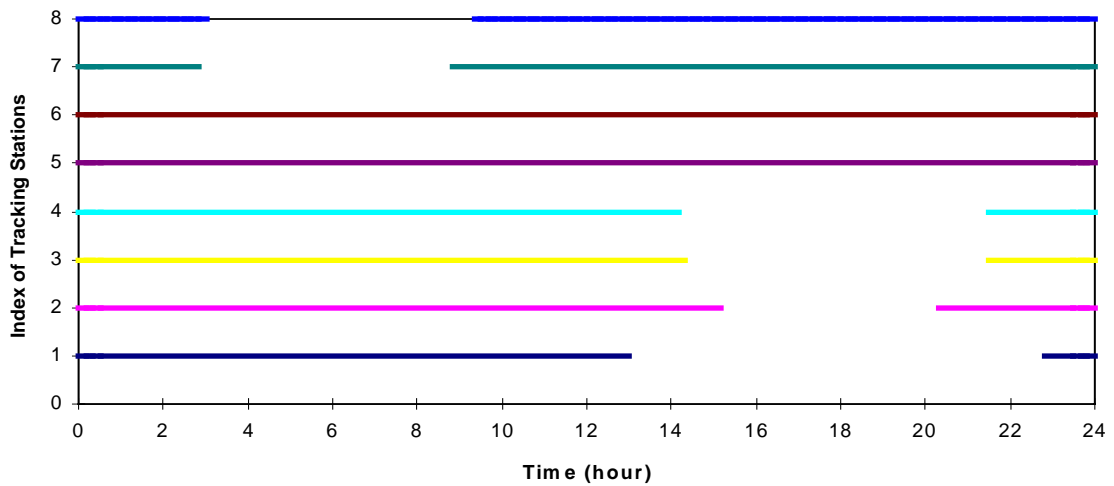
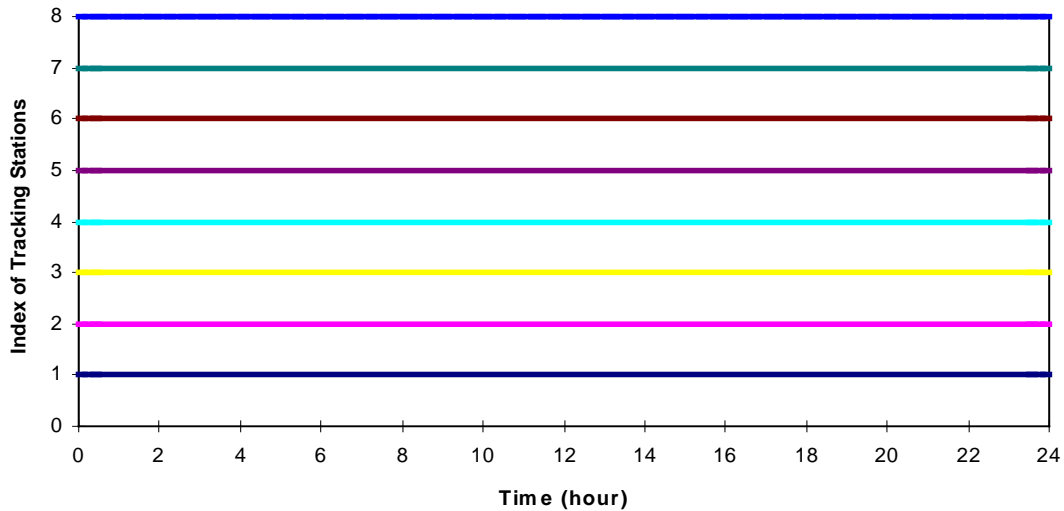


Figure 9-7 Visibility of an IGSO Satellite at  $\lambda = 60^\circ$

Figure 9-8 Visibility of a GEO Satellite at  $\lambda=20^\circ$ 

## 9.2 The Simulation Results of Dynamic Orbit Determination using Code Range Observations

Figure 9-9 shows the results of dynamic orbit determination using the algorithms, the tracking stations and software GEOKAL as discussed in former chapters and above.

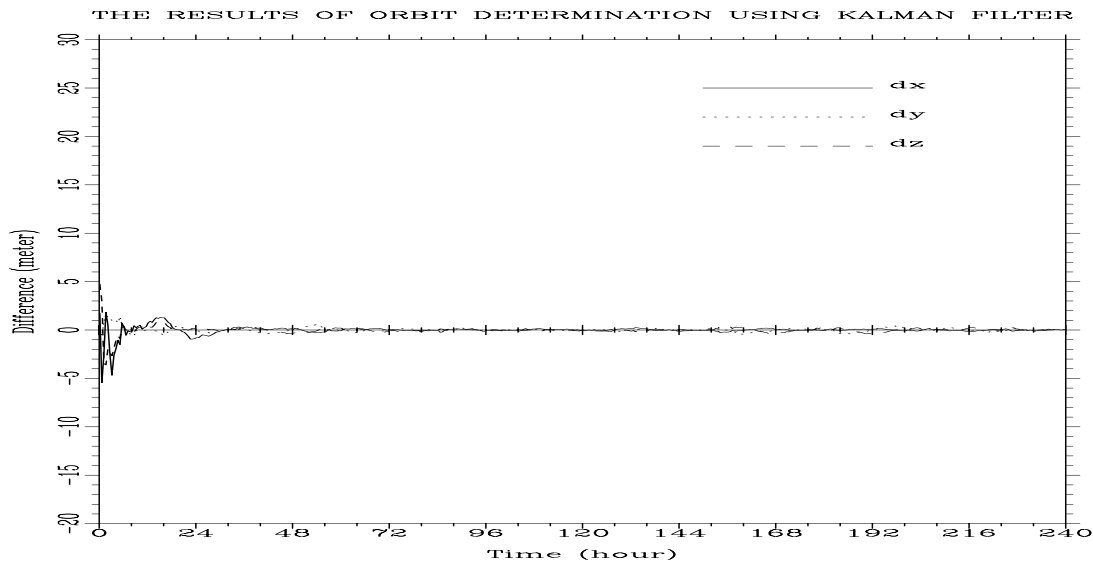


Figure 9-9 The accuracy of orbit determination using Kalman filter and 8 tracking stations

In Figure 9-9, about 10 days arc length of theoretical orbit has been produced. The satellite positions and velocities of theoretical orbit in the first epoch are chosen as initial orbit parameters for orbit determination. The initial orbit parameters are intentionally added with  $\pm 200$  meter errors in the position and  $\pm 0.1$  m/s errors in the velocity. Figure 9-9 shows the accuracy of orbit determination using Kalman filter for about 10 days arc length. The horizontal axis in the figure is time and the vertical axis is the difference between the theoretical orbit and the orbit determined by Kalman filter. From Figure 9-9 it can be seen that using Kalman filter discussed in the chapters 6 and 8, tracking stations presented in §9.1.2, the accuracies of  $x$ ,  $y$  and  $z$  coordinates of the satellite orbit determination are about  $\pm 0.24$ ,  $\pm 0.17$ ,  $\pm 0.18$  m respectively. In the results above, the satellite visibility is not considered in the orbit determination software GEOKAL. Under this situation it is assumed that the satellites

are always tracked at the ground tracking stations. Under this situation it can show the highest accuracy of dynamic orbit determination which can be achieved using Kalman filter. As a comparison, the results of the accuracy of dynamic orbit determination with the satellite visibility controlling (elevation mask=5°, 10° and 15°) are presented in the following figures.

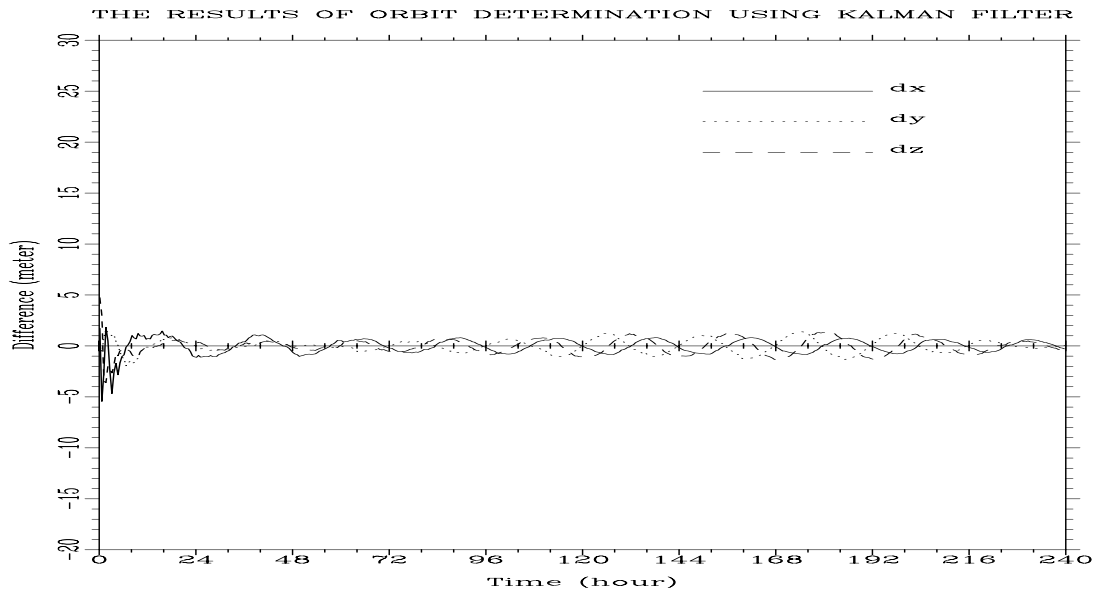


Figure 9-10 The Accuracy of Orbit Determination with Elevation Mask 5°

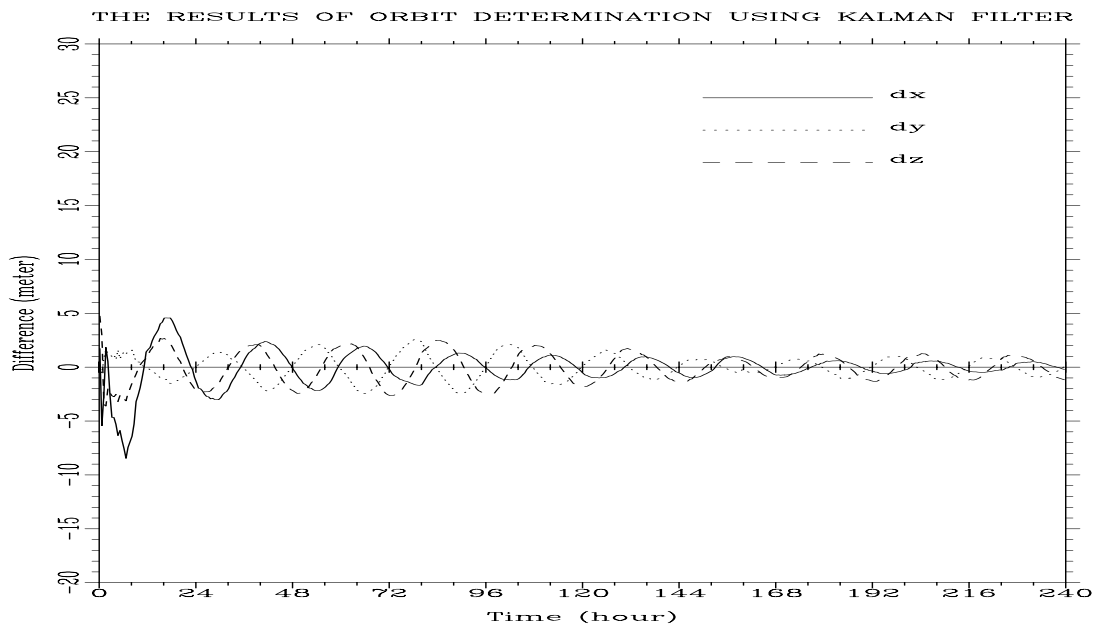


Figure 9-11 The Accuracy of Orbit Determination with Elevation Mask 10°

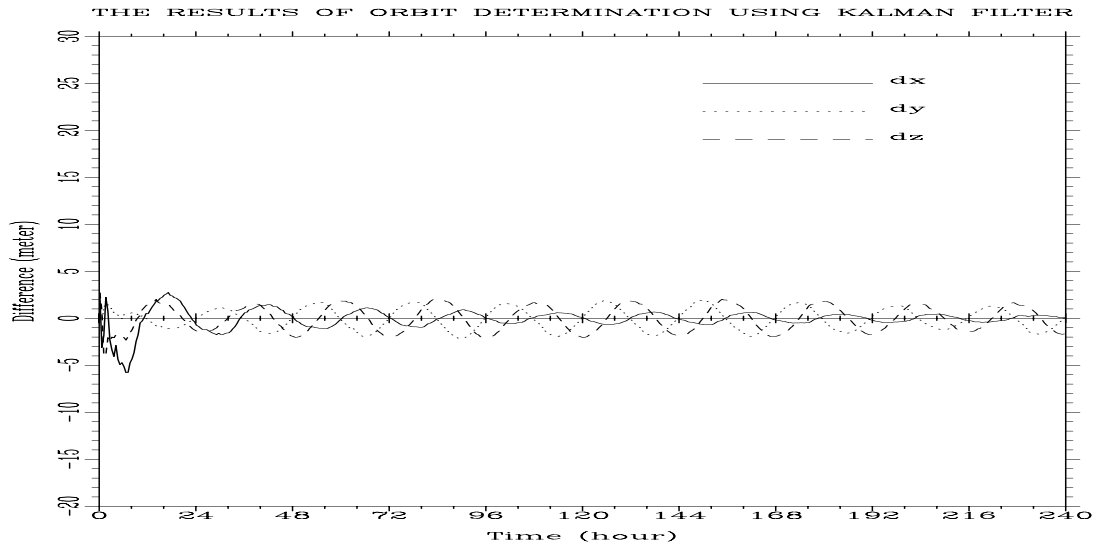


Figure 9-12 The Accuracy of Orbit Determination with Elevation Mask  $15^\circ$

The accuracies of  $x$ ,  $y$ ,  $z$  coordinates of the dynamic orbit determination with the satellite visibility control (elevation mask= $5^\circ$ ) are  $\pm 0.59$ ,  $\pm 0.63$ ,  $\pm 0.66$  meters respectively. For elevation mask= $10^\circ$ , the accuracies of dynamic orbit determination are  $\pm 1.41$ ,  $\pm 1.10$ ,  $\pm 1.35$  meters respectively. For elevation mask  $15^\circ$ , the accuracies of dynamic orbit determination are  $\pm 0.92$ ,  $\pm 1.19$ ,  $\pm 1.32$  meters respectively (see Figure 9-10, Figure 9-11 and Figure 9-12). Obviously, due to the satellite visibility, the number of the tracking stations which take the measurements of the satellite is decreased during some arcs of the satellite and the accuracy of the orbit determination is reduced. The related PDOP of the orbit determination using these 8 ground tracking stations is shown in Figure 9-13.

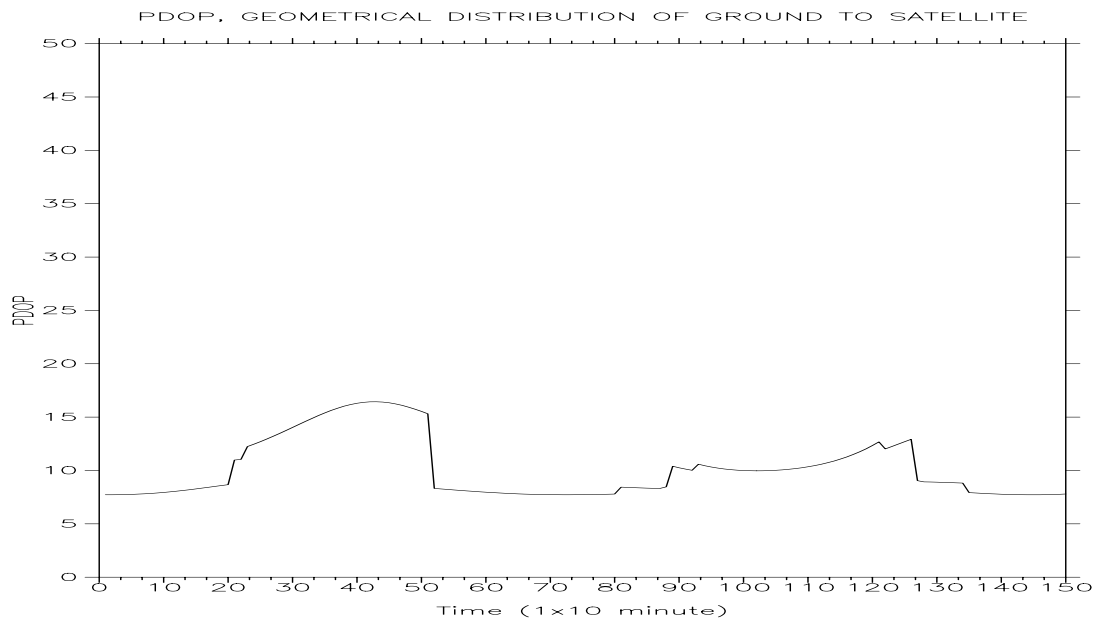


Figure 9-13 PDOP of the Orbit Determination with 8 Tracking Station Distribution (Elevation Mask  $10^\circ$ )

The results of orbit determination of an IGSO satellite located at  $\lambda=60^\circ$ ,  $-10^\circ$  are drawn in Figure 9-14 to Figure 9-17 (elevation mask  $10^\circ$ ).

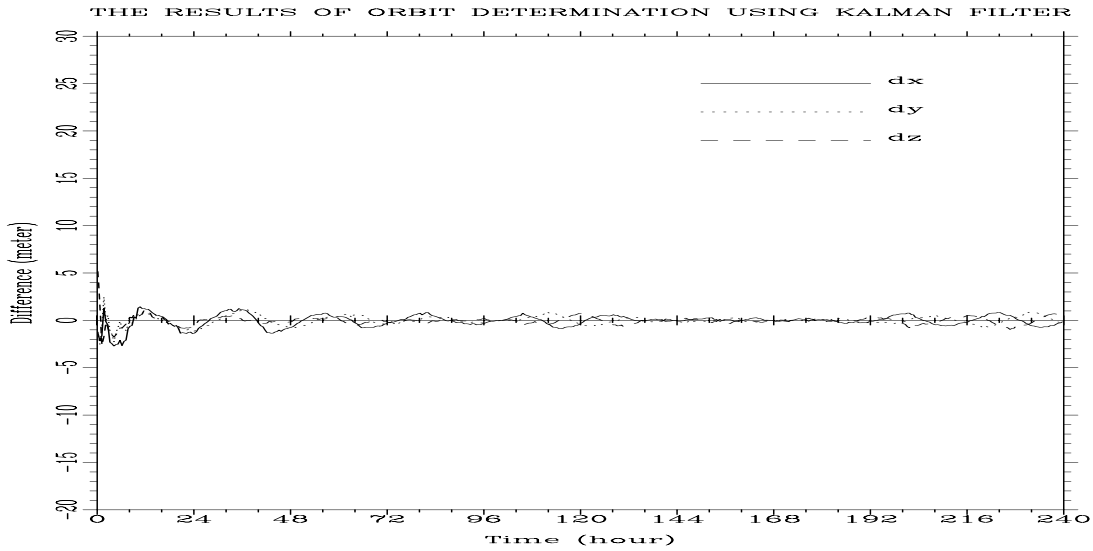


Figure 9-14 The Accuracy of the Orbit Determination of an IGSO Satellite Located at  $\lambda=60^\circ$

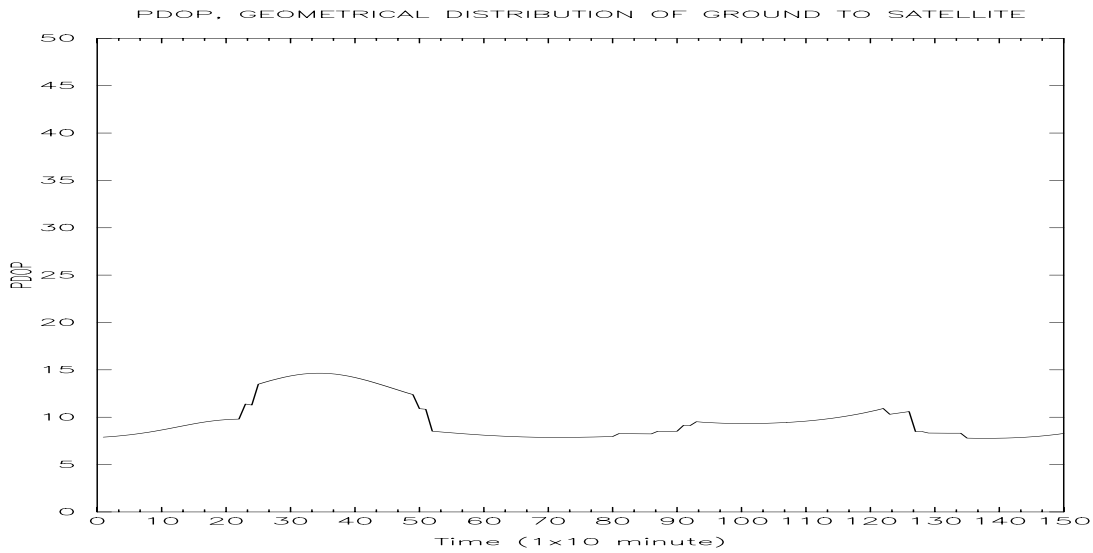


Figure 9-15 PDOP of the Orbit Determination of an IGSO Satellite Located at  $\lambda=60^\circ$

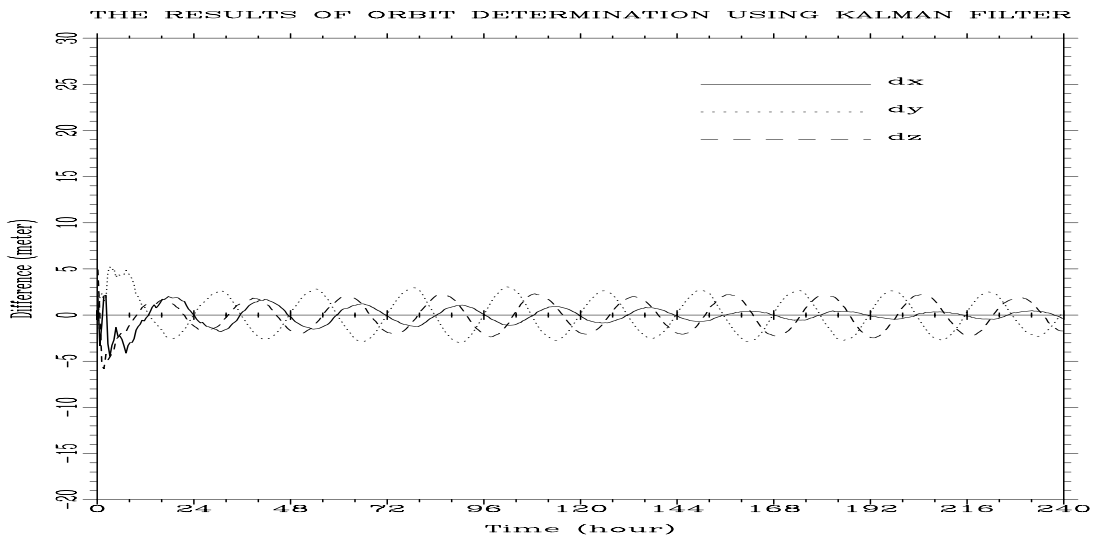


Figure 9-16 The Accuracy of Orbit Determination of an IGSO Satellite Located at  $\lambda=-10^\circ$



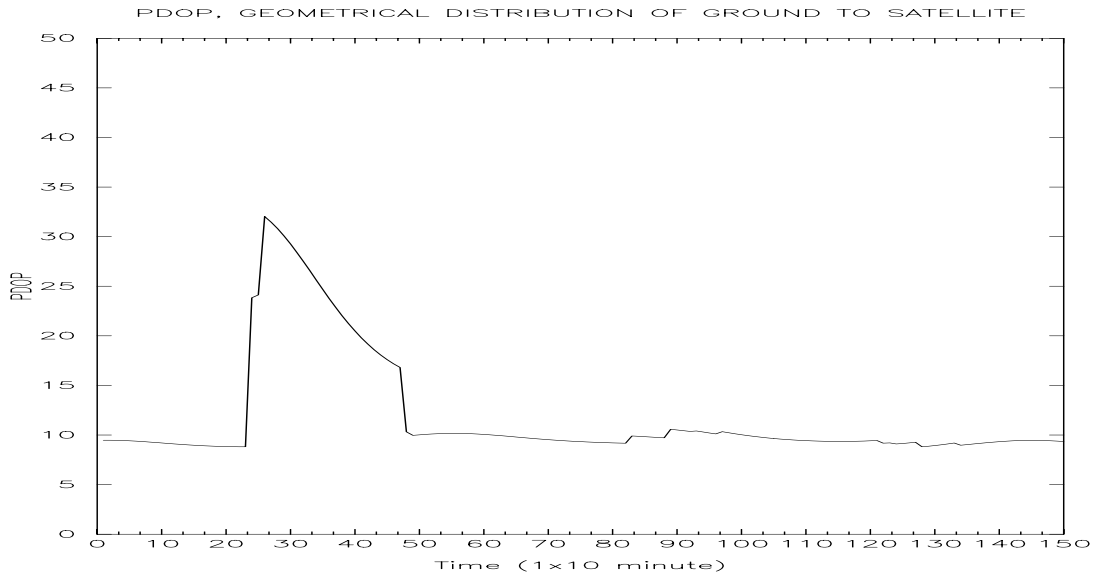


Figure 9-17 PDOP of the Orbit Determination of an IGSO Satellite Located at  $\lambda = -10^\circ$

The accuracies of  $x, y, z$  coordinates of dynamic orbit determination of an IGSO satellite located at  $\lambda = 60^\circ$  are  $\pm 0.54, \pm 0.41$  and  $\pm 0.33$  meters respectively. The accuracies of an IGSO satellite located at  $\lambda = -10^\circ$  are  $\pm 0.78, \pm 1.84$  and  $\pm 1.42$  meters respectively.

The figures above show the possible accuracy of dynamic orbit determination of IGSO satellites using 8 ESA ground tracking stations. Using Kalman filter and range observations with one meter error, 1 m accuracy of dynamic orbit determination of IGSO satellites can be achieved. If other conditions are the same as above, considering unmodeled errors in the satellite dynamic models, propagation and some unknown errors, the accuracy of IGSO satellite better than  $\pm 3$  meters can be achieved without difficulty.

The accuracies of GEO satellites are shown in Figure 9-18 to Figure 9-20

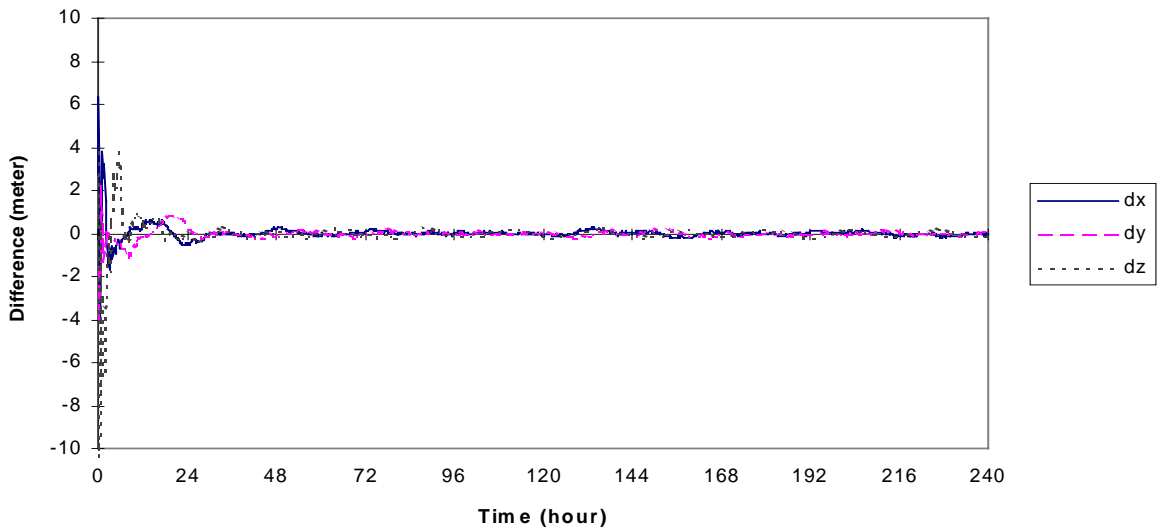


Figure 9-18 Accuracy of Orbit Determination of a GEO Satellite Located at  $\lambda = -10^\circ$

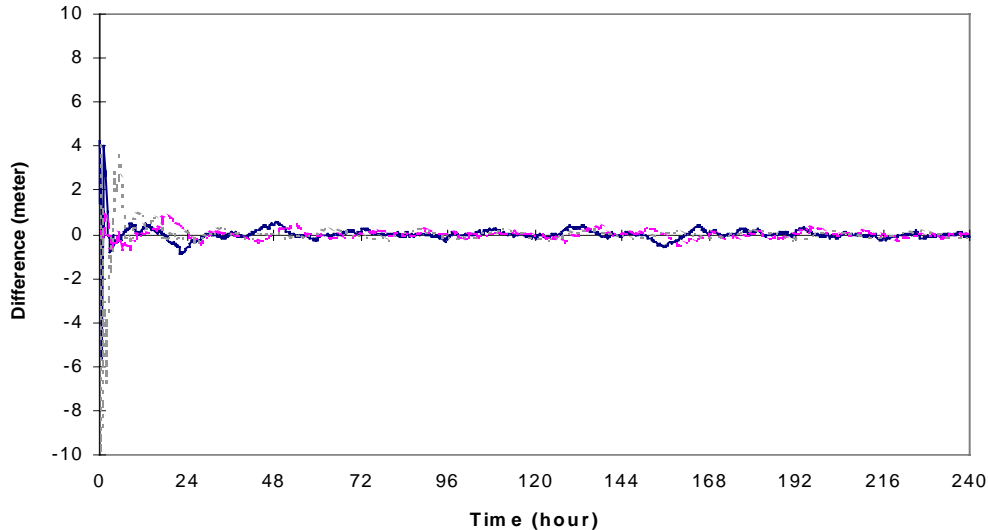


Figure 9-19 Accuracy of Orbit Determination of a GEO Satellite Located at  $\lambda=20^\circ$

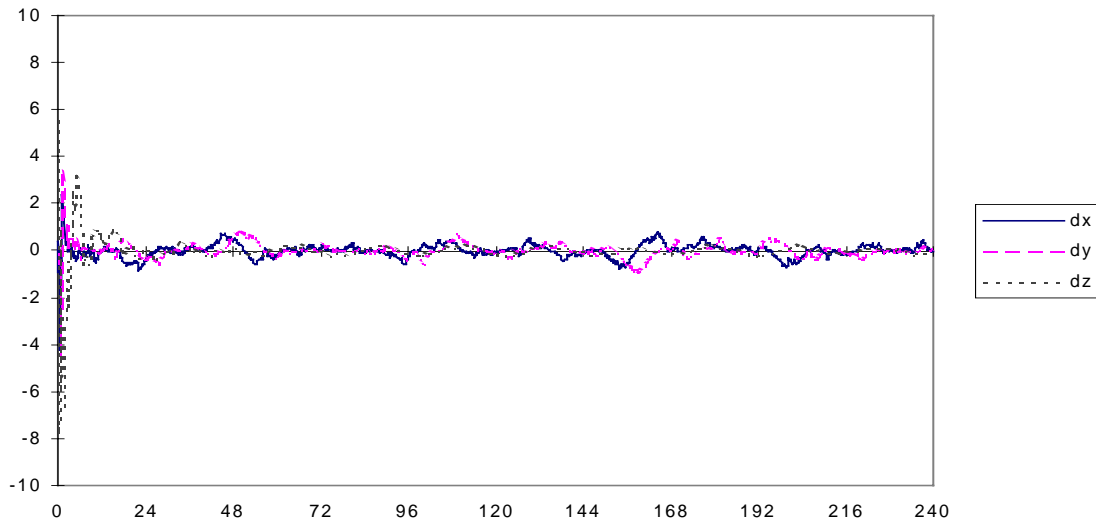


Figure 9-20 Accuracy of Orbit Determination of a GEO Satellite Located at  $\lambda=60^\circ$

The accuracy of  $x$ ,  $y$ ,  $z$  coordinates of dynamic orbit determination of a GEO satellite located at  $\lambda=-10^\circ$  are  $\pm 0.09$ ,  $\pm 0.09$  and  $\pm 0.13$  meters respectively. The accuracy of a GEO satellite located at  $\lambda=20^\circ$  are  $\pm 0.15$ ,  $\pm 0.16$  and  $\pm 0.13$  meters respectively. The accuracy of a GEO satellite located at  $\lambda=60^\circ$  are  $\pm 0.24$ ,  $\pm 0.25$  and  $\pm 0.14$  meters respectively.

Also considering the unmodeling errors in the satellite dynamic models, the propagation and some unknown errors, 1-10 m accuracy-level of dynamic orbit determination of GEO satellites can be achieved using range observations with 1 m errors.

Obviously, the accuracy of dynamic orbit determination of GEO satellites is better than that of IGSO satellites. This is related to satellite visibility, refer to Figure 9-5 to Figure 9-8.

### 9.3 Simulation Results using Carrier Observations

In order to carry out the simulation of dynamic orbit determination of IGSO and GEO satellite using carrier phase observation, a theoretical error-free orbit is produced using a numerical integration method. Four major

perturbation effects on the satellite orbit such as geopotential attraction ( $n, m \leq 10$ ), solar and lunar attraction and solar radiation pressure are included in the satellite dynamic model. The observation is a one-way carrier phase that is generated from the integrated theoretical orbit and the known coordinates of tracking stations described in §9.1.2. The white noise with  $\sigma = \pm 1 \text{ cm}$  are added to carrier phase observation. The elevation cut-off angle of observation is  $15^\circ$ . The sample rate is 10 minutes.

When observations are discontinuous due to the elevation mask limitation, new ambiguities of carrier phase observations will be added and solved during the orbit determination process. In the satellite dynamical models of orbit determination, the perturbation effects included are the same as those used for the theoretical error-free orbit integration, but there is a difference, for example, the degree and order of geopoturbation used in orbit determination are less than those used to determine the theoretical orbit. The accuracy of orbit determination is obtained using differences between the results of orbit determination and the theoretical error-free integration orbit.

### 9.3.1 Orbit Determination with Float Ambiguity Solution

#### 9.3.1.1 The Accuracy of Orbit Determination without Satellite Visibility Considered

The distribution of tracking stations used for orbit determination using carrier observations are drawn in Figure 9-2. In the following simulation results, the carrier phase observations are assumed to be continuous. The satellite visibility problem and cycle slips are not considered. All observations have to be set with true initial ambiguities according to their tracking stations as listed in Table 9-2.

Table 9-2 TRUE INITIAL AMBIGUITY SET FOR TRACKING STATIONS

Tracking Station	True Initial Ambiguity Set(Cycles)
Herstmonceux	20
Azoren	40
Kreta	60
Maspalomas	80
Kourou	100
Libreville	120
Hartebeesthoek	140
Perth	160

Float ambiguity solutions of IGSO satellite located at  $\lambda = -10^\circ$  are shown in Figure 9-21 to Figure 9-28.

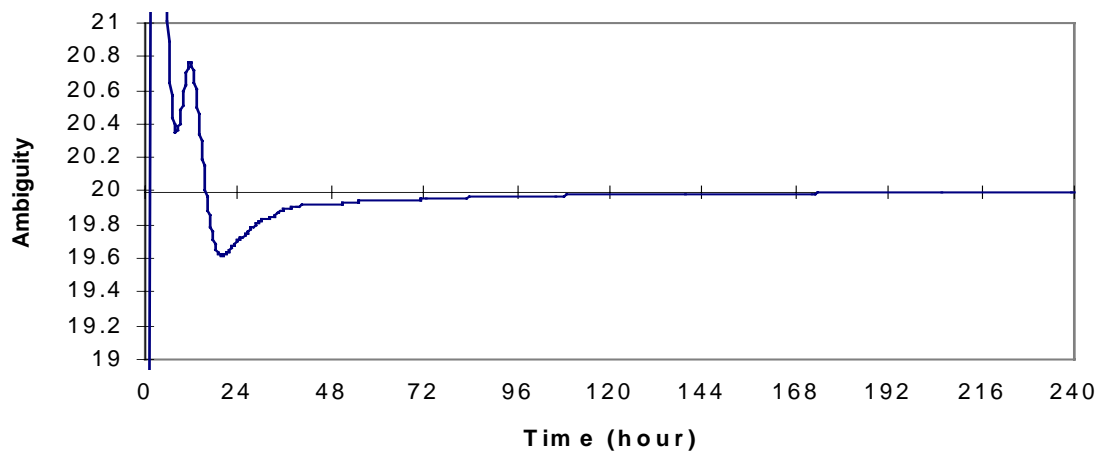


Figure 9-21 Float Ambiguity Solution of Tracking Station 1

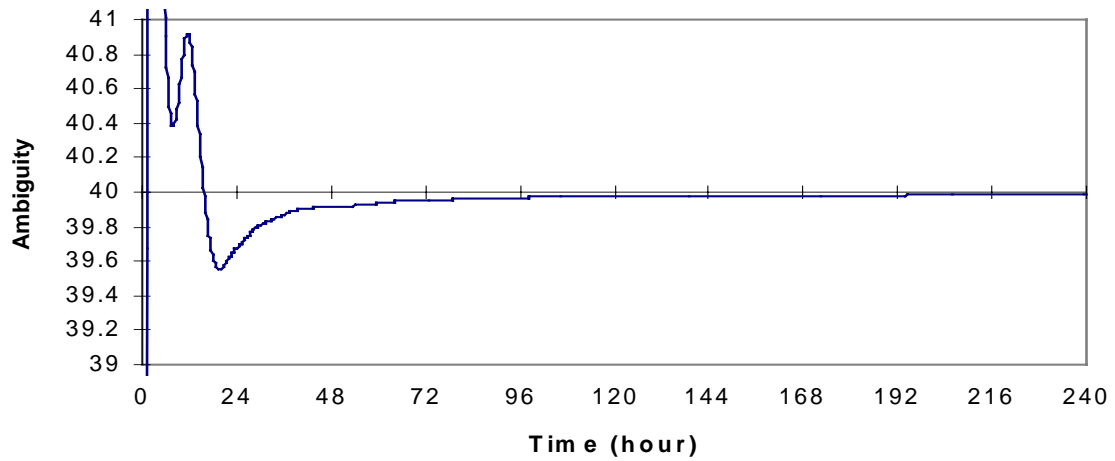


Figure 9-22 Float Ambiguity Solution of Tracking Station 2

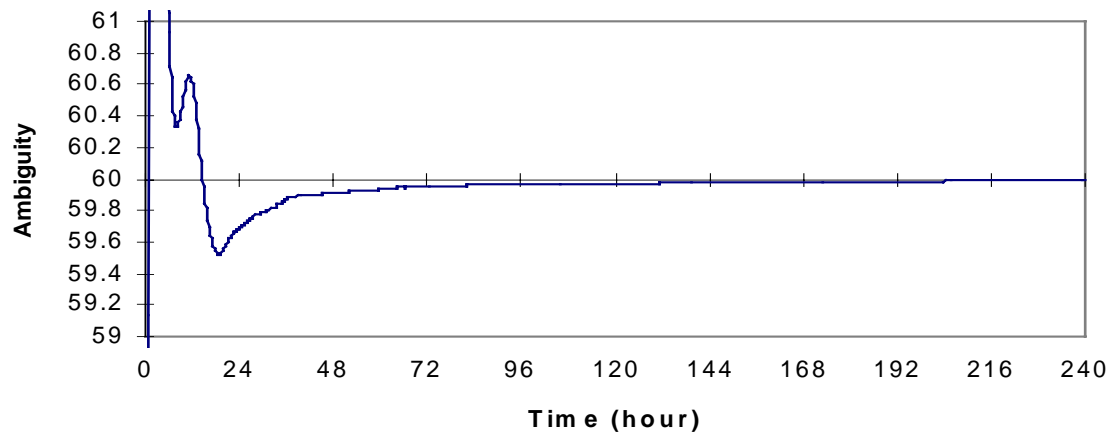


Figure 9-23 Float Ambiguity Solution of Tracking Station 3

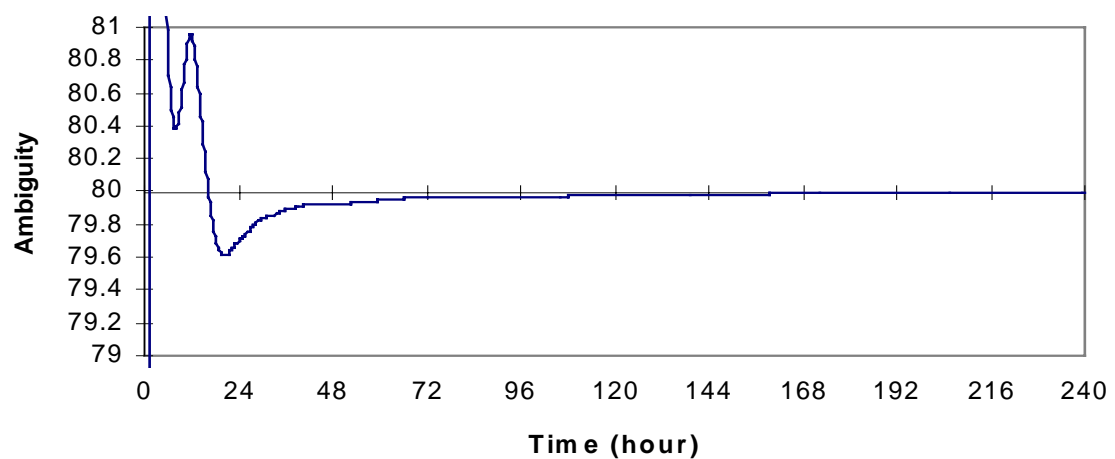


Figure 9-24 Float Ambiguity Solution of Tracking Station 4

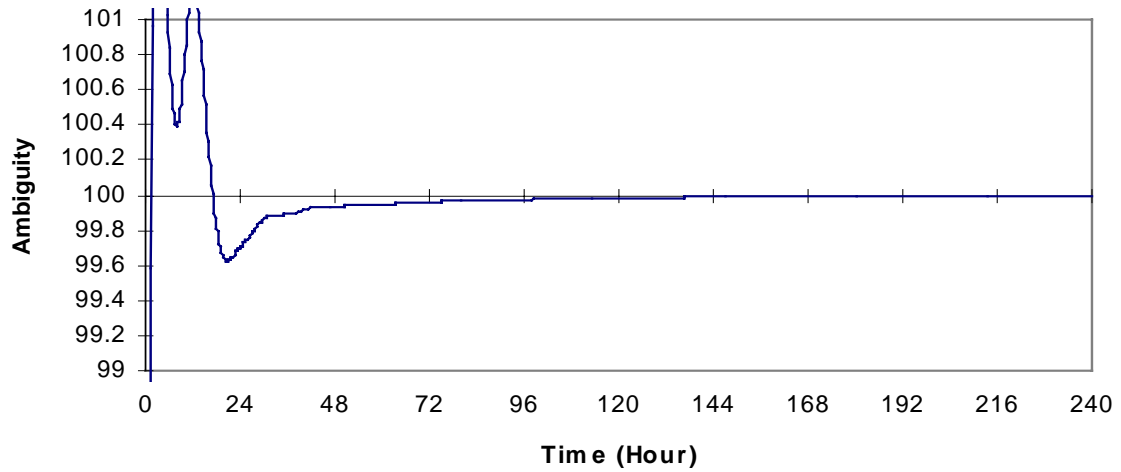


Figure 9-25 Float Ambiguity Solution of Tracking Station 5

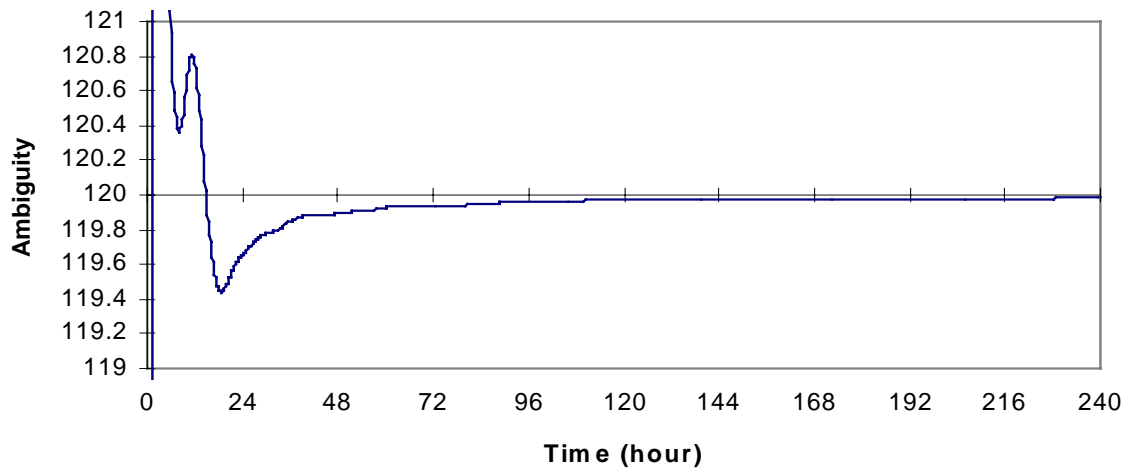


Figure 9-26 Float Ambiguity Solution of Tracking Station 6

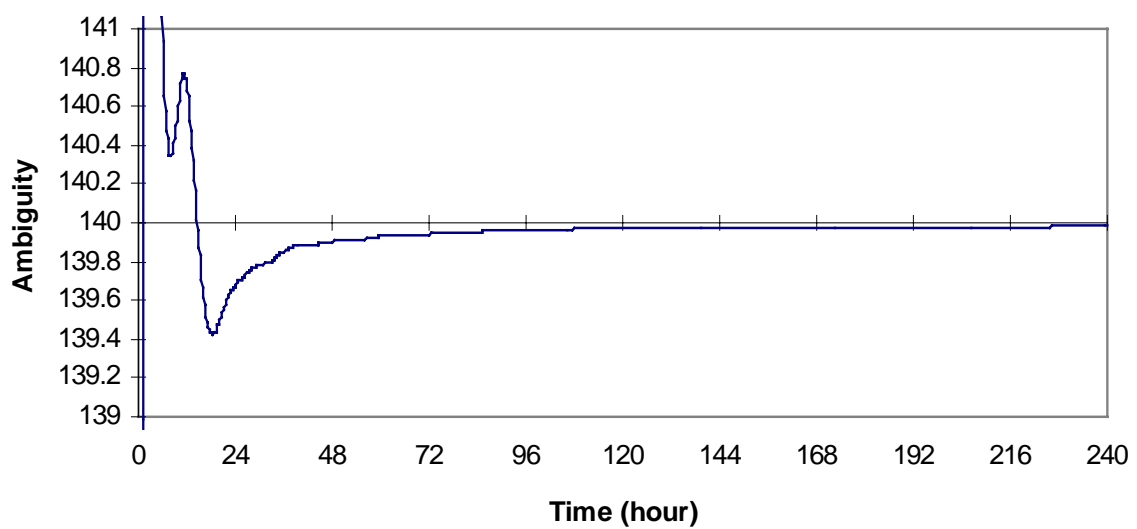


Figure 9-27 Float Ambiguity Solution of Tracking Station 7

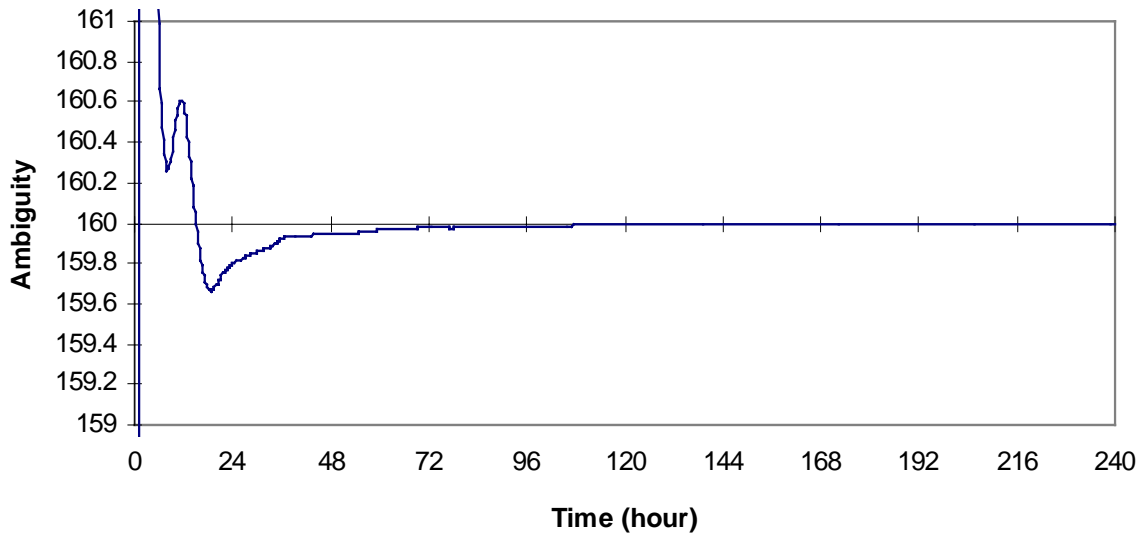


Figure 9-28 Float Ambiguity Solution of Tracking Station 8

In Figure 9-21 to Figure 9-28 most of the initial integer ambiguities have been solved as float solutions for one day and since then have had no great changes in the continuous processing.

The corresponding results of orbit determination of IGSO satellite located at  $\lambda = -10^\circ$  with float ambiguity solutions are drawn in Figure 9-29.

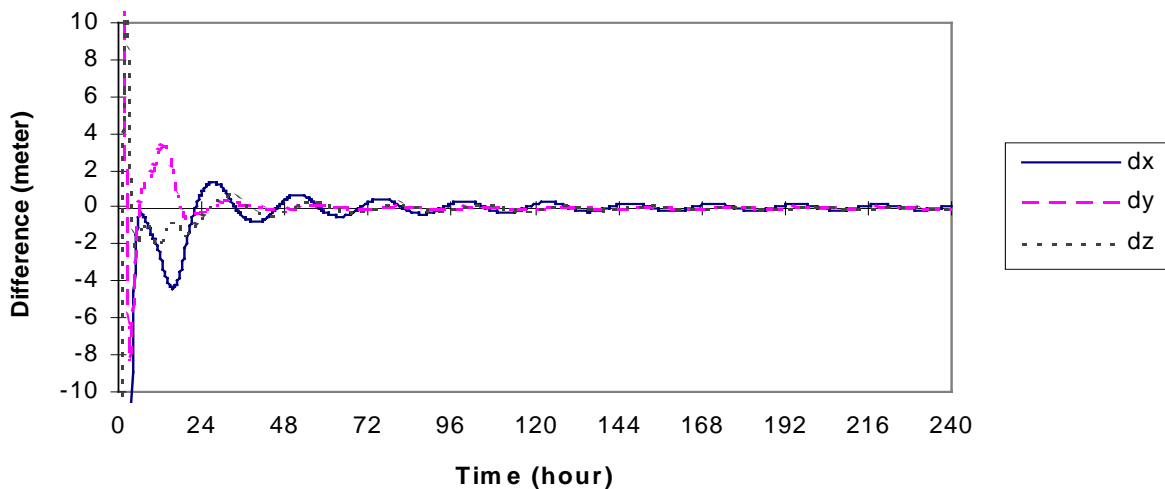


Figure 9-29 Accuracy of Dynamic Orbit Determination with Float Ambiguity Solution

The accuracies of  $x$ ,  $y$ ,  $z$  coordinates of orbit determination with float ambiguity solutions are  $\pm 0.23\text{ m}$ ,  $\pm 0.06\text{ m}$  and  $\pm 0.12\text{ m}$  respectively. In Figure 9-29 the accuracy of dynamic orbit determination has been significantly improved after the initial ambiguities are nearest integers (still as float solution), but not rounding to the nearest integers.

### 9.3.1.2 The Accuracy of Orbit Determination Considering Satellite Visibility

The accuracy presented above is the ideal accuracy of dynamic orbit determination of an IGSO satellite using carrier phase, because in the results above the satellite visibility problem at the tracking stations are not considered, therefore the observations to satellites are continuous for ten days, which is impossible in a practical

situation. In this section, the satellite visibility will be considered in the dynamic orbit determination. The satellite visibility, however, is a big problem for resolving initial ambiguity. The visibility of a IGSO satellite located at  $\lambda = -10^\circ$  with eight tracking stations has been shown in Figure 9-5.

From Figure 9-5 it can be seen that except the tracking stations Kourou (5) and Libreville (6), which are located near the equator, the observations of carrier phase from other tracking stations and IGSO satellites are discontinuous due to satellite visibility. After re-tracking the satellite at the tracking stations, the new initial ambiguities must be introduced in the observations. For example, from Figure 9-5, for tracking station 7 and 8, the first session of continuous observation is only about three hours. It is not enough time for this three-hour observation session to resolve all initial ambiguities due to the high altitude of the IGSO satellite (refer to §7.2.1, Chapter 7). Then observations are interrupted because the satellite is not visible from these two tracking stations. After a six hour interruption, the satellite will be seen again and re-locked, the new initial ambiguities must be introduced and solved, which will affect the accuracy of satellite orbit determination (see Figure 9-30, Figure 9-31 and Figure 9-32). But, if the accuracy with centimeter level of orbit determination has been achieved before observation interruption, the satellite visibility will not be a problem, because the satellite orbit can be precisely predicted by satellite dynamic models. The new initial ambiguities can be computed according to precise satellite orbit and the coordinates of ground tracking stations.

For convenience in simulation, the true initial ambiguities will be set according to Table 9-2. When the satellites are re-tracked, the same true initial ambiguities will be set as before. This assumption will not affect the actual accuracy of orbit determination. It is only convenient for graphical illustration. In order to save text volume, in the following figures only the ambiguity solutions from the tracking stations 1 and 5 are given. The observation from the tracking station 1 was not continuous, whereas tracking station 5 was continuous. The initial ambiguities solved as float ambiguities are shown as follows respectively.

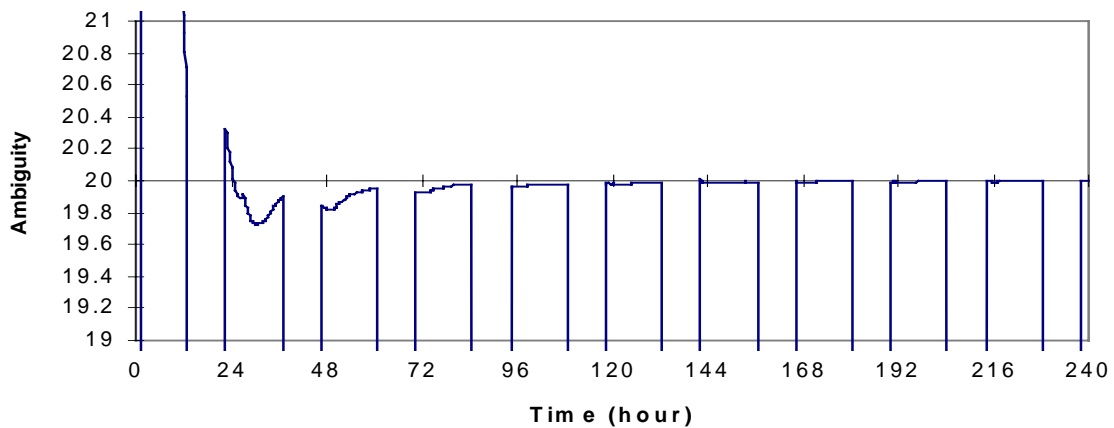


Figure 9-30 Float Ambiguity Solution of a IGSO Satellite at  $\lambda = -10^\circ$  at Tracking Station 1

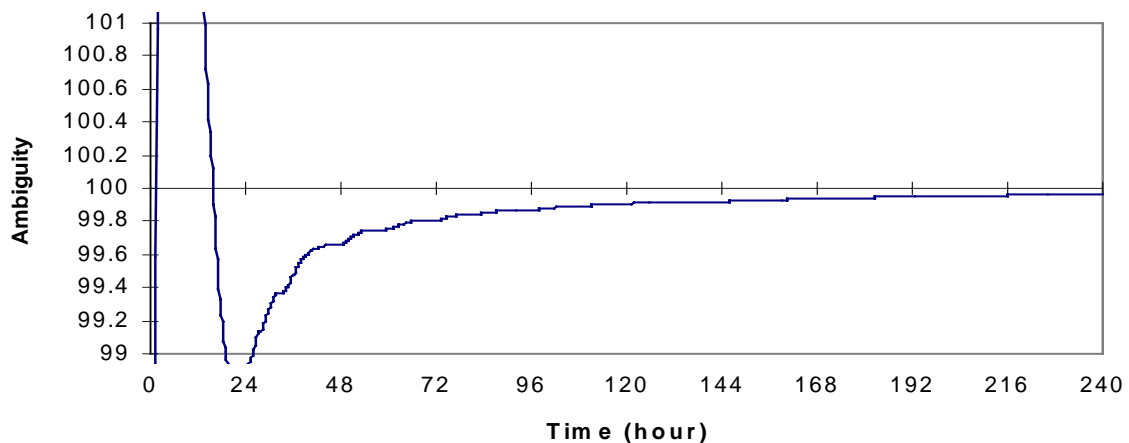


Figure 9-31 Float Ambiguity Solution of a IGSO Satellite at  $\lambda = -10^\circ$  at Tracking Station 5

Comparing Figure 9-21 and Figure 9-25 with Figure 9-30 and Figure 9-31, it can be found that the float ambiguity solution in Figure 9-30 (considering the satellite visibility) is not as good as that in Figure 9-27. When the tracking station loses the signal from the satellite, in the software GEOKAL, the initial ambiguity will be set to zero; when the signal is re-locked, the ambiguities are solved again. The same true ambiguities will be set before and after observation interruption. This is the reason why Figure 9-30 looks like a bar graph.

Figure 9-32 shows the accuracy of dynamic orbit determination of IGSO satellite at  $\lambda=-10^\circ$  using carrier phase observation considering the satellite visibility.

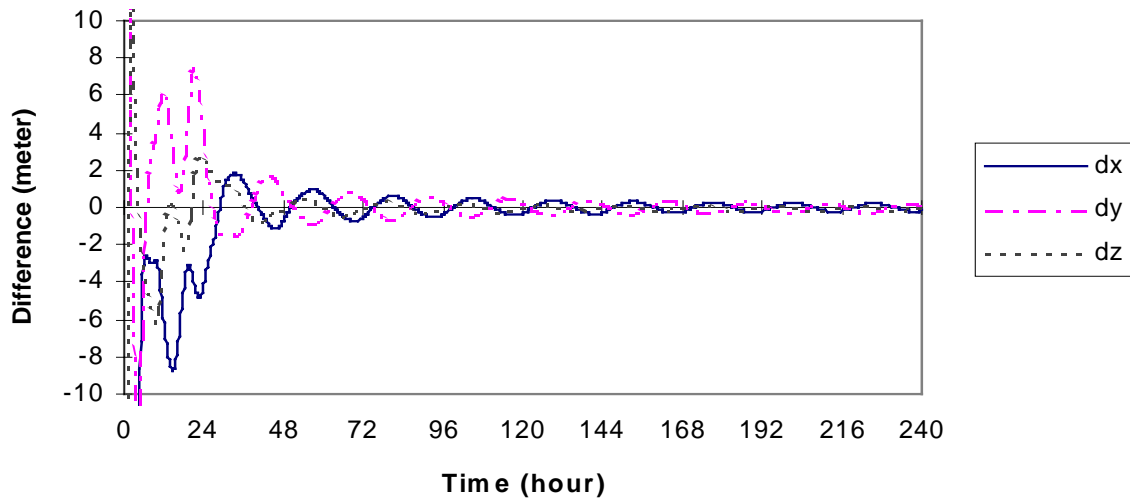


Figure 9-32 Accuracy of dynamic Orbit Determination of a IGSO Satellite at  $\lambda=-10^\circ$  with Float Ambiguity Solution

The accuracies of  $x$ ,  $y$ ,  $z$  coordinates of dynamic orbit determination with float ambiguity solution are  $\pm 0.32 m$ ,  $\pm 0.34 m$  and  $\pm 0.17 m$  respectively.

The results of other satellites are as follows.

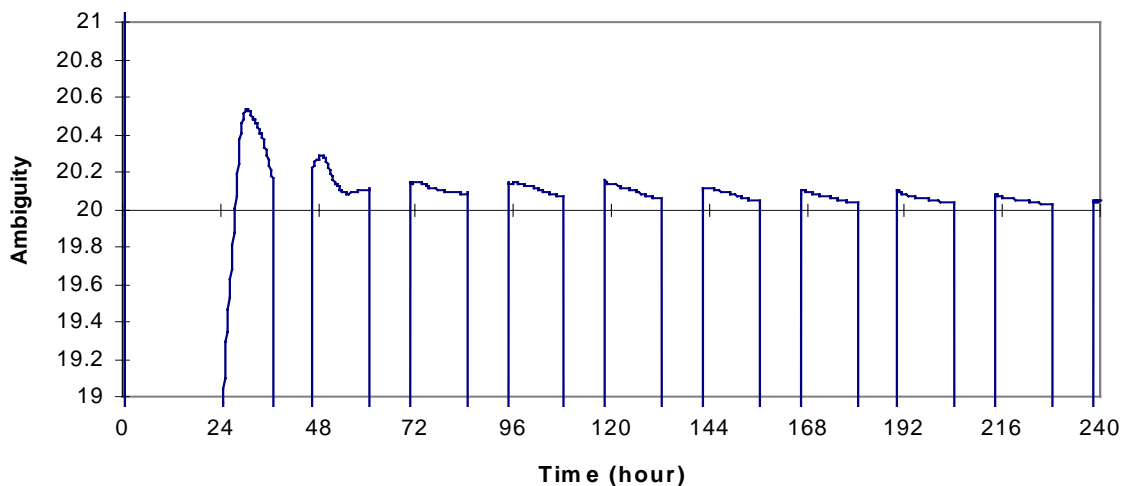


Figure 9-33 Float Ambiguity Solution of a IGSO Satellite at  $\lambda =20^\circ$  at Tracking Station 1



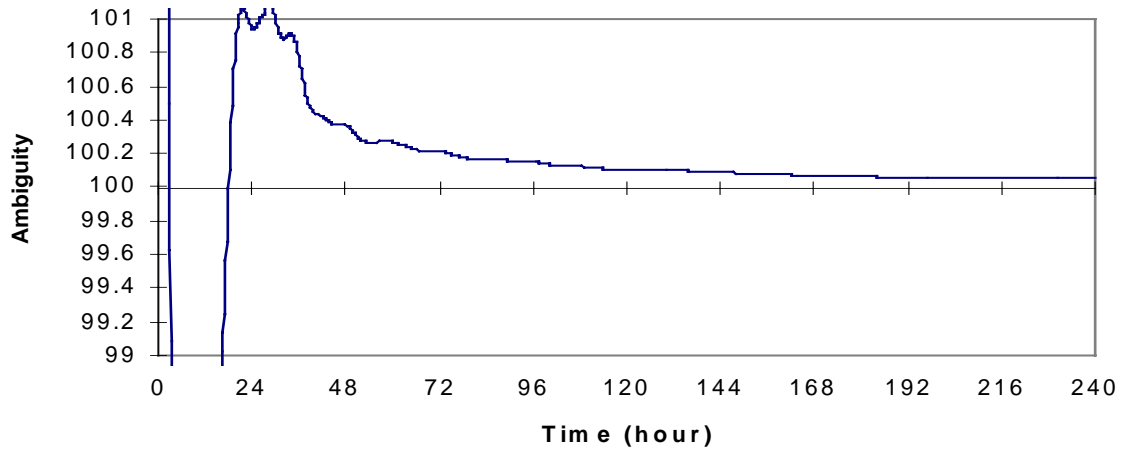


Figure 9-34 Float Ambiguity Solution of a IGSO Satellite at  $\lambda = 20^\circ$  at Tracking Station 5

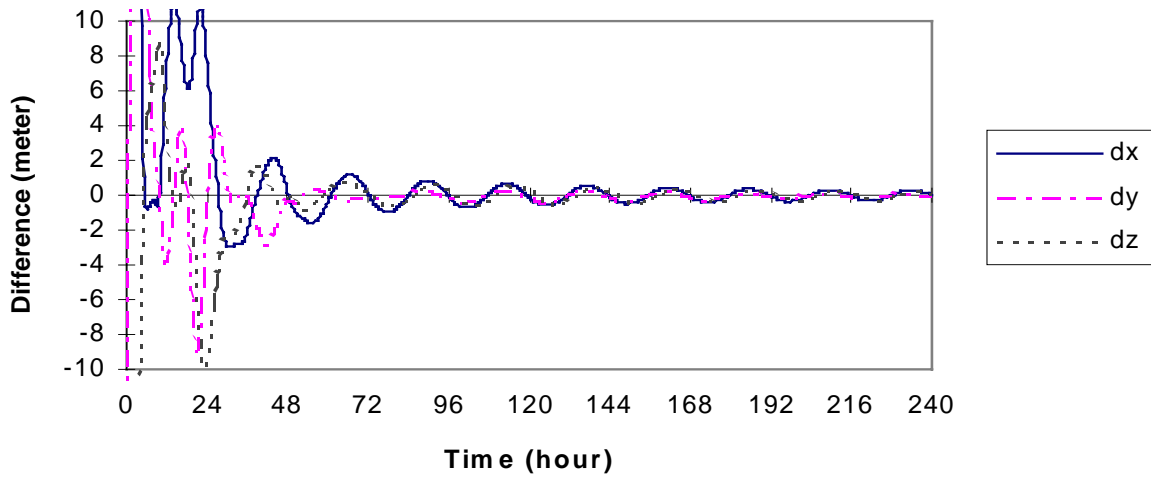


Figure 9-35 Accuracy of Dynamic Orbit Determination of a IGSO Satellite at  $\lambda = 20^\circ$  with Float Ambiguity Solution

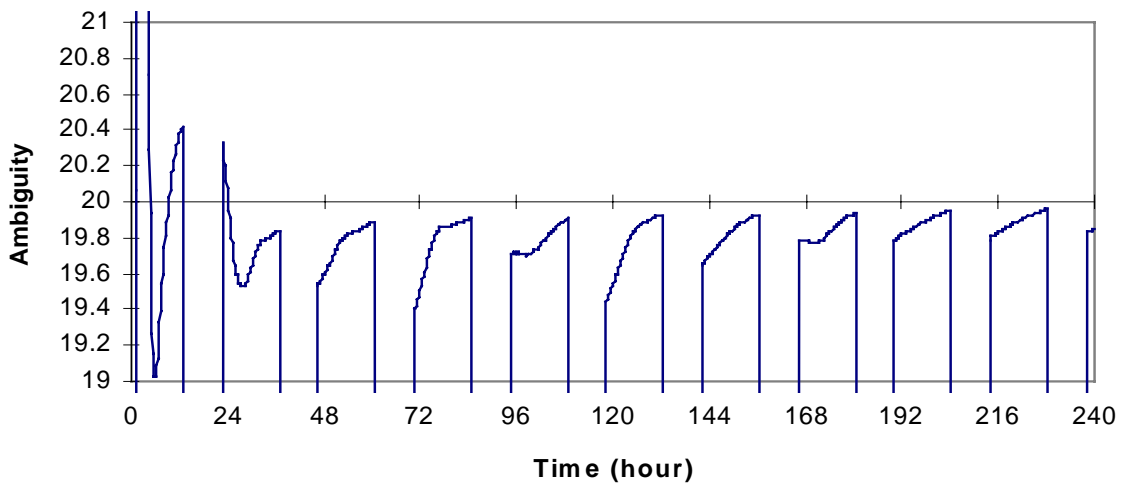


Figure 9-36 Float Ambiguity Solution of a IGSO Satellite at  $\lambda = 60^\circ$  at Tracking Station 1

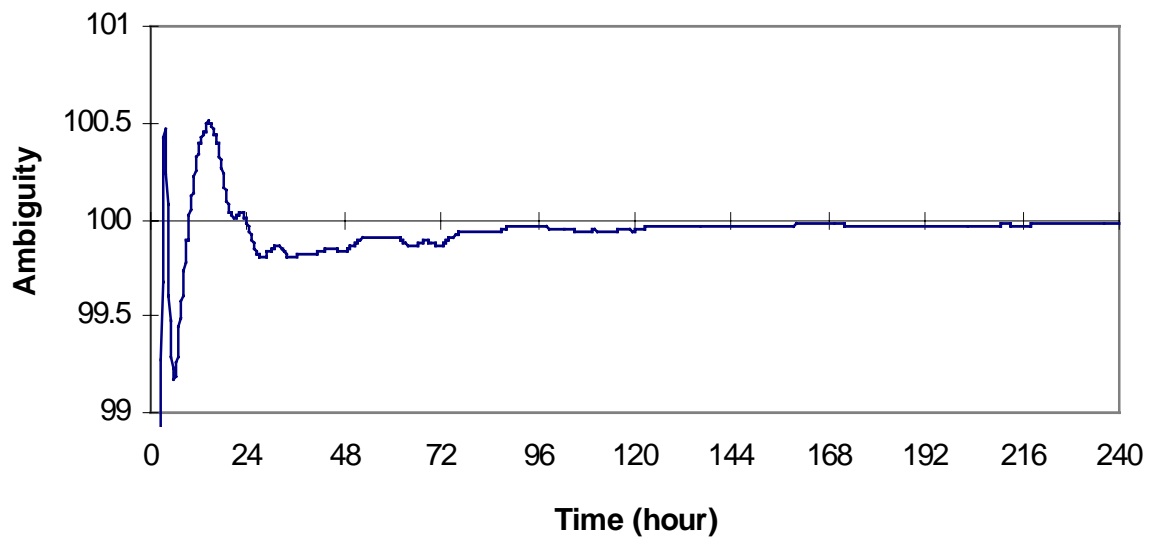


Figure 9-37 Float Ambiguity Solution of a IGSO Satellite at  $\lambda=60^\circ$  at Tracking Station 5

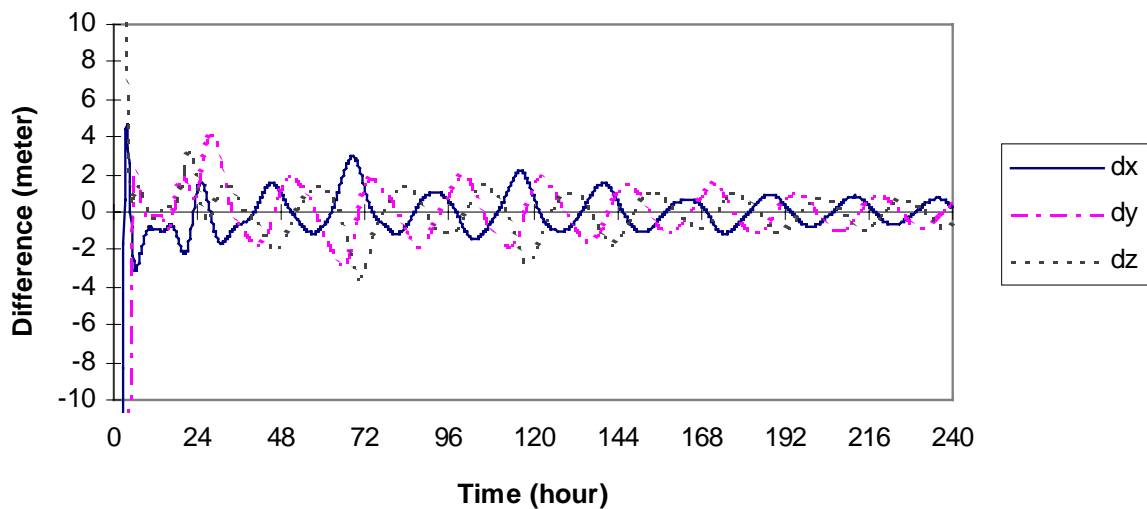


Figure 9-38 Accuracy of Dynamic Orbit Determination of a IGSO Satellite at  $\lambda=60^\circ$  with Float Ambiguity Solution

Considering the satellite visibility, the accuracies of  $x$ ,  $y$ ,  $z$  coordinates of orbit determination of an IGSO satellite located at  $\lambda = 20^\circ$  with float ambiguity solution are  $\pm 0.52 m$ ,  $\pm 0.18 m$  and  $\pm 0.34 m$  respectively. The accuracies of an IGSO satellite located at  $\lambda = 60^\circ$  with float ambiguity solution are  $\pm 0.91 m$ ,  $\pm 1.11 m$  and  $\pm 1.04 m$  respectively. The accuracies of these results are not better than that using range observations. One of the reason is that the convergence of the initial ambiguities estimated in Kalman filter to their true integer values is very slow, this is because the geometry changes between IGSO satellites and tracking stations are small.

### 9.3.2 Effects of Sample Rate on the Accuracy of Orbit Determination

In the results above, assume the sample rate of the observation is 10 min. What is the influence of sample rate of the observation on the accuracy of orbit determination? In the following simulation test, the observations with sample rate 1 and 5 min respectively are used for orbit determination. The results of orbit determination with observation sample rate 1 min are as follows (Figure 9-40 to Figure 9-48).

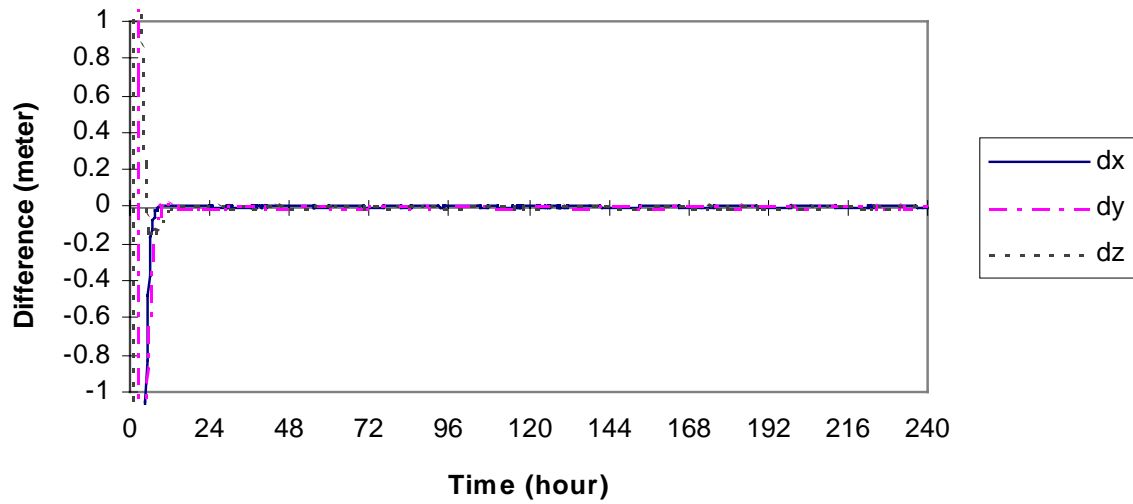


Figure 9-40 Accuracy of Dynamic Orbit Determination of an IGSO Satellite at  $\lambda=-10^\circ$  with Float Ambiguity Solution and Sample Rate 1 min.

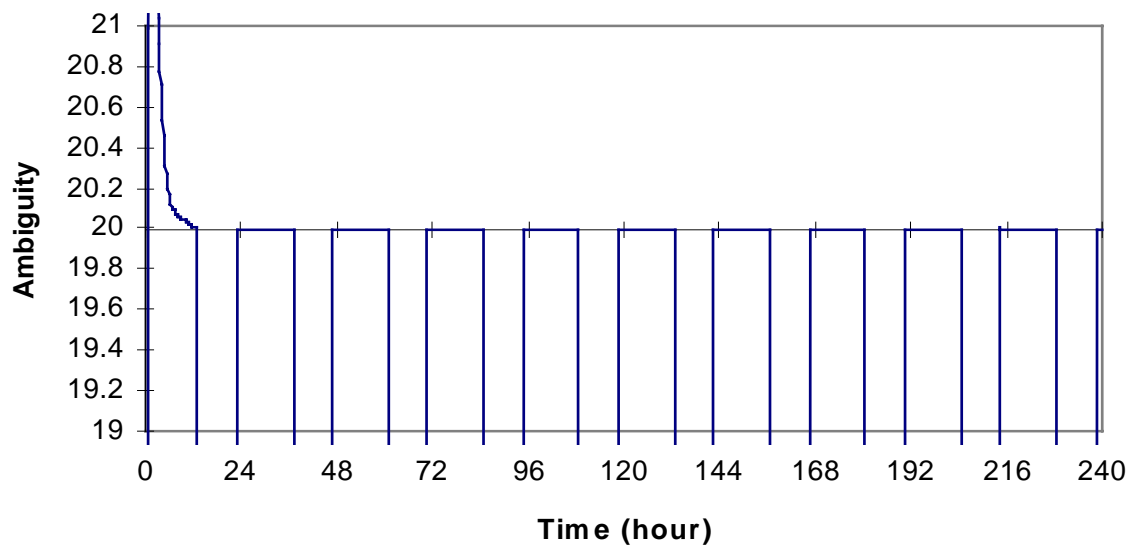


Figure 9-41 Float Ambiguity Solution of an IGSO Satellite at  $\lambda=-10^\circ$  with Sample Rate 1 min at Tracking Station 1

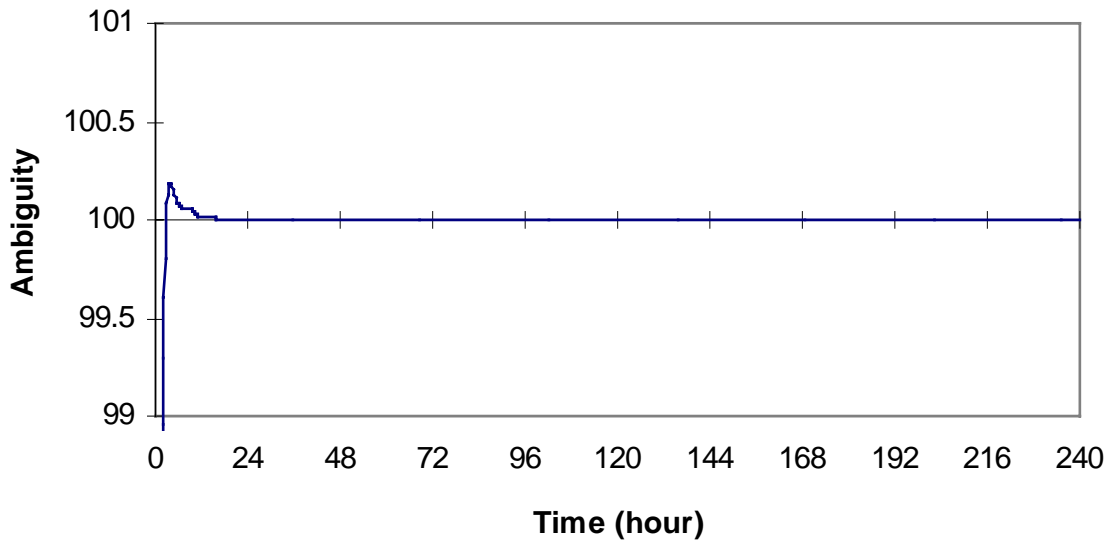


Figure 9-42 Float Ambiguity Solution of an IGSO Satellite at  $\lambda=-10^\circ$  at Tracking Station 5

Figure 9-40 shows the accuracies of  $x, y, z$  coordinates of orbit determination of an IGSO satellite located at  $\lambda=-10^\circ$  with float ambiguity solution considering the satellite visibility and observation sample rate 1 min are  $\pm 0.04 m, \pm 0.05 m$  and  $\pm 0.02 m$  respectively. Figure 9-41 and Figure 9-42 show the related ambiguity solution.

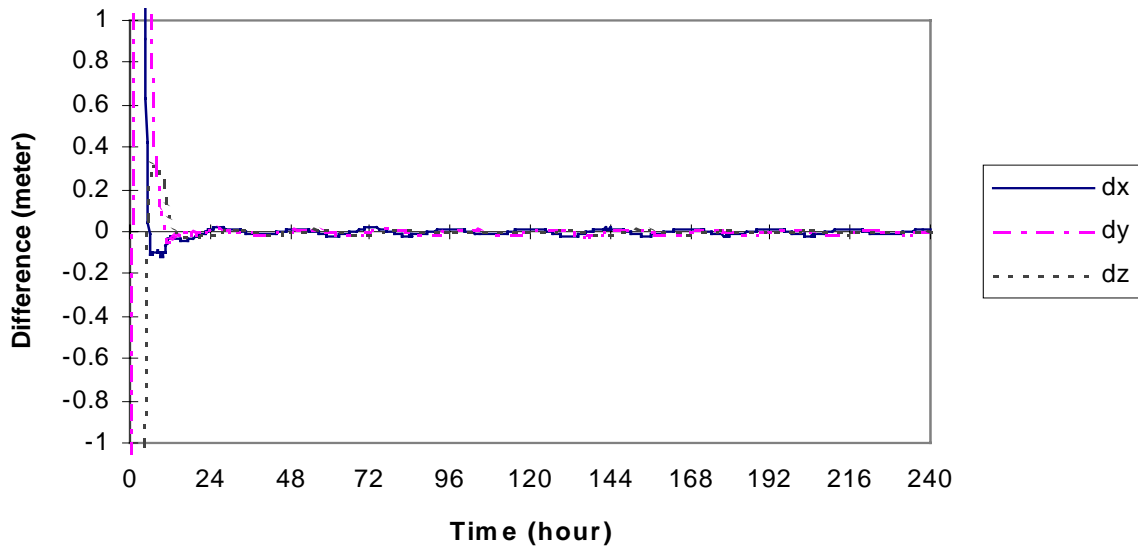


Figure 9-43 Accuracy of Dynamic Orbit Determination of an IGSO Satellite at  $\lambda=20^\circ$  with Float Ambiguity Solution and Sample Rate 1 min

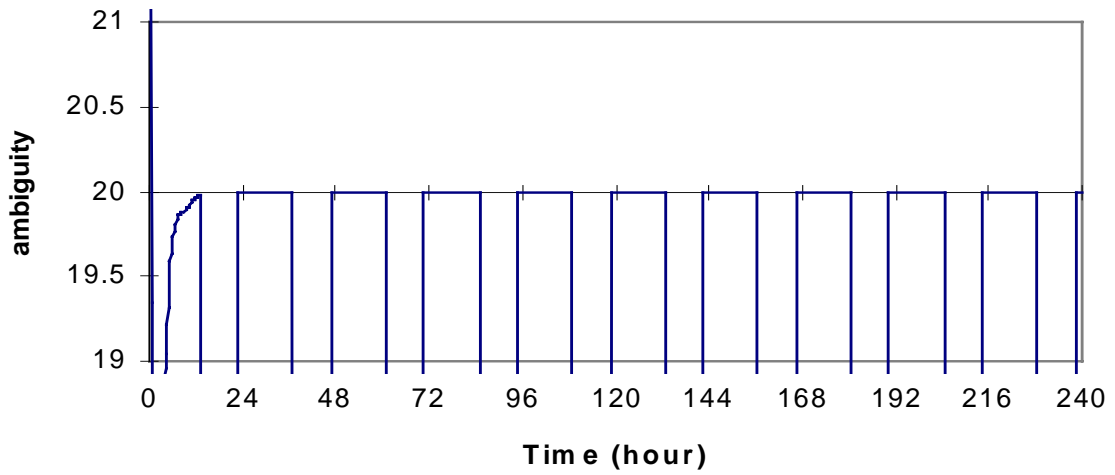


Figure 9-44 Float Ambiguity Solution of an IGSO Satellite at  $\lambda=20^\circ$  at Tracking Station 1

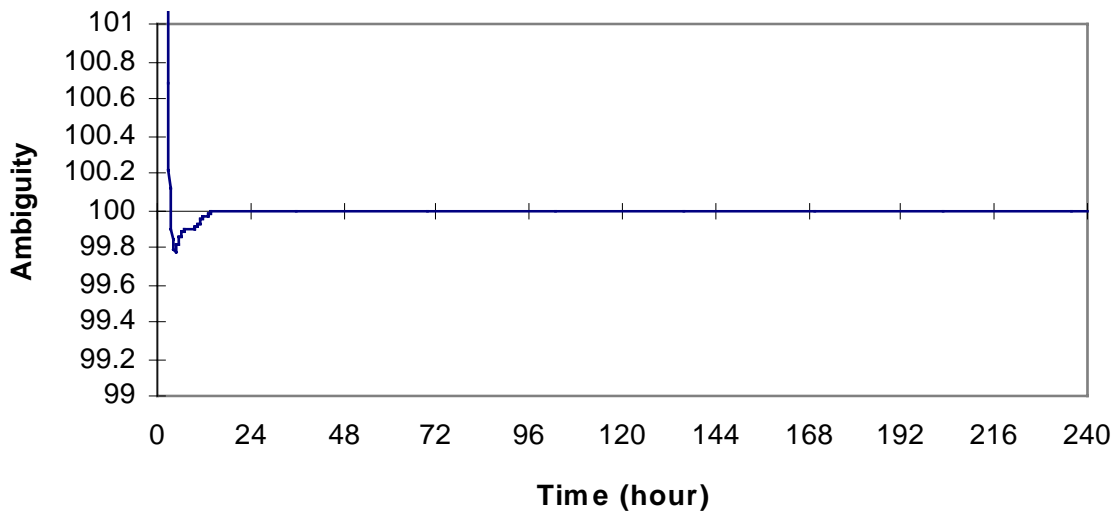


Figure 9-45 Float Ambiguity Solution of an IGSO Satellite at  $\lambda=20^\circ$  at Tracking Station 5

Figure 9-48 shows the accuracies of  $x$ ,  $y$ ,  $z$  coordinates of orbit determination of an IGSO satellite located at  $\lambda=20^\circ$  with float ambiguity solution considering the satellite visibility and observation sample rate 1 minute are  $\pm 0.02\text{ m}$ ,  $\pm 0.14\text{ m}$  and  $\pm 0.04\text{ m}$  respectively. Figure 9-49 and Figure 9-50 show the related ambiguity solution.

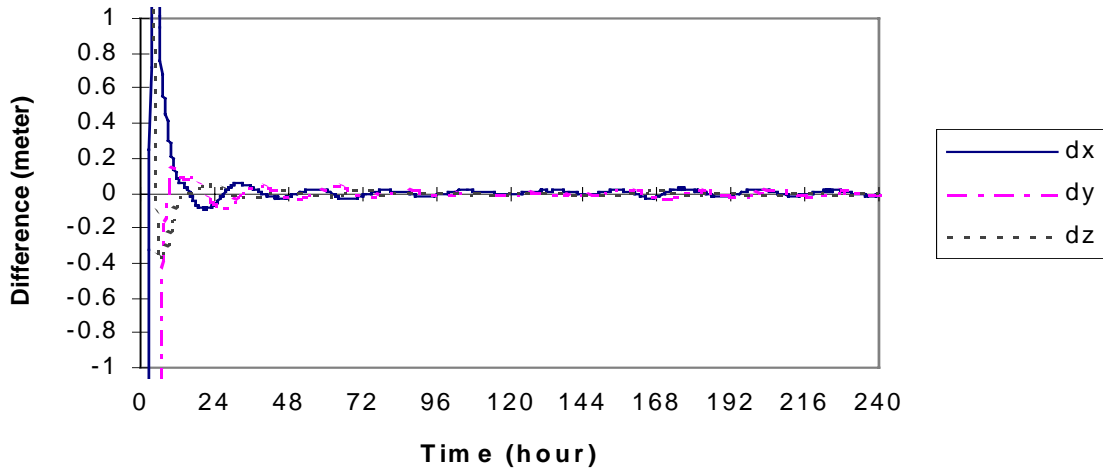


Figure 9-46 Accuracy of Orbit Determination of an IGSO Satellite at  $\lambda=60^\circ$  with Float Ambiguity Solution and Sample Rate 1 min

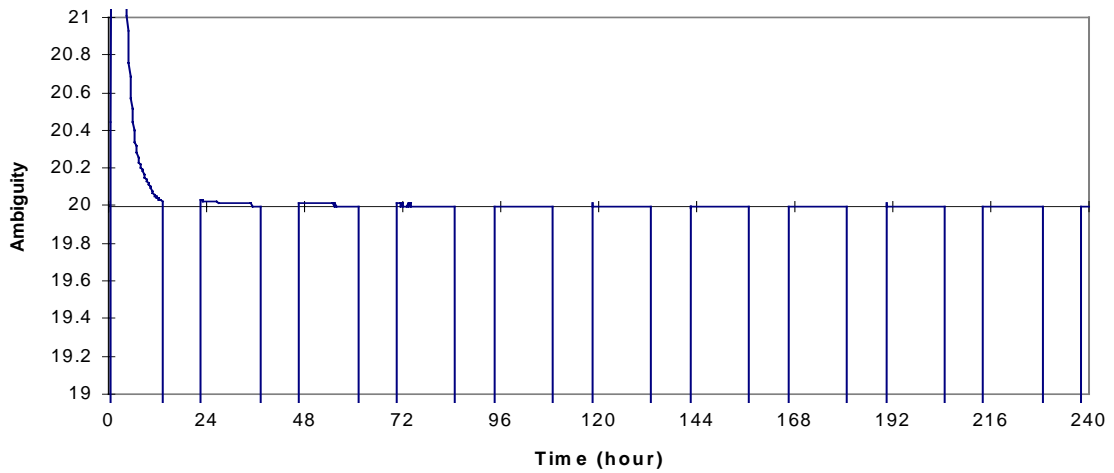


Figure 9-47 Float Ambiguity Solution of an IGSO satellite at  $\lambda=60^\circ$  at Tracking Station 1

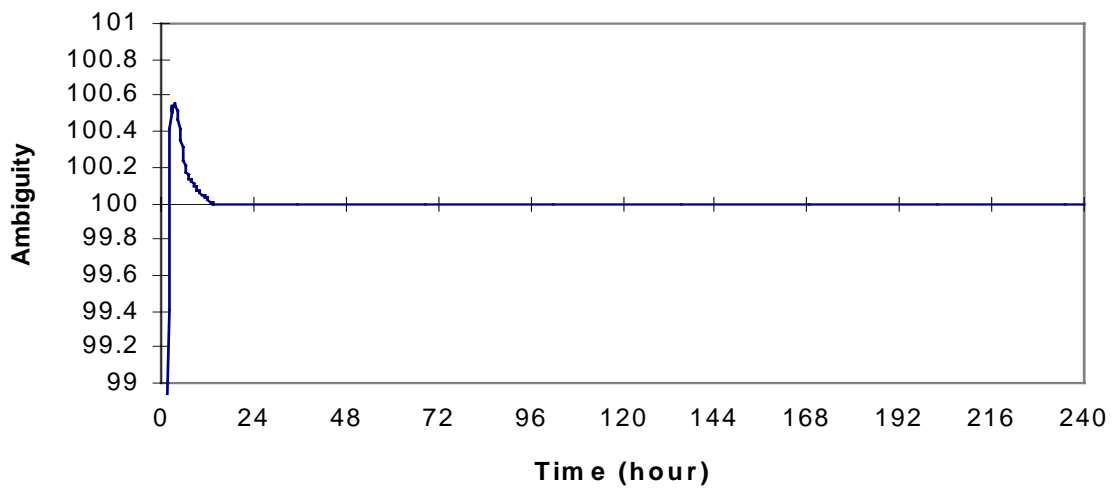


Figure 9-48 Float Ambiguity Solution of an IGSO satellite at  $\lambda=60^\circ$  at Tracking Station 5

Figure 9-51 shows the accuracies of  $x$ ,  $y$ ,  $z$  coordinates of orbit determination for a IGSO satellite located at  $\lambda=60^\circ$  with float ambiguity solution considering the satellite visibility and observation sample rate 1 minute are  $\pm 0.12\text{ m}$ ,  $\pm 0.12\text{ m}$  and  $\pm 0.05\text{ m}$  respectively. Figure 9-52 and Figure 9-53 show the related ambiguity solution.

The results above show that the accuracy of dynamic orbit determination has been significantly improved using carrier phase observation with a sample rate of 1 min. The initial integer ambiguities have been quickly resolved. This is because, using observations with a sample rate of 1 min, the satellite dynamic model errors and some time-related errors are reduced. The disadvantage of observations with a sample rate of 1 minute is that the amount of observation data will be too large to be processed for orbit determination. My suggestion is, after integer or float ambiguities are resolved, the observations with a sample rate of 10 min can be used for following orbit determination.

The following are the results of dynamic orbit determination using observations with a sample rate of 5 min.

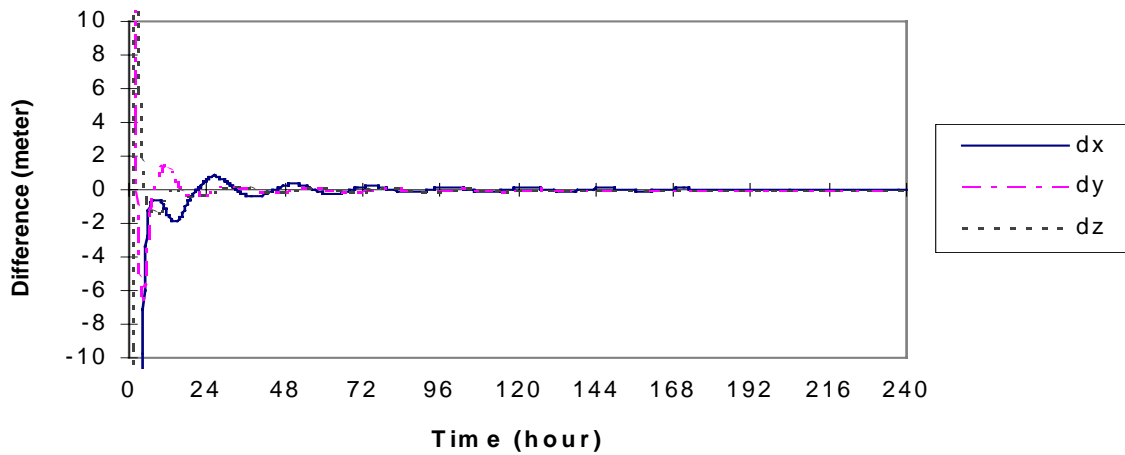


Figure 9-49 Accuracy of Orbit Determination of an IGSO Satellite at  $\lambda=-10^\circ$  with Float Ambiguity Solution and Sample Rate 5 min

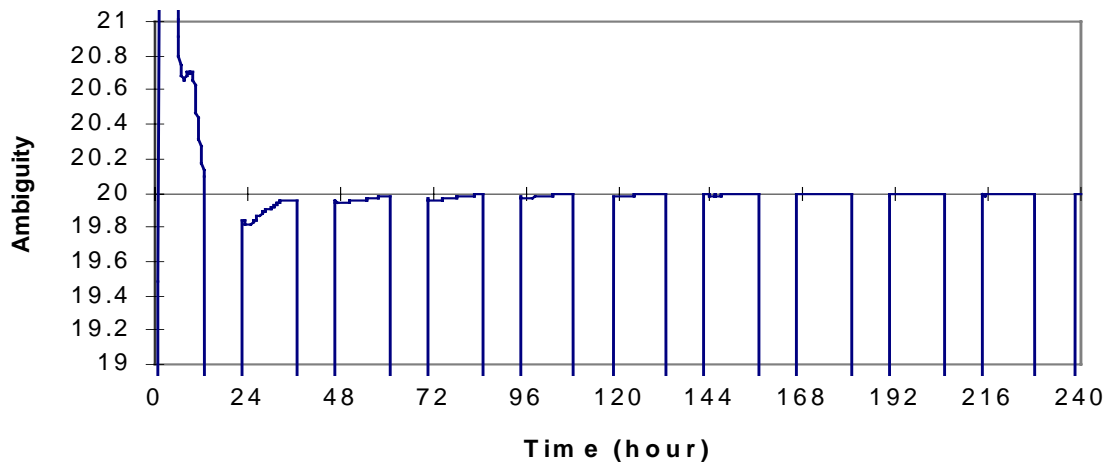


Figure 9-50 Float Ambiguity Solution of an IGSO satellite at  $\lambda=-10^\circ$  at Tracking Station 1

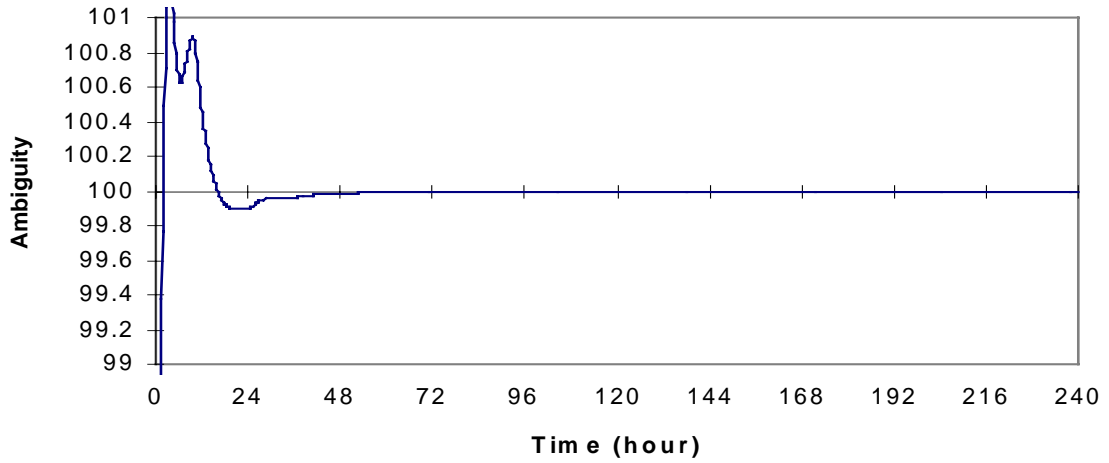


Figure 9-51 Float Ambiguity Solution of an IGSO satellite at  $\lambda=-10^\circ$  at Tracking Station 5

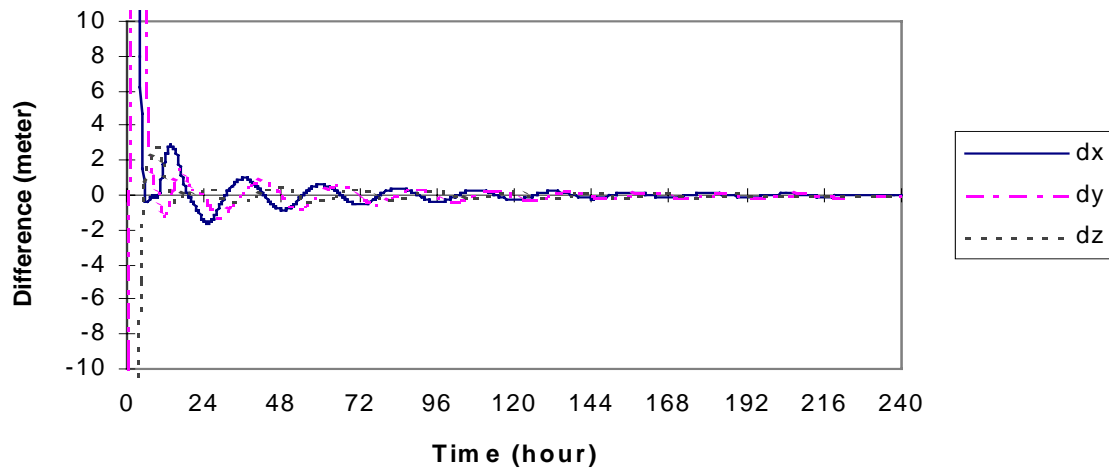


Figure 9-52 Accuracy of Orbit Determination of an IGSO Satellite at  $\lambda=20^\circ$  with Float Ambiguity Solution and Sample Rate 5 min

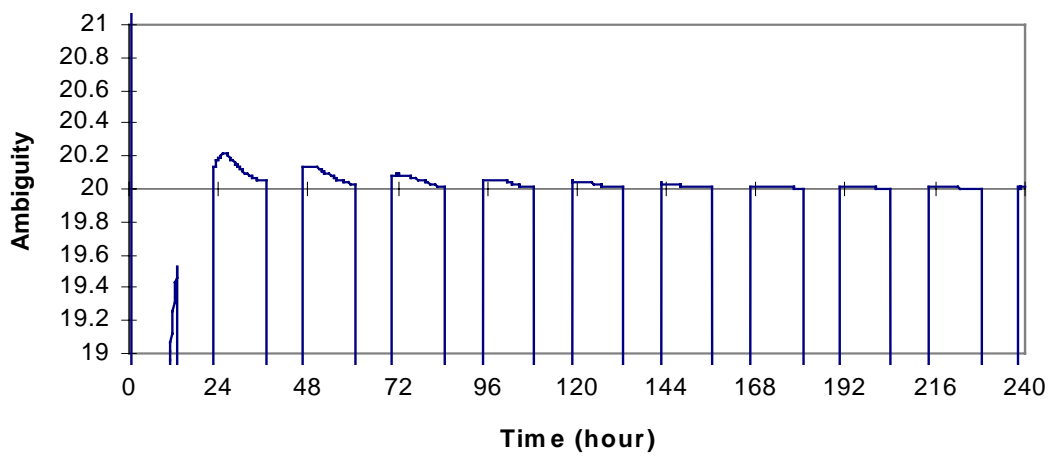


Figure 9-53 Float Ambiguity Solution of an IGSO satellite at  $\lambda=20^\circ$  at Tracking Station 1



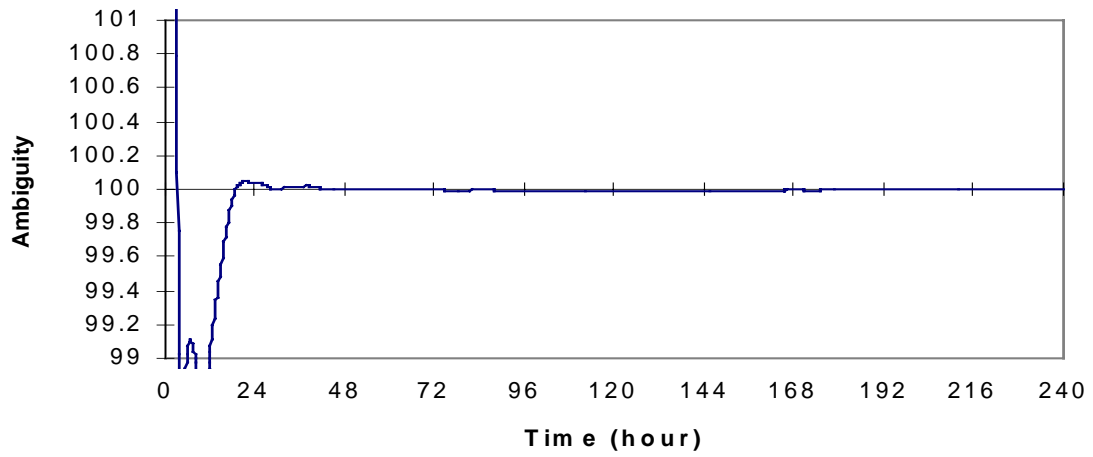


Figure 9-54 Float Ambiguity Solution of an IGSO satellite at  $\lambda=20^\circ$  at Tracking Station 5

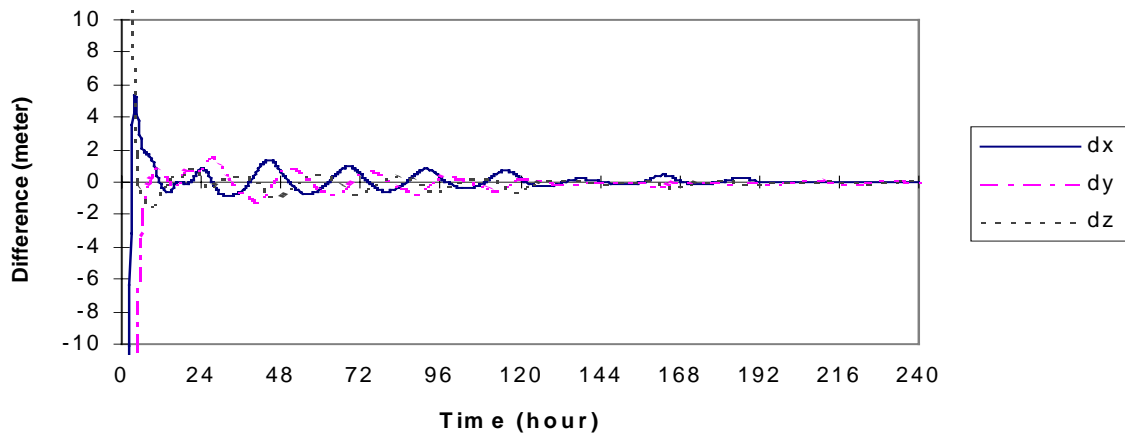


Figure 9-55 Accuracy of Orbit Determination of an IGSO Satellite at  $\lambda=60^\circ$  with Float Ambiguity Solution and Sample Rate 5 min

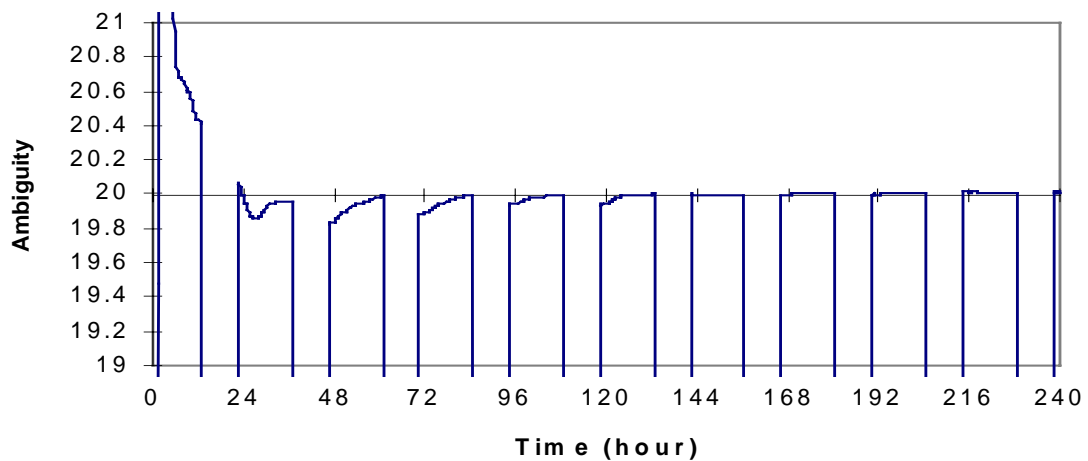


Figure 9-56 Float Ambiguity Solution of an IGSO satellite at  $\lambda=60^\circ$  at Tracking Station 1

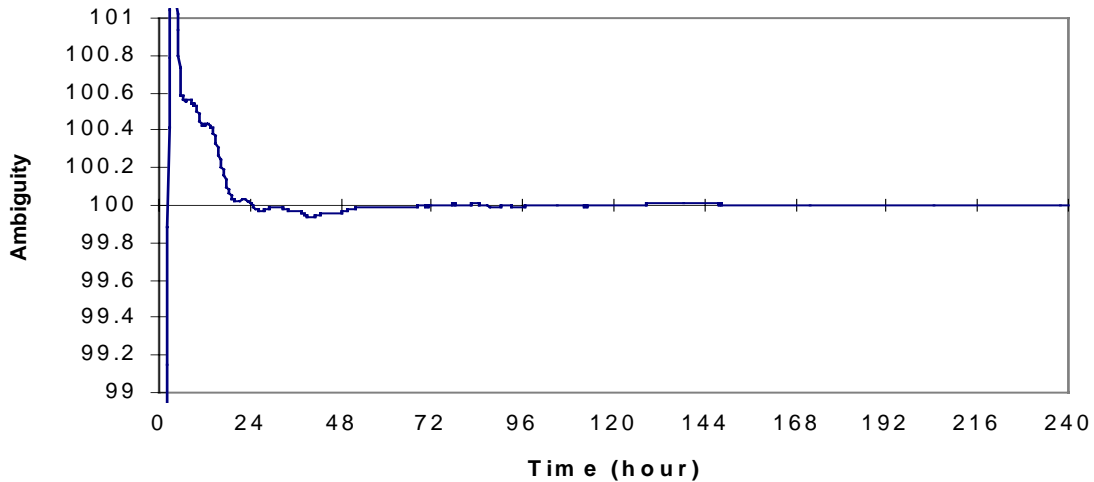


Figure 9-57 Float Ambiguity Solution of an IGSO satellite at  $\lambda=60^\circ$  at Tracking Station 5

The accuracies of  $x$ ,  $y$ ,  $z$  coordinates of dynamic orbit determination of an IGSO satellite located at  $\lambda=-10^\circ$  with float ambiguity solution considering the satellite visibility and observation with sample rate of 5 minutes are  $\pm 0.17\text{ m}$ ,  $\pm 0.07\text{ m}$  and  $\pm 0.07\text{ m}$  respectively. The accuracies of an IGSO satellite located at  $\lambda=20^\circ$  are  $\pm 0.34\text{ m}$ ,  $\pm 0.33\text{ m}$  and  $\pm 0.18\text{ m}$  respectively. The accuracies of a IGSO satellite located at  $\lambda=60^\circ$  are  $\pm 0.40\text{ m}$ ,  $\pm 0.41\text{ m}$  and  $\pm 0.29\text{ m}$  respectively.

### 9.3.3 The Effect of Distribution of Tracking Stations

It is very interesting that the effect of the geometrical distribution of tracking stations depends on the type of observations. Comparing Figure 9-40, Figure 9-43 and Figure 9-46 with the following figures it shows that there are different effects of distribution of tracking stations using range and carrier-phase observations. For range observations some tracking station networks constitute an optimal geometrical distribution, but for carrier phase observations this distribution may be bad. From the mathematical point of view, this difference is caused by the initial ambiguity parameters in the observation equations.

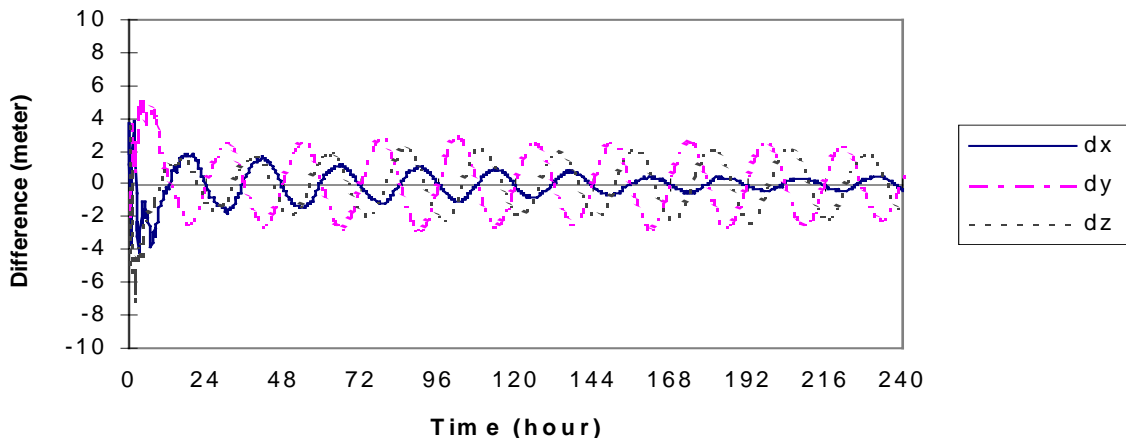


Figure 9-58 Accuracy of Orbit Determination of an IGSO Satellite at  $\lambda=-10^\circ$  using Range Observations

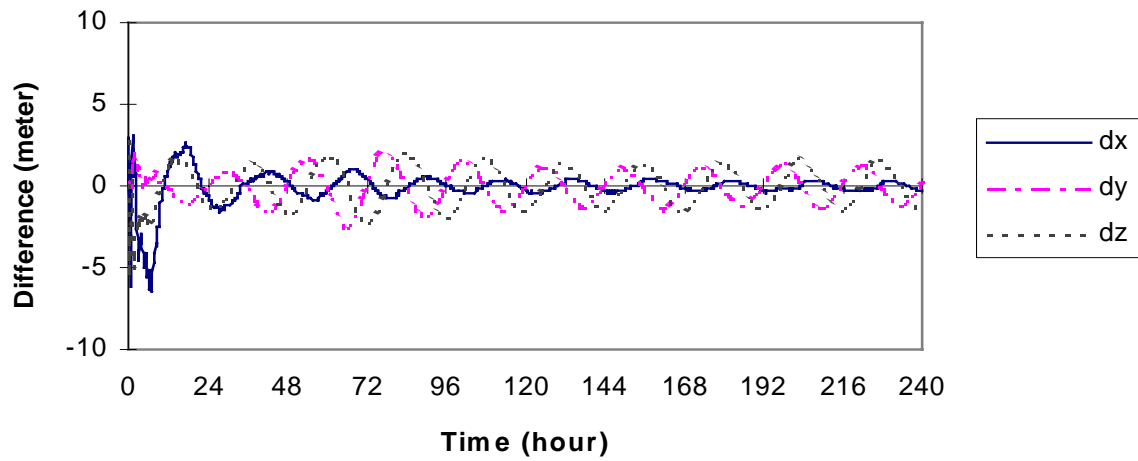


Figure 9-59 Accuracy of Orbit Determination of an IGSO Satellite at  $\lambda=20^\circ$  using Range Observations

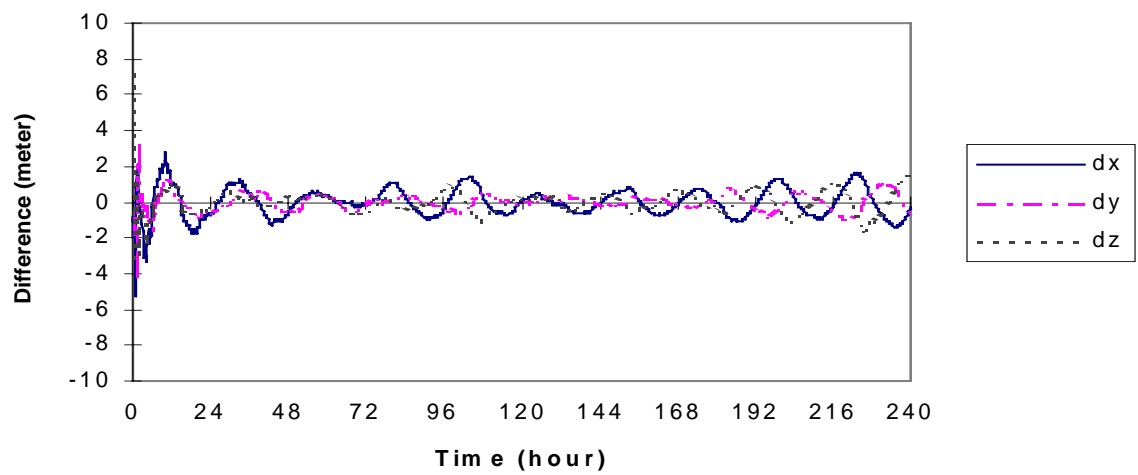


Figure 9-60 Accuracy of Orbit Determination of an IGSO Satellite at  $\lambda=-10^\circ$  with Range Observations

### 9.3.4 Orbit Determination With Integer Ambiguity Solution

Due to propagation errors, satellite clock drift and receiver noises, it is difficult to fix the initial ambiguities of carrier phase observations into integers during data processing for orbit determination. What accuracy of dynamic orbit determination can be achieved if the initial integer ambiguities of carrier phase observable are resolved? Figure 9-66 to Figure 9-69 show the results (sample rate =10min).

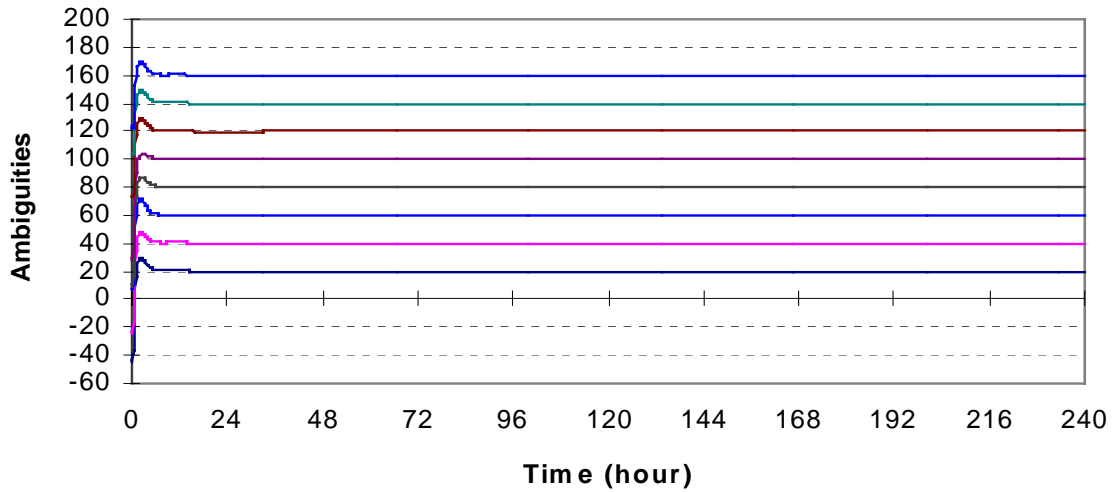


Figure 9-61 Integer Ambiguity Solutions

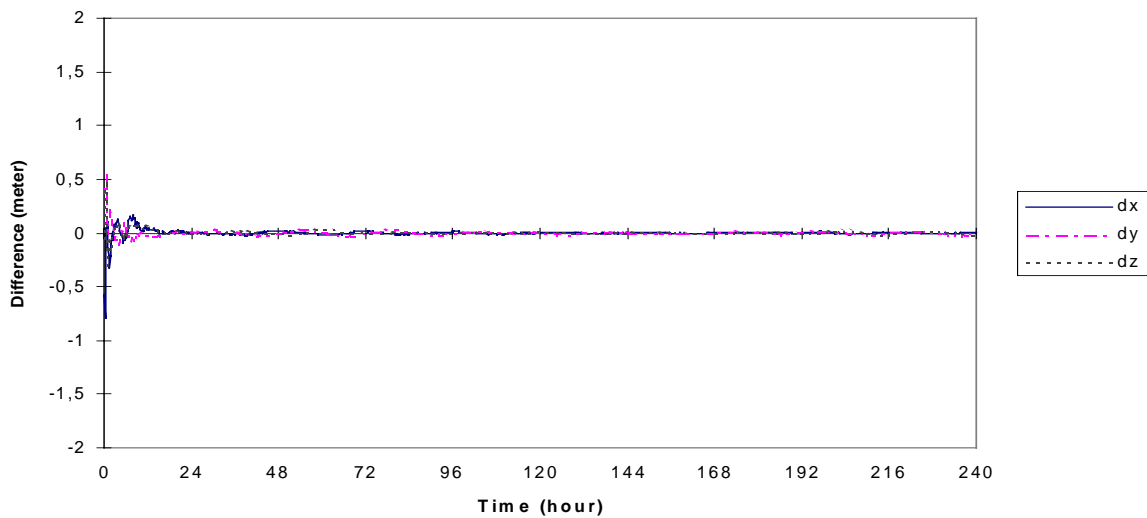


Figure 9-62 Accuracy of Orbit Determination of an IGSO Satellite at  $\lambda=-10^\circ$  with Integer Ambiguity Solution

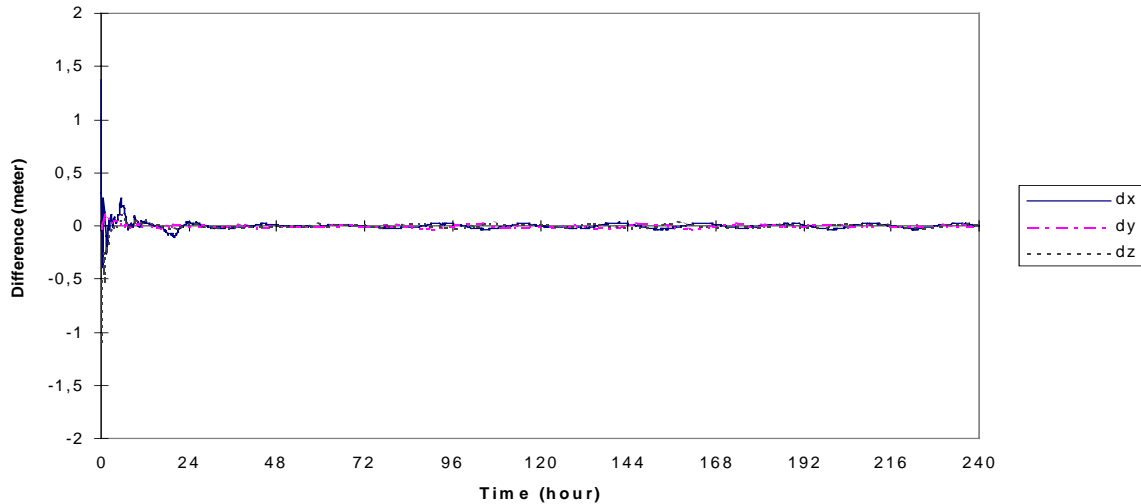


Figure 9-63 Accuracy of Orbit Determination of an IGSO Satellite at  $\lambda=20^\circ$  with Integer Ambiguity Solution

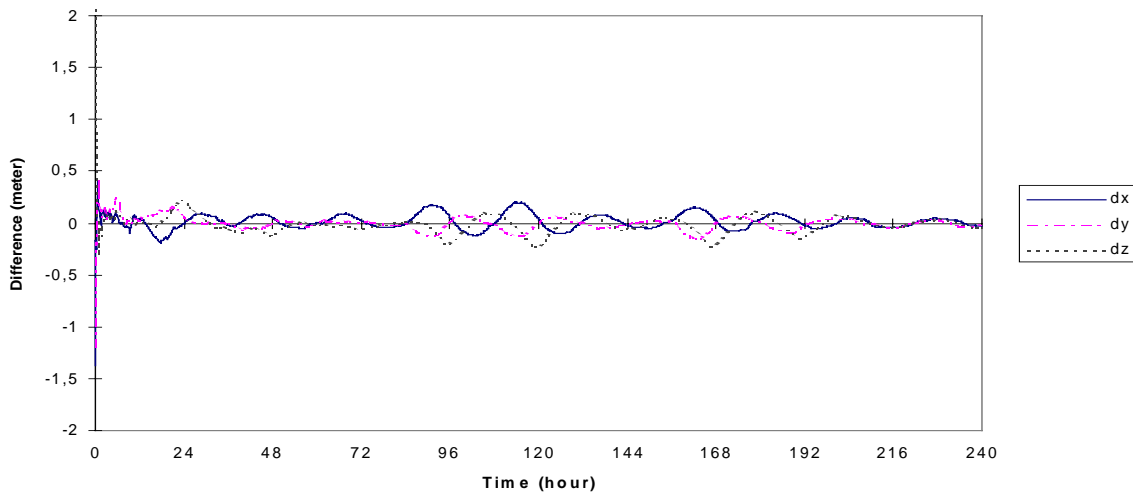


Figure 9-64 Accuracy of Orbit Determination of an IGSO Satellite at  $\lambda=60^\circ$  with Integer Ambiguity Solution

Figure 9-61 shows that data processing for  $45^{\text{h}} 20^{\text{m}}$ , all initial ambiguities of observations are fixed into integers. Figure 9-62, Figure 9-63 and Figure 9-64 show the promising accuracy of dynamic orbit determination of IGSO and GEO satellites. According to statistics from the differences between Kalman filter and theoretical error-free orbits, the accuracy of coordinate components of dynamic orbit determination of an IGSO satellite located at  $\lambda=-10^\circ$  are  $\pm 0.01$  m,  $\pm 0.01$  m and  $\pm 0.01$  m respectively; the accuracy of an IGSO satellite located at  $\lambda=20^\circ$  are  $\pm 0.02$  m,  $\pm 0.01$  m and  $\pm 0.01$  m respectively and the accuracy of an IGSO satellite located at  $\lambda=60^\circ$  are  $\pm 0.07$  m,  $\pm 0.05$  m and  $\pm 0.08$  m respectively. From these figures it can also be found that the wave-like variations in the accuracy of orbit determination have been significantly reduced. This means, that with the same error budget the effects of geometrical distribution of tracking station network and observation gaps due to the satellite visibility are largely eliminated. If the signal is lost after centimeter-accuracy of orbit determination has been reached, the initial integer ambiguities of recovered signals will be quickly resolved using high-precise orbit and coordinate of tracking stations, but this method is not suitable for orbit maneuvers.

It is difficult to resolve the initial ambiguity of carrier phase observation for GEO satellite, but if the initial ambiguity could be solved using other approaches, the accuracy of orbit determination of a GEO satellite would be significantly increased, see Figure 9-65.

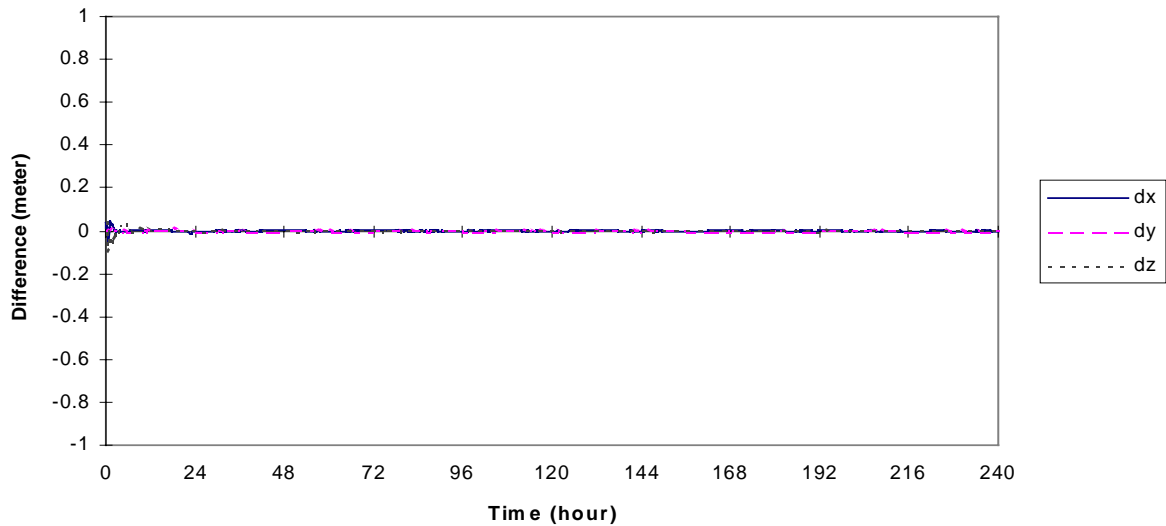


Figure 9-65 Accuracy of Orbit Determination of a GEO Satellite located at  $\lambda=20^\circ$  using Carrier Phase Observation

The accuracy of dynamic orbit determination of a GEO satellite located at  $\lambda=20^\circ$  is better than centimeter level.

In order to enhance the accuracy of orbit determination of IGSO and GEO satellites, the ambiguity resolution techniques of carrier phase observations are very important. Widely used ambiguity resolution algorithms available at present for GPS may be also suitable for future GNSS-2/Galileo satellite orbit determination. A new method of Three Carrier Ambiguity Resolution (TCAR) is proposed by Harris (1997). If TCAR method is successfully applied for future GNSS-2/Galileo system, it will significantly improve the accuracy of GNSS-2/Galileo orbit determination.

## CONCLUSION

The GNSS-2/Galileo system should be an open and global navigation satellite system(GNSS), developed by Europe and fully compatible with GPS, but independent of it. Galileo should provide three-dimensional performance, accurate to better than 10 meters horizontally, providing a universal independent time reference on a global basis. The Galileo system is based on a core constellation of MEO satellites. IGSO and GEO satellites are all possible candidates for GNSS-2 satellite constellations such as EGNOS.

In the dissertation the orbit determinations of IGSO, GEO and MEO satellites are discussed using dynamic and kinematic methods. The effort focused, however, on IGSO and GEO satellites, because MEO satellites are already adopted by both US and USSR for satellite navigation systems such as GPS and GLONASS and thus there is substantial literature available for GPS/Glonass orbit determination and applications.

From the discussion, IGSO satellites have many advantages. Fewer satellites are needed than are used in MEO for global coverage. Using range observations with one meter error, and partial global satellite tracking stations, 1-10 meter accuracy of real-time orbit determination of IGSO satellite can be achieved. When using carrier phase observations, the accuracy of real-time orbit determination will be much better. The disadvantage is that there is no actual application of IGSO satellites, therefore people have no experience of this type of satellite for navigation.

GEO satellites can be “fixed” at some point in the sky above the earth surface. For satellite tracking stations on the coverage of GEO, there is no visibility problem. Under the same conditions as IGSO satellites, using range observations, the accuracy of real time orbit determination of GEO satellites is better than that of IGSO satellites. The disadvantage is that the satellite orbit can not be determined using carrier phase observations. This is because of the very slow movement of the GEO satellite relative to the Earth’s surface. Another disadvantage is that maneuver operations are required weekly for GEO satellites due to quick drift. This is a serious problem for navigation and positioning users, because normally satellite orbit information will not be sent to navigation and positioning users during satellite maneuver and thus users can not perform navigation and positioning operations. This serious problem has been solved by using kinematic orbit determination discussed in chapter 8. If the initial ambiguity can be solved, very high accuracy of real time orbit determination can be achieved by using carrier phase observations.

For MEO satellites, the same accuracy as the IGSO and GEO satellites could be achieved.

The multipath effect has great influence on the initial ambiguity solution and the accuracy of orbit determination. In the dissertation, methods for mitigation of the multipath effect using linear combinations of original carrier phase observations are discussed.





## References

- Anderson, D. N. M., Mendillo, and B. Herniter, (1987): *A Semi-Empirical Low-Latitude Ionospheric Model*, Radio Sci. 22, 292, 1987.
- Anderson, D. N., J. M. Forbes, and M. Codrescu, (1989): *A Fully Analytical, Low- and Middle-Latitude Ionospheric Model*, J. Geophys. Res. 94, 1520, 1989.
- Balbach O, B. Eissfeller, G. Hein, T. Zink, W. Enderle, M. Schmidhuber and N. Lemke (1998): *Tracking GPS Above GPS Satellite Altitude: Results of the GPS Experiment on the HEO Mission Equator-S*, ION GPS-98, the Institute of Navigation, Nashville, Tennessee, September 15-18, 1998
- Bent, R. B., S. K. Llewellyn, and P. E. Schmid, (1972): *Ionospheric Refraction Corrections in Satellite Tracking*, Space Research XII, 1186-1194, Akademie-Verlag, Berlin, 1972.
- Beutler, G., W. Gurtner, M. Rothacher, U. Wild and E. Frei (1989): *Relative Static Positioning System: Basic Technical Considerations*: IAG Symposium No. 102, Global Positioning System: An Overview, Edited by Yehuda Bock and Norman Leppard, pp. 1-23, Springer-Verlag.
- Beutler, G. (1996): *GPS for Geodesy*, Lecture Notes in Earth Sciences, Springer Verlag 1996.
- Beutler, G, I. I. Mueller and R. E. Neilan (1996): *The International GPS Service for Geodynamics (IGS): The Story*, Beutler, Hein, Melbourne and Seeber edited GPS Trends in Precise Terrestrial, Airborne, and Spaceborne Applications, pp. 3-13, Springer-Verlag, 1996.
- Bisten, M. and Damiano, A.(1996): *Deutsche Telekom Automation in Satellite Flight Dynamics Operations*, Deutsche Telekom AG, Zentrale Satellite Systems Operation Postfach 10 00 03, 64296 Darmstadt
- Blaha, G. (1991): *Satellite-to-Satellite Tracking in the High-Low Mode - Line-of-Sight Acceleration in a Residual Gravity Field*, NASA Technical Report N92-32082/9INZ, 1992
- Blewitt, G. (1989): *Carrier Phase Ambiguity Resolution for Global Positioning System Applied to Geodetic Baselines up to 2000 km*, Journal of Geophysical Research, Vol. 94, No. B8, pp. 10187-10203, August 10, 1989
- Blitzer, Leon (1966): *Satellite Resonances and Librations Associated with Tesseral Harmonics of the Geopotential*, Journal of Geophysical Research, Vol. 71, No.14, July 15, 1966
- Borge, Tom Kare (1996): *GPS Carrier Phase Ambiguity Resolution and Cycle-Slip Processing on a Moving Platform*, PhD Dissertation, Department of Engineering Cybernetics, Norwegian University of Science and Technology.
- Braasch, Michael S.(1996): *Multipath Effects*, Parkinson et al edited *Global Positioning System: Theory and Applications, Chapter 14, Volume1* pp. 547-568, American Institute of Aeronautics and Astronautics, Inc.
- Braasch, Michael S.(1992): *On the Characterization of Multipath Errors in Satellite-based Precision Approach and Landing System*, Ph.D Thesis, Ohio State University.
- Breivik K., B. Forssell, C. Kee, P. Enge and T. Walter (1997): *Estimation of Multipath Error in GPS Pseudorange Measurements*, Navigation, Vol. 44, No.1, Spring 1997, Institute of Navigation.
- Byun, Sung H. and Bob E. Schutz (1998): *Satellite Orbit Determination Using GPS Carrier Phase in Pure Kinematic Mode*, ION GPS-98, Institute of Navigation, September 15-18, 1998, pp. 1519-1535, Nashville, Tennessee, USA
- Cappellari, J., C. Velez, A. Fuchs (1976): *Mathematical Theory of the Goddard Trajectory Determination System*. Goddard Space Flight Center, X-582-76-77.
- Carnebianca C., G. Mastini and R. Rizzo (1985): *NAVSAT SYSTEM CONFIGURATION STUDY*, Final Report, ESA ITS-TR-011/85, 1985.

Carpino M. (1995): *SAEG 0.2 User's Manual*.

Chadwell, C. D. (1995): *Investigation of Stochastic Models to Improve the Global Positioning System Satellite Orbits*. PhD Dissertation, Report No.429, The Ohio State University, March 1995

Chiu, Y. T.(1975): *An Improved Phenomenological Model of Ionospheric Density*, J. Atmos. Terr. Phys. 37, 1563, 1975.

Cohen, C.E. (1992): *Attitude Determination Using GPS*, Ph.D Thesis, Stanford University.

Colombo O. L. (1981): *Numerical Methods for Harmonic Analysis on the Sphere*, Report No. 310, Department of Geodetic Science, The Ohio State University 1981.

Comp C. J. and P. Axelrad (1996): *An Adaptive SNR-Based Carrier Phase Mitigation Technique*, ION GPS-96, pp. 683-697 Kansas City, Missouri, September 17-20, USA.

Costes, Murielle (1997): Private email communication.

Counselman III, C.C. and R. I. Abbot (1989): *Method of Resolving Radio Phase Ambiguity in Satellite Orbit Determination*, Journal of Geophysical Research, Vol. 94. No. B6, pp. 7058-7064, June 10, 1989

Degnan, J.J., and Pavlis, E.C.(1994): *Laser Ranging to GPS Satellites with Centimeter Accuracy*, GPS World, pp. 62-70, September, 1994.

Dow, M.(1999): private email communication

Eanes, R. J., Schutz, B., and Tapley, B. (1983): *Earth and Ocean Tide Effects on Lageos and Starlette*, in Proceedings of the Ninth International Symposium on Earth Tides, E. Schweizerbart'sche Verlagsbuchhandlung, Stuttgart.

Eissfeller, B. and G. W. Hein (1986): *A Contribution to 3D-Operational Geodesy*, Heft 17, Universitärer Studiengang Vermessungswesen der Universität der Bundeswehr München, 1986.

Eissfeller, B., O. Balbach and U. Rossbach (1996): *GPS Navigation on the HEO Satellite Mission EQUATOR-S, Results of the Feasibility Study*, ION GPS-96, September 17-20, Kansas City, Missouri, pp 1331-1340.

Eissfeller, B. (1997): *Ein dynamisches Fehlermodell für GPS Autokorrelationsempfänger*, Heft 55, Studiengang Vermessungswesen Universität der Bundeswehr München.

El-Rabbany, Ahmed (1995): *Temporal Characteristics of Multipath Errors*, ION GPS-95, pp.1493-1497, Palm Springs, California, September 12-15, 1995, USA.

Engeln-Müllges, Gisela and Frank Uhlig (1996): *Numerical Algorithms with FORTRAN*, Springer Verlag, Germany.

Escobal, P. R.(1976): *Methods of Orbit Determination*, Krieger Publishing Company, USA, 1976.

Euler, H.-J.; Landau, H. (1992): *Fast Ambiguity Resolution On-The-Fly for Real-Time Applications*, 6th International Geodetic Symposium on Satellite Positioning, March 1992, Columbus, Ohio.

Feltens, J. (1991): *Nicht-Gravitative Störeinflüsse bei der Modellierung von GPS-Erdumlaufbahnen*, PhD Dissertation, Deutsche Geodätische Kommission bei der Bayerischen Akademie der Wissenschaften, Reihe C, Heft Nr. 371, München 1991.

Feltman, A. J. (1999): *Trade-Off Analysis of Communications Capabilities of Inter-Satellite Links*, Technical Report, Air Force Inst. of Tech., Wright-Patterson AFB, OH. USA, 1999

Filippov, V., D. Tatarnicov, J. Ashjaee, A. Astakhov and I. Sutiagin (1998): *The First Dual-Depth Dual-Frequency Choke Ring*, ION GPS-98, Nashville, Tennessee, USA, September 15-18, 1998

- Flechtner, F., K. Kaniuth, Ch. Reigber, H. Wilmes (1990): *The Precise Range and Range Rate Equipment PRARE: Status Report on System Development, Preparations for ERS-1 and Future Plans*, Second International Symposium on Precise Positioning System with the Global Positioning System, September, Ottawa, 1990
- Flechtner, F. (2000): *PRARE System Description*, <http://op.gfz-potsdam.de/prare/>
- Fliegel, H. F. and T. E. Gallini (1992): *Global Positioning System Radiation Force*, Journal of Geophysical Research, Vol. 97, No. B1, pp 569-585, January 10, 1992.
- Forssell, B., Martin-Neira, M.; Harris, R. A. (1997): *Carrier Phase Ambiguity Resolution in GNSS-2*, Proceedings of ION-97, Kansas City.
- Frei, E., Beutler, G. (1990): *Rapid Static Positioning Based on the Fast Ambiguity Resolution Approach "FARA": Theory and First Results*, Manuscripta Geodaetica, Vol. 15, No. 6, pp. 325-356
- Frei, E., Yau, J., Sauer, D. (1993): *Ambiguity Resolution On The Fly (AROF); Results, Facts, Limitations*, ION GPS-93, The Institute of Navigation, September 22-24, Salt Lake City, Utah, pp. 1059-1067
- Gardner, C. S. and J. B. Abshire (1984): *Atmospheric Refraction and Target Speckle Effects on the Accuracy of Laser Ranging Systems*, fifth International Workshop on Laser Ranging Instrumentation, Herstmonceux Castle, September 10-14, 1984, Group de Recherches de Geodesie Spatiale, pp. 29-41.
- Gill E. and H. K. Kuga (1993): *ODEM - An Improved Approach Towards Rapid Satellite Maneuver*, AAS/AIAA Spaceflight Mechanics Meeting, Pasadena, California, Feb. 22-24, 1993, pp. 783-802.
- Gomez, S., R. Panneton, P. Saunders, S. Hwu and B. Lu (1995): *GPS Multipath Modeling and Verification Using Geometrical Theory of Diffraction*, ION GPS-95, pp. 195-204, Palm Springs, California, September 12-15, 1995, USA.
- Hagerman, L., 1973, *Effects of Multipath on Coherent and Noncoherent PRN Ranging Receiver*, Aerospace Rep. TOR-0073(3020-03)-3, Development Planning Division, The Aerospace Corporation, May 15, 1973.
- Hahn, J. (1996): *DLR's Research for Space-Maser Monitoring with Two-Way Microwave Links*, Institut für Hochfrequenztechnik, DLR Oberpfaffenhofen, Germany. pp.7.
- Harris, R. A. (1997): *Direct Resolution of Carrier-Phase Ambiguity by „Bridging the Wavelength Gap“*, ESA Publication TST/60107/RAH/Word, February, 1997.
- Hatch, R. (1990): *Instantaneous Ambiguity Resolution*, Proceedings of IAG International Symposium No. 107 on Kinematic Systems in Geodesy, Surveying and Remote Sensing, Springer Verlag, pp. 299-308
- Hein, G. W. (1995): *Geodetic Requirements of a Future Civil Global Navigation Satellite System (GNSS-2)*, Publication dedicated to Erwin Groten on the occasion of his 60th anniversary, Institute of Geodesy and Navigation (IfEN), University FAF Munich, pp. 152-163.
- Hein, G. W., H. Su and B. Eissfeller (1997): *Orbit Determination of Geosynchronous Satellites of a European Satellite Navigation System (ENSS2)*, International Symposium of Space Flight Dynamics, Darmstadt, Germany, June 2-6, 1997
- Hein, G. W., J. Pielmeier, Th. Zink and B. Eissfeller (1997): *GPS and GLONASS RAIM Availability Analysis Over Europe*, ION-GPS 97, pages 465-474
- Hofmann-Wellenhof, B., H. Lichtenegger, and J. Collins (1992): *GPS Theory and Practice*, Springer-Verlag.
- James, O. and M. Merrigan (1995): *Evaluation of DOD GPS Satellite Orbits Using NASA Laser Ranging Data*, ION-GPS 95, pages 45-54, September 12-15, 1995, Palm Springs, California.
- Jonge, de Paul and Ch. Tiberius (1996): *The LAMBDA-Method for Integer Ambiguity estimation: Implementation Aspects*, Delft Geodetic Computing Centre, Delft University of Technology, 1996

Klobuchar, J. A.(1996): *Ionospheric Effects on GPS*, Global Positioning System: Theory and Applications, Volume 1, edited by Bradford W. Parkinson, James J. Spilker Jr., Penina Axelrad and Per Enge, American Institute of Aeronautics and Astronautics, Inc.

Kouba, J. (1998): *Analysis Activities*, IGS Annual Report 1998, Pasadena, USA

Kovalevsky, J. (1967): *Introduction to Celestial Mechanics*, D. Reidel Publishing Company, Dordrecht-Holland, 1967

Landau, H., B. Eissfeller and G. W. Hein (1986): *GPS Research 1985 at the Institute of Astronomical and Physical Geodesy*, Heft 19, Universitärer Studiengang Vermessungswesen der Universität der Bundeswehr München, 1986.

Landau, H (1988): *Zur Nutzung des Global Positioning Systems in Geodäsie und Geodynamik: Modellbildung, Softwareentwicklung und Analyse*, Ph.D Dissertation, Studiengang Vermessungswesen, Universität der Bundeswehr München.

Lefebvre M. (1989): *DORIS system*, CNES/GRGS document, 1989

Leschiutta, S., S. Marra and R. Mazzucchelli (1984): *Thermal Effects on Detectors and Counters*, Fifth International Workshop on Laser Ranging Instrumentation, Herstmonceux Castle, September 10-14, 1984, Group de Recherches de Geodesie Spatiale, pp. 119-128.

Leick, A. (1995): *GPS Satellite Surveying*, 2nd Edition, John Wiley & Sons, USA, 1995

Lichten, S. and J. S. Border (1987): *Strategies for High-Precision Global Positioning System Orbit Determination*, Journal of Geophysical Research, Vol. 92, No. B12, pp. 12751-12762, November 10, 1987

McCarthy, D. D.(1992): *IERS Standards (1992)*, IERS Technical Note 13, Central Bureau of IERS - Observatoire de Paris.

Mireult, Y., J. Kouba and F. Lahaye (1996): *IGS Combination of Precise GPS satellite Ephemerides and Clocks*, Beutler, Hein, Melbourne and Seeber edited GPS Trends in Precise Terrestrial, Airborne, and Spaceborne Applications, pp. 14-23, Springer-Verlag, 1996.

Montalvo, A. and A. Brown (1995): *A Comparison of Three Multipath Mitigation Approaches for GPS Receivers*, ION GPS-95, pp.1511-1520 Palm Springs, California, September 12-15, USA.

Mueller, I. I. and S. Zerbini (1988): *The Interdisciplinary Role of Space Geodesy*, pp. 166, Springer-Verlag, 1988.

Nelson, Shane (1995): *Long Period Systematic Errors in GPS Measurements*, ION GPS-95, pp.1155-1163 Palm Springs, California, September 12-15, USA.

Noll C. E. and W. Gurtner (1996): *Global GPS Data Flow from Station to User within the IGS*, Beutler, Hein, Melbourne and Seeber edited GPS Trends in Precise Terrestrial, Airborne, and Spaceborne Applications, pp. 24-29, Springer-Verlag, 1996.

Parkinson, B.W., James J. Spilker Jr., Penina Axelrad and Per Enge (1996): *Global Positioning System: Theory and Application*.

Petway, J. (1995): *ARGOS Navigation and Attitude Determination System*, ION-GPS 95, pages 563-572, September 12-15, 1995, Palm Springs, California.

Raquet, C. J. and G. Lachapelle (1996): *Determination and Reduction of GPS Reference Station Multipath Using Multipath Receivers*, ION GPS-96, pp. 673-681, Kansas City, Missouri, September 17-20, USA.

Ray, J. K. and M. E. Cannon (1998): *Mitigation of Static Carrier Phase Multipath Effects Using Multiple Closely-Spaced Antennas*, ION GPS-98, Nashville, Tennessee, USA, September 15-18, 1998.

- Reigber, Ch., F.-H. Massmann and F. Flechtner (1997): *The PRARE System and the Data Analysis Procedure*, Advanced Space Technology in Geodesy - Achievements and Outlook -, CSTG Bulletin No.14, Munich, Germany, 1997.
- Rizos C. (1979): *An Efficient Computer Technique for The Evaluation of Geopotential From Spherical Harmonic Models*, Aust. J. Geod. Photo. Surv. No. 31 December 1979.
- Schillak, S. (1998): *Analysis of Quality of the Borowiec Satellite Laser Ranging System*, Proceedings 11<sup>th</sup> International Workshop on Laser Ranging, Deggendorf, Germany, September 20-25, 1998
- Schmid, P., Trudell, B. and Vonbun, F.(1975): IEEE Trans. Aerosp. Electr. Sys., 11, No.6
- Seeber, G. (1993): *Satellite Geodesy*, Walter de Gruyter, Berlin 1993.
- Sennott, J. W, D. Pietraszewski (1987): *Experimental Measurement and Characterization of Ionospheric and Multipath Errors in Differential GPS*, Navigation, Journal of the Institute of Navigation, Vol. 34, No.2, Summer 1987, pp. 160-173.
- Sleewaegen, Jean-Marie (1997): *Multipath Mitigation, Benefits from using the Signal-to-Noise Ratio*, ION GPS-97, pp. 531-540, Kansas City, Missouri, September 16-19, USA.
- Soop E. M. (1994): *Handbook of Geostationary Orbits*, European Space Agency and Microcosm Inc., 1994.
- Spilker, J. J.(1987): *GPS Signal Structure and Performance Characteristics*, Navigation, the Institute of Navigation, 25, 121-146.
- Spilker Jr., J. J.(1996): *Tropospheric Effects on GPS*, Global Positioning System: Theory and Applications, Volume 1, edited by Bradford W. Parkinson, James J. Spilker Jr., Penina Axelrad and Per Enge, American Institute of Aeronautics and Astronautics, Inc.
- Springer T.A., G. Beutler, M. Rothacher (1999): *Improving the Orbit Estimates of GPS Satellites*, Journal of Geodesy, 73, pp. 147-157, Springer-Verlag 1999
- Su, H. (1988): *Dynamic Collocation Model for NAVSTAR/GPS Satellite Orbit*, The 2nd National Symposium of Space Geodesy in China, Nov. 1988, Xi'an, PR China
- Su, H. (1993): *Kinematic GPS Positioning with Orbit Improvement*, Paper presented at IAG General Meeting, Aug. 9-13, 1993, Beijing, PR China
- Sussel J.et al (1989): *Location and Navigation Satellite System*, Centre National D'etudes Spatiales, 1989.
- Teunissen, P. J. G (1993a): *The Invertible GPS Ambiguity Transformations*, Delft Geodetic Computing Centre (LGR)
- Teunissen, P. J. G (1994a): *A New Method for Fast Carrier Phase Ambiguity Estimation*, IEEE Position Location and Navigation Symposium (PLANS-94), April, Las Vegas
- Teunissen, P.J.G (1994b): *On the Spectrum of the GPS DD-Ambiguities*, ION GPS-94, September, 1994, Salt Lake City
- Teunissen, P. J. G (1995): *The Least-squares Ambiguity Decorrelation Adjustment: a Method for Fast GPS Integer Ambiguity Estimation*, Journal of Geodesy, Springer Verlag, Vol. 70, pp. 65-82
- Teunissen, P. J. G and A. Kleusberg (1998): *GPS for Geodesy*, Springer Verlag, Germany, 1998
- Townsend, B., P. Fenton, K. Van Dierendonck and R. van Nee (1995): *Performance of the Multipath Estimating Delay Lock Loop*, Navigation, Vol. 42, No.3, Fall 1995, pp. 503-514, Institute of Navigation.
- Townsend, B., P. Fenton, K. Van Dierendonck and R. van Nee (1995): *L1 Carrier Phase Multipath Error Reduction Using MEDLL Technology*, ION GPS-95, pp.1539-1544 Palm Springs, California, September 12-15, USA.

- Traquilla, J. M. and J. P. Carr (1991): *GPS Multipath Field Observations at Land and Water Sites*, Navigation, Journal of the Institute of Navigation, Vol. 37, No.4, Winter 1990-1991, pp. 393-414.
- Tscherning, C. C. (1976): *Covariance Expressions for Second and Lower order Derivatives of the Anomalous Potential*. The Ohio State University, Department of Geodetic Science, Report No. 225, 1976.
- Tscherning, C. C.(1977): *Models for the Auto- and Crosscovariances between Mass Density Anomalies and First and Second Order Derivatives of the Anomalous Potential of the Earth*. In: Proc. Third International Symposium Geodesy and Physics of the Earth, 261-268, Potsdam, 1977.
- Van Dierendonck, A. J. (1996):*GPS Receivers*, Parkinson et al edited *Global Positioning System: Theory and Applications, Chapter 8, Volume1* pp. 329-407, American Institute of Aeronautics and Astronautics, Inc.
- Van Dierendonck, A.J., Fenton, P. and Ford, T.(1993): *Theory and Performance of Narrow Correlator Spacing in a GPS Receiver*, Navigation, Vol. 39, No.3, Fall 1993, pp. 265-283. Institute of Navigation.
- Van Nee, Richard D. J.(1991): *Multipath Effects on GPS Code Phase measurements*, ION GPS-91, pp. 915-924, Albuquerque, New Mexico, September 11-13, USA.
- Wahr, J. M. (1981): *The Forced Nutations of an Elliptical, Rotating, Elastic, and Oceanless Earth*, Geophys. J. Roy. Astron. Soc., 64, 705-727
- Weill, L. (1995): *Achieving Theoretical Accuracy Limits for Pseudorangeing in the Presence of Multipath*, ION GPS-95, Palm Springs, California, September 12-15, 1995, USA.
- Werner, W., B. Eissfeller, Z. Fu and G. W. Hein. (1998): *Performance of the TCAR Method in Multipath and Jamming Environments*, ION GPS-98, pp.1385-1394 Nashville, Tennessee, September 15-18, 1998, USA.
- Wild, U. (1994): *Ionosphere and Geodetic Satellite systems: Permanent GPS Tracking Data for Modelling and Monitoring*, Geodätisch-geophysikalische Arbeiten in der Schweiz, Schweizerischen Geodätischen Kommission, Band 48
- Willis, P. (1995): *DORIS Coordinating Center Report*, IERS Annual Report 1995
- Willis, P. (1997): Private e-mail communication.
- Yang, M. (1995): *New GPS Measurement Modeling Techniques of Orbit Determination and Precise Kinematic Positioning*. Ph.D Dissertation, Report No. 431, The Ohio State University, August 1995
- Yunk, T. P., W. I. Bertiger, S. C. Wu, Y. E. Bar-Sever, E. J. Christensen, B. J. Haines, S. M. Lichten, R. J. Muellerschoen, Y Vigue and P. Willis (1994): *First Assessment of GPS-based Reduced Dynamic Orbit Determination on TOPEX/Poseidon*, Geophysical Research Letters, Vol. 21, No. 7, pages 541-544, April 1, 1994
- Xu, Q. (1989): *GPS Navigation and Precise Positioning*, Changzheng Press, Beijing, 1989
- Zhu, S.Y., Ch. Reigber and Z. Kang (1997): *Apropos Laser Tracking to GPS Satellites*, Journal of Geodesy (1997) 71.
- Zhu, S.Y., and E. Groten (1988); *Relativistic Effects in GPS, GPS Techniques Applied to Geodesy and Surveying*, Lecture Notes in Earth Science 19, Springer-Verlag.

## ACKNOWLEDGMENTS

I would like to express my sincere gratitude to my supervisor, Prof. Dr.-Ing. Günter W. Hein for his guidance, valuable comments and improvement. Without his support, I cannot finish this work. My many thanks also give to Prof. Dr.-Ing. Bernd Eissfeller and Prof. Dr.-Ing. Erwin Groten for their comments and suggestions. The help and valuable information from Dr. John M. Dow, European Space Operation Center (ESOC) at Darmstadt, Germany; Dr. Eberhard Gill, Germany Space Operation Center (GSOC) at Wessling, Germany; Dr. TS Kelso, US Air Force Institute of Technology (AFIT) at Wright-Patterson AFB in Ohio, USA; Dr. Dirk Oscam, Astrium GmbH at Fridrichhafen, Germany; Dr. Herbert Landau, Mr. Daniel Grossmith and Ms. Monika Jennert, Trimble TerraSat GmbH at Höhenkirchen, Germany and Mr. Daniel König, University FAF Munich at Neubiberg, Germany are also great appreciated.

The Education Ministry of Chinese government which supports my stay in Germany as visiting scholar from January 1996 to December 1996 is also acknowledged.





## RESUME

### Personal Data

Name Hua Su  
Date of Birth: Aug. 24, 1959  
Place of Birth: Jiangsu Province, PR China  
Languages English, German and Chinese

### Education

1974 - 1977 High School Student  
Wuxi No.1 High School, Jiangsu Province PRC

1978 - 1982 Undergraduate Student  
Wuhan Technical University of Surveying and Mapping, PRC  
(Graduated: B.S.)

1984 - 1987 Graduate Student  
Wuhan Technical University of Surveying and Mapping, PRC  
(Graduated: M.S.)

### Working Experience

1982 – 1984 Research Assistant  
Xi'an Research Institute of Surveying and Mapping, PRC

1987 – 1995 Research Associate  
Xi'an Research Institute of Surveying and Mapping, PRC

1996 – 2000 Ph.D Candidate and Research Associate  
Institute of Geodesy and Navigation, University FAF Munich, Germany